The Formulation of a Bioresponsive Ceramic Bone Replacement

By
Aminat Oyebola Bolarinwa

A thesis submitted to the
School of Chemical Engineering
of the
University of Birmingham
for the degree of
Doctor of Philosophy

School of Chemical Engineering,
University of Birmingham,
Edgbaston,
Birmingham, UK
B15 2TT.
June 2010

ABSTRACT

The long-term stability and brittle nature of ceramic bone replacements in physiological conditions makes them prone to mechanical failure. These problems have led to the development of bioresorbable bone replacement materials. Bioresorbable biomaterials are expected to degrade at a rate which is proportional to the rate of formation of new bone tissue. In the majority of cases, however, resorption is driven by simple dissolution and so it is difficult to ensure an appropriate degradation rate for all patients. This thesis seeks to develop a material that can degrade in response to the bone formation process, thus linking implant resorption to tissue formation. We have shown that this can be achieved by linking implant resorption to a biological stimulus, such as the enzyme alkaline phosphatase (ALP), which is found on the surface of bone forming cells (osteoblasts). ALP causes bone mineralisation by removing the pyrophosphate ($P_2O_7^{4-}$) ion, a known inhibitor to calcium phosphate formation. By removing the $P_2O_7^{4-}$ ions from solution the dissolution of calcium pyrophosphate ($Ca_2P_2O_7$) crystals were accelerated in accordance with Le Chetalier's principle. We demonstrated that for this accelerated dissolution to occur, the ALP did not require access to the crystal surface. This is contrary to previous work which suggested that CPPD dissolution occurred as a result of ALP cleaving the crystal surface. Bulk $Ca_2P_2O_7$ ceramics were successfully produced by sintering brushite cement at temperatures $\geq 400°C$, the dissolution of which could accelerated in the presence of ALP but was heavily dependent on material specific surface area. The process of sintering limits the possibility of producing biomaterials of complex morphology; therefore the final part of this thesis involved the fabrication of $Ca_2P_2O_7$ ceramic using stereolithography.

ACKNOWLEDGEMENTS

I would like to thank my supervisor Dr Liam Grover for his support and guidance throughout my PhD. I would also like to thank Dr Adrian Wright and Dr Rachel Bridson, their considerable knowledge of Rietveld analysis and dynamic vapour sorption respectively was of major benefit to me in my research.

Many thanks to Dr Covington and Ms Marina Talib at the University of Warwick for their expertise and allowing me the use of their stereolithography equipment.

I would also like to thank staff members: Dr Alan Smith, Dr James Bowen, Mrs Hazel Jennings and Ms Elaine Mitchell for their assistance with various laboratory equipments and techniques. My sincere gratitude extends to my fellow PhD students who have provided me with both technical and moral support throughout my PhD.

Finally my sincerest thanks go to my parents for their constant encouragement, financial and emotional support. The love and support of my brothers and sister did not go unnoticed either. My thanks also go to Ms Binuyo, Dr Agbabiaka, Ms Adeoshun, Zebiba Ali and to my loving husband Fadil Sanni. Your unending support, prayers and encouragement provided me with added strength.

To mum, dad, Ismail, Ishaq, Aliyyah and Fadil

TABLE OF CONTENTS

LIST OF FIGURES

LIST OF TABLES

LIST OF EQUATIONS

LISTS OF ABBREVIATIONS

ACP	Amorphous calcium phosphate
ALP	Alkaline phosphatase
ANOVA	Analysis of variance
ATP	Adenosine triphosphate
BET	Brunauer Emmett Teller
BMU	Basic multicellular unit
CAD	Computer aided design
CDHA	Calcium deficient hydroxyapatite
CPPD	Calcium pyrophosphate dihydrate
CRT	Cathode ray tube
DCPA	Dicalcium phosphate anhydrous (monetite)
DCPD	Dicalcium phosphate dihydrate (brushite)
DPA	Dipentaerrythritol penta/hexa acrylate
DSC	Differential scanning calorimetry
DTA	Differential thermal analysis
DVS	Dynamic vapour sorption
FTIR	Fourier transform infrared spectroscopy
HA	Hydroxyapatite
HDDA	1,6-Hexanediodiacrylate
HDeDA	1,6-Hexanediol ethoxylate diacrylate
Ksp	Solubility product
MCPM	Monocalcium phosphate monohydrate
MVs	Matrix vesicles

MWCO	Molecular weight cut off
NCP	Non-collagenous proteins
NTPs	Nucleoside triphosphate pyrophosphohydrolase
OCP	Octacalcium phosphate
P:L	Powder liquid ratio
PBS	Phosphate buffered saline
PC-1	Plasma cell membrane glycoprotein-1
PTFE	Polytetrafluroethylene
Pyrolidon	N-Methyl-2-pyrolidone
RGD	Arginine-glycine-aspartate sequence
SDCP	Sintered dicalcium pyrophosphate
SEM	Scanning electron microscopy
SLS	Selective laser sintering
STA	Simultaneous thermal analysis
TCP	Tricalcium phosphate
TGA	Thermogravimetric analysis
TMPTA	Trimethylolpropane triacrylate
TTCP	Tetracalcium phosphate
UV	Ultraviolet
XRD	X-ray diffraction
α'-TCP	α'-Tricalcium phosphate
α-TCP	α-Tricalcium phosphate
β-DCP	β-Dicalcium pyrophosphate
β-TCP	β-Tricalcium phosphate

1. INTRODUCTION

There is increased demand for bone replacement materials worldwide due to an ageing population (Hing, 2004). Annually around 2.2 million bone grafting procedures are carried worldwide with most of them using autograft tissue (Malak and Anderson, 2008). Other biological bone grafting options include allograft and xenograft. The disadvantages associated with these biological bone grafts such as immune rejection and disease transmission outweigh their advantages driving research into alternative bone replacement materials (Precheur, 2007). Synthetic materials such as metals, glass ceramics, polymers, hydrogels, cements and ceramics have been studied for use as bone replacements (Frame, 1975; Levine, 2008). A suitable bone replacement material is expected to be osteoconductive, non-cytotoxic and bioresorbable.

Hydroxyapatite (HA) is a calcium phosphate material which forms a strong bond with hard tissue and as such it has found extensive use in the repair of bone defects (Bucholz et al., 1987; Jarcho, 1981). HA is the most thermodynamically stable calcium phosphate in physiological conditions (Ishikawa et al., 2003) meaning that the implant will remain *in situ* for an extended period of time and present a significant chance of failure during the lifetime of the patient (Uemura et al., 2003). Brushite cement is another calcium phosphate which is more soluble than HA in physiological conditions and so can be more rapidly replaced with bone. As brushite cement degrades and the local environment becomes supersaturated with HA, HA is formed within the cement. This prevents resorption of the material and can lead to implant failure. One way to avoid this long term implant stability is to develop a

bioresorbable material. The degradation of such a material would be linked to a biological stimulus associated with the process of bone mineralisation.

Alkaline phosphatase (ALP) is an enzyme associated with bone mineralisation and found on the surface of osteoblasts. It is thought to aid bone mineralisation by removing pyrophosphate ($P_2O_7^{4-}$) ions from solution (Balcerzak et al., 2003; Johnson et al., 2000). The $P_2O_7^{4-}$ ion inhibits bone mineralisation by suppressing HA crystallisation; it adsorbs to the surface of the crystals, blocking further crystal growth (Addison et al., 2007; Hessle et al., 2002). ALP hydrolyses $P_2O_7^{4-}$ ion into orthophosphate (PO_4^{3-}) ions which initiate mineralisation. The hydrolysis of $P_2O_7^{4-}$ by ALP has been exploited by Xu et al. (Xu et al., 1991b) as a means for dissolving calcium pyrophosphate dihydrate (CPPD) crystals in arthritic joints. The dissolution of CPPD crystals was found to be faster in the presence of ALP (Xu et al., 1991b). This suggested that it would be possible to develop a calcium pyrophosphate based ceramic whose degradation can be linked to the bone mineralisation process. The ability to link both processes makes it possible to overcome variations in bone repair which occurs due to differences in age, health and gender of patients (Fahrleitner-Pammer et al., 2005; Havill, 2004).

This thesis begins with the precipitation of phase pure CPPD and brushite crystals which were characterised using X-ray diffraction, fourier transform infrared and scanning electron microscopy. The dissolution of these crystals in the presence and absence of ALP was investigated and quantified using a colourimetric phosphate assay. The mechanism by which ALP accelerated dissolution was investigated by ageing the crystals in the same solution as the ALP, but isolated from the surface of the crystals by visking tubing.

Following this, calcium pyrophosphate ceramics were formed by sintering brushite cements at temperatures $\geq$ 400°C. The influence of process parameters on the composition and mechanical properties of the ceramic were investigated and selected formulations were aged in the presence of ALP to determine whether bulk ceramic dissolution could be accelerated by the enzyme. Finally, stereolithography was evaluated as a means to produce complex calcium pyrophosphate structures.

2. BONE

Bone is a mineralised connective tissue: it protects the internal organs and provides structural support in vertebrates and in conjunction with the muscles facilitates movement (Dorozhkin, 2007; Hing, 2004). The main constituents of bone are: calcium phosphate crystals (65 wt%) (mainly HA); an organic phase consisting of type I collagen; cells and other macromolecules (25 wt%) and water (10 wt%) (Kuhn, 2001; Currey, 2001; Olszta et al., 2007). The high toughness of bone is as a result of the presence of collagen (Wang and Puram, 2004). The organic component of bone is responsible for giving bone its form and its ability to resist tension (Hedberg and Mikos, 2001). The inorganic component is important for the stiffness and compressive strength of bone (Hedberg and Mikos, 2001; Wang and Puram, 2004). Bone is an important reservoir and regulator of mineral ions; it contains 99% of the body's calcium and about 88% of the phosphates (Ng et al., 1997; Hedberg and Mikos, 2001). Bone is heterogeneous and anisotropic with a hierarchal structure which can be divided into four parts: macrostructure, microstructure, nanostructure and sub-nanostructure (Figure 2.1) (Rho et al., 1998).

2.1. BONE STRUCTURE

2.1.1. Macrostructure

Mature bone is composed of two types of tissue: the cortical (compact) bone found on the outer surface of most bones and cancellous (spongy or trabecular) bone found near the ends of long bones (e.g. tibia) and at the centre of flat bones (e.g. the skull and ribs) (Rho et al., 1998; Hing, 2004; Hedberg and Mikos, 2001; Dorozhkin, 2007). Cortical bone is denser than cancellous bone with a porosity of 5% - 10%

(Martin et al., 1998) (Table 2.1). It consists of regular cylindrical lamellae. Cancellous bone is composed of trabecular struts and marrow filled cavities which give it a relatively high surface area (Rho et al., 1998); its porosity is 75% - 95% (Martin et al., 1998). Cancellous bone can be categorised as either coarse or fine (Hing, 2004). The coarse cancellous bone is found in the body of healthy adult while fine cancellous bone is characteristic of a foetal skeleton (Hing, 2004). Generally cancellous bone is more metabolically active and it is therefore remodelled more often than cortical bone (Rho et al., 1998). As shown in table 2.1 cortical bone has a higher compressive, tensile and flexural strength than cancellous bone.

Table 2.1: Mechanical properties exhibited by cortical and cancellous bone (Hedberg and Mikos, 2001; Lawson and Czernuszka, 1998).

Property	**Cortical bone**	**Cancellous bone**
Compressive strength (MPa)	106 - 215	0.5 - 50
Tensile strength (MPa)	55 - 146	10 - 20
Flexural strength (MPa)	130 - 180	2 - 25
Young's modulus (GPa)	10 - 22	0.05 - 1.0
Density (gcm^{-3})	1.8	0.1 - 1.0

2.1.2. Microstructure

The bone microstructure consists of the lamellae, haversian canals and osteons which are then arranged to form either compact or cancellous bone (Olszta et al., 2007; Rho et al., 1998). Osteons are large hollow fibres with a diameter of 200 μm (Lakes, 1993); they consist of concentric lamellae (3 - 7 μm wide; (Rho et al., 1998)) and pores containing osteocytes cells (Lakes, 1993). The lamellae consist of fibrils which

on a sub-microstructural level consist of calcium phosphates and collagen (Lakes, 1993). As shown in figure 2.1b, osteons are made up of haversian canals which contain blood vessels carrying the necessary nutrients to the surrounding tissue (Lakes, 1993).

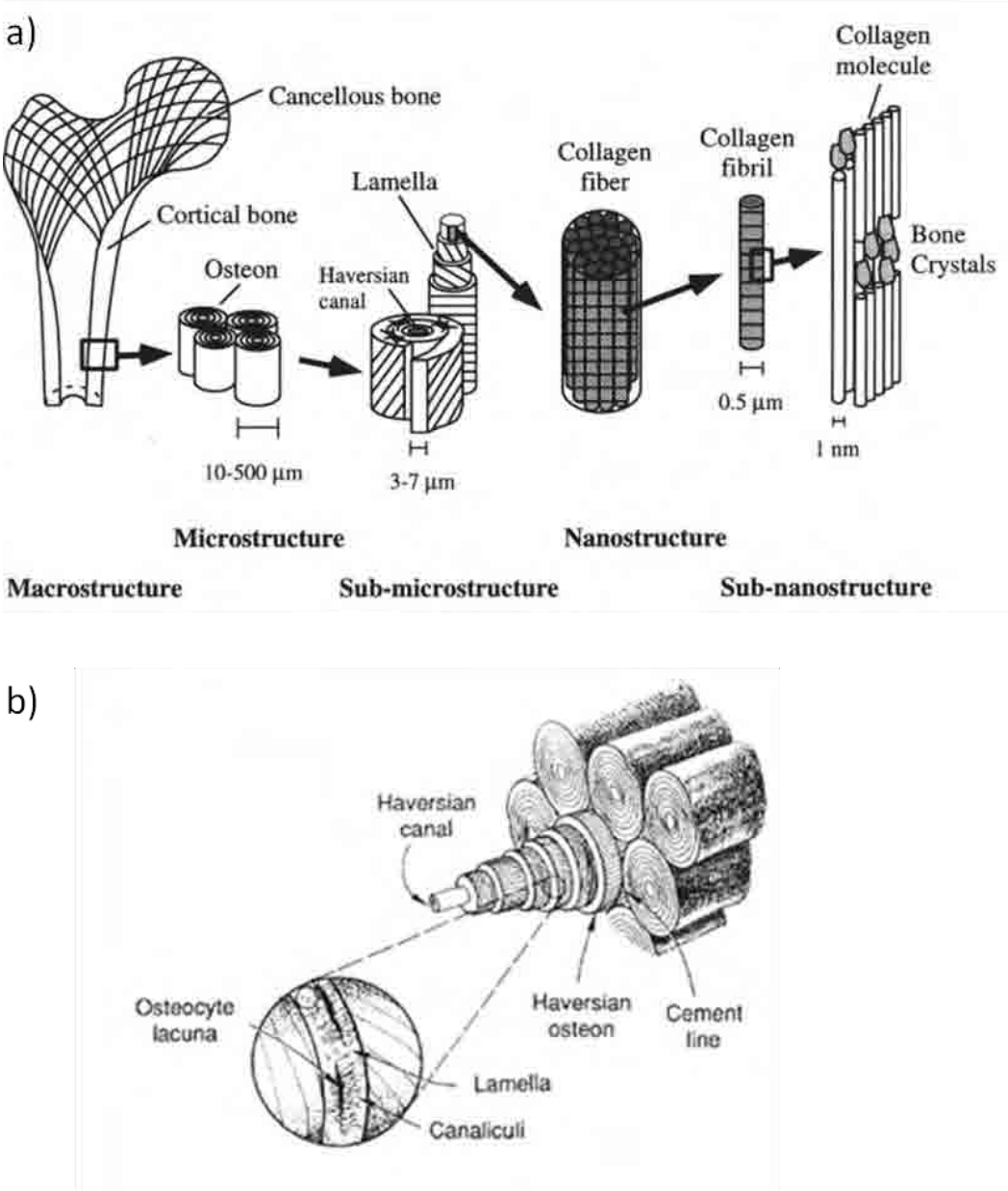

Figure 2.1: a) The hierarchal structure of the human bone (Kuhn, 2001; Rho et al., 1998) and b) microstructural division of bone (Lakes, 1993).

2.1.3. Nanostructure and sub-nanostructure

Collagen fibres and apatite make up 95% of the dry weight of bone and the remainder of the bone matrix consists of other organic molecules (known as non-collagenous protein), which are outlined in the following section.

2.1.3.1. Collagen

Collagen is the most abundant protein found in the body; it occurs in both calcified and non-calcified tissues and accounts for 70-90% of non-mineralised component of bone (Hing, 2004). Bone consists mostly of type-I with some type-V collagen. Type-I accounts for 90% of the body's total collagen (Hing, 2004) and is characterised by its fibrous nature (Weiner and Wagner, 1998). It consists of carefully arranged arrays of tropocollagen molecules which are long rigid molecules (300 nm in length, 1.5 nm wide), consisting of three polypeptides chains about 1000 amino acids in length; these are wound together in a triple helix (Weiner and Wagner, 1998; Hing, 2004). The flexibility and tensile strength of bone arises from its collagen structure (Martin et al., 1998).

2.1.3.2. Mineral

Since 1926, bone mineral has been known to be a calcium phosphate with an apatite-like structure (de Jong, 1926); it has a similar crystallographic structure to HA and calcium to phosphate ratio (Ca:P = 1.67). Apatite is often described by the formula $A_4B_6(MO_4)_6X_2$; in bone A and B are mostly calcium ion (Ca^{2+}), MO_4 is a PO_4 group and X is mostly hydroxyl ion (OH^-) with some fluoride ions (F^-) (Brown and Chow, 1976). In this thesis apatite has been used to mean a calcium phosphate with the same chemical formula of HA ($Ca_{10}(PO_4)_6(OH)_2$). The crystals of bone are plate or needle shaped with an average length between 40 – 60 nm, 20 nm wide and 1.5 – 5

nm thick (Suchanek and Yoshimura, 1998). The apatitic calcium phosphates crystals are deposited in discrete spaces of the collagen fibril (Figure 2.2). It is described as poorly crystalline (amorphous) because of the presence of impurities such as acid phosphates (HPO_4), sodium (Na), magnesium (Mg) and carbonates (Rho et al., 1998; Olszta et al., 2007; Fratzl et al., 2004).

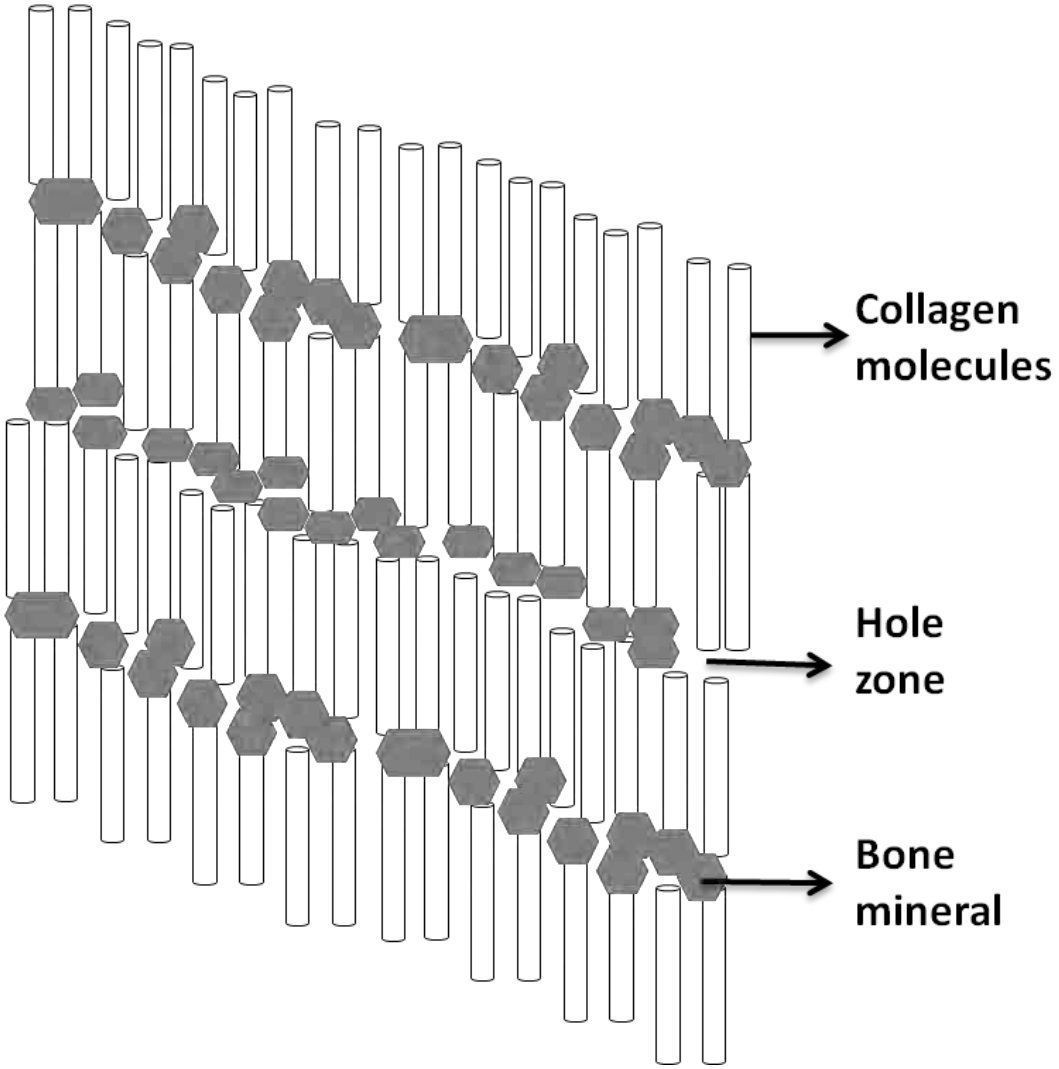

Figure 2.2: Schematic diagram illustrating the assembly of collagen fibrils and apatitic calcium phosphate in bone.

2.1.3.3. Non-collagenous proteins

Non-collagenous proteins (NCP) in bone include glycoproteins, proteoglycans and phosphoproteins such as osteocalcin, osteopontin, osteonectin and bone sialoprotein. These phosphoproteins are produced by bone cells and are responsible for regulating bone mineralisation and remodelling (Hing, 2004; Rho et al., 1998). Of these proteins bone sialoprotein and osteocalcin are specific to mineralised tissue (Hunter et al., 1996).

Osteocalcin

Osteocalcin, also known as bone Gla protein and it is one of the most abundant NCPs comprising up to 20% of the total NCP in bone (Hing, 2004). Osteocalcin is thought to inhibit HA formation by delaying crystal nucleation (Hunter et al., 1996).

Osteonectin

Osteonectin is expressed by osteoblast cells and is present in high concentrations in bone (Hunter et al., 1996; Hing, 2004). Osteonectin is believed to lack all inhibitory effect on HA crystal growth at concentrations ≤ 10 μg/ml (Hunter et al., 1996) and it is thought to be involved in cell-matrix interactions (Hing, 2004).

Bone sialoprotein

Bone sialoprotein and osteopontin are phosphorylated sialoproteins containing an arginine-glycine-aspartate (RGD) sequence required for cell adhesion (Hing, 2004; Hunter et al., 1996; Mckee and Nanci, 1996). Bone sialoprotein makes up 15% of the total NCP in bone (Hing, 2004; Wuttke et al., 2001). It does not inhibit HA formation at concentrations below 10 μg/ml; it is also thought to be involved in the nucleation of HA thereby promoting bone mineralisation (Hunter et al., 1996; Hunter and Goldberg, 1993).

Osteopontin

Osteopontin is a multifunctional protein involved in various physiological and pathological processes including: cell migration, adhesion and signalling, and regulation of osseous and ectopic calcification (Pampena et al., 2004). Osteopontin has been shown to inhibit calcification *in vitro*, studies also show osteopontin is a potent inhibitor of the *de novo* formation and seeded growth of HA (Pampena et al., 2004; Hunter et al., 1994; Boskey et al., 1993).

2.2. BONE CELLS

2.2.1. Osteoclasts

Osteoclasts originate from haematopoietic stem cell lineage and maintain mineral homeostasis by resorbing the surface of bone (Zaidi, 2007). Osteoclasts are large and multinuclear because they are formed from the fusion of monocytes (20 - 100 μm in diameter) (Kuhn, 2001; Martin et al., 1998).

2.2.2. Osteoblasts

Osteoblasts are mononuclear, cubodial cells that produce osteoid (Martin et al., 1998; Kuhn, 2001; Ng et al., 1997). They are derived from bone marrow mesenchymal stem cells (Martin et al., 1998; Hing, 2004). Differentiation of mesenchymal stem cells into osteoblasts occurs within 2-3 days. The osteoblasts lay down osteoid at a rate of 1 μm/day, mature osteoblasts become embedded in the matrix and differentiates to become osteocytes (Martin et al., 1998).

2.2.2.1. Role of osteoblast cells in bone mineralisation

Osteoprogenitor cells differentiate to become osteoblasts which express alkaline phosphatase and secrete type 1 collagen and NCPs (Johnson et al., 2000; Zaidi, 2007). The collagen formed is arranged in fibrillar structures, the spaces between the end of the collagen fibres are known as hole zones as shown in figure 2.2. Apatite crystals are formed in the interior of matrix vesicles (MVs) (Johnson et al., 2000; Hessle et al., 2002; Anderson et al., 2005; Tomatsu et al., 2006). MVs are sub-microscopic, extracellular membranes located on osteoblasts and enriched in ALP, Ca^{2+} and PO_4^{3-} ions (Anderson et al., 2005; Johnson et al., 2000; Tomatsu et al., 2006; Hessle et al., 2002; Balcerzak et al., 2003; Hsu and Anderson, 1978). The formation of apatite is followed by its extrusion into the hole zones. Besides the presence of Ca^{2+} and PO_4^{3-} ions, apatite formation is also aided by the removal of $P_2O_7^{4-}$ ion a known inhibitor to bone mineralisation by alkaline phosphatase as shown in figure 2.3 (Anderson et al., 2005; Hessle et al., 2002). $P_2O_7^{4-}$ ion suppresses the formation and growth of hydroxyapatite (Hessle et al., 2002) and at high concentrations of $P_2O_7^{4-}$ osteopontin is expressed (Addison et al., 2007; Moochhala et al., 2008). Osteopontin is a known inhibitor of HA formation (Pampena et al.,

2004; Hunter et al., 1994; Boskey et al., 1993). ALP hydrolyses the $P_2O_7^{4-}$ ion into PO_4^{3-} ion which is then used to form bone mineral (hydroxyapatite). Further mineralisation of the collagen occurs by the nucleation of crystals already formed within the hole zone. Once the available space within the hole zone is filled the crystals grow and extend beyond the hole zones and into pore spaces between the collagen fibrils (Kuhn, 2001).

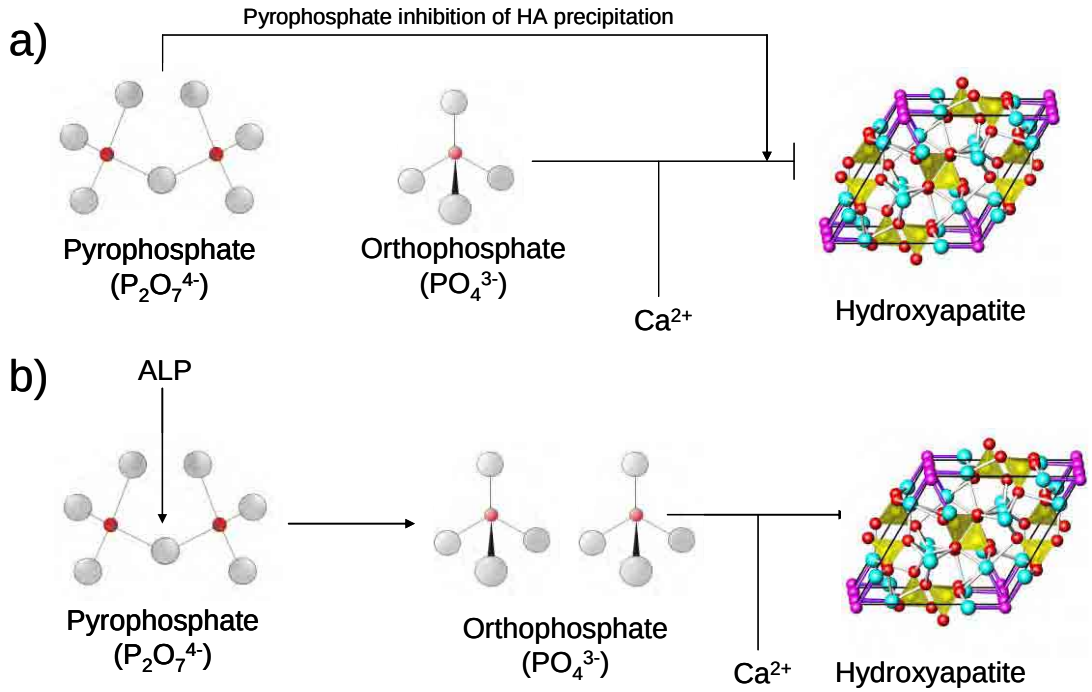

Figure 2.3: a) Effect of pyrophosphate ion on the mineralisation of bone and b) alkaline phosphatase aids bone mineralisation by hydrolysing pyrophosphate ion into phosphate ion which is then precipitated as hydroxyapatite.

2.2.3. Osteocytes

Osteocytes are the most common cell type in bone; they are responsible for its maintenance (Hing, 2004; Nijiweide et al., 2002). Osteocytes are spaced throughout the mineralized matrix confined within cavities called lacunae (Nijiweide et al., 2002). Osteocytes maintain a link with osteoblasts through small canals within the bone matrix known as canuliculi (Nijiweide et al., 2002; Martin et al., 1998). Osteocytes receive stimuli that enable response to ionic concentrations of calcium and phosphate and mechanical strain through this network of canuliculi (Kuhn, 2001).

2.3. BONE FORMATION AND REMODELLING

This section discusses the formation of bone in humans from childhood to adulthood, the roles of the various bone cells and proteins and the process by which bone remodels and repairs itself.

2.3.1. Bone formation

Bone formation occurs by the intramembranous ossification or endochondral ossification process (Kuhn, 2001). The intramembranous ossification forms flat bones such as the skull and pelvis while endochondral ossification produces long bones such as the femur that bear weight and are linked to joints (Kuhn, 2001; Martin et al., 1998; Marks and Odgren, 2002).

Endochondral ossification

Endochondral ossification occurs during embryonic development when the chondroprogenitor cells become chondrocytes which then forms a cartilaginous model of bone (Kuhn, 2001). Other undifferentiated cells in the surrounding areas form osteoblasts which forms a bony collar in centre of the cartilaginous long bones (Kuhn, 2001). The bony collar starves the cells which lead to the degradation of the cartilage. As the cartilage degrades the product of the degradation is transported via blood vessels leaving empty canals. This is then filled with bone forming cells which deposit osteoid forming a network of spongy bone (Kuhn, 2001; Schoenau et al., 2004).

Intramembranous ossification

Intramembranous ossification occurs during embryonic development (Marks and Odgren, 2002). It involves the formation of fibrous connective tissue which is used as a scaffold (Kuhn, 2001). The fibrous connective tissue is formed by mesenchymal progenitor cells (Kuhn, 2001). Unmineralised osteoid matrix is secreted around the fibrils of the connective tissue membranes by osteoblasts. The osteoid matrix is then mineralised to become a network of porous cancellous bone (Kuhn, 2001). A periosteum is a multilayered connective tissue which encloses the cancellous bone. Over time new bone fills the spaces beneath the periosteum and at the outer portion of the cancellous bone thereby forming a compact bone shell (Kuhn, 2001). This encloses the cancellous bone in a sandwich structure.

Bone modelling

Bone modelling involves the growth and reshaping of bone in childhood and adolescence (Ng et al., 1997). Longitudinal growth of long bones depends on the proliferation and differentiation of cartilage cells at growth plates which are then transformed to bone tissue in the metaphysis (Ng et al., 1997; Schoenau et al., 2004). The growth of bone in width occurs by the formation of bone at the periosteal surface with resorption at the endosteum (Schoenau et al., 2004; Ng et al., 1997). In adults, bone growth in length and endochondral bone formation ceases once the epiphyses close but the process of bone remodelling continues throughout life (Ng et al., 1997).

2.3.2. Bone remodelling

Bone remodelling refers to the process whereby old bone is replaced by new bone (Ng et al., 1997). This occurs throughout adult life in both cancellous and cortical bone. It is estimated that 25% of cancellous bone and 3% of cortical bone is resorbed and replaced annually (Parfitt, 1994). The process of remodelling is initiated by osteoclasts which bind to the bone surface using cell attachment proteins called integrins (Ng et al., 1997; Kuhn, 2001). Osteoclasts release H^+ lowering the pH of the local environment this causes the dissolution of bone crystals and other organic components thereby producing "resorption pits" (Ng et al., 1997; Kuhn, 2001). After the resorption process, osteoblasts deposit osteoid which is later mineralised (Ng et al., 1997). The newly deposited osteoid has a new (lamellae) microstructure (Kuhn, 2001; Ng et al., 1997). The remodelling process involves the removal and replacement of bone in this particular order and on the same site (Martin et al., 1998). The group of cells which partake in these processes are called the basic

multicellular unit (BMU). The link between osteoblast and osteoclasts activity is called coupling (Ng et al., 1997; Schoenau et al., 2004).

2.4. ALKALINE PHOSPHATASE

Alkaline phosphatase (ALP) is a plasma bound enzyme which occurs widely in many organisms (McComb et al., 1979; Millan, 2006; Muginova et al., 2007). ALP is a metalloenzyme that forms an isologous dimer with two reactive centres in which magnesium and zinc are present (Balcerzak et al., 2003; Mornet et al., 2001; McComb et al., 1979). It is known to catalyse the hydrolysis of phosphomonoesters (Schwartz and Lipmann, 1961) and has inorganic pyrophosphatase activity (Cox et al., 1967) and can therefore hydrolyse pyrophosphates and polyphosphates ions, releasing inorganic phosphate (Anderson et al., 2005; Hessle et al., 2002; Omelon et al., 2009). $P_2O_7^{4-}$ ions are produced by the nucleoside triphosphate pyrophosphohydrolase (NTPs) activity of a family of enzyme which includes plasma cell membrane glycoprotein-1 (PC-1). In conjunction with PC-1 ALP seeks to control bone mineralisation by regulating the concentration of pyrophosphate ions present within the MVs as seen in figure 2.4 (Hessle et al., 2002). The process of regulating the concentrations of $P_2O_7^{4-}$ and PO_4^{3-} is important in order to avoid abnormalities in bone mineralisation (Hessle et al., 2002).

2.4.1. Forms of alkaline phosphatase

Alkaline phosphatase is divided into four isozymes. Three forms of the enzyme are tissue specific - intestinal, placental and germ cells (Moss, 1982; Muginova et al., 2007). The tissue specific ALP is 90 – 98% homologous and their genes are located on chromosome 2 (Mornet et al., 2001). The fourth isozyme, which is 50% identical to the other three is tissue non-specific as it is widely distributed in the liver, bone and kidney (Mornet et al., 2001; Llinas et al., 2006). The genes of the tissue non-specific ALP can be found on chromosome 1 (Mornet et al., 2001).

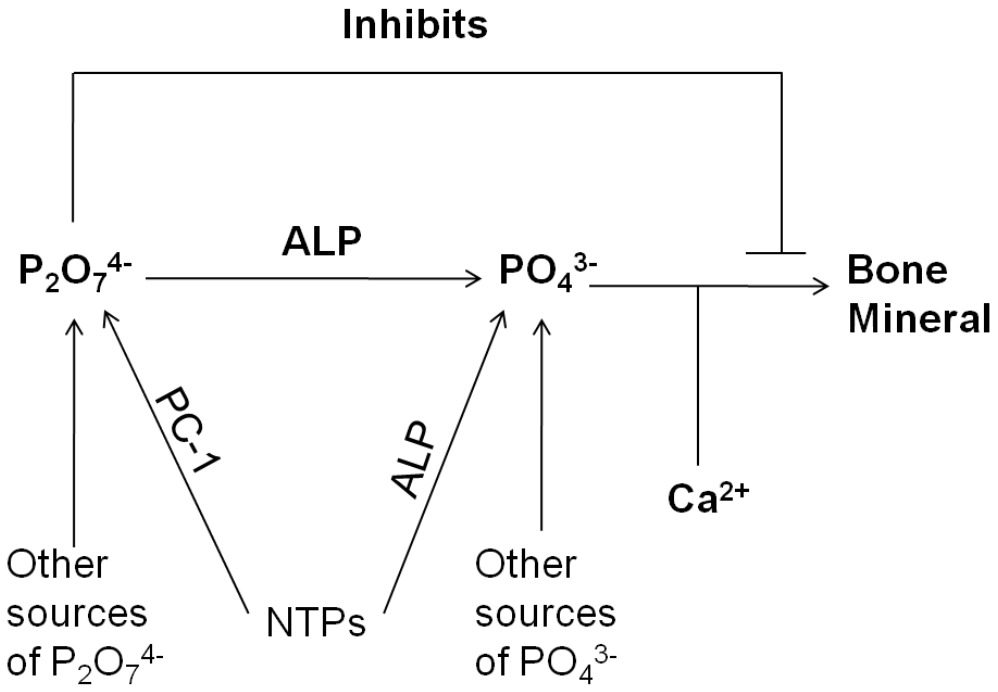

Figure 2.4: Schematic diagram showing the role of ALP and PC-1 activity in regulating bone mineralisation by controlling inorganic phosphate and pyrophosphate ion concentrations (Balcerzak et al., 2003; Hessle et al., 2002).

3. BONE REPLACEMENT MATERIALS

One of the earliest modern applications of a biomaterial as a bone replacement was in the early 1900's when bone plates conventionally made from stainless steel, chromium-cobalt, titanium alloys were used to successfully stabilise fractures and accelerate its healing (Ben-Nissan and Pezzotti, 2004). Although bone can regenerate to a certain extent following injury, beyond a critical size defect it is impossible for bone tissue to regenerate and fibrous in growth will occur. The advancement in technology and an ageing population has increased the focus on finding various means and methods by which bone can be replaced. Key properties of bone replacement materials include: non-toxicity, availability, osteoconductivity and wherever possible bioresorbability. Osteoconductivity refers to the ability of the material to act as a scaffold on which new bone tissue can grow across (Ilan and Ladd, 2002). Osteoinductivity is the ability of a bone replacement material to induce the formation of new bone tissue (Ilan and Ladd, 2002). Bone replacement materials can be classified as either biological or synthetic. This chapter discusses the relative merits and drawbacks of synthetic and biological bone graft replacements.

3.1. BIOLOGICAL BONE REPLACEMENT

3.1.1. Autograft

It has been estimated that approximately 500,000 bone grafting procedures are carried out annually in the USA and about 2.2 million procedures worldwide in the orthopaedics and dental industry (Lewandrowski et al., 2000; Giannoudis et al., 2005; Ilan and Ladd, 2002). Autograft tissue is the 'gold standard' for bone graft procedures; the bone graft is transferred from one site to another within the same

individual (Precheur, 2007). The tissue can be harvested from either cortical or cancellous bone (e.g. iliac, femur and tibia); a mixture of both types of bone tissue can also be used (Precheur, 2007; Ludwig et al., 2000). Autologous tissue provides osteogenic, osteoinductive and osteoconductive properties (Giannoudis et al., 2005). The problems associated with the autografting procedure include: donor site morbidity, increased surgery and patient recovery time (Giannoudis et al., 2005; Ludwig et al., 2000).

3.1.2. Allograft

Allograft tissue is taken from another individual of the same species and it is the most frequently chosen bone graft where autograft is not available. Allograft tissue is available as either dowels, strips or chips (Giannoudis et al., 2005; Sandhu et al., 1999). It is prepared fresh but it's rarely used in this state as it ignites an immune response or can transmit disease (Friedlander et al., 1999). Allograft tissue is persevered by freezing or freeze drying, these processes could result in the destruction of osteoprogenitor cells leading to some loss in osteoinductive properties, but the osteoconductive property is retained (Giannoudis et al., 2005; Ludwig et al., 2000; Ilan and Ladd, 2002). The problems associated with allograft tissue include: antigenicity and disease transmission (Precheur, 2007). As allograft tissue is cadaveric in origin (Precheur, 2007), it is sometimes difficult to obtain reproducible bone tissue for grafting (Giannoudis et al., 2005; Vaccaro, 2002).

3.1.3. Xenograft

Xenograft tissue involves the transplantation of bone tissue from one species to another, it is often bovine in origin (Precheur, 2007). Bovine bone is non-toxic to human osteoblasts (Blom, 2007; Doherty et al., 1994). The main disadvantages of xenograft is the theoretical risk of transmission of bovine spongiform encephalopathy although there is no firm evidence that it can be transmitted to humans (Precheur, 2007). It has also been documented that xenografts could cause an intense inflammatory response (Begley et al., 1995). The source of xenograft bone tissue could also raise strong ethical issues.

3.2. SYNTHETIC BONE REPLACEMENT

The use of synthetic materials in humans dates as far back as ancient Phoenicia where gold wires were used to bind artificial teeth with the neighbouring ones (Ben-Nissan and Pezzotti, 2004). Developments in technology have led the research into synthetic bone replacement materials; the aim is to overcome the disadvantages associated with biological bone tissue replacement. Synthetic bone replacement materials include: metals, polymers, hydrogels, cements, ceramics and glasses. The basic properties required of a suitable bone replacement materials include non-toxicity, reproducibility and osteoconductivity (Ben-Nissan and Pezzotti, 2004; Vaccaro, 2002; Giannoudis et al., 2005). Any material placed into the body elicits a response from the surrounding tissue (Table 3.1) (Ben-Nissan and Pezzotti, 2004; Hulbert et al., 1982; Hench, 1998). As a result of this interaction materials may be described as nearly inert, bioactive or bioresorbable (Hench, 1991).

Bioinert (nearly inert)

Bioinert materials have little or no interaction with the surrounding tissues (Hench, 1991). They do not bond chemically or biologically with the bone tissue, this results in the formation of a fibrous tissue layer at the bone-tissue interface (Hench, 1991). Any movement at this interface can cause implant failure (Hench, 1991). To resolve this, biomaterials with pore sizes between 100 – 150 μm have been developed, enabling biological fixation to the host tissue through the growth of healthy and viable bone tissue (Hench, 1991). Table 3.1 gives some examples of nearly inert biomaterials.

Bioactive (surface reactive)

Bioactive biomaterials were discovered in 1969 when Hench reported the first *in vivo* results and *in vitro* tests from the use of Bioglass® (Hench et al., 1972). The glass material was found to form a stable bond with bone due to the kinetic modification of the surface in a time dependent manner when implanted (Hench, 1991). Although the implant is strongly attached there is a possibility that the bone or implant (bulk) could fail (Hench, 1991). Bioactive materials are also known to enhance bone tissue formation (Precheur, 2007). Due to these properties HA has been used as coatings for various bioinert materials especially in hip replacement (Hench and Wilson, 1984; Nagano et al., 1996; Geesink et al., 1988; Ducheyne et al., 1980).

Bioresorbable

Resorbable materials are designed to degrade slowly in the body before they are replaced by the host tissue (e.g. bone) (Hench, 1991; Hench, 1998). Due to the resorbable nature of these materials there is little interface layer formed (Hench, 1991). A suitable resorbable material should be made up of ions which are tolerated in the body and easily removed from circulation therefore limiting the risk of toxicity. The limitations of designing suitable resorbable biomaterial include: (1) maintaining the strength of the implant and the stability of the interface throughout degradation and new tissue formation and (2) matching the rate of material degradation to new tissue formation (Hench, 1991).

Table 3.1: Interaction between the biomaterial and host tissue (Hench, 1991; Hulbert et al., 1982; Ben-Nissan and Pezzotti, 2004; Dubok, 2000).

Biomaterial type	Tissue reaction	Example
Nearly inert	Undergoes little or no chemical change, formation of a fibrous tissue layer	Al_2O_3, ZrO_2, titanium and stainless steel.
Bioactive	Chemical bond between the tissue and implant surface	Hydroxyapatite, Bioglass® and glass ceramic.
Resorbable	Gradual dissolution in the body while it is replaced by the new bone tissue	Calcium phosphate salts and polylactic-polyglycolic acid copolymers.

3.2.1. Metals

Metals were first used in orthopaedic procedures by the ancient Greeks to treat bone fractures (Sumita and Teoh, 2004). In 1991 over half of the total market for implants and instrumentation in orthopaedics was for joint prostheses made of metallic materials (Brunski JB, 1996). Metallic implants take the form of nails, screws, bone plates and staples amongst others (Sumita and Teoh, 2004). The main advantage of using metallic implant is their high mechanical strength and fracture toughness making them suitable for use in load bearing applications (Brar et al., 2009; Staiger et al., 2006). Unfortunately their usually low corrosion resistance means they release potentially toxic ions that could lead to tissue inflammation (Staiger et al., 2006; Sumita and Teoh, 2004; Jacobs et al., 1998). The material does not form a significant bond with bone and the patient would require a secondary surgery to remove the implant (Staiger et al., 2006). There is also a problem with implant failure due to fracture arising from corrosion or fretting fatigue (Sumita and Teoh, 2004). Examples of metallic implants currently available on the market are: stainless steel, titanium, cobalt-chromium based alloys and magnesium.

3.2.1.1. Magnesium

Magnesium's properties make it suitable for use in bone tissue repair. It is lightweight, non-toxic and biodegradable; it has a similar density to that of bone (Staiger et al., 2006; Tan et al., 2009). Magnesium is essential for human metabolism with work showing that magnesium enhances cell adhesion on alumina and has no inhibitory effect on cell growth (Li et al., 2004; Pietak et al., 2008; Brar et al., 2009; Zreiqat et al., 2002). Magnesium was first used in 1907 by Lambotte (Lambotte, 1932) to secure a fractured leg bone (Brar et al., 2009; Staiger et al., 2006). This

biomaterial failed to provide sufficient mechanical support to the surrounding tissue as it corroded and degraded too rapidly (Staiger et al., 2006; Lambotte, 1932). Furthermore, as magnesium undergoes corrosion hydrogen gas is released and this was found to have been accumulated underneath the skin were the implant was placed (Staiger et al., 2006; Lambotte, 1932). The low corrosion resistance of magnesium has led to the development of various magnesium alloys which have a higher resistance at physiological pH.

3.2.1.2. Stainless steel

Stainless steel is made from iron alloyed with various other elements such as silicon, molybdenum, carbon, and chromium (Sumita and Teoh, 2004). The addition of 12 wt% or more of chromium to steel increases corrosion resistance due to the formation of a chemically stable oxide layer (Sumita and Teoh, 2004). The most common grade of stainless steel used for tissue transplantation is 316L as it contains less than 0.03 wt% carbon because this reduces the possibility of corrosion *in vivo* (Brunski JB, 1996). Nickel is sometimes added to stainless steel to promote the higher corrosive resistance austenitic phase (Sumita and Teoh, 2004). The disadvantage of using nickel is its toxicity to the surrounding tissue therefore the material is used in temporary devices (Sumita and Teoh, 2004).

3.2.2. Ceramics, Bioglass and Glass Ceramics

3.2.2.1. Alumina

α-Alumina is the form of alumina used in bioceramics; it is the most stable form when free from impurities (Ishikawa et al., 2003). In 1963 alumina ceramic (Al_2O_3) was mixed with epoxy resin before implantation into rabbits (Smith, 1963). After 40 days implantation the biomaterial was found to have been kept in place by cancellous bone and fibrous tissue (Hulbert et al., 1982; Hulbert et al., 1972). High purity, polycrystalline alumina was developed and used for total hip prostheses and tooth implants as a replacement to surgical metal alloys (Ben-Nissan and Pezzotti, 2004; Boutin et al., 1988; Hench, 1991). The advantage of using alumina in articulating areas is its low wear rate due to its high hardness, low friction coefficient and high corrosion resistance (Ben-Nissan and Pezzotti, 2004; Hench, 1991).

3.2.2.2. Zirconia

Zirconia is of interest in the orthopaedics field due to its mechanical strength, high fracture toughness and relatively low Young's modulus (Ishikawa et al., 2003); about 600,000 zirconia femoral heads have been implanted worldwide (Chevalier, 2006). These properties enable the production of smaller femoral heads for total hip prostheses than alumina (Hench, 1998). Zirconia occurs in three forms: monoclinic, cubic and tetragonal (Ishikawa et al., 2003; Piconi, 2001). From room temperature up to 1170°C zirconia exists in the monoclinic form, above this temperature it changes to the tetragonal phase (Ishikawa et al., 2003; Piconi, 2001). Biomedical grade zirconia has been shown to exhibit the best mechanical strengths of the oxide ceramics due to phase transformation toughening (Chevalier, 2006). Phase transformation involves the application of stress, inducing the transformation from

the metastable tetragonal to monoclinic phase. Zirconia is prone to ageing in the presence of water due to this metastability (Chevalier, 2006; Ben-Nissan and Pezzotti, 2004). The addition of calcium oxide (CaO), magnesium oxide (MgO), cerium oxide (CeO_2) or Yttrium oxide (Y_2O_3) has been shown to prevent phase transformation in the material (Ishikawa et al., 2003; Piconi, 2001). The products of the degradation of zirconia leads to osteolysis which is thought to be the major cause of long term failure of total hip replacements (Ben-Nissan and Pezzotti, 2004; Ishikawa et al., 2003).

3.2.2.3. Bioglass and glass-ceramics

Bioglass and glass ceramics are used in spinal surgery, maxillofacial reconstruction, coatings for inert biomaterials, and as bone and dental implants (Hench, 2001; Hench, 1998; Rezwan et al., 2006). Hench (Hench et al., 1972) discovered that bioactive glasses containing Na_2O, CaO, P_2O_5 and SiO_2 bonded to femoral bone in rats 10 days after implantation. Bioglass®, PerioGlas®, BioGran®, 45S5® and S53P4® are types of bioglass and glass ceramics currently in use in clinics (Hench, 2001). The 45S5 (45% SiO_2, 24.5% CaO, 24.5% Na_2O and 6% P_2O_5 by weight) bioglass is commonly used. The products of its degradation are found to upregulate the expression of genes that control osteogenesis and the production of growth factors thereby enhancing osteoblast proliferation (Rezwan et al., 2006). The extent of bone bonding is thought to be affected by the silica content of the biomaterial; the upper limit is 60% (Hench, 2001). It has also been suggested that 45S5 bioglass enhances the growth of osteoblast on its surface than hydroxyapatite due to the rapid exchange of ions at the surface (Rezwan et al., 2006; Ben-Nissan and Pezzotti, 2004). CaO-SiO_2-B_2O_3 glass ceramic was investigated as a possible bone replacement material

but the tensile strength was lower than that of HA and when implanted into New Zealand white male rabbits (Lee et al., 2006). $CaO\text{-}SiO_2\text{-}B_2O_3$ glass ceramic was also found to show a higher biodegradation than β-TCP and HA *in vivo* (Lee et al., 2006).

3.2.3. Polymers

Biodegradable polymers can be classified as either natural polymers e.g. polysaccharides, collagen or synthetic polymers e.g. poly(glycolide), poly(ε-caprolactone), poly(lactic-coglycolide). The success in the late 1960s of a poly(-glycolic acid) based wound suture has led to the design and development of a variety of polymer biomaterials (Gilding and Reed, 1979; Middleton and Tipton, 2000). Since then there has been considerable interest in polymers as dental materials (Kulkarni et al., 1971; Miller et al., 1977), coatings for orthopaedic implants (Gollwitzer et al., 2005; Seal et al., 2001; Ignjatovic et al., 2007), orthopaedic biomaterials (Middleton and Tipton, 2000; Nair and Laurencin, 2007; Rezwan et al., 2006; Athanasiou et al., 1998) and as drug delivery matrices (Rezwan et al., 2006; Seal et al., 2001; Ramchandani and Robinson, 1998). Due to the versatility of polymers in 2003, the sale of polymeric biomaterials was in excess of $7 billion (Nair and Laurencin, 2007).

3.2.4. Hydrogels

Hydrogels are a network of macromolecular hydrophilic polymers forming a gel, which have the ability to hold water many times their weight (Patel and Mequanint, 2007; Ulijn et al., 2007; Li, 2004; Griesser and Kambouris, 2001). The first hydrogel to be used in the 1950's was poly(hydroxyethyl methacrylate) (poly-HEMA); it was found to be well tolerated in the body (Griesser and Kambouris, 2001; Wichterle and Lim, 1960). Poly-HEMA resists protein adsorption and lubricity making it an ideal material for contact lenses (Batich and Leamy, 2003). Hydrogels can be classified as either chemical or physical based on the bonding of the crosslinks present and also as either natural, synthetic or a combination of both based on the source (Li, 2004). Chemical hydrogels are also known as permanent hydrogels as they cannot be dissolved using water or other solvents (Li, 2004). The polymer network of a chemical hydrogel is formed by covalent bonding (Li, 2004). The polymer networks for physical hydrogels are formed by cohesion forces such as ionic bond, hydrogen bond and van der Waals forces (Li, 2004). Hydrogels are employed in a variety of applications including: wound dressing (Rosiak et al., 1989), coatings for orthopaedic materials (Zdrahala, 1996; Griesser and Kambouris, 2001), drug delivery (Schmaljohann et al., 2003; Ulijn et al., 2007; Peppas et al., 2006) and in tissue engineering (Ulijn et al., 2007; Peppas et al., 2006). The mechanical properties of hydrogels have been vastly improved (Gong et al., 2003) although it is still comparatively lower than that of metals, metallic alloys, cements and ceramics (Grimm, 2003).

4. CALCIUM PHOSPHATES

Calcium phosphate materials have been in use in medicine (Friedman et al., 1998; Jarcho, 1981; de Groot K., 1984; de Groot, 1980) and dentistry (Brown and Chow, 1985; LeGeros, 1988) for over 30 years (Hench, 1998). The applications include: coatings for orthopaedic implants (Geesink, 1990; Geesink et al., 1988; Stephenson et al., 1991), maxillofacial surgery (Hench, 1998), scaffolds for bone growth (Hench, 1998), materials in total hip and knee surgery (Hench, 1998; Gatti et al., 1990; van Hemert et al., 2004) and as a drug release matrices (Ginebra et al., 2006; Paul and Sharma, 1999; Itokazu et al., 1998; Hamanishi et al., 1996). Calcium phosphates are widely available and are of interest to a variety of fields including geology, chemistry, biology and medicine (Dorozhkin, 2007). As the name suggests they comprise calcium (Ca), phosphorus (P) and oxygen (O) atoms but could also consist of hydrogen (H^+) ions either as an acidic phosphate e.g. HPO_4 or as water (H_2O). Calcium phosphates are all soluble in acids and insoluble in alkaline solution while the vast majority are sparingly soluble in water (Dorozhkin, 2007). The chemical similarity of bone with calcium phosphate materials (Kuhn, 2001; Currey, 2001; Olszta et al., 2007) and their osteoconductive nature makes them suitable materials for bone replacement (Gatti et al., 1990; Kitsugi et al., 1993). A benefit of using calcium phosphates is the non-toxicity of its degradation products which are easily cleared from the body (del Valle et al., 2007; Constantz et al., 1995; Suchanek and Yoshimura, 1998; Anee et al., 2003; Ng et al., 2008). A brief description of some of the calcium phosphates used in the production of bone replacement materials are provided below.

4.1. CALCIUM ORTHOPHOSPHATES

4.1.1. β – Tricalcium phosphate (β-TCP)

There are three polymorphs of TCP: β-TCP, α-TCP and α'-TCP (Choi and Kumta, 2007). α'-TCP is the high temperature phase and exists above 1470°C (Ryu et al., 2002; Elliot J.C., 1994). Due to its unstable nature it has not found any use as bone replacement. β-TCP is the most stable form at temperatures below 1180°C (Elliot J.C., 1994). A combination of β-TCP, HA and their derivatives form the basis of most calcium phosphate bone cements used in bone replacement (Navarro et al., 2008) as it is considered to be non-toxic and resorbable (Peters and Reif, 2004). The powder and highly porous blocks of β-TCP degrade too rapidly resulting in no bone formation at the implant site of the implant (Lin et al., 1995b; Uemura et al., 2003). Pure β-TCP ($Ca_3(PO_4)_2$) does not occur in biological calcifications and cannot be precipitated in aqueous solution (Dorozhkin, 2007). It can be produced only through thermal decomposition at temperatures above 800°C (Dorozhkin, 2007). β-TCP is also used as a coating for orthopaedic appliances (Hulbert et al., 1982; Peters and Reif, 2004) and is added to some brands of toothpaste as a gentle polishing agent and in multivitamin complexes (Dorozhkin, 2007).

4.1.2. α – Tricalcium phosphate (α-TCP)

α-TCP is stable at temperatures between 1180 -1400ºC and is formed by the phase transformation of β-TCP at temperatures above 1125ºC (Choi and Kumta, 2007; Dorozhkin, 2007). α-TCP has the same chemical composition as β-TCP but a different crystallographic structure (Table 4.1) (Dorozhkin, 2007). This is thought to be responsible for the higher solubility of α-TCP when compared to β-TCP (Bohner,

2000). Compared to β-TCP, α-TCP is less stable and more reactive in aqueous systems (Peters and Reif, 2004). It hydrolyses and reprecipitates as apatitic products (Peters and Reif, 2004). α-TCP was shown to degrade faster *in vivo* than β-TCP and was surrounded by new bone (Yamada et al., 2007). α-TCP does not occur in biological calcification and in its pure form it is occasionally used in bone cement (Dorozhkin, 2008; Dorozhkin and Epple, 2002; Bermudez et al., 1994; Driessens et al., 1994; Kurashina et al., 1997; Constantz et al., 1995).

4.1.3. Tetracalcium phosphate (TTCP)

TTCP ($Ca_4(PO_4)_2O$) is also known as hilgenstockite and is the most basic calcium orthophosphate (Dorozhkin and Epple, 2002; Dorozhkin, 2007). TTCP has a higher solubility than HA in water (Table 4.2) and cannot be precipitated from aqueous solution (Kalita et al., 2007). TTCP is not stable in aqueous conditions and it hydrolyses slowly to HA and calcium hydroxide (Kalita et al., 2007; Elliot J.C., 1994). It can be prepared by solid state reactions at temperatures above 1300°C in a dry atmosphere, in vacuum or with rapid cooling to prevent water uptake and HA formation (Elliot J.C., 1994; Dorozhkin, 2007). TTCP is never found in biological calcification (Kalita et al., 2007). It is widely used for the preparation of various self setting calcium phosphate cements such as HA (Elliot J.C., 1994).

Table 4.1 : Crystallographic data for calcium phosphates (Dorozhkin, 2007; Elliot J.C., 1994)

Compound	**Space group**	**Unit cell**					
		a (Å)	b (Å)	c (Å)	α (°)	β (°)	γ (°)
β-TCP	Rhombohedral R3Ch	10.4183(5)	10.4183(5)	37.375(6)			120
α-TCP	Monoclinic $P2_1/a$	12.887(2)	27.280(4)	15.219(2)		126.20(1)	
OCP	Triclinic *P*1	19.692(4)	9.523(2)	6.835(2)	90.15(2)	92.54(2)	108.65(1)
MCPM	Triclinic *P*1	5.6261(5)	11.889(2)	6.4731(8)	98.633(6)	118.262(6)	83.344(6)
DCPD	Monoclinic *I*a	5.812(2)	15.180(3)	6.239(2)		116.42(3)	
TTCP	Monoclinic $P2_1$	7.023(1)	11.986(4)	9.473(2)		90.90(1)	
HA	Monoclinic $P2_1/b$	9.84214(8)	2a	6.8814(7)			120
HA	Hexagonal $P6_3/m$	9.4302(5)	9.4302(5)	6.8911(2)			120

4.1.4. Amorphous calcium phosphate (ACP)

ACP [(($Ca_3(PO_4)_2$). nH_2O; n = 3 - 4.5; 15-20% H_2O) (Bohner, 2000; Dorozhkin, 2007)] was previously reported to be a component of bone the concentration of which decreases with age (Termine and Posner, 1966). Further investigations carried out by Grynpas et al. (Grynpas et al., 1984) indicated that ACP was not present in bone. ACP often occurs as a transient phase in the formation of calcium phosphates in aqueous solutions (Dorozhkin and Epple, 2002; Elliot J.C., 1994). ACP is used to produce calcium phosphate cements (Takagi et al., 1998; Bohner, 2000). The chemical composition of ACP, in the final mixing solutions, is dependent on the pH, calcium and phosphate ion concentrations (Dorozhkin and Epple, 2002; Dorozhkin, 2007). Electron microscopy has shown that ACP consists of spherical particles with diameters in the range of 20 – 200 nm without distinct morphology (Dorozhkin and Epple, 2002; Dorozhkin, 2007). It is also thought to have apatitic structure but with a crystal size that is X-ray amorphous (Dorozhkin and Epple, 2002; Dorozhkin, 2007). It has also been proposed that ACP has a basic structural unit 9.5 Å diameter, roughly spherical, cluster of ions comprising $Ca_9(PO_4)_6$ (Betts and Posner, 1974).

4.1.5. Monocalcium phosphate monohydrate (MCPM)

MCPM ($Ca(H_2PO_4)_2.H_2O$) is the most acidic and soluble of all the calcium phosphates (Elliot J.C., 1994), at temperatures above 100°C it loses its water of crystallisation and becomes anhydrous (Dorozhkin, 2007). Due to its high acidity and solubility MCPM is not found in biological calcifications and is not cytotoxic with bone in its pure form (Koster et al., 1977). Mirtchi et al (Mirtchi et al., 1989) used MCPM in conjunction with β-TCP to form self hardening cement (DCPD; brushite)

for use as bone replacement material. This cement has been reported to be non-toxic and osteoconductive (Ohura et al., 1996). MCPM is used in food, beverages and as mineral supplement in dry baking powders in addition it is used in agriculture as a fertilizer (Dorozhkin, 2007). According to the European Union classification MCPM is a food additive marked as E34 (Dorozhkin, 2007).

Table 4.2: Properties of some calcium orthophosphates (Dorozhkin, 2007; Dorozhkin, 2008; Fernandez et al., 1999).

Compound	**Ca/P molar ratio**	**Density (gcm^{-3})**	**Solubility at 25ºC –Log(Ksp)**	**Solubility at 37ºC -Log(Ksp)**
MCPM	0.5	2.23	1.14	-
DCPD	1.0	2.32	6.59	6.59
OCP	1.33	2.61	96.6	95.9
TTCP	2.0	3.05	38 – 44	37 – 42
β-TCP	1.5	3.08	28.9	29.5
α-TCP	1.5	2.86	25.5	25.5
HA	1.67	3.16	58.4	58.6

4.1.6. Octacalcium phosphate (OCP)

OCP ($Ca_8(HPO_4)_2(PO_4)_4.5H_2O$) is found biologically in dental and urinary calculi (Dorozhkin, 2007). It often occurs as an intermediate phase during the precipitation of more stable calcium orthophosphate from aqueous solution (Dorozhkin and Epple, 2002). It has been proposed that OCP is an intermediate phase in the mineralisation of bone and teeth (Brown et al., 1987; Tomazic et al., 1994; Nancollas and Wu, 2000; Suzuki et al., 1991; Bohner, 2000; Brown, 1962; Brown et al., 1962).

Therefore OCP has been investigated for use as an implant coating as well as promoting bone formation *in vivo* and *in vitro* due to its bioactive and osteoconductive properties (Barrere et al., 2003; Kamakura et al., 1999; Shelton et al., 2006). OCP consists of apatitic layers separated alternately by hydrated layers (Elliot J.C., 1994; Dorozhkin and Epple, 2002; Suzuki et al., 2006). The presence of apatitic layers explains the structural similarities with HA (Brown et al., 1962) and the transition of OCP to HA is thermodynamically favoured (Suzuki et al., 2006). This transition in physiological conditions is thought to be responsible for the low detection of OCP in vascular calcification (Suzuki et al., 2006).

4.1.7. Hydroxyapatite (HA)

HA ($Ca_{10}(PO_4)_6(OH_2)$) is the most stable and the least soluble of all the calcium orthophosphates in physiological conditions (Table 4.2) (Ben-Nissan and Pezzotti, 2004; Dorozhkin and Epple, 2002). It has a chemical composition similar to the mineral content of bone (Vallet-Regi and Gonzalez-Calbet, 2004; Kalita et al., 2007; Bow et al., 2004). It is osteoconductive and bioactive therefore bonds well with bone (Ng et al., 2008; Vallet-Regi and Gonzalez-Calbet, 2004; Ben-Nissan and Pezzotti, 2004) and soft tissue (Hench, 1991; Suchanek and Yoshimura, 1998). HA has been widely used in orthopaedic (Dorozhkin and Epple, 2002) and dental applications (Denissen and Degroot, 1979; LeGeros, 1988) either in powder or bulk form. It is used as a coating for metallic prostheses due to its bioactive properties (Ben-Nissan and Pezzotti, 2004; Liu et al., 2001; Suchanek and Yoshimura, 1998; Willmann, 1999). HA is also used as a matrix for drug release (Paul and Sharma, 1999; Liu et al., 2005; Palazzo et al., 2005; Lin et al., 1996). A composite of HA and poly(vinyl

alcohol) gel have also been investigated for use as a biomaterial in articular cartilage repair (Pan et al., 2007).

4.1.8. Dicalcium phosphate dihydrate (DCPD)

DCPD is commonly known as brushite and can be easily crystallized from aqueous solutions (Dorozhkin, 2007). It is often found in pathological calcifications dental calculi, chondrocalcinosis (LeGeros, 2001) and urinary stones (Hesse and Heimbach, 1999). It has been proposed as an intermediate in the formation of bones and teeth i.e. bone mineralization and dissolution of enamel in acids (dental erosions) (Sainz-Diaz et al., 2004). Brushite cement can be produced by a mixture of phosphoric acid and β–TCP (Bohner et al., 1996), which is transformed into its anhydrous form (dicalcium phosphate anhydrous; DCPA) at temperatures above 55°C (Grover et al., 2005). Brushite cement has been developed as a bone replacement material in place of HA due to its higher solubility at pH 7.4 in physiological conditions. Other uses of brushite are as a texturizer in the food industry and as a water retention additive (Dorozhkin, 2007).

4.2. CALCIUM PHOSPHATE CEMENT

Calcium phosphate cements were discovered in the 1980's by Brown and Chow (Brown and Chow, 1985) and are widely used as bone substitutes due to their osteoconductive properties (Bucholz, 2002). Calcium phosphate cements are produced by the reaction of one or more calcium phosphate powders in an aqueous solution (Bohner et al., 2005). The calcium phosphate cement dissolves depending on the chemical composition and pH of the solution before the final product is

precipitated (Dorozhkin, 2008). During precipitation the newly formed crystals form a web as they grow providing mechanical rigidity to the calcium phosphate cement (Bohner, 2000). Calcium phosphate cements can also be implanted into patients as a workable paste to fit various shape defects (Alkhraisat et al., 2008) leading to the development of a wide variety of commercially available calcium phosphate cements (Table 4.3) (Bohner et al., 2005). Depending on the end product of the cement setting reaction calcium phosphate cement can be classified as apatite or brushite cement (Bohner, 2000).

Table 4.3: Examples of commercially available calcium phosphate cements and their compositions (Bohner et al., 2005; Dorozhkin, 2008; Ishikawa et al., 2003).

Brand Name	**Cement type**	**Powder component**	**Liquid component**	**Company**
BoneSource®	Apatite	TTCP + DCPA	H_2O, mixture of Na_2HPO_4 and NaH_2PO_4	Stryker-Leibinger Corp.
Norian SRS®	Apatite	α-TCP + MCPM + $CaCO_3$	H_2O, Na_2HPO_4	Synthes-Norian
Mimix™	Apatite	TTCP + α-TCP	Citric acid	Biomet
Biopex®	Apatite	α-TCP + TTCP + DCPD + HA	Succinic acid and chonroitin sulphate	Mitsubishi materials
Eurobone®	Brushite	β-TCP + $Na_4P_2O_7$	H_2O, H_3PO_4 and H_2SO_4	Kasios
chronOS™ Inject	Brushite	β-TCP, MCPM, $MgHPO_4.3H_2O$, $MgSO_4$ and $Na_2H_2P_2O_7$	H_2O, sodium hyaluronate	Synthes-Norian

4.2.1. Apatite cements

The formation of calcium deficient apatite (CDHA) cement by the hydrolysis of α-TCP between 60 - 100°C was first reported by Monma and Kanazawa (Monma and Kanazawa, 2000). The presence of calcium phosphate crystals which are closely similar to CDHA and carbonated apatite in bone and teeth is thought to be responsible for its osteoconductive nature and non-cytotoxic properties *in vivo* (Dorozhkin, 2008). Brown and Chow (Brown and Chow, 1985) reported on the formation of apatite from the combination of TTCP and DCPA or DCPD powders in an aqueous medium. The setting period for this apatite cement (Brown and Chow, 1985) was shorter at physiological temperature than that of CDHA (Monma and Kanazawa, 2000) but could be further reduced by adding MCPM, orthophosphoric ions and phosphoric acid which lower the pH of the mixture (Dorozhkin, 2008). Apatite cements are formed at near physiological pH (> 4.2) (Xia et al., 2006). As DCPA and TTCP powders in aqueous solution dissolve and calcium and phosphate ions are released these results in the supersaturation of the solution with respect to apatite. Apatite, crystals are then precipitated to form the hardened apatite cement mass (equation 4.1). This process is known as "dissolution-precipitation mechanism" (Ishikawa et al., 2003). Due to the thermodynamic stability of apatite cement at neutral pH most calcium phosphates are hydrated to form apatite (Ishikawa et al., 2003).

$$2Ca_4(PO_4)_2O + 2CaHPO_4 \rightarrow Ca_{10}(PO_4)_6(OH)_2 \ldots (4.1)$$

4.2.2. Brushite cements

Brushite cement was first introduced in 1987 by (Lemaitre et al., 1987) and can only be produced by an acid base reaction (Bohner, 2000). It has a faster setting time than apatite cement and citric acid and sodium citrate delay the hardening reaction. Brushite cement is formed when the pH of the setting cement past is acidic i.e. pH ≤ 4.2 (Bohner et al., 1997). Brushite cement can be produced from a mixture of β-TCP, MCPM and water (equation 4.2) (Mirtchi et al., 1989). When MCPM is replaced with orthophosphoric acid (equation 4.3) it is easier to control the physico–chemical properties of the cement such as longer setting times and larger tensile strengths due to a higher homogeneity as well as the chemical composition and reactivity of the cement (Dorozhkin, 2008).

$$Ca(H_2PO_4)_2.H_2O + Ca_3(PO_4)_2 + 7H_2O \rightarrow 4CaHPO_4.2H_2O \ldots (4.2)$$

$$Ca_3(PO_4)_2 + H_3PO_4 + 6H_2O \rightarrow 3CaHPO_4.2H_2O \ldots (4.3)$$

Brushite cements are osteoconductive and also more soluble than apatite cements (Dorozhkin, 2008). They are metastable and more soluble at physiological pH than apatite cement (Vereecke and Lemaitre, 1990) making them more resorbable *in vivo* (Apelt et al., 2004). The linear degradation rate of brushite cement is calculated as 0.25 mm/week (Ohura et al., 1996) which is thought to be too fast as not to allow the formation of mature bone. The release of orthophosphoric acid when large amounts of brushite cement are implanted *in vivo* is thought to be responsible for the inflammation of the surrounding tissue (Bohner, 2000). The inflammation is thought to occur by the transformation of DCPD into CDHA which increases the resorption time leading to cement implant failure (Dorozhkin, 2008; Grover et al., 2003). $P_2O_7^{4-}$

ions or magnesium salts of low solubility can be incorporated into the brushite cement to inhibit apatite formation (Grover et al., 2006; Apelt et al., 2004; Bohner and Matter, 2004).

4.2.2.1. Pyrophosphate modified brushite cement

Pyrophosphate ions prevent the seeding of calcium phosphate crystals by binding onto the crystal surface therefore stopping it from reaching its critical size (Caswell et al., 1991). This property has been exploited in reducing setting times for brushite cement. Grover et al. reported the formation of a new type of brushite cement containing calcium pyrophosphate (Grover et al., 2003). This cement was found to degrade faster than brushite cement in phosphate buffered saline solution (Figure 4.1) (Grover et al., 2006). This is due to pyrophosphate ion inhibiting the formation of apatite within the brushite cement (Grover et al., 2006). This property of $P_2O_7^{4-}$ ion as well as its interaction with ALP has ensured the possibility of developing a pyrophosphate based bone replacement material (Whited et al., 2006).

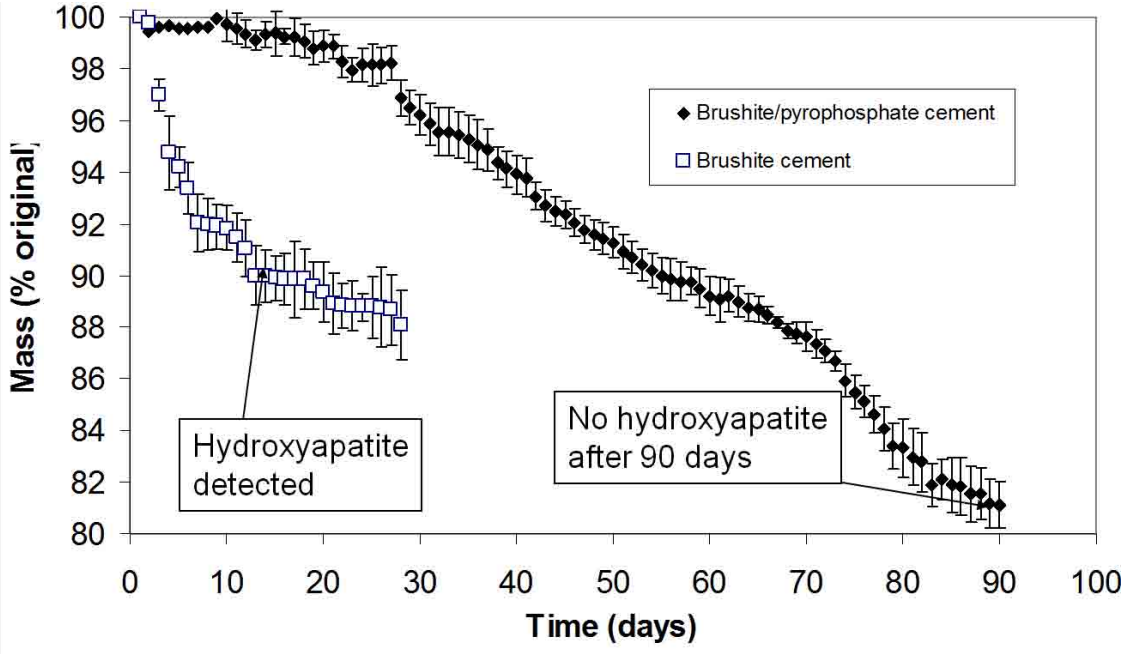

Figure 4.1: Degradation of brushite and pyrophosphate modified brushite cement in phosphate buffered saline solution (Grover et al., 2006).

5. CONDENSED PHOSPHATES

Condensed phosphates were discovered in 1827 (Vanwazer and Holst, 1950). They can be formed either by an enzymatic reaction using polyphosphatase kinases (Kornberg et al., 1999) or a condensation reaction. The condensation reaction involves the elimination of the water component of orthophosphoric acids and other phosphate species (Greenfield and Clift, 1975). Condensed phosphates have a wide variety of applications such as in drug delivery matrices (Dion et al., 2005) and as a multivalent electrolyte in aqueous solutions (Van Wazer, 1974). They can be classified as: polyphosphates, cyclophosphates and ultraphosphates. Linear and ultra (branched) - phosphates are formed by the condensation of phosphoric acids with the empirical formula:

$$H_{(n+2)}P_nO_{(3n+1)} \; or \; n(H_3PO_4).(n-1)H_2O$$

While cyclophosphates are salts of cyclic acids with an empirical formula of:

$$(HPO_3)_n \; or \; (H_3PO_4.H_2O)_n$$

Where n is the number of phosphates in the linear or cyclic chain.

Biological occurrence of condensed phosphate salts

McCarty (Mccarty et al., 1962) first discovered the presence of CPPD crystals in articular cartilage and synovial fluid of humans. The presence of these crystals leads to the clinical disease known as calcium pyrophosphate deposition disease, with patients exhibiting arthritic symptoms (Song et al., 2002). High concentrations of $P_2O_7^{4-}$ ions were also found in fluid collected from the joints of patients suffering with osteoarthritis (Hearn and Russell, 1980). Polyphosphates have also been

identified in a wide variety of microorganisms such as bacteria, fungi and algae (Kornberg et al., 1999) and in higher plants and animals (Harold, 1966).

5.1. TYPES OF CONDENSED PHOSPHATES

5.1.1. Pyrophosphates

PO_4^{3-} ion consists of a central phosphorous atom surrounded by four oxygen atoms at the corners of a tetrahedron (Vanwazer and Holst, 1950). Pyrophosphate, the simplest form of condensed phosphates is formed by linking two phosphate ions together by a central oxygen atom as illustrated in figure 5.1b. Pyrophosphates are usually non-linear and the P-O-P (phosphoanhydride) bond angle is rarely 180° (Greenfield and Clift, 1975).

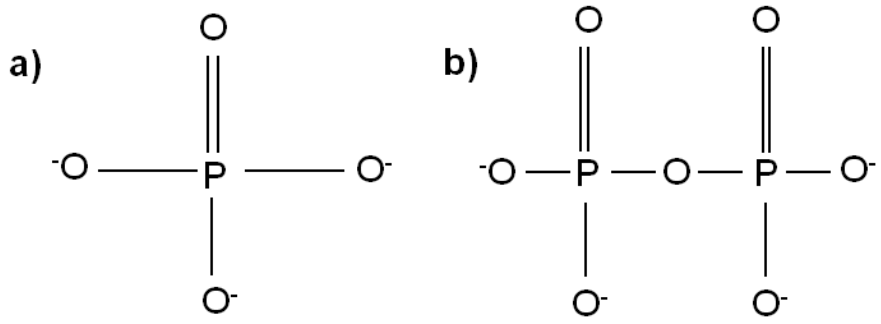

Figure 5.1: A diagram representing the structure of a) orthophosphoric ion and b) pyrophosphate ion.

5.1.2. Linear polyphosphates

Linear polyphosphates are represented by the general formula $M_{(n+2)}P_nO_{3n+1}$, where n is the number of phosphorous atoms in the chain. In the polyphosphate chain, the phosphorous atoms are linked another by an oxygen atom as shown in figure 5.2. The degree of polymerisation n, varies from 2 (pyrophosphate) to10^6 (Kualev et al., 2004). Polyphosphates chains between 2 and 5 can be obtained in a pure and crystalline phase while polyphosphates of higher chain length are obtained in mixtures with each other (Kualev et al., 2004; Vanwazer and Callis, 1958). Polyphosphates are stable at neutral pH, room temperature (Kualev et al., 2004) and alkali solution but reactive in acids (Harold, 1966).

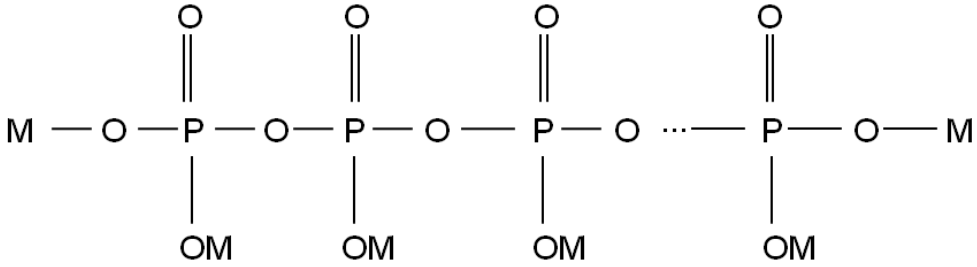

Figure 5.2: Structure of linear condensed phosphate, where M is a hydrogen ion or a monovalent metal cation.

Linear polyphosphates contains terminal hydroxyl groups which are weakly acidic and intermediate hydroxyl groups that are strongly acidic (Kualev et al., 2004). This property makes it possible to determine the type of condensed phosphate and the length of the polymer chain. The alkali metal salts are more soluble in water with the exception of Kurrol's (large macromolecular potassium polyphosphate) and Maddrell's (high molecular weight sodium polyphosphate) salt (Kualev et al., 2004). Polyphosphates salts produced from divalent metals are either completely insoluble or sparingly soluble in aqueous solution (Kualev et al., 2004).

5.1.3. Cyclophosphates

Cyclophosphates also known as “metaphosphates” have the general formula $M_nP_nO_{3n}$. Most common compounds in this group of condensed phosphates are the tri- and tetra-methaphosphates (Figure 5.3). Cyclophosphates are weak BrØnsted bases due to the absence of terminal hydroxyl groups, however, they hydrolyse faster in strongly acidic and basic solutions (Kualev et al., 2004; Kura, 1987a). They are also very stable in neutral aqueous solutions (Kura, 1987a).

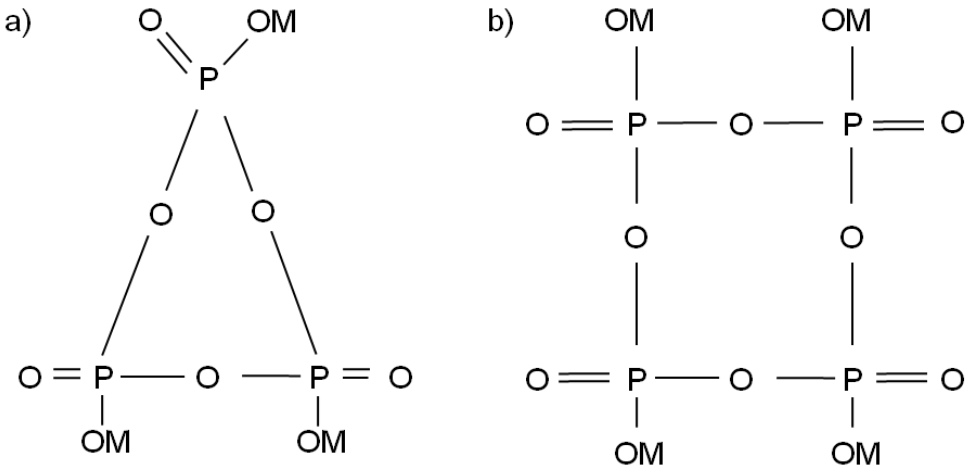

Figure 5.3: Structure of cyclophosphates: a) tri-metaphosphate and b) tetra-metaphosphate.

5.1.4. Ultraphosphates

Ultraphosphates contain branched phosphates i.e. phosphorous atom shares three oxygen atoms with the neighbouring phosphorous atom (Harold, 1966). The branching points on the chain are easily hydrolysed in aqueous solution irrespective of pH or temperature therefore ultraphosphate salts are difficult to detect in living organisms (Harold, 1966; Kualev et al., 2004).

5.2. STABILITY OF CONDENSED PHOSPHATES

5.2.1. Hydrolytic degradation of condensed phosphates

Linear polyphosphates and cyclophosphates hydrolyse very slowly at neutral pH and room temperature. The hydrolysis of these condensed phosphate salts is increased in the presence of complex ion, by reducing pH and increasing temperature (Greenfield and Clift, 1975; Kura and Tsukuda, 1993). The hydrolysis of linear polyphosphates occurs faster in acidic solution through the nucleophilic attack of water on the phosphorous atoms in the P-O-P bonds (Kura, 1991). This is initiated by the reaction of the linear polyphosphates a strong BrØnsted base with hydrogen ion (H^+) in the acidic solution (Kura, 1991).

The degradation of cyclophosphates occurs in two stages: (i) it is converted into linear polyphosphate of the same chain length in strong alkali solution and (ii) the linear polyphosphate is degraded in acidic solution in a manner similar to that described above (Kura, 1987b). Pyrophosphates breakdown into PO_4^{3-} ions which are the end product of hydrolytic degradation of all condensed phosphates (Kura et al., 1998), polyphosphates do not degrade directly and completely into only phosphate ions (Greenfield and Clift, 1975). For example the degradation of tetrapolyphosphate into orthophosphate ions occurs in three stages as shown below:

$$P_4O_{13}^{6-} \rightarrow P_3O_{10}^{5-} + PO_4^{3-}$$

$$\downarrow$$

$$P_2O_7^{4-} + PO_4^{3-}$$

$$\downarrow$$

$$2PO_4^{3-}$$

5.2.2. Enzymatic degradation of condensed phosphates

Karl-Kroupa (1950) found that polyphosphates are degraded in the presence of various living organisms (Karlkroupa et al., 1957). Polyphosphatase enzymes degrade polyphosphates by cleaving orthophosphate ion from the end of the chain (exopolyphosphatase) or by breaking the chain in the middle to produce two shorter polyphosphate chains (endopolyphosphatase) (Omelon and Grynpas, 2008). The phosphorlaytion of glucose is catalysed by the polyphosphate glucose phosphotransferase enzyme which uses adenosine triphosphate (ATP) or polyphosphate as its source of orthophosphate (Omelon and Grynpas, 2008; Harold, 1966). ALP can hydrolyse both pyrophosphate and polyphosphate to produce orthophosphate thereby contributing to the overall pool of orthophosphate ion which is then used in bone mineralisation (Omelon et al., 2009; Hessle et al., 2002).

5.2.3. Degradation of CPPD by polyphosphates

Polyphosphate materials with at least three PO_3 units were found to be effective in dissolving CPPD crystals (Cini et al., 2001). There was no significant effect on CPPD dissolution when the PO_3 units were increased further (Cini et al., 2001). These crystals were removed from female patients suffering from degenerative meniscal lesions. Linear polyphosphates (sodium tripolyphosphate; $Na_5O(PO_3)_3.6H_2O$) are found to be more effective in increasing CPPD crystal dissolution than cyclic trisodium metaphosphate ($Na_3(PO_3)_3$) (Cini et al., 2001). It is thought that the higher negative charge and complexing ability of linear $Na_5O(PO_3)_3.6H_2O$ enables it to remove and bind effectively and more tightly to calcium ion on the crystal surface than cyclic $Na_3(PO_3)_3$ (Cini et al., 2001).

5.3. APPLICATION OF CONDENSED PHOSPHATES

5.3.1. Enhanced biological phosphorous removal; EBPR

Polyphosphate accumulating organisms are used in wastewater treatment (Kualev et al., 2004). Wastewater contains orthophosphate ions from the run off of fertilizers, detergents and other industrial discharges (Kualev et al., 2004). The presence of PO_4^{3-} ions in wastewater encourages the growth of destructive blue algae blooms in natural waters (Kualev et al., 2004). These microorganisms consume large amount of phosphates than that needed for their growth by storing and accumulating it within their cells as polyphosphates (Kualev et al., 2004; Seviour et al., 2003).

5.3.2. Food and agriculture

Calcium ammonium pyrophosphate and ammonium polyphosphates are some of the condensed phosphates widely used in fertilizers (Kualev et al., 2004; Brown et al., 1963). Polyphosphates are added to food to maintain its pH at optimal level prolonging the lifetime of the food as well as preventing changes in colour and fat decomposition during storage (Kualev et al., 2004).

5.3.3. Biological applications

Polyphosphates have been identified as a phosphate storage in many microorganisms such as *Saccharomyces cerevisiae* (Urech et al., 1978) and it was proposed that the microorganisms obtain orthophosphates from the polyphosphates during periods of starvation (Harold, 1966). It has also been proposed that the storage of phosphates as polyphosphate is favoured due to the efficiency of the system and it produces little effect on the osmotic pressure (Harold, 1966). As explained previously pyrophosphates and polyphosphates perform an important role in bone mineralisation as they are known inhibitors to the growth of apatite crystals (Johnson et al., 2000; Omelon et al., 2009). Excess orthophosphate is also polymerised to form polyphosphates (Omelon et al., 2009).

5.3.4. Orthopaedic biomaterials

Calcium pyrophosphate ceramics are non-toxic and osteoconductive (Kitsugi et al., 1993; Lin et al., 1995b). It also forms very good bond with bone (Kitsugi et al., 1993). Calcium pyrophosphate is also thought to be an intermediate product in bone mineralisation. Its calcium to phosphorus ratio (Ca/P = 1.0) is lower than that of

tricalcium phosphate (Ca/P = 1.5) and therefore more soluble (Lin et al., 1995a). These properties have made it favourable to be evaluated as a possible bone replacement material. Some calcium pyrophosphate and calcium polyphosphate ceramic materials have been discussed below.

5.3.4.1. Sintered calcium pyrophosphate

Kitsugi et al. produced and implanted bulk dicalcium pyrophosphate ceramic into mature male rabbits and found the ceramic to be non-toxic and osteoconductive (Kitsugi et al., 1993). It was reported that no fibrous tissue layer was formed at the bone and ceramic interface (Kitsugi et al., 1993). The mechanical strength of sintered $Ca_2P_2O_7$ ceramic was found to improve when a liquid additive, sodium pyrophosphate ($Na_4P_2O_7.10H_2O$) up to 5 wt% was added (Lin et al., 1995b). The porous β-$Ca_2P_2O_7$ with 5 wt% $Na_4P_2O_7.10H_2O$ ceramic was implanted into New Zealand white rabbits where it was found to form a strong bond with the bone tissue without the formation of a fibrous tissue layer (Lin et al., 1995b). The bone tissue grew into the macropores of the ceramic and gradually dissolved over time to be replaced by a bony structure (Lin et al., 1995a). Sintered calcium pyrophosphate particles were also found to have no inhibitory effect on the growth of osteoblast cells (Sun et al., 1997). Sun et al. evaluated the use of $Ca_2P_2O_7$ as a possible treatment for osteoporosis (Sun et al., 2002). Postmenopausal osteoporosis is a disorder which affects elderly women and is characterised by increase bone resorption relative to bone formation. This occurs generally with an increase bone turnover. In ovariectomized rats the increased bone turnover and increased bone porosity was treated with sintered dicalcium pyrophosphate ($Ca_2P_2O_7$) (Sun et al., 2002). The increase in bone mineral content in long bones was higher in rats which

ingested $Ca_2P_2O_7$ than those which ingested alendronate (Sun et al., 2002). The porosity of the trabecular bone was decreased when $Ca_2P_2O_7$ was ingested (Sun et al., 2002).

5.3.4.2. Pyrophosphate glass ceramic

Phosphate based glass ceramics are easily machinable using conventional tools (Kasuga, 2007). It is possible to incorporate a wide range of compositions in glass ceramics which in conjunction with heat treatment makes it easy to control chemical and physical properties of glass ceramics (Kasuga, 2007). Phosphate based glass ceramics are degradable and non-toxic (Ahmed et al., 2004). Osteoblasts and fibroblasts cells were successfully seeded onto phosphate based glass ceramics with no adverse cell reactions (Bitar et al., 2004). Calcium pyrophosphate glass ceramics consisting of β-$Ca_3(PO_4)_2$ and β-$Ca_2P_2O_7$ crystals was made by sintering a powder consisting of 60 mol% CaO, 30 mol% P_2O_5, 7 mol% Na_2O and 3 mol% TiO_2 at 850°C (Kasuga and Abe, 1998). This glass ceramic was found to be bioactive due to the formation of a calcium phosphate phase on the surface of the ceramic when soaked in simulated body fluid (Kasuga et al., 1999). Dias et al. developed two glass ceramics; MK5B consisting of $KCa(PO_3)_3$, β-$Ca(PO_3)_2$, β-$Ca_2P_2O_7$ and $Ca_4P_6O_{19}$ and MT13B consisting of $CaTi_4(PO_4)_6$, TiP_2O_7, α- and β-$Ca_2P_2O_7$ phases (Dias et al., 2006). When implanted into the tibiae of Japanese white rabbits both glass ceramics were found to be osteoconductive and allowed the formation of new bone tissue (Dias et al., 2006). The MK5B ceramic was found to have been almost completely surrounded by bone whereas some spaces where found surrounding the MT13B glass ceramic (Dias et al., 2006).

5.3.4.3. Calcium polyphosphate ceramic

Calcium polyphosphate biomaterials have been synthesised for use in tissue engineering (Nelson et al., 1993) and in cartilaginous tissue repair (Waldman et al., 2002). Lagow et al. used a calcium polyphosphate material to repair mandibular bone defects *in vivo* (Lagow et al., 1991). Pilliar et al. have manufactured a highly porous calcium polyphosphate ceramic through the process of sintering (Pilliar et al., 2001). This was then implanted in New Zealand white rabbits where it was shown to encourage bone growth (Grynpas et al., 2002). Calcium polyphosphate biomaterials can also be manufactured by the solid freeform fabrication process (Porter et al., 2001). This process would then be used to design a 'tailor made' bone replacement. Calcium polyphosphate fibres have been synthesised (Griffith, 1982) with application in the repair of tendon tissue (Sun and Zhao, 2002).

6. MATERIAL CHARACTERISATION

This thesis investigates the possibility of forming $Ca_2P_2O_7$ ceramic which is to be used as a bioresponsive bone replacement material. It is therefore important to thoroughly characterise the ceramic material with regards to the sintering process, porosity and mechanical strength. To further develop the ceramic material for clinical application it is important to study the *in vitro* degradation of the $Ca_2P_2O_7$ ceramic. Other characterisation techniques used in this thesis involved the characterisation of precipitated crystals and colorimetric testing procedures. This chapter briefly outlines the characterisation techniques carried out in this thesis.

6.1. COMPOSITION CHARACTERISATION

6.1.1. X-ray diffraction (XRD)

X-ray diffraction enables the determination of the crystal structure of unknown materials. XRD is also used to measure the spacings between the layers of atoms and the structural properties e.g. preferred orientation, phase composition and grain size of the crystals. X-rays are electromagnetic radiation generated from two metal electrodes enclosed in a vacuum chamber. The electrons are produced by heating a tungsten filament cathode. The highly negative potential cathode produces high accelerating electron which hit the water cooled anode (usually at ground potential) to produce X-rays (loss of energy upon impact). In 1912 Laue found that crystals diffracted X-rays (Figure 6.1) (Bragg, 1975). Bragg's law (equation 6.1) is an alternative way of expressing Laue's equation which fulfils the three conditions which need to occur before the X-rays are diffracted by crystals.

$$n\lambda = 2d\ sin\theta \quad \text{... (6.1)}$$

Where d is the distance between atomic layers in a crystal, θ (theta) is the angle of incidence, λ (lambda) is the wavelength of the incident X-ray beam and n is an integer.

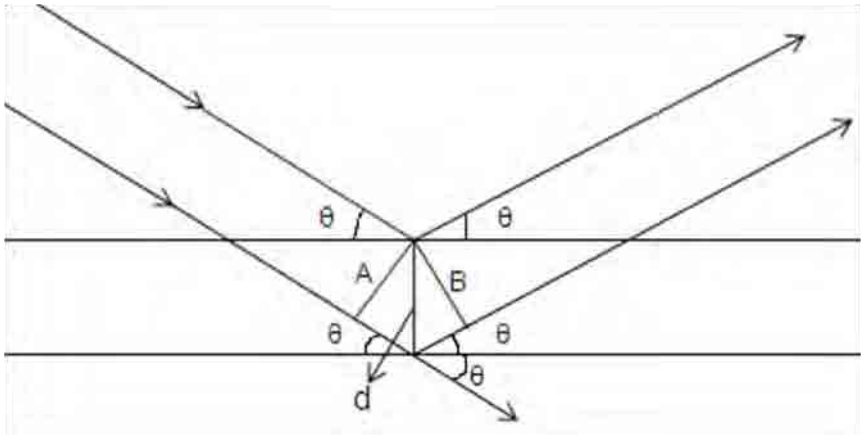

Figure 6.1: Schematic diagram showing the diffraction of X-rays by the crystal lattice.

6.1.2. Rietveld refinement phase analysis

Rietveld refinement phase analysis can be used to determine the composition of a multiphase ceramic. The Rietveld refinement phase analysis compares a calculated pattern to the measured diffraction pattern ensuring it fits as best as possible. The difference between the measured and calculated pattern is minimized by using the least-square method to adjust structural parameters such as unit cell dimensions, atomic coordinates and scale factors, displacement parameters, lattice parameters and parameters associated with the instrument or experiment. The X-ray diffraction peaks are assumed to be Gaussian in shape and the calculated intensity at each point (e.g. 0.2° at 2θ) is a sum of the constituent Gaussian peaks representing that individual reflections. The profile refinement using the least square method is minimised by the function M, where w_i is the weighting factor, c is an overall scale factor, y_i (obs) is the observed profile and y_i (calc) is the calculated profile.

$$M = \sum_i w_i \left\{ y_i(obs) - \frac{1}{c} y_i(calc) \right\}^2 \ldots (6.2)$$

The goodness of fit is measured by x^2 comparing the agreement of the weighted pattern (R_{wp}) to the agreement of the expected pattern (R_{exp}).

$$x^2 = \left\{ \frac{{R_{wp}}^2}{R_{exp}} \right\} \ldots (6.3)$$

$$R_{wp} = \left\{ \frac{\sum_i w_i [y_i(obs) - y_i(calc)]^2}{\sum_i w_i [y_i(obs)]^2} \right\}^{\frac{1}{2}} \ldots (6.4)$$

$$R_{exp} = \left\{ \frac{(N-P)}{\sum_{i=1}^{n} w_i [y_i(obs)]^2} \right\}^{\frac{1}{2}} \ldots (6.5)$$

N is the number of observations and P is the number of parameters.

6.1.3. Fourier transform infrared spectroscopy (FTIR)

FTIR is used to identify unknown chemicals by identifying the chemical bonds present within the material. Infrared radiation is absorbed by the material causing the chemical bonds present to vibrate (Smith, 1996). The functional groups present absorb the infrared radiation at the same wavenumber range irrespective of the rest of the molecule in which it was present (Smith, 1996). Therefore based on the functional group present the structure of the unknown molecule could be identified. It is also possible to derive quantitative information such as the concentration of the molecule from the FTIR spectrum. The relationship between absorbance and concentration is given by Beer's law (equation 6.6).

$$A = \varepsilon l c \ldots 6.6$$

Where: A – Absorbance, ε – Absorptive, l – Pathlength and c – Concentration.

Infrared spectroscopy is the study of the interaction of infrared light with matter (Smith, 1996). The interferometer takes a beam of light, splits it into two and makes one of the light beam travel a different distance than the other. The difference in the distance travelled by the two light beams is referred to as the optical path difference. The Michelson was the first interferometer to be used in FTIR instruments and is still in use in commercially available machines. A Michelson interferometer (Figure 6.2) consists of a source for infrared light, a stationary mirror and a moving mirror. The Beamsplitter which is present between the stationary and moving mirror and it is designed to transmit half of the radiation that falls to the movable mirror and reflect the other half onto the fixed mirror. The lights then recombine at the beamsplitter before leaving to interact with the sample and the detector. The variations in the light intensity as it move from the detector to the source as a function of the optical path difference generates the spectrum which is obtained from the FTIR machine (Smith, 1996; Griffiths and de Haseth, 2007).

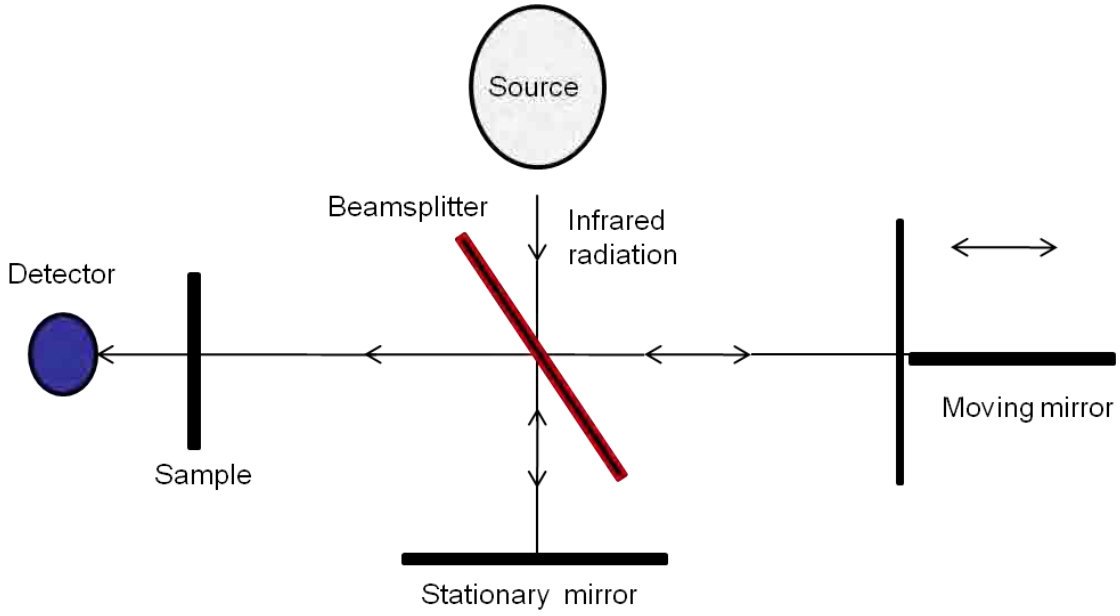

Figure 6.2: An optical diagram of a Michelson interferometer (adapted from Smith, B.C (Smith, 1996)).

6.1.4. Differential scanning calorimetry (DSC)

DSC is a technique for measuring the energy necessary to obtain a near zero temperature difference between a sample and the reference material, when both materials are subjected to identical temperature regimes. The materials are heated and cooled at a constant rate. DSC is used in a wide variety of applications including: characterisation of materials, investigating stability of materials, evaluation of phase diagrams, relative comparison measurements, determining the purity and safety of material. There are two types of DSC's:

Heat-flux DSC

In heat-flux DSC the exchange of heat (temperature difference) between the sample and the reference material is measured via a thermal resistance. Both samples are placed in the same furnace. The heat capacity changes in the sample causes a temperature difference between the reference material and the sample.

Power-compensation DSC

In the power-compensation DSC the temperature of the material and reference material are controlled independently by using identical but separate furnaces. To maintain both materials at the same temperatures the power input into both furnaces was varied. The energy required to maintain similar temperatures is a measure of the capacity changes in the sample relative to the reference material.

6.2. PARTICLE SIZE MEASUREMENT

6.2.1. Scanning electron microscopy (SEM)

The sintering of calcium pyrophosphate ceramic results in the changes to the topography and composition of the material. The surface morphology of calcium pyrophosphate dihydrate crystals could also be changed by the presence of dissolution products therefore it is essential to observe the effect of these processes using a scanning electron microscope. The electron column consists of an electron gun and two or more magnetic lenses as shown in figure 6.3. The electron gun generates electrons which accelerate to energy in the range of 1 – 40 keV. The condensed (projective and objective) lenses reduce the diameter of the electron beam to about 5-100 nm (Sarkar et al., 2001) making it small and focused on the specimen. The electrons then interact with the atoms at or near the surface of the material resulting in the release of signals which are formed as images. Secondary electrons, backscattered electrons, Auger electrons, X-rays and transmitted electrons are some of the signals which can be produced from an SEM and collected if the appropriate detector. The deflection system is used to control the magnification of the image. It operates by generating a raster which is controlled by the scanning coils on both the specimen and the screen (Goldstein et al., 1992). The two pairs of scanning coils are used to control the raster of the beam. The magnification of the sample image is the ratio of the linear size of the cathode ray tube (CRT) to the linear size of the raster on the sample. Therefore the magnification can be increased by exciting the scanning coils less strongly thereby deflecting the beam a smaller distance onto the specimen.

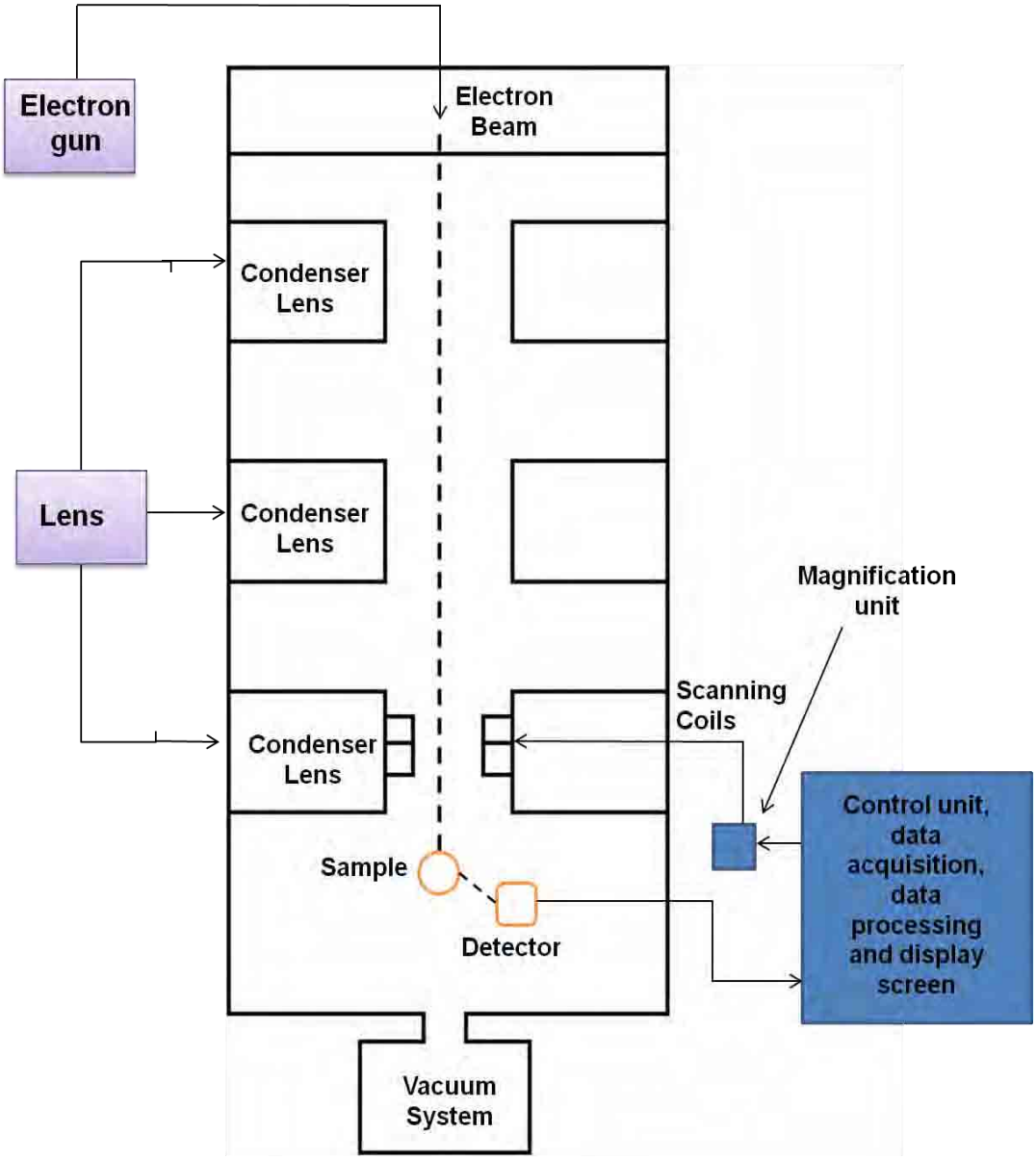

Figure 6.3: A diagrammatic representation for the setting of a scanning electron microscope.

6.3. SPECIFIC SURFACE AREA (SSA) MEASUREMENT

Along with other properties the chemical and physiochemical reactivity of a biomaterial could be controlled by the size and quality of the surface of the solid biomaterial (Skalny and Hearn, 2001). The degree of control can be linked to the SSA which is defined as the surface area per unit mass and expressed in centimetre squared per gram (cm^2/g) or metre squared per kilogram (m^2/kg). The SSA of a biomaterial depends on the shape and size of the particle and also the size and shape of flaws present at the surface of the material (Skalny and Hearn, 2001). Sintering process leads to the presence/absence of flaws and changes to the particle size and shape of the ceramics. Therefore SSA measurement enables the effect of changes in temperature to be monitored on the change in particle size which can also be related to the porosity (pore fraction). The SSA is determined by applying Brunauer-Emmett-Teller (BET) equation to sorption isotherm data. Sorption is the interaction between a gas (adsorbate) which can be nitrogen or octane gas and the solid ceramic surface. The adsorption experiment works on the assumption that gas molecules are strongly attracted to the surface of the ceramic and that the adsorbate is small enough to reach all the pores on the ceramic surface. By increasing the pressure of the gas the amount of gas adsorbed to the ceramic surface can be increased and another layer of gas can be formed onto the initial one.

The BET equation is given below:

$$V = \frac{V_m .c.P}{(P_o - P)\left\{1+(c-1)\frac{P}{P_o}\right\}} \quad \ldots (6.7)$$

Where: V – is the volume of gas adsorbed (cm^3), V_m is the monolayer capacity (cm^3), c is a constant related to the average heat of adsorption of the monolayer, P is the vapour pressure (kPa) and P_o is the saturation vapour pressure (kPa).

6.4. MECHANICAL STRENGTH

Compressive strength

It is important to understand the mechanical behaviour of a newly fabricated biomaterial when placed under stresses that it may experience *in vivo*. The biomaterial which is developed as a bone replacement should be able to withstand such stresses as failure would lead to trauma and implant site morbidity. The mechanical failure of such a material would culminate in the patient undergoing further surgical procedure to retrieve and replace the biomaterial. The material studied in this thesis was produced by sintering; this process introduces microscopic defect into the ceramic. Unlike tensile fracture which occurs as the result of a single severe flaw, compression failure occurs when the accumulation of numerous flaws within the ceramic results in structural collapse. Therefore the sintered ceramic studied in this thesis was subjected to compressive testing. The cylindrical sintered ceramic with an aspect ratio of 2 was loaded perpendicularly along its long axis until the ceramic fails. The compression test consists of two load blocks exerting a compressive force on the cylindrical ceramic material (Figure 6.4). The compressive stress of the sintered ceramic (σ_c) can be calculated in accordance with equation 6.8:

$$\sigma_c = \frac{4F}{\pi d^2} \ldots (6.8)$$

Where F is the load at failure (N) and d is the diameter of the ceramic sample (mm).

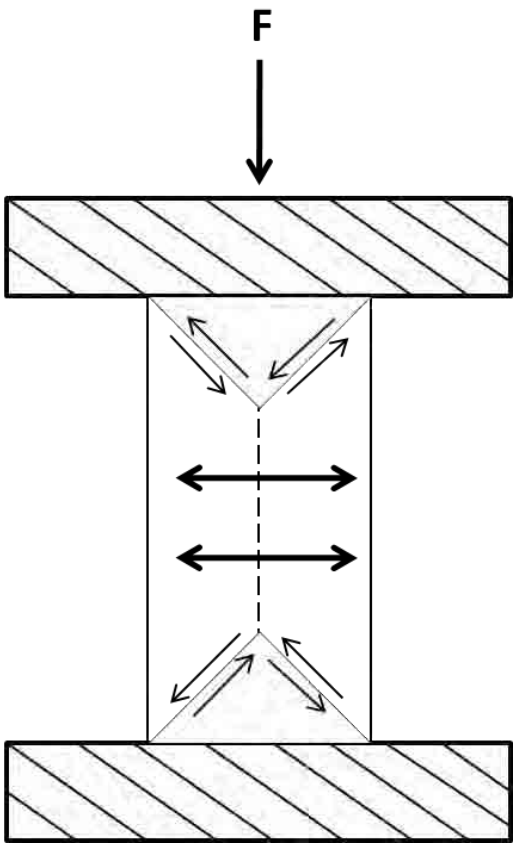

Figure 6.4: The stresses and causes of failure in a cylindrical ceramic loaded along its long axis.

6.5. POROSITY

The porosity of the sintered ceramic was determined by using either a helium pycnometer or an Archimedes balance. Using an Archimedes balance the specific gravity of the sintered ceramic was calculated from the weight of the ceramic measured in air and in water according to equation 6.9.

$$Specific\ gravity = \frac{Weight\ in\ air}{Weight\ in\ air - Weight\ in\ water} \ldots (6.9)$$

The true density of the ceramic was calculated by multiplying the specific gravity by 1000 Kg/m^3 (density of water at 25°C). Relative density was calculated by dividing the apparent density by the true density (equation 6.10a) and the apparent density was calculated by dividing the mass of the ceramic by its volume (equation 6.10b).

$$Relative\ density = \frac{Apparent\ demsity}{True\ density} \ldots (6.10a)$$

$$Apparent\ density = {}^{Mass}/_{Volume} \ldots (6.10b)$$

The porosity of the ceramic was then calculated by subtracting the relative density from 1.

$$\therefore Relative\ porosity = 1 - Relative\ density \ldots (6.11)$$

Helium pycnometry is used to obtain an accurate measurement of the volume of the ceramic which in turn gives the true density of the material. The helium atom is small and able to penetrate very small pores within the ceramic to the limit of 0.1 nm (Asthana et al., 2006; Ayral et al., 1992; Petropoulos et al., 1983). Helium pycnometer measures the total porosity by calculating the volume of the sample from the changes in pressure between the two chambers in the machine when the porous sample is introduced into one of the chambers (Figure 6.5). The chamber with

volume V_I is filled with helium at a pressure P_1, the gas is then allowed to flow into the second chamber (when there is no sample present) (Figure 6.5).

The pressure in the whole system is P_1^* and the cell volume is given by V_C (equation 6.12).

$$V_C = V_I\left(\frac{P_1}{P_1^*} - 1\right) \ldots 6.12$$

When the sample is present in the chamber the volume of the sample (V_S) is given by equation 6.13:

$$V_S = V_I\left(1 - \frac{P_2}{P_2^*}\right) + V_C \ldots 6.13$$

Where P_2 and P_2^* is the pressure in the chamber and the whole system when the sample is present.

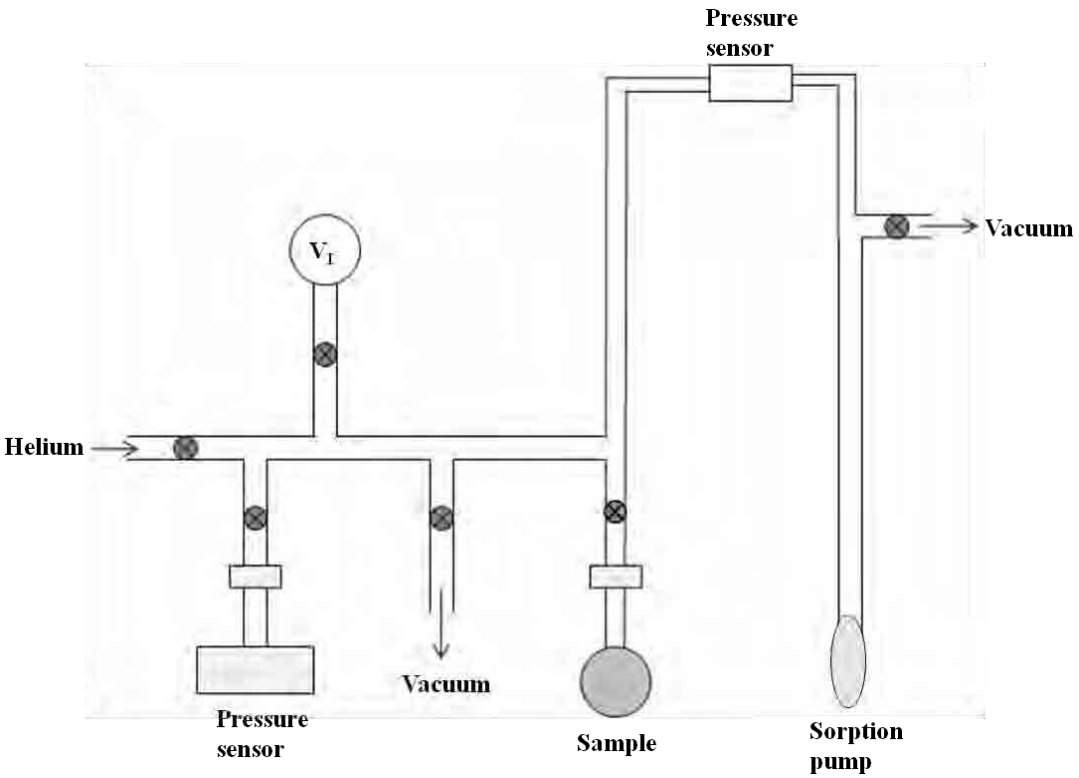

Figure 6.5: Schematic diagram of apparatus which allows helium density measurements (redrawn from (Ayral et al., 1992)).

7. ALP MEDIATED DEGRADATION OF CALCIUM PYROPHOSPHATE DIHYDRATE CRYSTALS

Alkaline phosphatase (ALP) is an enzyme associated with bone mineralisation (Hessle et al., 2002; Johnson et al., 2000). It acts by removing the $P_2O_7^{4-}$ ion, an inhibitor to bone mineralisation (Anderson et al., 2004). ALP hydrolyses $P_2O_7^{4-}$ ion to produce the PO_4^{3-} ion which is then added to the pool of PO_4^{3-} ion resulting in localised supersaturation with respect to apatite and therefore precipitation of bone mineral. The ability of ALP to break down $P_2O_7^{4-}$ ion has been exploited by Xu et al. (Xu et al., 1991b) in removing CPPD crystals which are deposited in the joints of patients suffering from calcium pyrophosphate deposition disease (Mccarty et al., 1962; Pritzker, 1980; Song et al., 2002). Xu et al. found that CPPD degraded faster in the presence of yeast inorganic pyrophosphatase and ALP (Xu et al., 1991a; Xu et al., 1991b). This chapter describes the precipitation of phase pure CPPD and brushite crystals as well as investigating the mechanism by which crystal dissolution occurs in the presence of ALP, this has previously been reported to be enzyme attachment mediated (Shinozaki et al., 1995). The dissolution of CPPD and brushite crystals in control Tris HCl solution was also investigated as well as the changes to the surface morphology of both crystals once exposed to the ALP and control solutions. The effect of saturation on the rate of crystal dissolution and the adhesion of ALP onto the crystal surface was also investigated.

7.1. MATERIALS AND METHODS

7.1.1. Precipitation of CPPD, brushite and OCP crystals

7.1.1.1. CPPD

CPPD crystals were precipitated according to the method of Shinozaki et al. (Shinozaki et al., 1995) from a mixture of 500 mL calcium chloride ($CaCl_2$) and 1300 mL sodium pyrophosphate ($Na_4P_2O_7$) solution at 37°C and pH 5.5 for 21 days. The 40 mM $Na_4P_2O_7$ solution (Sigma Aldrich, Dorset, UK) and 3.6 mM $CaCl_2$ solution (Sigma Aldrich, Dorset, UK) at pH of 5.5 were mixed and the pH of the resulting solution was adjusted to pH 5.5 using either hydrochloric acid (HCl) (Fluka, Dorset, UK) or sodium hydroxide (NaOH) (Fluka, Dorset, UK). The solution, which was in a 2 L beaker, was placed in the 37°C incubator and its pH was adjusted daily using HCl and/or NaOH. After 21 days the crystals were filtered using a Buchner funnel. The crystals were then washed using double distilled water to remove excess NaCl and NaOH before drying overnight at room temperature.

7.1.1.2. Brushite

Brushite crystals were precipitated by the method outlined below. Calcium chloride dihydrate solution ($CaCl_2.2H_2O$) (Sigma Aldrich, Dorset, UK) 0.50 M and 500 mL was poured into a burette; 500 mL solutions of 0.50 M sodium acid phosphate (Na_2HPO_4) (Sigma Aldrich, Dorset, UK) and 0.04 M potassium dihydrogen phosphate (KH_2PO_4) (Sigma Aldrich, Dorset, UK) was poured into another burette. The 0.15 M 250 mL solution of KH_2PO_4 which was placed in the 2.5 L beaker was continuously stirred using a magnetic stirrer. The solutions from both burettes were allowed to flow into the beaker in a drop wise manner over the period of 2.5 – 3 h at 25˚C (room temperature). The solution was continuously stirred and the pH was

maintained between 4 and 5 by adjusting the flow of either of the reactants from the burettes.

7.1.1.3. OCP

OCP crystals were precipitated at a temperature of 60°C in a 250 mL jacketed vessel. 20 mM 100 mL Na_2HPO_4 was placed into the jacketed vessel and allowed to attain the set temperature. The pH was also adjusted to 5 using HCl. To this solution 20 mM 100 mL calcium acetate $Ca(CH_3COO)_2$ (Sigma Aldrich, Dorset, UK) was added in a drop wise manner from the burette. The solution in the jacketed vessel was constantly stirred throughout the experiment. After 3 – 4 h the solution was filtered and the crystals were washed with distilled water before drying at room temperature.

7.1.2. Characterisation of brushite and CPPD crystals using XRD, FTIR and SEM

The chemical composition of all the precipitated crystals were determined using an X-ray diffractometer (D5000 Brucker, Siemens, Germany) with CuKα1 radiation (λ = 1.5406 Å). The precipitated crystals were scanned over a 2θ range of 3 - 50° at 25°C using a step size of 0.020° and a step time of 0.3 s. Further chemical analysis was conducted by using FTIR (NICOLET 380, Thermo Scientific). The absorption mode scanning was from 400 to 4000 cm^{-1}. The shape of the precipitated brushite and CPPD crystals were observed under the light microscope (OLYMPUS BX50, Japan).The surface morphology of the crystals which were precipitated and used in the experiments was observed using the SEM (Philips XL 30).

7.1.3. Measuring dissolution in the presence and absence of ALP

The interaction between CPPD crystals and ALP enzyme (calf intestinal mucosa; Fluka, Dorset) was investigated by incubating 10 mg of the crystals with 10 U ALP in 5 mL Tris HCL solution. The Tris HCl solution used in these experiments had a concentration of 100 mM and pH 7.4, it contained 1 mM $MgCl_2$ and 0.01% sodium azide (NaN_3, Sigma Aldrich, Dorset). The solutions were placed on a rack and into a 37°C rotating incubator (Mk X Incubator Shaker, LH Engineering, UK) at 150 rpm. The amount of PO_4^{3-} ion released into solution was determined by modifying the method of Chen et al. and Xu et al. (Xu et al., 1991b; Chen et al., 1956). For the first hour at intervals of 15 min and 30 min subsequently, the mixture was removed from the incubator and centrifuged separating the crystals from the medium before 300 µL aliquot was removed. To the aliquot, 3.7 mL of distilled water was added to make the solution up to 4 mL. 1600 µL of distilled water, 800 µL 3 M sulphuric acid (H_2SO_4) (Fisher Scientific, Loughborough UK), 800 µL of ammonium molybdate ($(NH_4)_6Mo_7O_{24}.4H_2O$) (Riedel – de Haen, Germany) and 800 µL ascorbic acid ($C_6H_8O_6$, Sigma Aldrich, Dorset UK) was added and the resulting solution was thoroughly mixed before placing into a 37°C incubator for 1.5 h. The mixture was allowed to cool to room temperature and the absorbance was measured at 620 nm in Uvikon 922 spectrophotometer (Kontron Instruments). A control experiment was carried out by following the same procedure as above without the ALP enzyme. The interaction of brushite crystals with ALP was also investigated. A standard calibration curve was plotted using a phosphate standard (KH_2PO_4) with known orthophosphate ion concentration (Figure 7.1). Using this calibration curve unknown orthophosphate ion concentrations were determined.

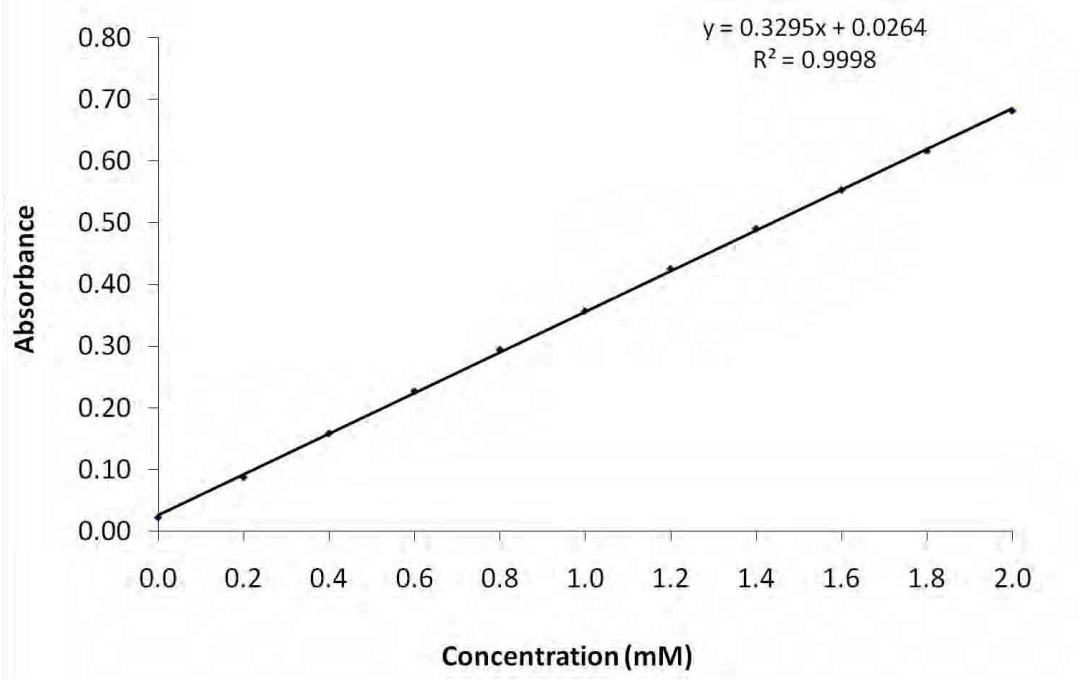

Figure 7.1: Calibration curve for orthophosphate ion determination.

7.1.3.1. Effect of saturation on the dissolution of CPPD crystals

As CPPD crystals dissolve in solution the ageing medium becomes saturated with respect to either PO_4^{3-} or $P_2O_7^{4-}$ ion. This could reduce the amount of crystals which are then dissolved in solution. To overcome this problem the same experiment described in section 7.1.3 was carried out but 4 mL aliquot was removed instead of 300 µL. The 4 mL aliquot removed was replaced with fresh ageing media of the same volume.

7.1.4. Protein attachment on CPPD crystals

7.1.4.1. Crystals surface staining

The method Shinozaki et al. (Shinozaki et al., 1995) used to determine enzyme attachment was employed in this research to understand the adhesion behaviour of ALP to CPPD and brushite crystals surface. 2.5 mg of CPPD crystals were placed into a 2 mL eppendorf with 75 U of ALP before adding 750 µL of the Tris HCl

buffer (without sodium azide). The solution was then placed in a shaker at 1000 rpm for 60 min at room temperature after which the crystals were washed several times with 750 µL of the Tris HCl solution. The crystals were then placed in another eppendorf and the staining solution of 0.025% naphthol AS-MX phosphate (Sigma Aldrich, Dorset) at pH 7.4 containing 1 mg/ml of fast red TR salt (5-chloro-2-toluenediazonium chloride hemi [zinc chloride]) (Sigma Aldrich, Dorset) was added. The mixture stood at room temperature for 1 h before the crystals were washed with double distilled water to remove non-specific products. To determine enzyme attachment the washed crystals were then observed using the light microscope (OLYMPUS BX50, Japan). The control experiment was carried out by following a similar procedure as above in the absence of ALP. The attachment of ALP to the surface of the crystal is expected to decrease if the experiment is carried out at higher temperatures (this was not measured here).

7.1.4.2. Bichinchoninic Assay (BCA)

To quantify ALP attachment to CPPD crystal surface in solution, the BCA protein assay procedure was used. 10 mg of CPPD crystals were incubated with 10 U of ALP (calf intestinal mucosa, Fluka) in 1.5 mL Tris HCl solution (without sodium azide). The mixture was placed in an eppendorf that was shaken at room temperature on a shaker operating at 1250 rpm. At intervals of 30 s for the first 5 min and every five minutes afterwards 100 µL of aliquot was taken from the mixture; to this 2 mL of the BCA working reagent was added. The mixture was gently shaken before it was placed in the 37ºC incubator for 30 min. The absorbance of the solution was measured using the Uvikon 922 spectrophotometer at 562 nm. The interaction of brushite crystals with ALP was studied using the same procedure as above. To

determine the concentration of enzyme (from which the amount on the crystal can be determined) in solution a calibration curve was drawn based on known concentration of bovine serum albumin (BSA) as shown in figure 7.2.

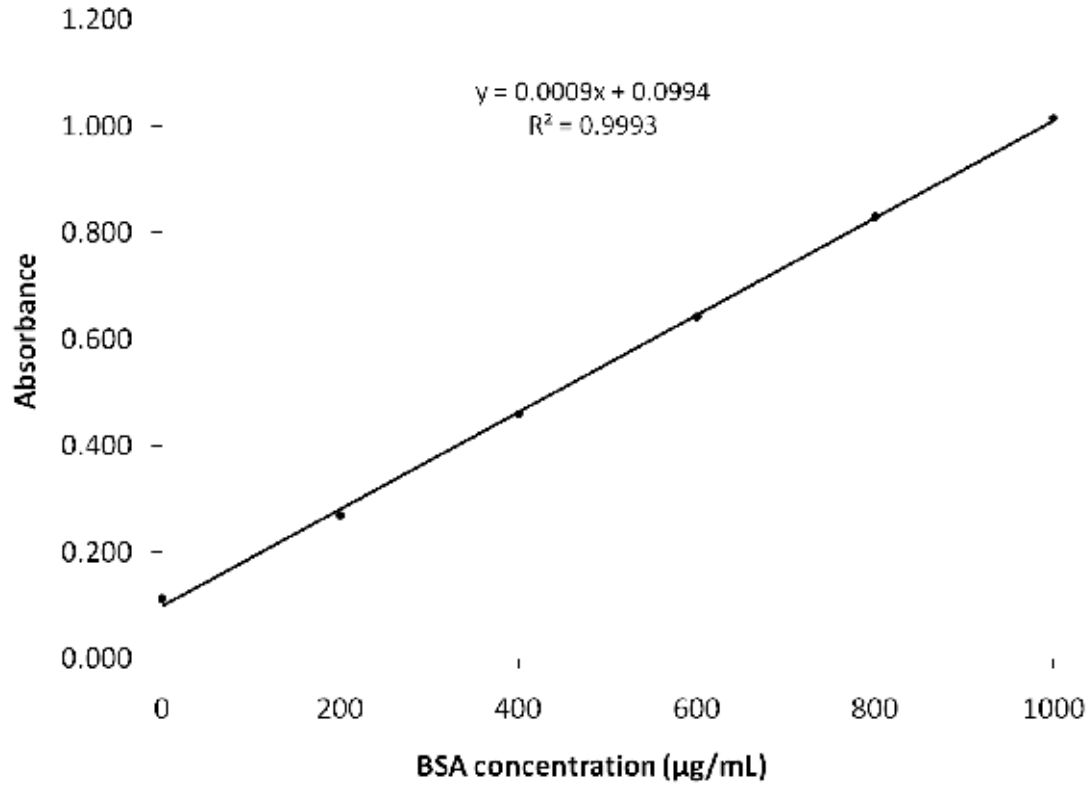

Figure 7.2: Calibration curve of BCA using known concentrations of bovine serum albumin (BSA) at ambient conditions. The calibration curve was obtained from three separate calibration experiments.

7.1.5. Dissolution of CPPD crystals in visking tubing

To fully understand the mechanism of CPPD crystal dissolution in ALP solution, the crystals were placed in a SnakeSkin® pleated dialysis tubing (visking tube) (Thermo Scientific, Rockford, USA) with a molecular weight cut of (MWCO) of 3500. This was used to separate the ALP enzyme in solution from the crystals. The enzyme is not expected to pass through the visking tube as it has a very high molecular weight of 160 kDa. 10 mg of CPPD crystals were placed in the visking tube this was then placed in a Tris HCl solution containing ALP; the control experiment had no ALP

present. Every 30 min aliquots were removed from the solution to test for the presence of PO_4^{3-} ion using a CECIL CE7500 spectrophotometer as described in section 7.1.3.

7.1.6. Protein interaction with pyrophosphate ion

ALP activity in solution was measured by studying the rate of $P_2O_7^{4-}$ ion breakdown in ALP containing solution using the method of Xu et al. and Woltgens et al. (Woltgens and Ahsmann, 1970; Xu et al., 1991b). $Na_4P_2O_7$ was dissolved in 100 mM Tris HCl solution. This solution was then diluted using the Tris HCl buffer into concentrations of 0.04, 0.05, 0.06, 0.07 and 0.08 mM. To carry out the experiment ten samples at the same concentration each 1 mL in volume was used. To each volume placed in a 5 mL Bijou bottle 1 mL 2 U ALP (Bovine intestinal mucosa, Sigma Aldrich, Dorset) was added and then mixed for 10 seconds using a test tube shaker. The first of the ten samples stood at room temperature for 1 min, the second sample for 2 min and so on until the tenth sample stood at room temperature for 10 min. After the experimental time has elapsed the reaction was stopped by adding 2 mL of solution A (10% TCA and 5 mM $CuSO_4$) and 3 mL of solution B (5% $FeSO_4$, 1% $(NH_4)_6Mo_7O_{24}.5H_2O$ and 0.5 M H_2SO_4). The colour of the solution was allowed to develop for 5 min at room temperature before measuring the absorbance at 690 nm in Uvikon 922 spectrophotometer. Using a calibration curve it was therefore possible to plot a graph of PO_4^{3-} concentration against time for each of the $P_2O_7^{4-}$ ion solutions. From these graphs the initial rates were determined from the gradient of the curve and documented in table 7.1.

7.2. RESULTS

7.2.1. Characterisation of CPPD crystals

Crystals were precipitated from the reaction mixture and over 21 days of ageing exhibited a blade-like morphology typical of CPPD (Figure 7.3a).

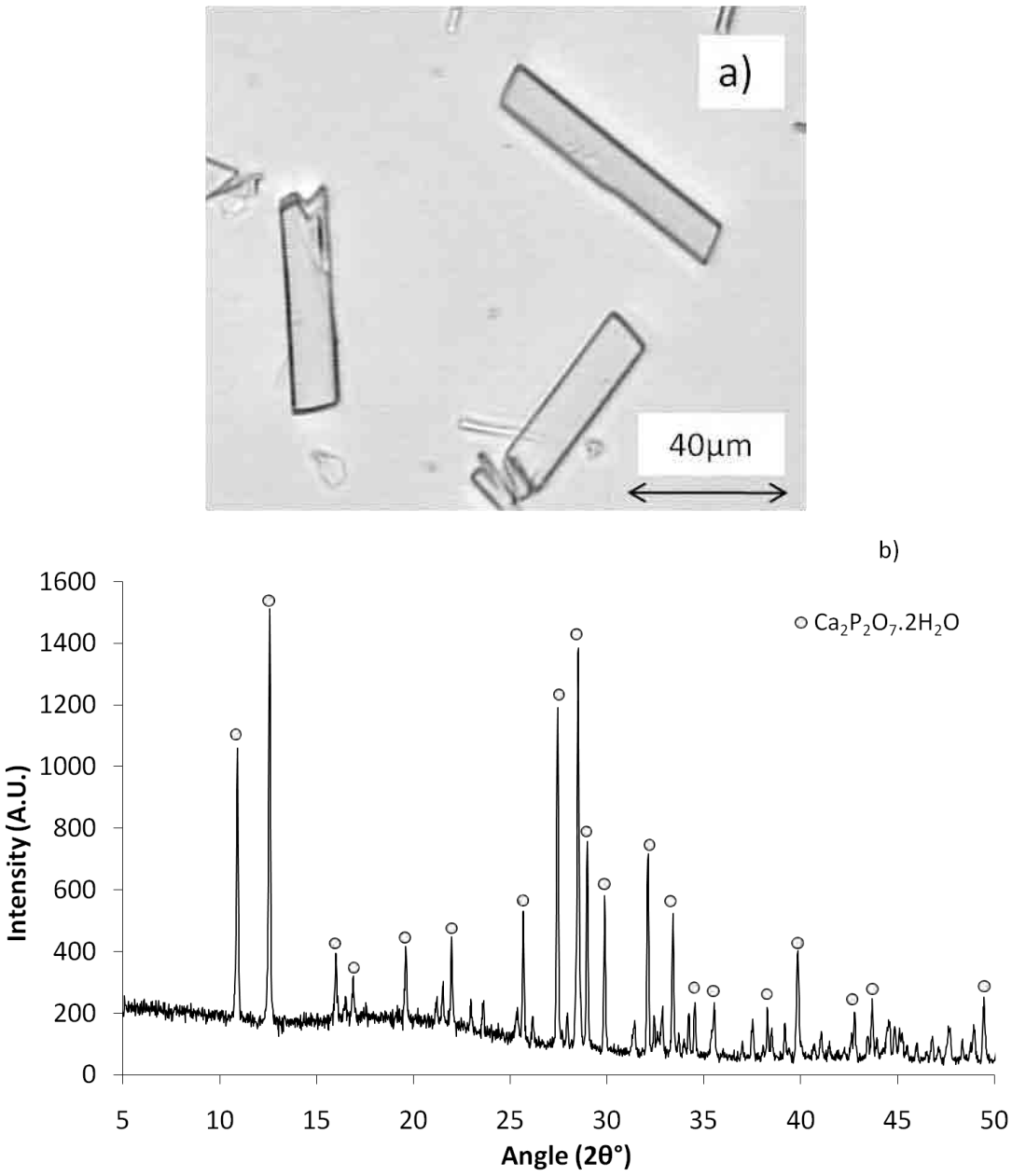

Figure 7.3: a) Image of the precipitated triclinic CPPD crystals taken with the light microscopy and b) XRD pattern for calcium pyrophosphate dihydrate crystals precipitated at 37°C and pH 5.5 for 21 days.

The crystals precipitated at pH 5.5 and a temperature of 37°C were shown to be CPPD and were phase pure (Figure 7.3b). The peaks identified on figure 7.3b are indicative of triclinic CPPD as opposed to the monoclinic isoform. The precipitated CPPD crystals were shown to vary in length from 10 - 40 μm and width from 2 - 4 μm (Figure 7.3a and 7.4a).

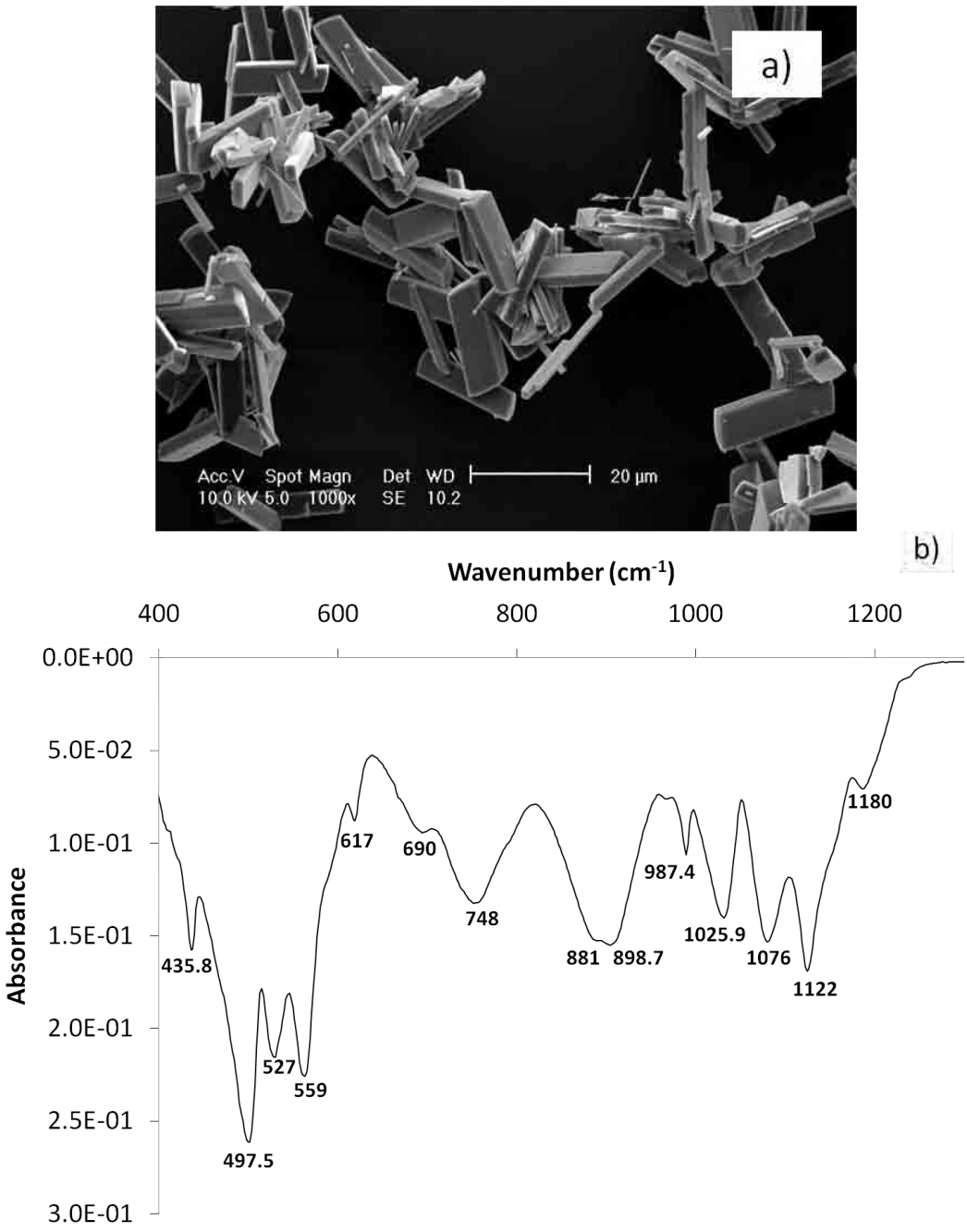

Figure 7.4: a) SEM micrograph of CPPD crystals precipitated at pH 5.5 and temperature 37°C and b) the FTIR spectrum of the precipitated CPPD crystals.

An FTIR spectrum of CPPD on figure 7.4b shows peaks associated with phosphoanhydride (P-O-P) bonds at 748, 987 and 1122 cm^{-1}. The peak at 1076 cm^{-1} indicates the presence of hydroxyl bond (P-OH) which is associated with water of crystallisation and is present in CPPD. The presence of the phosphate and oxygen bond (P-O) is identified at 527, 1025.8, 1180 cm^{-1} (Figure 7.4b). The uniform shape and size of the precipitated triclinic CPPD crystals can be clearly observed on the SEM micrograph in figure 7.4a.

7.2.2. Characterisation of brushite crystals

Crystals of plate like morphology, similar to that reported for brushite were precipitated from a solution of KH_2PO_4, Na_2HPO_4 and $CaCl_2$ at room temperature as shown in figure 7.5a. The crystalline composition of the precipitate was confirmed using XRD, the peaks which are clearly marked is indicative of the monoclinic brushite crystal (Figure 7.5b).

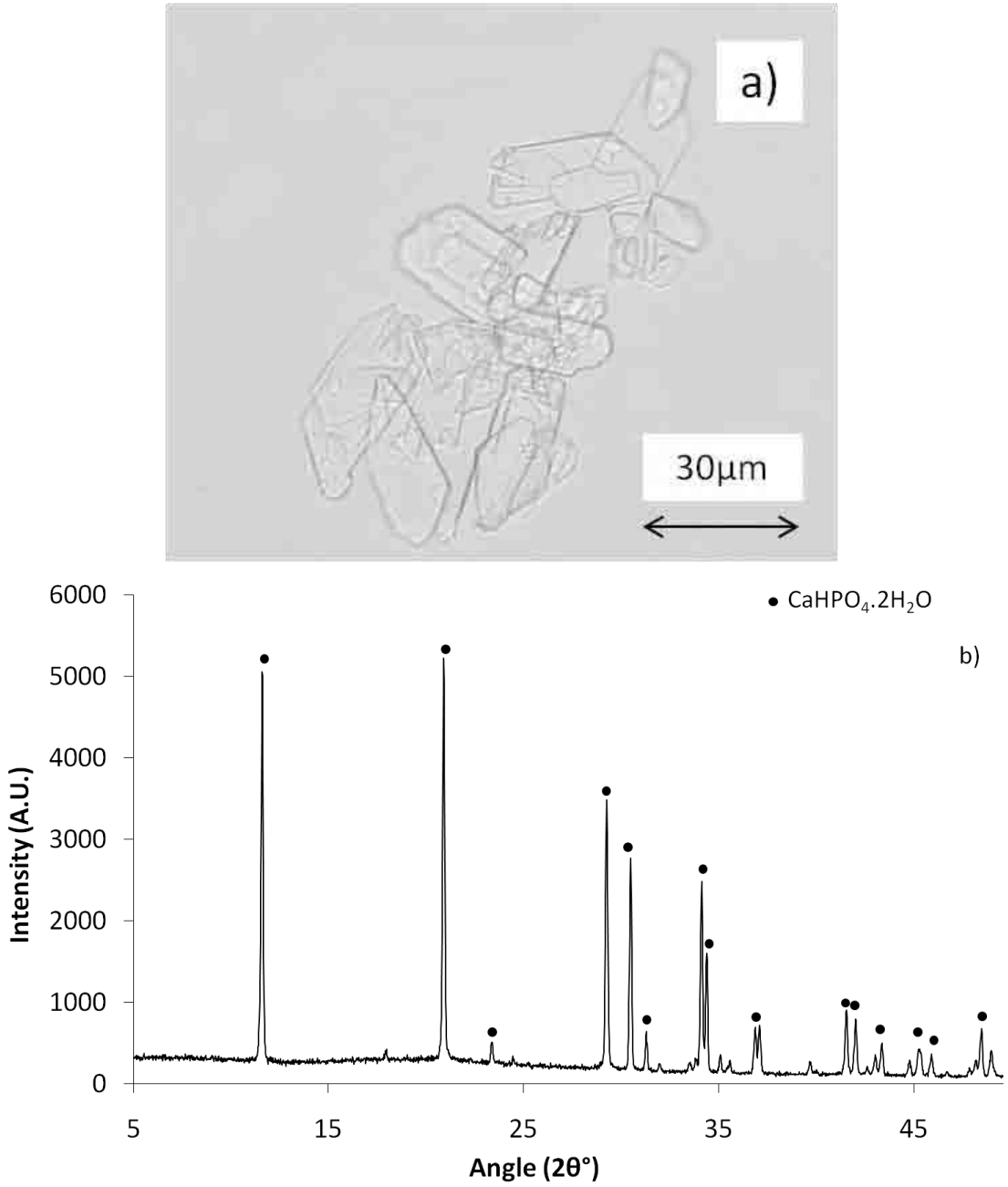

Figure 7.5: a) Image of the precipitated brushite crystals taken with the light microscopy and b) XRD pattern for brushite crystals precipitated at room temperature and pH between 4 and 5.

The SEM micrograph shows that the precipitated monoclinic brushite crystals were plate like in shape (Figure 7.6a). Acid phosphate bonds (HPO_4^{2-}) present in brushite crystals were clearly identified in figure 7.6b at 517, 575 and 866 cm^{-1}. The FTIR spectrum also shows the peaks which indicate the presence of phosphate bonds (P-O) at 771, 982 and 1050 cm^{-1} and of water molecule at 1641 cm^{-1}.

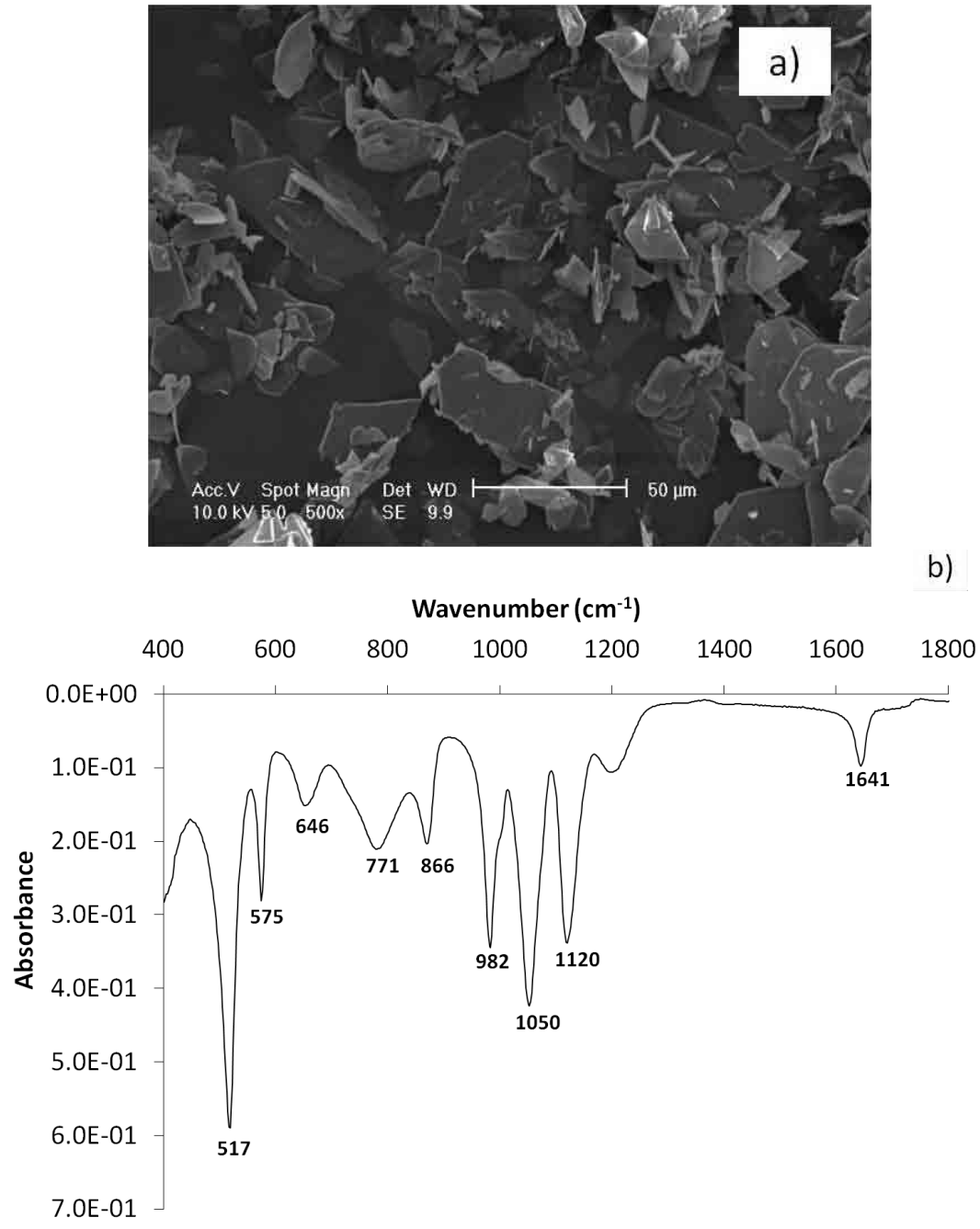

Figure 7.6: a) SEM micrograph of precipitated brushite crystals at pH 4-5 and room temperature and b) FTIR spectrum for the precipitated brushite crystals.

7.2.3. Characterisation of OCP crystals

Crystals of needle like morphology were precipitated from a reaction mixture of calcium acetate and sodium phosphate (Figure 7.7). The crystals were precipitated at pH 5 and temperature of 60°C.

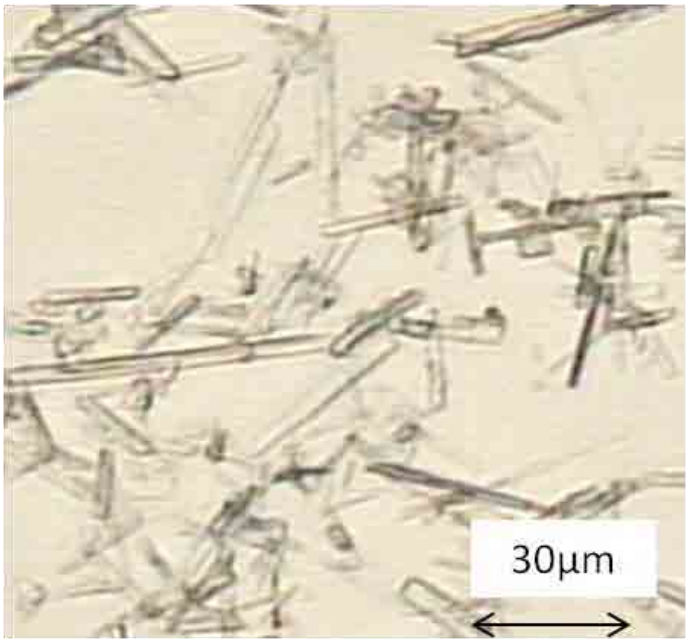

Figure 7.7: Light microscopy image of needle like precipitated OCP at 60°C.

The characteristic primary (100) peak of OCP at 2θ° = 4.7 was clearly identified on XRD patterns collected from the sample (Figure 7.8a). The precipitated triclinic OCP was phase pure and all the peaks which identify it are clearly identified on figure 7.8a. The peaks identified on the FTIR spectrum in figure 7.8b are indicative of that reported for OCP (Suzuki et al., 2006). Although it has been shown that it is possible to precipitate phase pure OCP crystals, there was no corresponding experiment carried out using the crystals in this thesis. Since brushite and CPPD crystals have similar Ca/P brushite crystals were used as the negative control in the dissolution experiments rather than OCP.

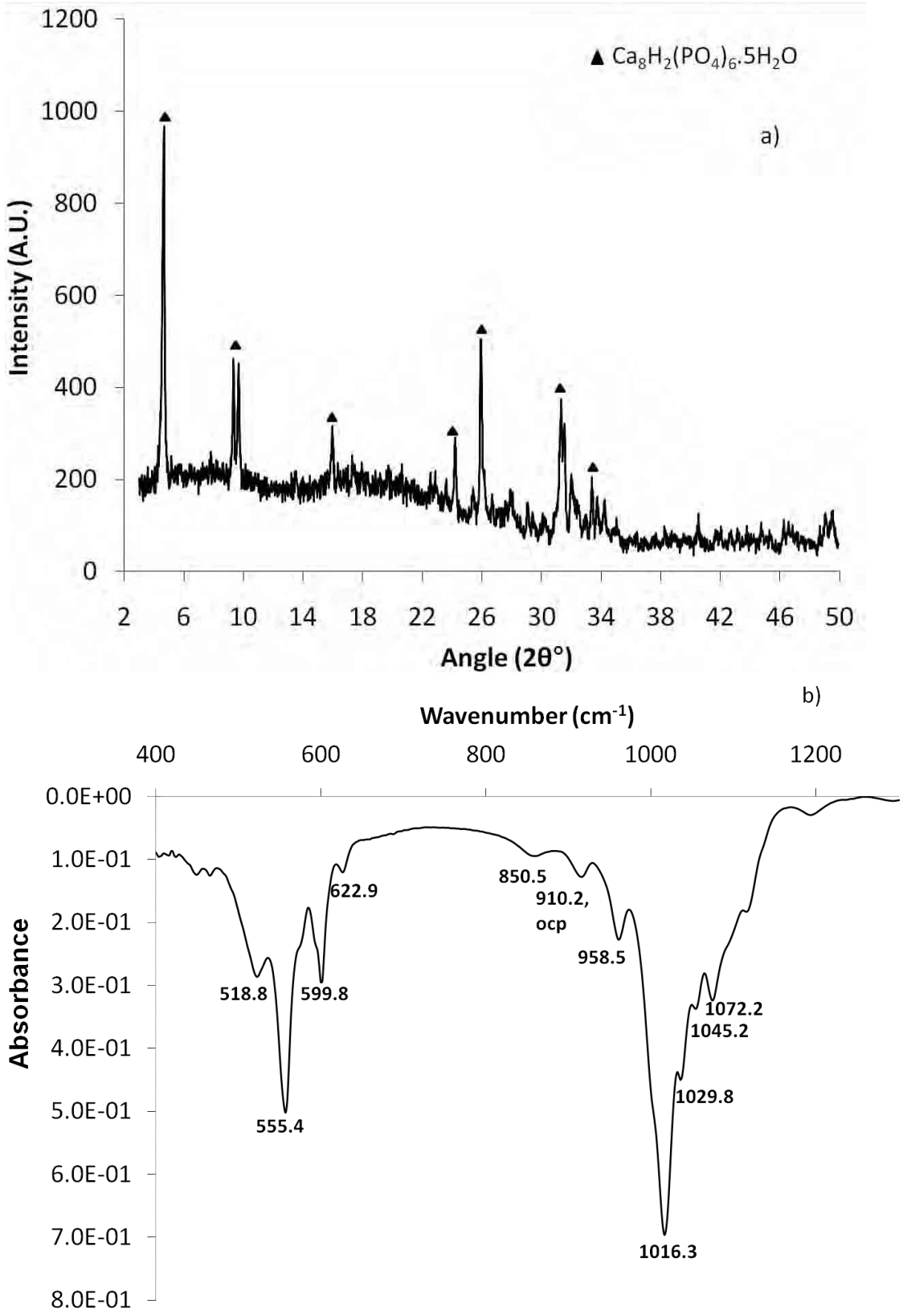

Figure 7.8: a) XRD pattern of precipitated triclinic OCP crystals and b) FTIR spectrum of OCP crystals precipitated at 60°C.

7.2.4. Dissolution of CPPD crystals

The rate of CPPD crystal dissolution in the ageing medium was determined by measuring the concentration of PO_4^{3-} ion in solution with time. Figure 7.9a shows that the concentration of PO_4^{3-} ion detected in the ALP solution was greater than that in the control. After ageing CPPD crystals in ALP containing solution for 6 h the concentration of PO_4^{3-} ion was four times greater than that in the control Tris HCl solution (Figure 7.9a). There was a gradual increase in PO_4^{3-} ion concentration from 15 min to 1 h, a slight reduction between 1 – 4 h and then an increase until the end of the experiment (Figure 7.9a). Once the aliquot was taken it was replaced with a fresh ageing solution of the same volume and this change was accounted for when calculating the concentration of PO_4^{3-} ion released into solution. Using the molecular mass of CPPD crystals the concentration of PO_4^{3-} ion detected at each time point was converted to the mass of CPPD crystals dissolved as shown in figure 7.9b. The shape of the graph on figure 7.9b is the same as that in figure 7.9a in that there was a gradual increase in the mass of CPPD crystals which dissolved from 15 min to 1 h before a period where there was little increase in the mass of crystals dissolving. After ageing for 6 h 6.9 wt% of CPPD was found to have dissolved in the presence of ALP, four times that which dissolved in the control solution (1.7 wt%) (Figure 7.9b). The error bars on figure 7.9 were obtained by calculating the standard deviation of three PO_4^{3-} ion concentration at each time point and three mass loss data at each time point.

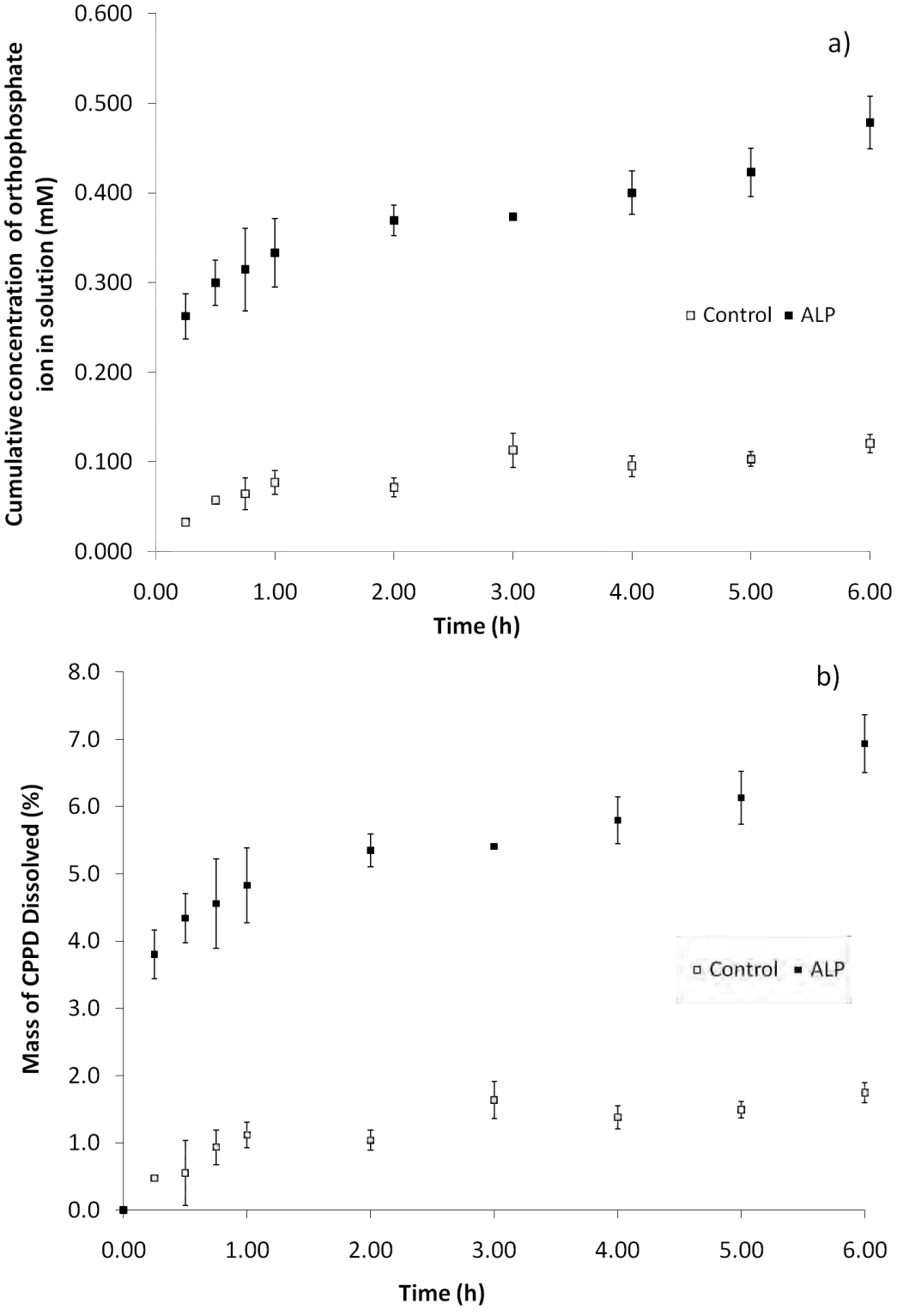

Figure 7.9: a) Cumulative concentration of orthophosphate ions detected in solution from the dissolution of CPPD crystals at 37°C and pH 7.4 and b) percentage mass of CPPD crystals dissolved in ALP and control solution over 6 h at pH 7.4 and temperature 37°C.

7.2.5. Dissolution of brushite crystals

The dissolution of brushite crystals in the presence and absence of ALP was carried out at pH 7.4 and 37°C. Figure 7.10 shows that ALP had no effect on the rate or amount of brushite dissolved in solution. The concentration of PO_4^{3-} ion detected when brushite was aged in ALP solution was six times that detected when CPPD crystals of the same weight were aged in similar solution. This is due to the higher solubility of brushite crystals as compared to triclinic CPPD crystals. Over the 6 h experimental period there was little increase in the total concentration of PO_4^{3-} ion detected in solution (Figure 7.10a). This could be due to the saturation of the solution with respect to PO_4^{3-} ion which causes the reprecipitation of apatite in the sample. 22.0 wt% of brushite crystals were dissolved in both the ALP and control solutions (Figure 7.10b).

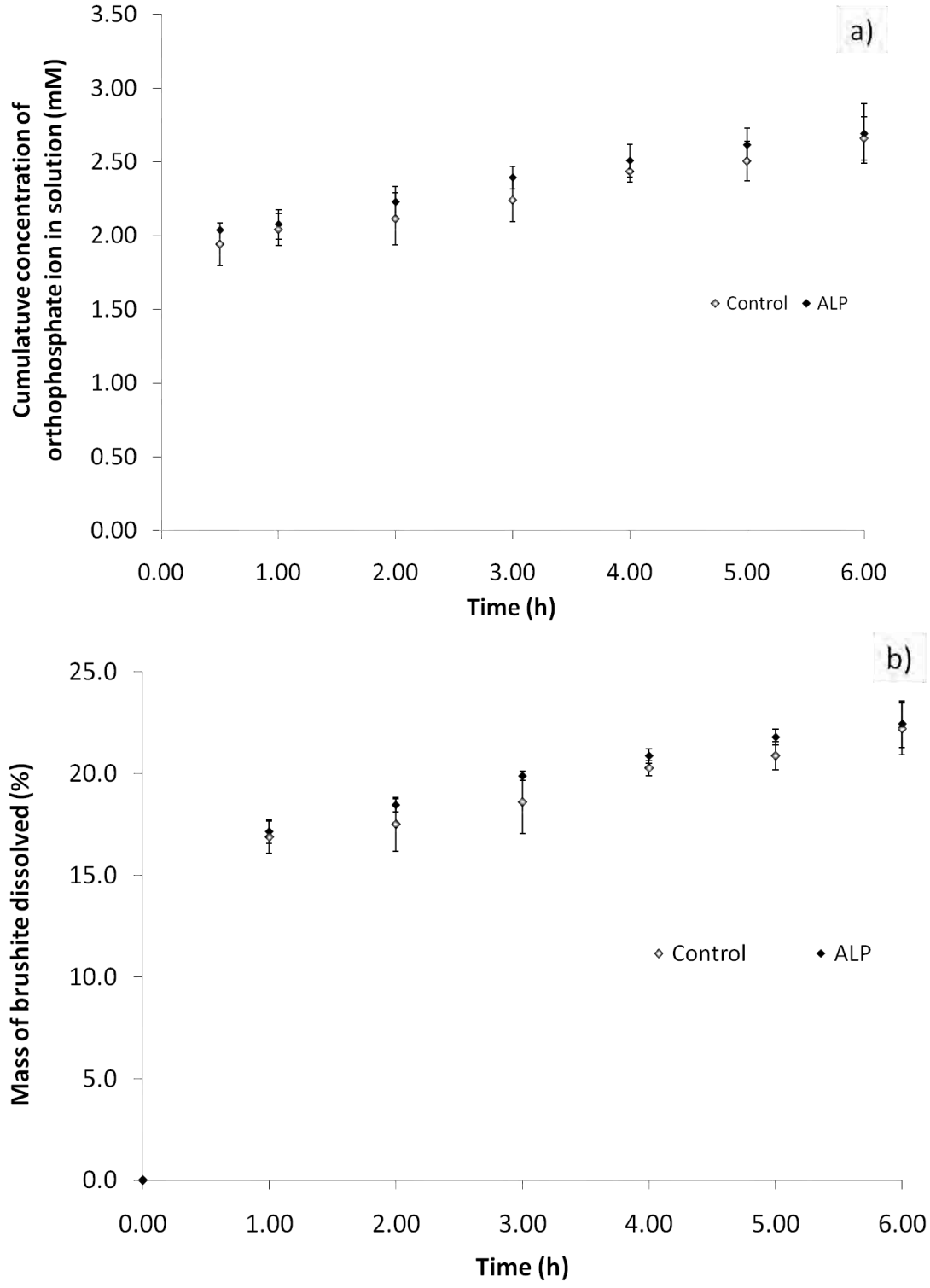

Figure 7.10: Cumulative concentration of orthophosphate ion detected in solution from the dissolution of brushite crystals and b) percentage mass of brushite crystals dissolved in ALP and control solution over 6 h at pH 7.4 and temperature 37°C.

7.2.6. Effect of ageing on the chemical composition and surface morphology of CPPD and brushite crystals

Figure 7.9 shows that there was very little increase in PO_4^{3-} concentration after the initial burst of PO_4^{3-} ion in solution. SEM was used to observe what was happening on the crystal surface during ageing. Figure 7.11a shows the surface morphology of typical triclinic CPPD crystals after precipitation. After the crystals were exposed to an ageing medium the surface morphology was found to change as shown in figures 7.11b and 7.11c. Figure 7.11c shows signs of CPPD crystals dissolution as well as the presence of reprecipitated crystals on the surface which could have been apatite. These were not identified on the XRD pattern (Figure 7.12) and this could be attributed to the small size of the reprecipitated crystal and the low sensitivity of XRD which can detect masses of a minimum of 2 mg. The micrograph of the crystals aged in Tris HCl (control) solution (Figure 7.11b) also show the presence of reprecipitated crystals although it was of a smaller quantity to that observed on figure 7.11c. There was no sign of cleaving on crystal surface when aged in either the control or ALP solution as has previously reported (Figure 7.11) (Shinozaki et al., 1995). After the dissolution experiment the remaining crystals were dried and the chemical composition determined using XRD (Figure 7.12).

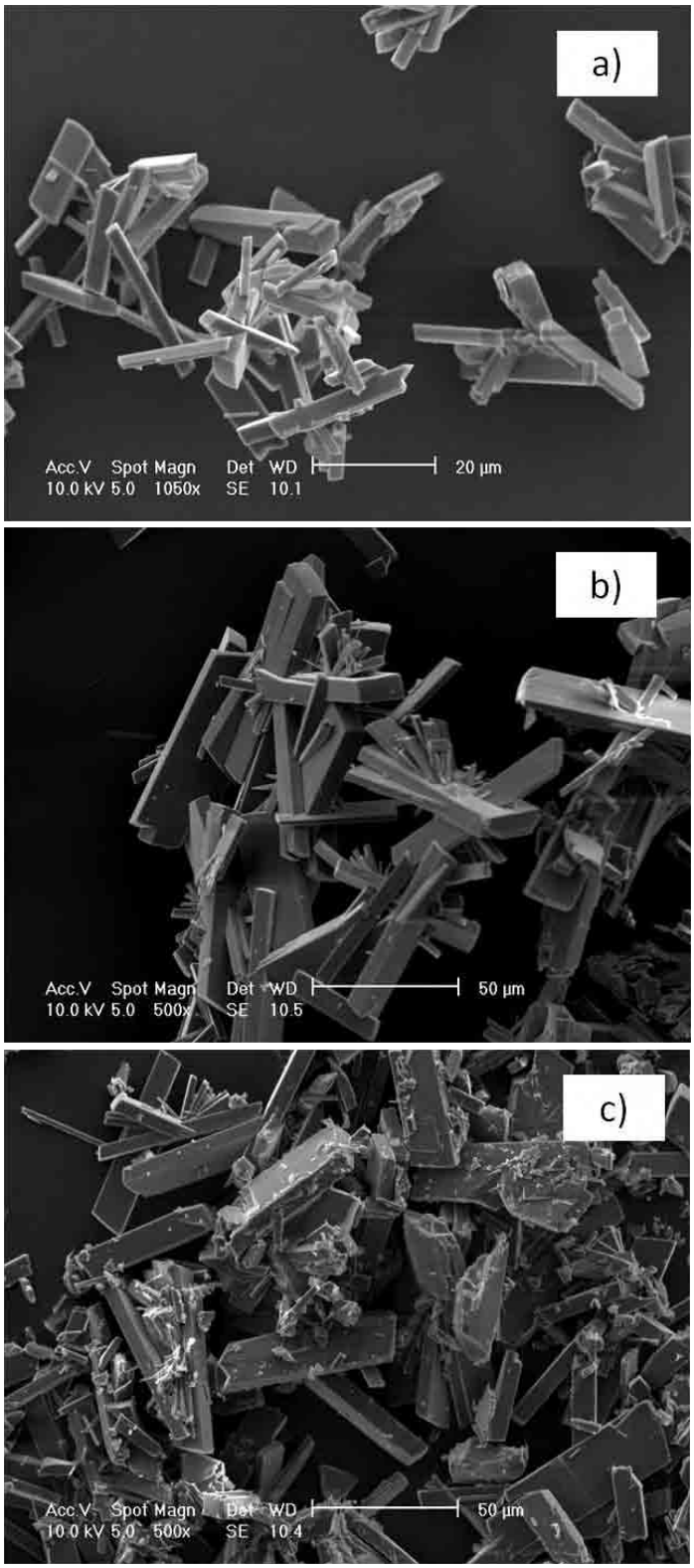

Figure 7.11: Surface morphology of a) precipitated CPPD crystals, b) CPPD crystals aged in Tris HCl solution and c) CPPD crystals aged in ALP containing Tris HCl solution.

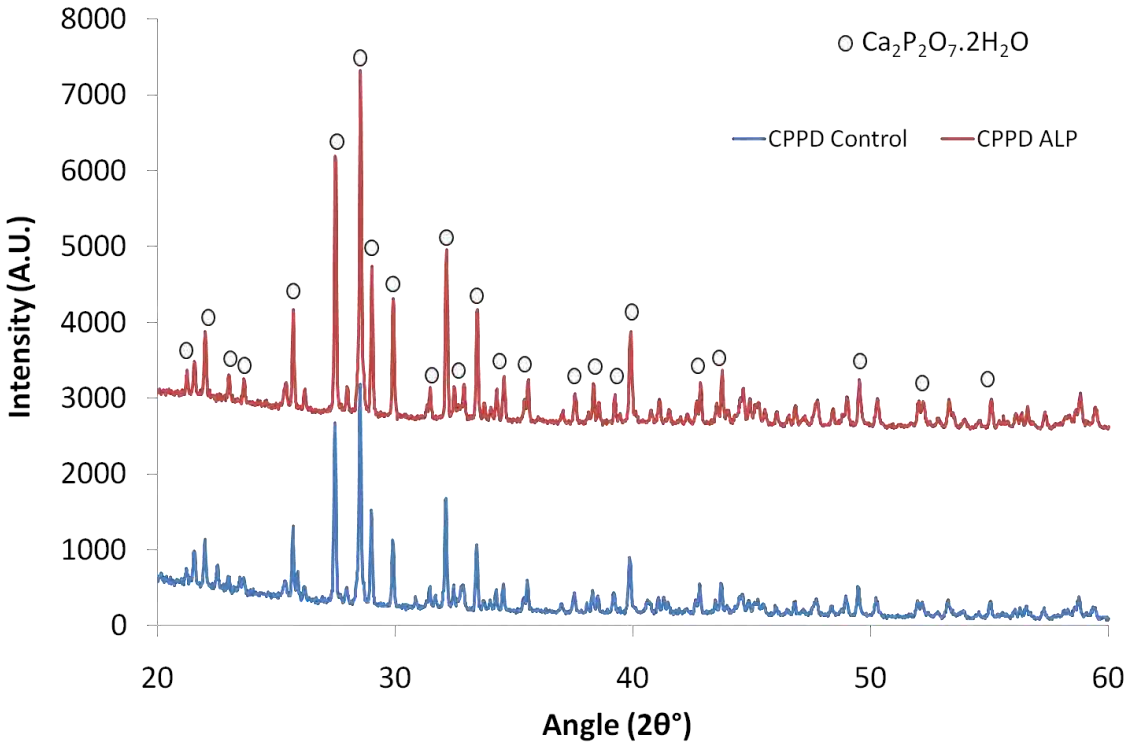

Figure 7.12: Chemical composition of CPPD crystals after ageing in Tris HCl solution and ALP containing Tris HCl solution at 37°C.

The peaks in figure 7.12 are clearly identified as that of CPPD crystals. There was little change in diffraction pattern suggesting no change in crystalline composition (Figure 7.12). Figure 7.13 shows the surface morphology of brushite crystals when precipitated and after ageing in Tris HCl and ALP containing solution. The micrographs in figure 7.13b and 7.13c show signs of crystal dissolution as well as the presence of smaller crystals. These smaller crystals are thought to be reprecipitated crystals although this could not verified by XRD. There was no significant difference in the SEM micrographs of the brushite crystals incubated in the control solution (Figure 7.13b) and those incubated in the ALP solution (Figure 7.13c).

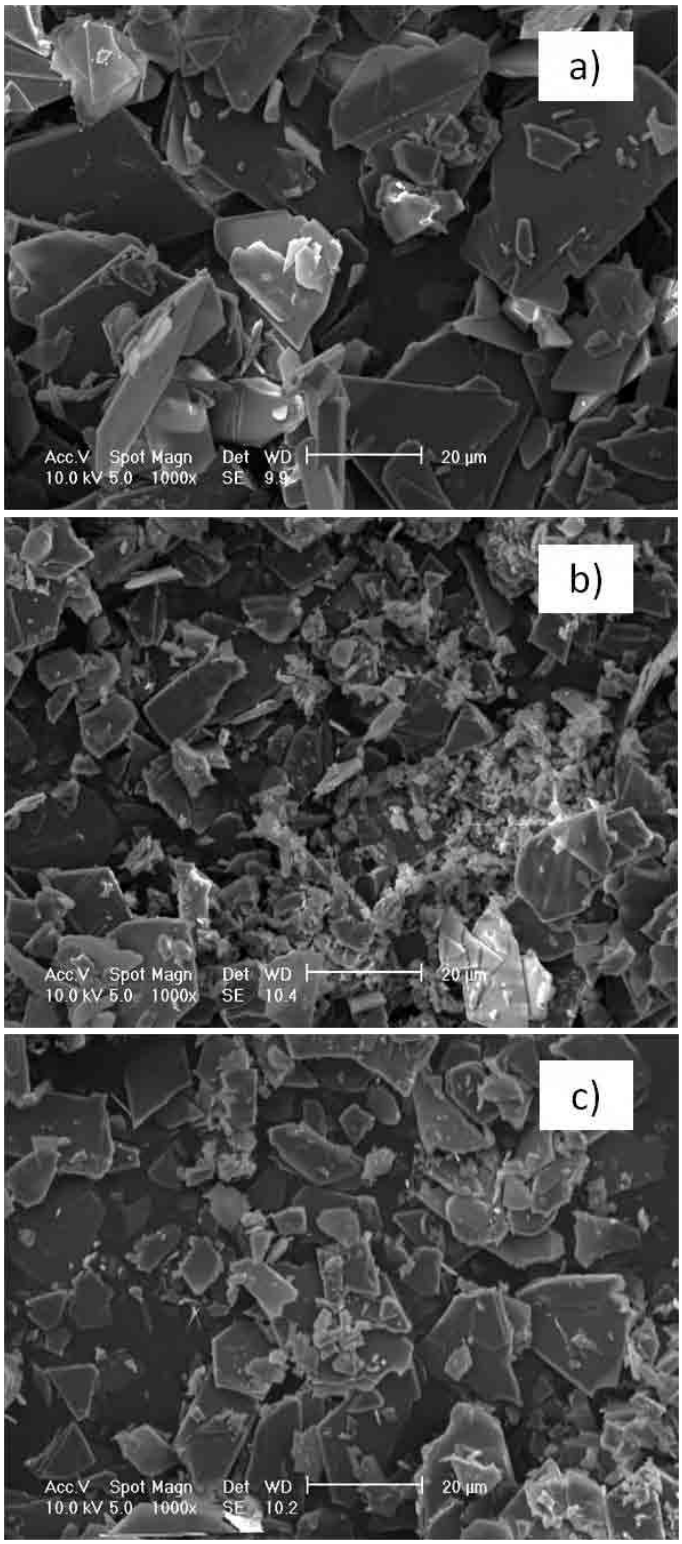

Figure 7.13: Surface morphology of a) precipitated brushite crystals, b) brushite crystals aged in Tris HCl solution and c) brushite crystals aged in ALP containing Tris HCl solution.

7.2.7. Effect of saturation on crystal dissolution

The results shown previously suggest that the rate of crystal dissolution was severely affected by the saturation of the ageing solutions with PO_4^{3-} ions. This problem was overcome by increasing the volume of the aliquot which was taken at each time point from 6% (300 μL) to 80% (4 mL). The concentration of PO_4^{3-} ion released into solution was found to increase significantly in both CPPD and brushite experiment (Figure 7.14). In the ALP solutions the concentration of PO_4^{3-} ion released from both CPPD and brushite crystals when 80% of the aliquot was removed was four times greater than that detected when only 6% aliquot was removed (Figure 7.9a, 7.10a and 7.14). Figure 7.14a shows that the concentration of PO_4^{3-} ion released into ALP solution from CPPD crystals was greater than that detected in the control solution; this follows a similar trend to that observed in figure 7.9a when only 6% of the solution was removed as aliquot. Figure 7.14b shows a slight difference in the mass of brushite which degraded in ALP solution as compared to the control solution. The difference in mass in both solutions was of no statistical significance (i.e. $P>0.05$). Figure 7.15a shows that 24.8 wt% of CPPD was dissolved in the ALP solution an increase from 6.9 wt% when only 6% aliquot was removed. There was also an increase in the percentage of CPPD crystals which dissolved in the control solution from 1.7 wt% to 2.2 wt%. Refreshing 80% of the ageing solution also produced a marked increase in the mass of brushite which was dissolved in solution (Figure 7.15b). In the ALP solution the increase was from 22.0 wt% to 91.2 wt% of brushite crystals dissolved (Figure 7.15b). The error bars i.e. standard deviation of the three concentration or mass data on figures 7.14 and 7.15 are very small therefore not visible.

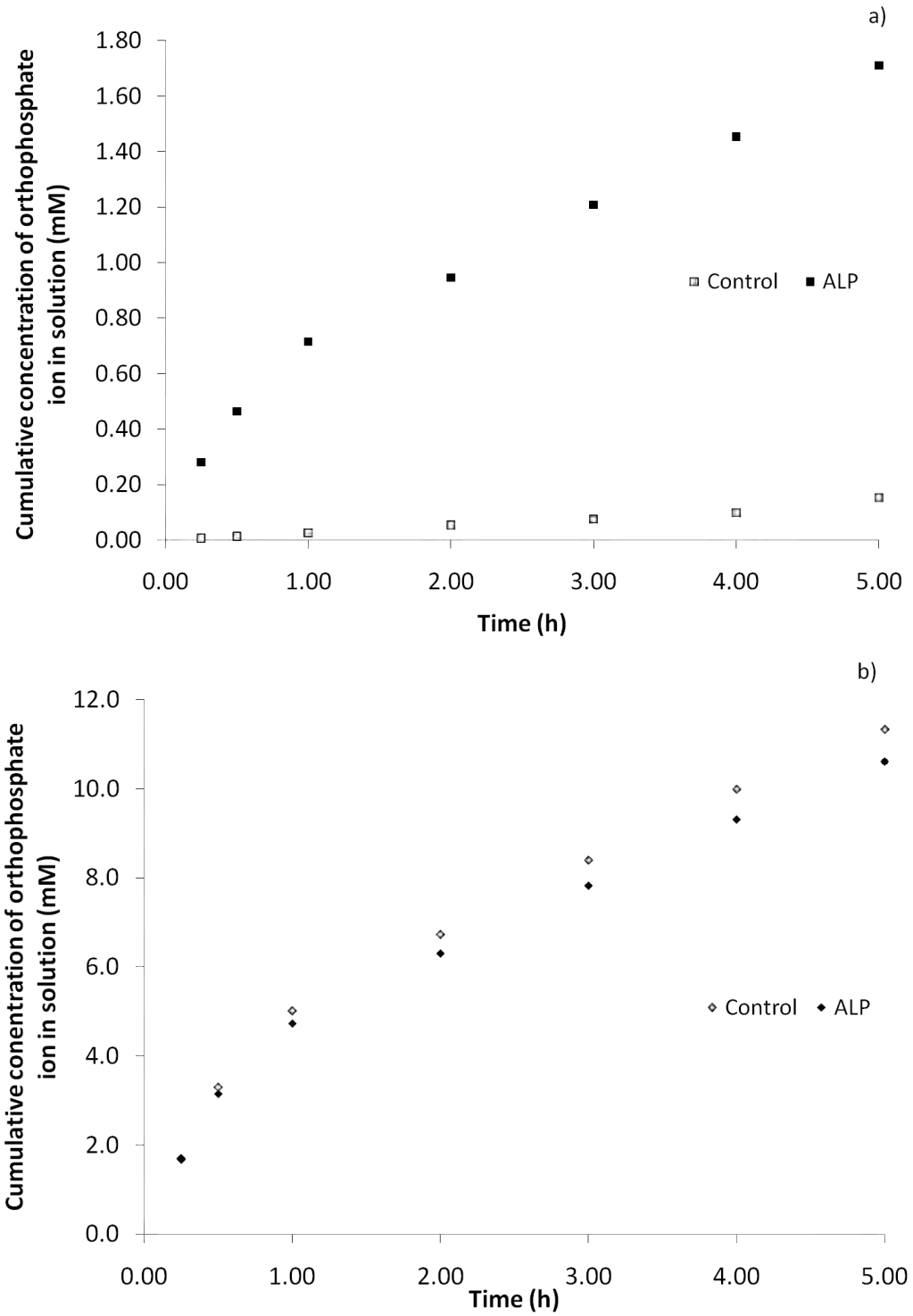

Figure 7.14: Cumulative concentration of orthophosphate ion released when 80% of the solution was replaced at each time point from a) CPPD and b) brushite crystals.

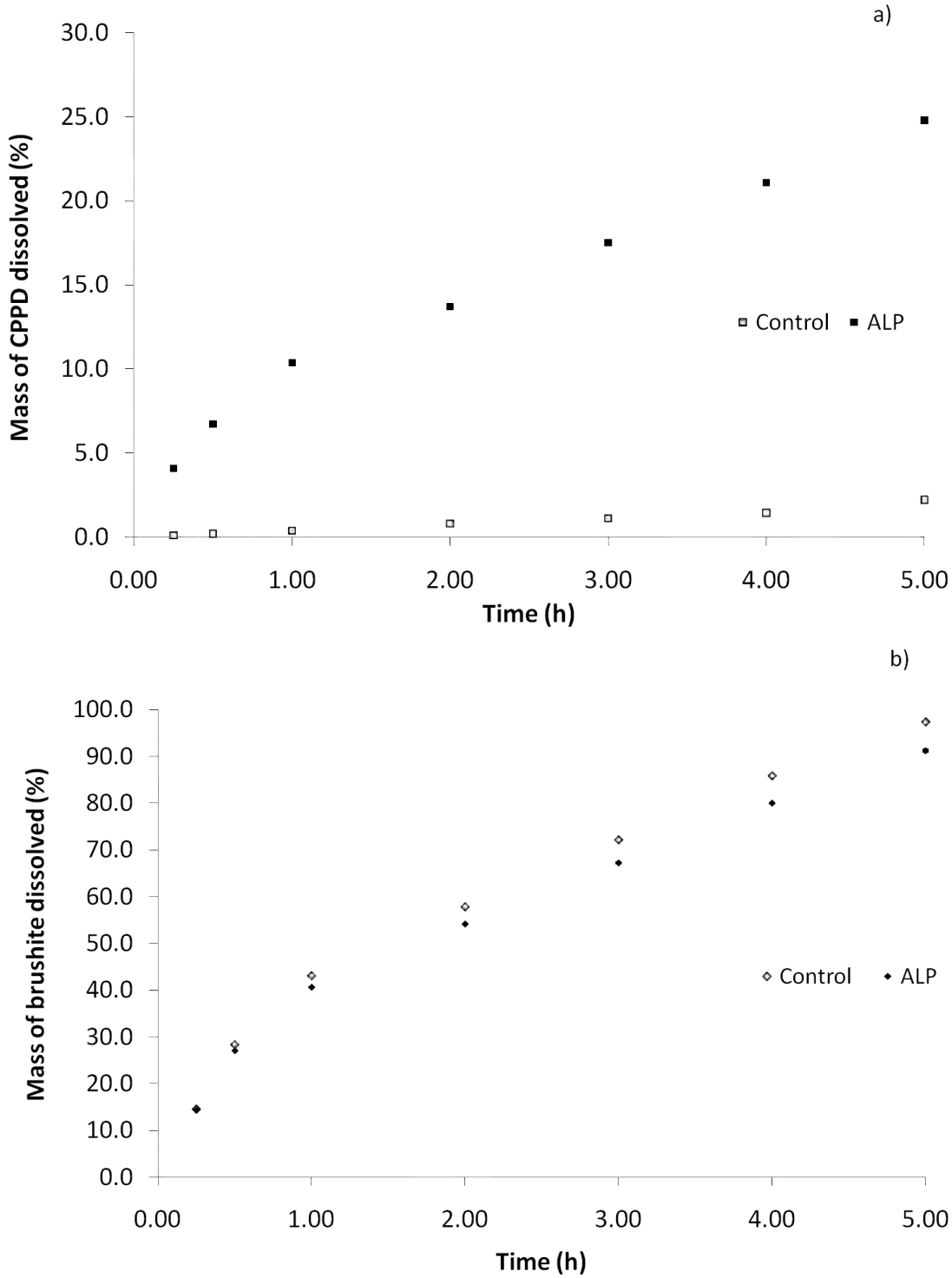

Figure 7.15: Percentage mass of a) CPPD and b) brushite crystals dissolved in the ageing solutions when 80% of the solution was replaced at each time point.

7.2.8. ALP activity in pyrophosphate solution

Mathematical evaluation of enzyme kinetics is used to understand the rate and mechanism of enzyme catalysed reactions. It helps to understand and determine the affinity with which the ALP binds to $P_2O_7^{4-}$ ion in a single substrate reaction as well as the turnover rate of the enzyme. The activity of ALP on the $P_2O_7^{4-}$ ion was investigated to understand the rate at which CPPD crystals would be dissolved when ALP enzyme is present. Michaelis-Menten is the equation which describes an enzyme catalysed reaction and is given by equation 7.1.

$$V = Vmax \left[\frac{[S]}{Km + [S]}\right] \ldots (7.1)$$

Lineweaver – Burk equation (equation 7.2) is the linear form of the Michaelis-Menten equation.

$$\frac{1}{V} = \left[\frac{Km}{Vmax}\right]\left[\frac{1}{[S]}\right] + \frac{1}{Vmax} \ldots (7.2)$$

Where V = rate of enzyme activity, Km = Michaelis-Menten constant, Vmax = maximum rate of the enzyme and [S] = substrate concentration in mM. Km relates to the affinity of the enzyme to the substrate and Vmax is the maximum rate it takes the enzyme to breakdown the substrate. The Vmax and Km values are determined from the initial rates; the initial rate in table 7.1 was calculated from the gradient of a graph of concentration with time.

Table 7.1: Initial rate values for ALP activity experiments carried out at varying concentrations and ambient conditions.

Concentration of $P_2O_7^{4-}$ ion (mM)	1/[S] (mM^{-1})	Initial rate (mM/min)	1/rate (min/mM)
0.04	25.0	0.0068	147.1
0.05	20.0	0.0086	116.3
0.06	16.7	0.0102	98.0
0.07	14.3	0.0119	84.0
0.08	12.5	0.0127	78.7

Using the initial rate values a Lineweaver-Burk graph was plotted on figure 7.16. The Vmax was calculated from the intercept of the graph on the y-axis graph while the Km was calculated from the gradient of figure 7.16. Therefore Vmax = 161.2 μM/min and Km = 898.9 μM.

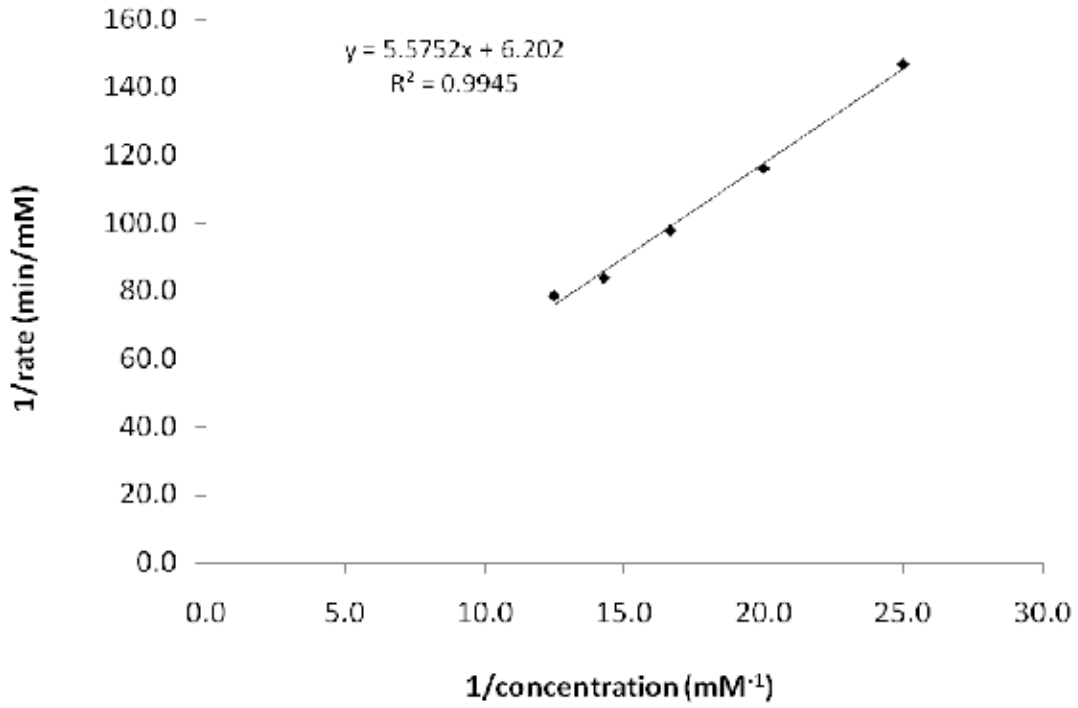

Figure 7.16: Lineweaver-Burk graph for ALP activity in pyrophosphate solution under ambient condition.

7.2.9. Enzyme mineral interaction

Since it has been established that CPPD crystals dissolve faster in the presence of ALP the mechanisms by which this occurs was investigated. The BCA assay was used to observe the attachment of ALP to the surface of both brushite and CPPD crystals. CPPD and brushite crystals were aged in Tris HCl buffer containing known concentrations of ALP. The mass of ALP in the buffer solution was determined using the BCA assay. To determine the mass of ALP which adhered to the surface of the crystals at each time point, the mass of ALP in solution was subtracted from that in the original buffer solution (Figure 7.17). Figure 7.17 shows that there was a continuous process of adsorption and desorption of ALP enzyme on both CPPD and brushite crystals over the duration of the experiment, no particular relationship was evident between protein adsorption and dissolution. Since the pattern observed in figure 7.17 was not observed in figures 7.9 and 7.10 it can be understood that the adsorption of ALP onto the crystal surface is not solely responsible for crystal dissolution. Figure 7.17b also shows that a larger quantity of enzyme is adhered to the surface of brushite crystals as compared with CPPD crystals this could be due to the larger surface area of the brushite crystals. As the crystals dissolve the amount in solution decreases resulting in the decrease in the amount enzyme which adheres to the crystal (Figure 7.17b). The adhesion of ALP onto CPPD crystal was confirmed by staining as shown in figure 7.18. ALP was present on the crystal surface as well as the surrounding areas. In the control experiment (Figure 7.18a) there was no red stain as no ALP enzyme was present in solution.

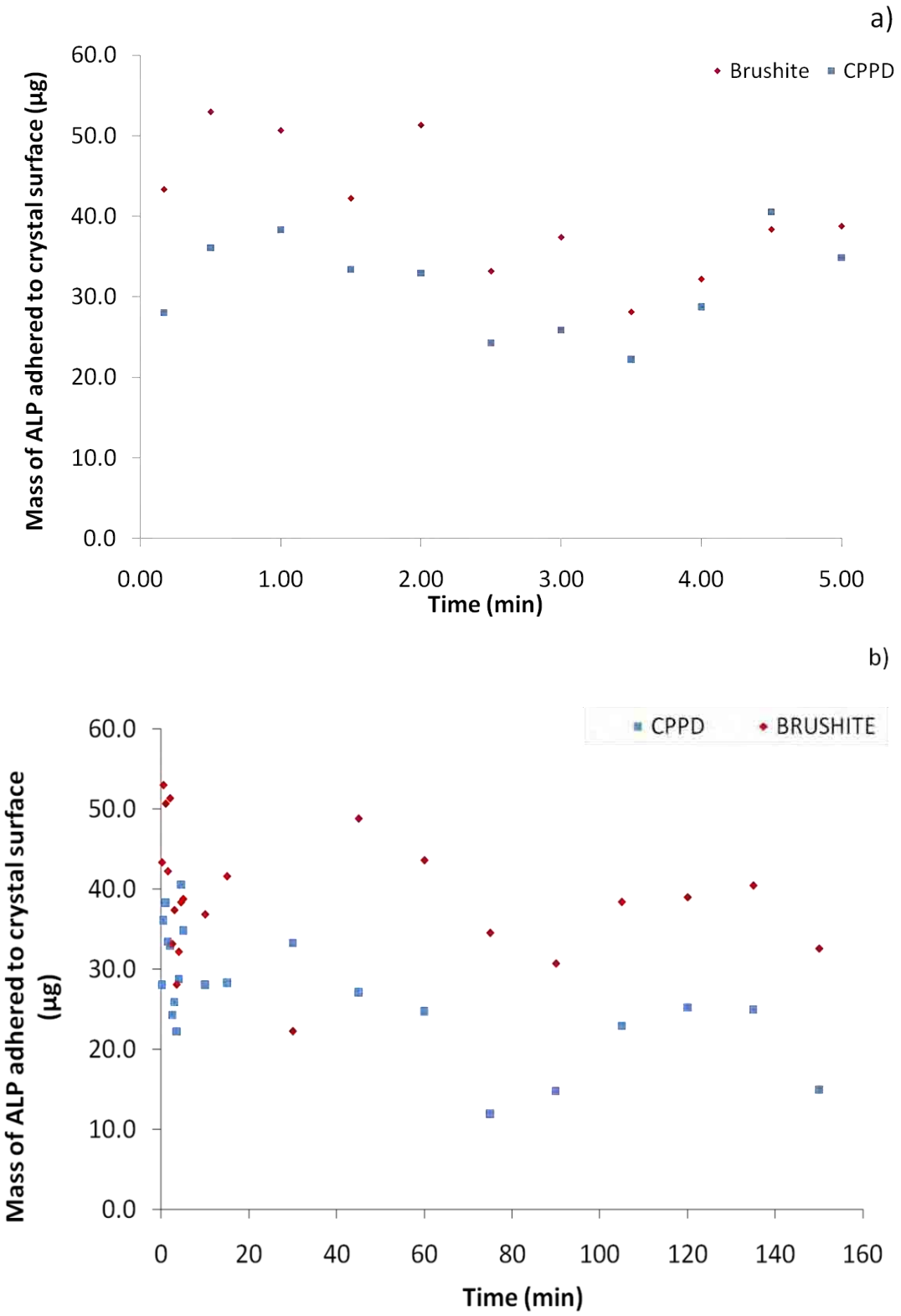

Figure 7.17: a) mass of ALP adhered to CPPD and brushite crystal surface over 5 min and b) mass of ALP enzyme adhered to the surface of CPPD and brushite crystals over 160 min.

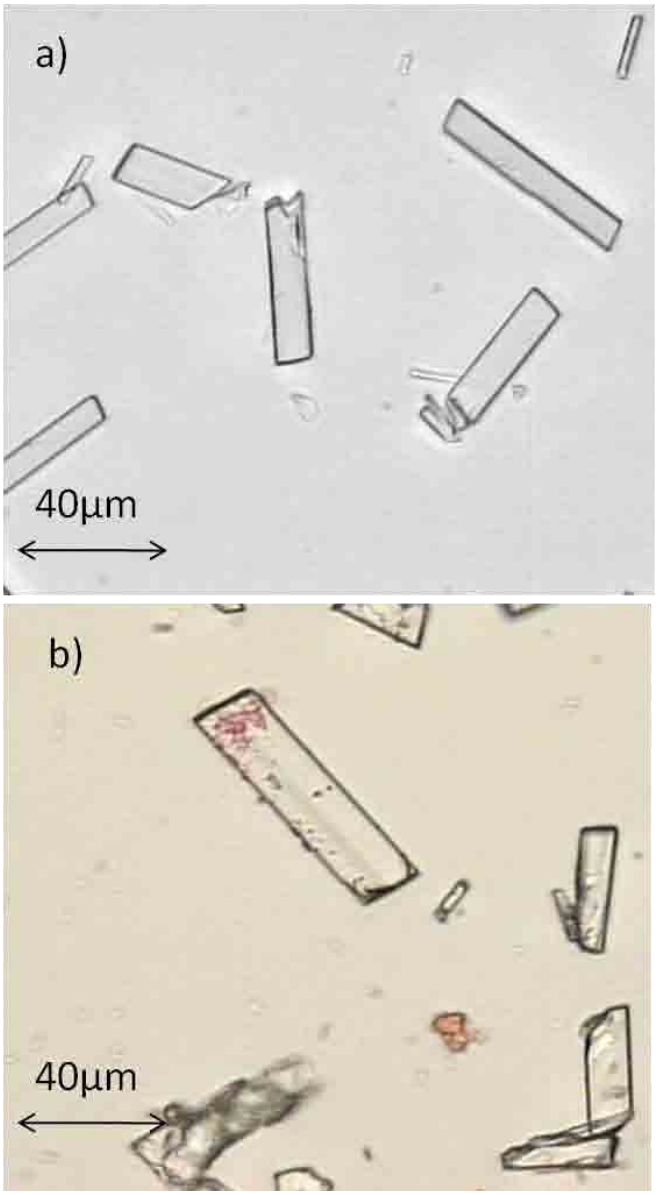

Figure 7.18: a) CPPD surface staining in the absence of ALP and b) CPPD staining in the presence of ALP using naphthol phosphate.

7.2.10. CPPD dissolution mechanism

The final experiment in understanding CPPD dissolution in the presence of ALP was to repeat the dissolution experiment but placing the crystals in a visking tube to separate it from the ALP enzyme. CPPD crystals were placed in a visking tube before placing in the ALP and control solutions. The MWCO of the visking tube was low (3500) so as to prevent the enzyme from passing through to interact directly with the crystals. The crystals are also too large to pass through the visking tube into the ageing solution. The control experiment was carried out in a similar manner without the ALP enzyme. Figure 7.19 show that the mass of CPPD crystal which degraded in the visking tube and ALP solution was greater than that when the ALP was not present. This follows the same trend observed in figure 7.9 when the crystals were exposed directly to the ALP enzyme.

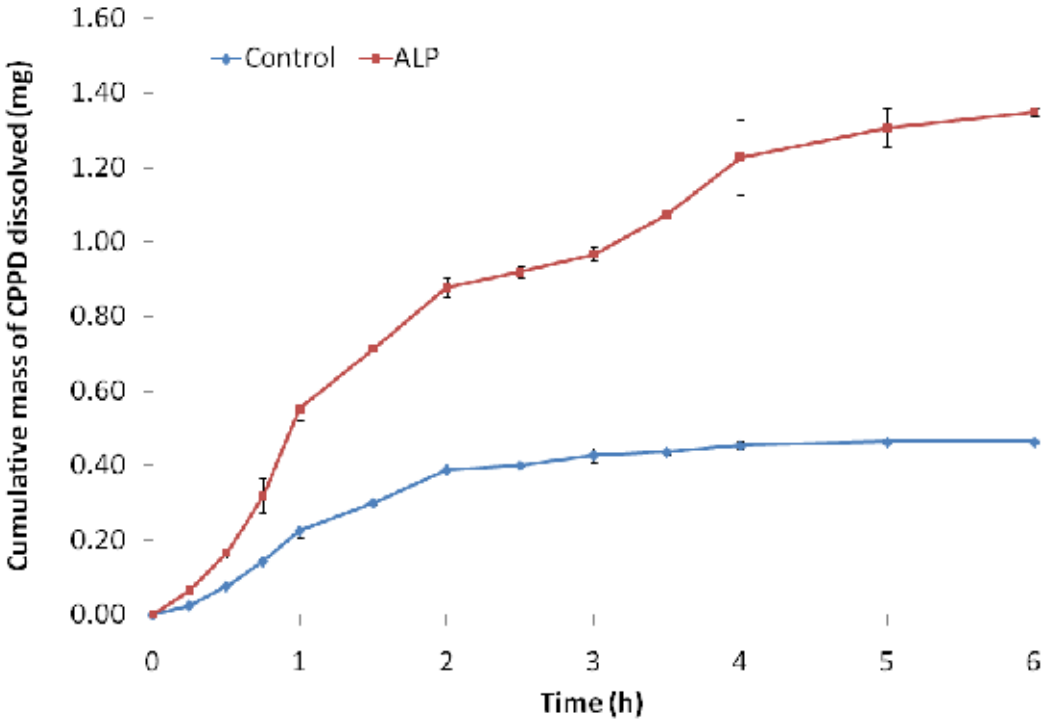

Figure 7.19: Dissolution of CPPD crystal in a visking tube ALP and control solution.

There was a gradual increase in the mass of CPPD crystals which dissolved in solution although between 1 - 4 h the solution appeared saturated with PO_4^{3-} and $P_2O_7^{4-}$ ion resulting in reprecipitation. Figure 7.19 shows that CPPD crystals dissolve in solution (equation 7.3) to produce calcium and pyrophosphate ion. ALP enzyme then hydrolyses the pyrophosphate ion to produce orthophosphate ion. This shows that the accelerated dissolution was not solely mediated by surface attachment as has previously been reported Shinozaki et al. (Shinozaki et al., 1995).

$$Ca_2P_2O_7.2H_2O \rightarrow 2Ca^{2+} + P_2O_7^{4-} \quad \ldots (7.3)$$

7.3. DISCUSSION

7.3.1. Crystal precipitation and dissolution in the presence and absence of ALP

The rate of bone turnover is known to vary with the age and health of a patient, making it difficult to link the rate of implant degradation to the formation of new bone tissue (Fahrleitner-Pammer et al., 2005; Havill, 2004). A suitable biomaterial would be one that degrades at a rate proportional to the formation of new bone tissue. One way to achieve this is to link the degradation of a biomaterial to the presence of a suitable biological stimulus. In bone ALP is an enzyme present on osteoblast cells and it aids bone mineralisation by removing $P_2O_7^{4-}$ ion an inhibitor to bone mineralisation (Anderson et al., 2004; Hessle et al., 2002). The ability of ALP to remove the $P_2O_7^{4-}$ ion has been exploited by Xu et al. (Xu et al., 1991b) with the aim of removing CPPD crystals present in the joints of patients suffering from calcium pyrophosphate dihydrate disease. This chapter further investigates the possibility of enhancing CPPD dissolution in the presence of ALP as well as the mechanism by which the process occurs. Initial investigation involved the precipitation of phase pure CPPD, brushite and OCP crystals (Figures 7.3b, 7.5b and 7.8b). Triclinic CPPD crystals were precipitated using the method of Shinozaki et al. (Shinozaki et al., 1995) according to equation 7.4. The crystals which were produced at pH 5.5 and temperature 37°C contained were phase pure and confirmed to be CPPD (Figure 7.3b).

$$2CaCl_2 + Na_4P_2O_7 + 2H_2O \rightarrow Ca_2P_2O_7.2H_2O + 4NaCl \ldots (7.4)$$

The peaks on the FTIR spectrum in figure 7.4a indicate the presence of pyrophosphate bonds, phosphate and phosphorous hydroxyl (P-OH) bonds which are present in CPPD crystals. Monoclinic brushite crystals were also successfully precipitated as verified using XRD (Figure 7.5b). The FTIR spectrum of brushite crystals shows the presence of PO_4^{3-}, HPO_4^{2-} and H_2O (Figure 7.6b). The triclinic and monoclinic shape of CPPD and brushite crystals respectively can be clearly observed figures 7.4a and 7.6a. Phase pure triclinic OCP crystals were successfully precipitated as verified by the presence of the characteristic primary (100) peak of OCP at $2\theta° = 4.7$ (Figure 7.8a). OCP was not used as the negative control to CPPD as it is less stable than brushite and it converts easily to HA (Arellano-Jimenez et al., 2009; Lu and Leng, 2005).

The trend observed by Xu et al. (Xu et al., 1991b) was confirmed on figure 7.9 where the mass of CPPD dissolved in ALP solution was four times that which dissolved in the control solution (ALP absent). The percentage mass of CPPD crystals dissolved was derived from the concentration of PO_4^{3-} ions released into solution at each time point as shown in figure 7.9b. ALP had no effect on the degradation of brushite crystals in solution due to the absence of pyrophosphate bonds (Figure 7.10). The percentage mass of brushite crystals (22.0 wt%) which dissolved in solution was higher than that of CPPD crystals (6.9 wt%) due to its lower solubility product (Table 7.2) i.e. brushite is more soluble than CPPD crystals. The dissolution of CPPD crystals in both ALP and control solution shows that after the initial increase in PO_4^{3-} ions there was a period between 1 - 4 h where very little increase in PO_4^{3-} ions concentration was observed (Figure 7.9). Figure 7.10a shows that the dissolution

of brushite crystals resulted in very little increase in the concentration of PO_4^{3-} ions over the 6 h experimental period (0.655 mM). The reduction in the concentration of PO_4^{3-} ions over the experimental time is thought to be due to the reprecipitation of apatite crystals. The presence of reprecipitated crystals was confirmed on SEM micrographs in figures 7.11c and 7.13c. The amount of reprecipitated crystals observed on the surface of CPPD crystals was higher on crystals aged in ALP solution than on that aged in control solution (Figure 7.11). The small quantities of reprecipitated crystals and low sensitivity of XRD made it difficult for the chemical composition of the reprecipitated crystals to be determined on figure 7.12. Solubility products was used to determine the concentration of PO_4^{3-} and $P_2O_7^{4-}$ ion required in solution for apatite and CPPD reprecipitation to occur.

Table 7.2: Properties of calcium pyrophosphate dihydrate, brushite and HA crystals precipitated at 37°C (Christoffersen and Christoffersen, 2003; Elliot J.C., 1994; Fernandez et al., 1999).

	CPPD; $Ca_2P_2O_7.2H_2O$	**Brushite; $CaHPO_4.2H_2O$**	**HA; $Ca_5(PO_4)_3OH$**
Crystal system	Triclinic	Monoclinic	Monoclinic
Cell data	a = 6.70, b = 7.38, c = 8.31 Å and β = 102.48°	a = 6.361(3), b = 15.191(4), c = 5.814(2) Å and β = 118.45(4)°	a = 9.84214(8), b = 2a, c = 6.8814(7) Å and γ = 120°
Density (g/cm^3)	2.46	2.32	3.15
Solubility product	18.35	6.63	58.6

7.3.2. Determining the concentration at which HA reprecipitation was likely to occur

Solubility product (Ksp) of HA and CPPD crystals (Table 7.2) was used to calculate the minimum concentration of PO_4^{3-} and $P_2O_7^{4-}$ ion required for the precipitation of HA and CPPD crystals in solution at 37°C. The dissolution of HA crystal is given by equation 7.5:

$$Ca_5(PO_4)_3(OH) \rightarrow 5Ca^{2+} + 3PO_4^{3-} + [OH^-] \ldots (7.5)$$

$$Ksp = \frac{[Ca^{2+}]^5[PO_4{}^{3-}]^3[OH^-]}{[Ca_5(PO_4)_3(OH)]}$$

$$Ksp = 2.51E10^{-59} = [Ca^{2+}]^5[PO_4{}^{3-}]^3[OH^-]$$

$$= [5x]^5\ [3x]^3[x\ ]$$

$$= 84375x^9$$

$$\therefore x = 86.8 \text{ x } 10^{-9}\text{M}$$

Therefore the concentration of PO_4^{3-} required for apatite to be reprecipitated in solution is 0.260 µM (i.e. 3 x 86.8 E -09 M). Equation 7.6 represents the mechanism by which CPPD crystal is dissolved in solution. At 37°C the concentration of $P_2O_7^{4-}$ ion is given by:

$$Ca_2P_2O_7.2H_2O \rightarrow 2Ca^{2+} + P_2O_7^{4-} \ldots (7.6)$$

$$Ksp = \frac{[Ca^{2+}]^2[P_2O_7{}^{4-}]}{[Ca_2P_2O_7]}$$

$$Ksp = 4.47E10^{-19} = [Ca^{2+}]^2[P_2O_7{}^{4-}]$$

$$= [2x]^2[x]$$

$$= 4x^3$$

$$\therefore x = 0.482\mu M$$

Therefore the concentration of $P_2O_7^{4-}$ ion required for the reprecipitation of CPPD crystal in solution is 0.482 μM. From figure 7.9a and 7.10a it can be noted that the concentration of PO_4^{3-} ion at 15 min is much greater than 0.260 μM (the minimum concentration required for apatite precipitation) strongly supporting the hypothesis that the reprecipitated crystals are apatite (equation 7.7b). The excess PO_4^{3-} ion in solution can also be condensed to form $P_2O_7^{4-}$ which is then reprecipitated as CPPD (equation 7.7a).

$$2PO_4^{3-} \leftrightarrow P_2O_7^{4-} \leftrightarrow Ca_2P_2O_7.2H_2O \ldots (7.7a)$$

$$Ca_2P_2O_7.2H_2O \leftrightarrow 2Ca^{2+} + P_2O_7^{4-} \leftrightarrow 2Ca^{2+} + 2PO_4^{3-}$$

$$\leftrightarrow Ca_5(PO_4)_3(OH) \ldots (7.7b)$$

To increase the amount of crystals dissolved in solution by reducing the effect of saturation of the ageing solution the volume of aliquot removed at each time point was increased from 300 μL to 4 mL. By removing 80% (4 mL) of the ageing medium there was an increase of 75% in the mass of CPPD which dissolved in ALP solution (Figure 7.15a) and 76% increase in the mass of brushite crystal which dissolved in a similar solution (Figure 7.15b). There was also a significant increase in the mass of crystals which dissolved in the control solution 23% for CPPD crystals and 79% for brushite crystals. The increase in concentration of PO_4^{3-} ion can be explained by Le Chatelier's principle (Figure 7.14). By increasing the volume of aliquot the concentration of PO_4^{3-} ion in solution is reduced i.e. the concentration of CPPD and brushite crystals is higher than PO_4^{3-} therefore the equilibrium position moves to the right (equation 7.8a and 7.8b). This means that the dissolution of CPPD and brushite crystals is favoured i.e. the mass of CPPD and brushite crystals dissolved in solution increases (Figure 7.14 and 7.15).

$$Ca_2P_2O_7.2H_2O \leftrightarrow Ca^{2+} + P_2O_7^{4-} \leftrightarrow 2PO_4^{3-} \ldots (7.8a)$$

$$CaHPO_4.2H_2O \leftrightarrow Ca^{2+} + HPO_4^{2-} \leftrightarrow H^+ + PO_4^{3-} \ldots (7.8b)$$

In reactions containing ALP it was important to understand the rate at which the enzyme breaks down $P_2O_7^{4-}$ into PO_4^{3-} ions. Km value for ALP determined from Michealis – Menten kinetics was 898.9 μM showing that the enzyme has a high affinity for $P_2O_7^{4-}$ ion. The Ksp value for CPPD crystals reveal that the maximum concentration of $P_2O_7^{4-}$ ion which leads to the formation of the crystals in solution is 0.482 μm. The maximum rate at which ALP hydrolyses $P_2O_7^{4-}$ ion to produce PO_4^{3-} ion is 161.2 μM/min. This shows that ALP will breakdown the $P_2O_7^{4-}$ ion released into solution producing PO_4^{3-} ion with a concentration greater than 0.260 μm. Therefore the solution becomes saturated with respect to PO_4^{3-} ion resulting in the reprecipitation of apatite crystals as illustrated by equation 7.8a (Figure 7.11c). If most of the PO_4^{3-} ion is converted to apatite the amount detected in solution would be reduced, this explains what was observed in solution between 1 – 4 h (Figure 7.8).

7.3.3. Surface interaction of CPPD and brushite crystals with ALP

The adhesion of ALP onto the surface of CPPD and brushite crystals was investigated to further understand if crystal dissolution was surface mediated. The adhesion of ALP onto the surface of CPPD and brushite crystals was shown to increase and decrease throughout the experiment (Figure 7.17b). The adhesion of ALP onto CPPD crystal was confirmed using light microscopy (Figure 7.18b). Shinozaki et al. suggested that the dissolution of CPPD crystals occurs through surface mediation i.e. the ALP that adheres to CPPD crystal stereo selectively cleaves it surface therefore results in crystal dissolution (Shinozaki et al., 1995).

Figure 7.17b suggests that there is continuous adsorption and desorption of ALP from the surface of the crystals. In figure 7.9a and 7.10a the concentration of PO_4^{3-} ion in solution was found to increase gradually and not as suggested by the BCA assay to increase and decrease. In conjunction with figures 7.11c and 7.13c which shows no evidence that ALP cleaved the surface of both CPPD and brushite crystals it can be concluded that crystal dissolution was not surface mediated. The visking experiment in figure 7.19 provides conclusive evidence that CPPD dissolution was not surface mediated. Figure 7.19 shows that the crystals (in visking tube) in the ALP solution degraded faster than that which was aged in the control solution. This result confirms the mechanism of CPPD crystal dissolution to be (1) dissolution of CPPD into calcium and pyrophosphate ions and then (2) the hydrolysis of the $P_2O_7^{4-}$ ion by ALP (equation 7.8a).

7.4. CONCLUSION

Phase pure CPPD, brushite and OCP crystals were successfully precipitated and this was confirmed using XRD, FTIR and SEM. CPPD crystals dissolved faster in the presence of ALP but brushite crystals were not affected by the enzyme. A higher percentage of brushite crystals were dissolved in solution than CPPD as it is more soluble in physiological conditions. SEM micrographs of CPPD crystals aged in the control and ALP solution show the presence of reprecipitated crystals which is due to the saturation of the ageing solution with respect to PO_4^{3-} ion. The Michaelis-Menten kinetics showed the high affinity ALP had for $P_2O_7^{4-}$ ion and therefore releasing orthophosphate ion at very high concentrations that result in reprecipitation. The mass of CPPD and brushite crystals which were dissolved in the ageing solutions increased significantly with increase in the volume of aliquot removed. This confirms that the solubility of the precipitated crystals is inhibited by the reprecipitation of apatite and CPPD crystals. Although ALP was shown to adsorb to the surface of CPPD crystals the adhesion experiment (BCA assay) does not support the hypothesis that CPPD dissolution occurs when ALP cleaves to the surface of the crystal on which it was attached. CPPD crystal dissolution was found to increase in ALP solution than the control even though the crystals were placed in a visking tube which would prevent direct interaction with the enzyme. It can be concluded that the dissolution of CPPD in the presence of ALP occurs in two stages: (1) hydrolytic degradation of the crystals and (2) enzymatic degradation of the pyrophosphate bonds resulting in the release of phosphate ions.

8. FORMULATING AND PROCESSING A BULK CALCIUM PYROPHOSPHATE CERAMIC

The human body is limited in its ability to regenerate bone defects caused by infection and trauma. Therefore various materials have been investigated as a possible bone replacement material. ALP which is found on the surface of osteoblasts cells plays an important role in bone mineralization by hydrolyzing the $P_2O_7^{4-}$ ion to PO_4^{3-} ion which causes supersaturation and apatite formation (Balcerzak et al., 2003). Although CPPD crystals were shown to dissolve faster in the presence of ALP (chapter 7), CPPD crystals are not suitable biomaterials as they cannot be produced phase pure in large quantities. The presence of CPPD crystals in the body is also associated with calcium pyrophosphate dihydrate deposition disease and pseudogout (Mccarty, 1976; Mccarty et al., 1971). Therefore this chapter seeks to investigate the formulation and processing of a bulk calcium pyrophosphate ceramic which is reproducible and can be produced in large quantities. The ceramic is also expected to degrade in the presence of ALP therefore acting as a bioresponsive bone replacement. A ceramic is an inorganic, non-mettalic solid prepared by the action of heat and subsequent cooling (Dorozhkin, 2010). Ceramics can be crystalline, partly crystalline or amorphous (Dorozhkin, 2010). Sintered dicalcium pyrophosphate (SDCP) and β-dicalcium pyrophosphate (β-DCP) particles have been shown to encourage osteoblast cell growth (Sun et al., 1997). Calcium pyrophosphate ceramic is also osteoconductive and well tolerated *in vivo* (Lin et al., 1995b). When Lin et al. implanted β-DCP doped with sodium pyrophosphate ($Na_4P_2O_7.10H_2O$) into the femur of New Zealand white male rabbit the ceramic was found to be degradable *in vivo* and new bone tissue was formed within the

macropores of the compacted ceramic (Lin et al., 1995b). Another experiment showed that bone mineral was increased and porosity of trabeculae bone was decreased in the long bone of ovariectomized rats when the Wistar rats ingested SDCP (Sun et al., 2002), suggesting that the material could play a broader therapeutic role. The presence of a glass phase within the SDCP ceramic could result in a low SSA, a factor known to influence the biological reaction to the material (Lin et al., 1995b; Barralet et al., 2002). In this chapter the process of producing calcium pyrophosphate ceramic from brushite based cement was investigated. The effect of varying process conditions and cement compositions on the microstructure, porosity and compressive strength of the ceramic was also investigated. The mass loss and volumetric shrinkage of the ceramic was also investigated with respect to varying powder liquid (P:L) ratio and sintering temperature. Finally the degradation of the sintered ceramic in ALP containing solution and in serum was investigated. The effect of SSA, sintering temperature and P:L ratio on ceramic degradation was also determined.

8.1. MATERIALS AND METHODS

8.1.1. Synthesis of calcium pyrophosphate ceramics

The brushite cement for thermal treatment was synthesized by combining β-TCP with 3.5 M H_3PO_4 (Fisher Scientific, Dorset, UK) containing citric acid at a concentration of 50 mM (Fluka, Dorset, UK) (equation 8.1). The β-TCP was mixed with H_3PO_4 solution at powder to liquid ratio (P:L) of 1.25 g/mL. The resulting paste was cast into a polytetrafluroethylene (PTFE) split mould to form cylindrical samples of diameter 6 mm and height 12 mm. The cylinders were allowed to harden at 37°C for 24 h prior to testing or further heat treatment. The hardened cement cylinders were subsequently sintered at temperatures between 400 and 1200°C for 5 h using a muffle furnace (CWF 1300; Carbolite, UK), the heating and cooling rate of the furnace was set at 10°C/min converting the brushite cement into monetite and then calcium pyrophosphate ceramic ($Ca_2P_2O_7$) in accordance with equation 8.2 and 8.3.

$$\beta - Ca_3(PO_4)_2 + H_3PO_4 + 6H_2O \rightarrow 3CaHPO_4.2H_2O \ldots (8.1)$$

$$2CaHPO_4.2H_2O \rightarrow 2CaHPO_4 + 4H_2O \ldots (8.2)$$

$$2CaHPO_4 \rightarrow Ca_2P_2O_7 + H_2O \ldots (8.3)$$

8.1.2. Monitoring phase transitions

Dried brushite cement (P:L = 1.25 g/mL) was ground and then placed in a temperature controlled X-ray diffractometer. The X-ray diffractometer (D5005 Brucker, Siemens, Germany) with CuKα1 radiation λ = 1.5406 Å and CuKα2 radiation λ = 1.5444 Å was used in determining the crystal composition of the powder as it was heated from 27 to 1000°C over a 2θ range of 5 - 70° using a step

size of 0.036° and a step time of 0.5 s. Thermogravimetric analysis (TGA) and differential thermal analysis (DTA) was carried out on brushite cement powder over a temperature range of 25 – 1200°C with a flow rate of 50 mL/min and at a heating rate of 20°C/min using a simultaneous thermal analysis machine (STA 1500, Stanton Redcroft).

8.1.3. Effect of varying cement composition

The concentration of H_3PO_4 acid determines the amount of β-TCP that reacts to form brushite (equation 8.1) and hence subsequent amount of pyrophosphate within the ceramic. The acid concentration was varied from 1.5 – 4.5 M and the effect on the porosity and mechanical strength of the ceramic was investigated. The effect of mixing incremental amounts of β-TCP with H_3PO_4 acid at P: L between 1.25 and 3.0 g/mL was studied. The effect of increasing the P:L on the porosity and mechanical strength of the ceramic was investigated as increasing P:L should result in increased amount of unreacted β-TCP. The changes to surface morphology, mass and volume loss with increasing P:L was also observed.

8.1.4. Effect of varying process conditions

Sintering time and temperature are driving forces in the process of sintering and therefore affect the microstructure and composition of the resulting ceramic. The sintering time was varied over 3 – 10 h and the effect on the porosity and mechanical strength of calcium pyrophosphate ceramic was investigated. The effect of varying sintering temperature from 400 – 1200°C on microstructure, porosity, mass and

volume loss and mechanical strength while keeping the sintering rate and time constant was also investigated.

8.1.5. Characterisation of calcium pyrophosphate ceramic

8.1.5.1. Mass and volume change

At each operating condition geometrical and mass measurements of each sample (n=9) were made and from these data, volumetric shrinkage and mass loss were calculated. The mass loss is given by:

$$M_s(\%) = \frac{M_i - M_f}{M_i} \times 100 \ldots (8.4a)$$

Where M_s is the mass loss from the ceramic upon sintering, M_i is the mass of brushite cement and M_f is the mass of the sintered $Ca_2P_2O_7$ ceramic. The volumetric shrinkage of $Ca_2P_2O_7$ ceramic is given by:

$$V_s(\%) = \frac{V_i - V_f}{V_i} \times 100 \ldots (8.4b)$$

Where V_s is the volumetric shrinkage, V_i is the volume of brushite cement and V_f is the volume of the sintered $Ca_2P_2O_7$ ceramic.

8.1.5.2. Ceramic microstructure

The new microstructure formed within the ceramic was observed using SEM. The changes to the cement and ceramic microstructure with varying P:L and sintering temperature was observed using SEM (Philips XL 30 and Joel 6060). The fracture surface of the cement and ceramic was gold plated (depth of 1 mm) to make them conductive and potentials of 10 kV were applied to obtain clear pictures.

8.1.5.3. Porosity

The conversion of brushite to $Ca_2P_2O_7$ results in density changes within the material. There are also additional density changes when phase change occurs between the different isoforms of $Ca_2P_2O_7$ at temperatures above 400°C. The changes to density as well as composition would affect the porosity and therefore the compressive strength of the ceramic according to equation 8.5:

$$\sigma_c = \sigma_o \exp(-KP) \ldots (8.5)$$

Where σ_c is compressive strength at porosity P, σ_o is compressive strength at zero porosity, K is a constant and P is the porosity of the ceramic. Using Archimedes principle, the porosity of the ceramic was determined from apparent and true density measurements. True density was calculated from the mass of the ceramic in air (dry) and in water (wet) while the apparent density was calculated from the mass and volume (measured using the outer dimensions of the ceramic) of the ceramic.

$$True\ density = \left(\frac{mass\ in\ air}{mass\ in\ air - mass\ in\ water}\right) \times 100 \ldots (8.6a)$$

$$Apparent\ density = \left(\frac{mass\ in\ air\ (Kg)}{volume\ of\ ceramic\ (m^3)}\right) \ldots (8.6b)$$

$$Density\ (\%) = \left({Apparent\ density}/{Theoretical\ density}\right) \ldots (8.6c)$$

$$\therefore Porosity\ (\%) = 100 - Density\ (\%) \ldots (8.6d)$$

8.1.5.4. Compressive strength

Prior to testing in compression, ceramic samples were immersed in double distilled water for a period of 2 h and stored at 37°C. The wet ceramic samples were mounted on the testing machine (Dartec HCIO, UK) so that the long axes of the ceramic cylinders were perpendicular to the lower anvil. A compressive force was then

applied to the upper surface of the ceramic samples at a constant crosshead displacement rate of 1 mm/min until failure occurred. Mean strength was determined from the average of nine measurements. The applied load was measured using a 1 kN load cell (Dartec HCIO, UK). Compressive strength was determined in accordance with equation 8.7:

$$\sigma_c = \left(\frac{4F}{\pi d^2}\right) \quad \ldots (8.7)$$

Where σ_c is compressive strength (MPa), F is load at failure (N) and d is the diameter of the cylindrical sample (mm).

8.1.5.5. Specific surface area

The changes to SSA of $Ca_2P_2O_7$ ceramic with sintering temperature was measured and calculated according to Brunauer Emmet Teller (BET) method by a Tristar II 3020 apparatus (Tristar Gemini, Micrometrics) with the nitrogen liquid at 77 K.

SSA measurements for the ceramics degraded in ALP, Tris HCl, serum and PBS solutions was calculated by applying BET equation to the data collected from a DVS Advantage II (Surface Measurement Systems, UK). Octane was used as the probe molecule. 35 – 50 mg ± 1mg of sample was loaded onto one side of the twin pan balance, before running the software-controlled sequence that held the sample at 0% relative humidity (dry nitrogen) for 12 h to remove any surface moisture followed by humidity steps from 0% relative humidity up to 90% relative humidity in 3% increments. This procedure was repeated three consecutive times on each sample except were stated. The temperature throughout was 25°C ± 0.1°C. The sample was allowed to reach a near equilibrium state (% d*m*/d*t* = 0.002%/min) at each humidity stage before progressing to the next.

8.1.5.6. Statistical analysis

One-way analysis of variance (ANOVA) was employed to determine the statistical significance of differences between mass loss, volumetric loss, porosity and compressive strengths of the ceramics. Comparison of these raw data was performed using the post-hoc Tukey test. Differences between sample groups was deemed significant when $p \leq 0.05$. All statistical analysis was performed using Primer of Biostatistics for windows version 4.

8.1.6. Degradation of calcium pyrophosphate ceramics

Bulk $Ca_2P_2O_7$ ceramics were aged in the presence of ALP; this is to determine if ALP accelerated the degradation of calcium pyrophosphate ceramic as was the case with CPPD crystals. To provide a more realistic simulation of body fluid, the ceramic was also aged in serum which should contain pyrophosphatase enzymes.

8.1.6.1. Degradation in ALP solution

Bulk $Ca_2P_2O_7$ ceramics sintered at 1200ºC with varying P:L of 1.25 - 1.5 g/mL were aged in 20 mL Tris HCl solution containing ALP (10 – 75 U). The Tris HCl buffer was at a pH of 7.4 and it contained 0.01% sodium azide (NaN_3, Sigma Aldrich, Dorset) and 1 mM magnesium chloride ($MgCl_2$, Sigma Aldrich, Dorset). As a control experiment the bulk ceramics were aged in the Tris HCl buffer without ALP. The experiments were carried out in a rotating incubator at 37°C with the rotor speed of 150 rpm. The ageing solution was changed daily and the mass of the ceramic was measured daily.

8.1.6.2. Degradation in Foetal Bovine Serum (Serum)

$Ca_2P_2O_7$ ceramic (n=3) was aged in 20 mL foetal bovine serum (PAA laboratories, Somerset, UK) containing 0.01% sodium azide (NaN_3, Sigma Aldrich, Dorset) in a rotating incubator at 37°C with the rotor speed set at 150 rpm. As a control experiment $Ca_2P_2O_7$ ceramic (n=3) with the same composition and sintering conditions was degraded in 20 mL phosphate buffered saline (PBS). The ageing solutions were changed daily over the duration of the study, the ceramics were dried and the mass was measured daily.

8.2. RESULTS

8.2.1. Synthesis of $Ca_2P_2O_7$ ceramic

The change in the microstructure of brushite cement (P:L = 1.25 g/mL) after sintering is illustrated by figure 8.1. Before heat treatment the cement consisted predominantly of rectangular shaped crystals of 10 – 30 μm in length (Figure 8.1a). Following heat treatment the microstructure of the ceramic consisted of very small pores which are formed when the crystals of the cement diffuse into one another (Figure 8.1b).

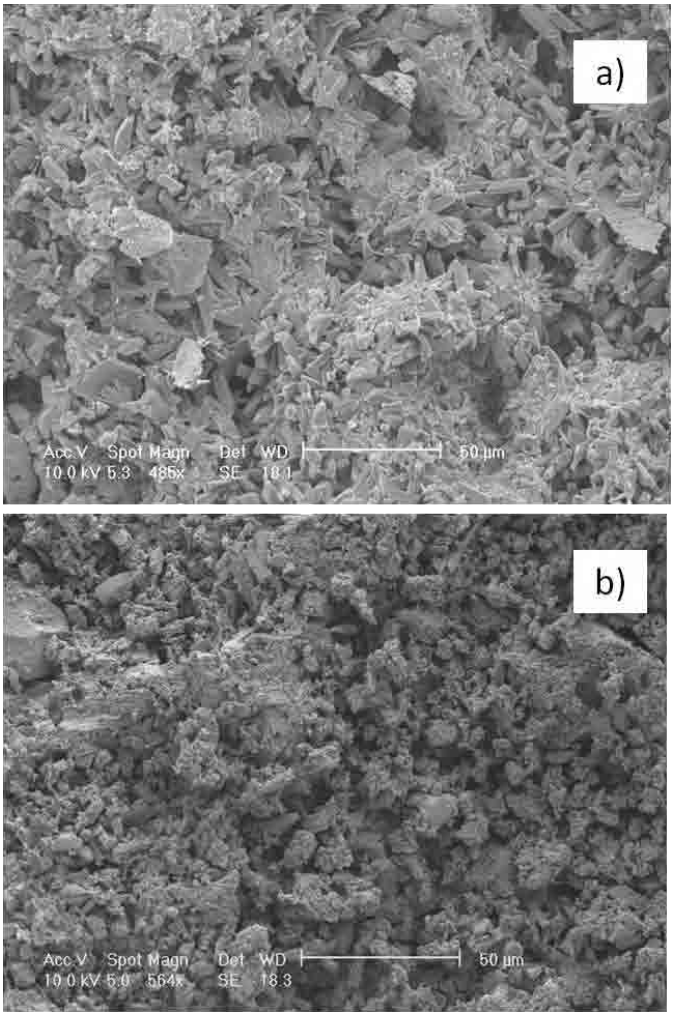

Figure 8.1: Microstructure of a) brushite based cement prior to sintering and b) $Ca_2P_2O_7$ ceramic sintered at 1000°C.

The particles of the sintered ceramic consist of irregularly shaped particles (5 – 50 μm long) and coarsened (densified) crystals with interconnected pores associated with neck formation and crystal growth (Figure 8.1b). X-ray diffraction showed that prior to heat treatment, the cement consisted in the most part of brushite, with some residual unreacted β-TCP (Figure 8.2). Sintering brushite cement to 200°C resulted in the conversion of all the brushite crystals within the cement into calcium hydrogen phosphate anhydrous (monetite; $CaHPO_4$) in accordance with equation 8.8a. Figure 8.2 also shows that monetite was completely converted to $Ca_2P_2O_7$ when sintered at temperatures ≥400°C in accordance with equation 8.8b.

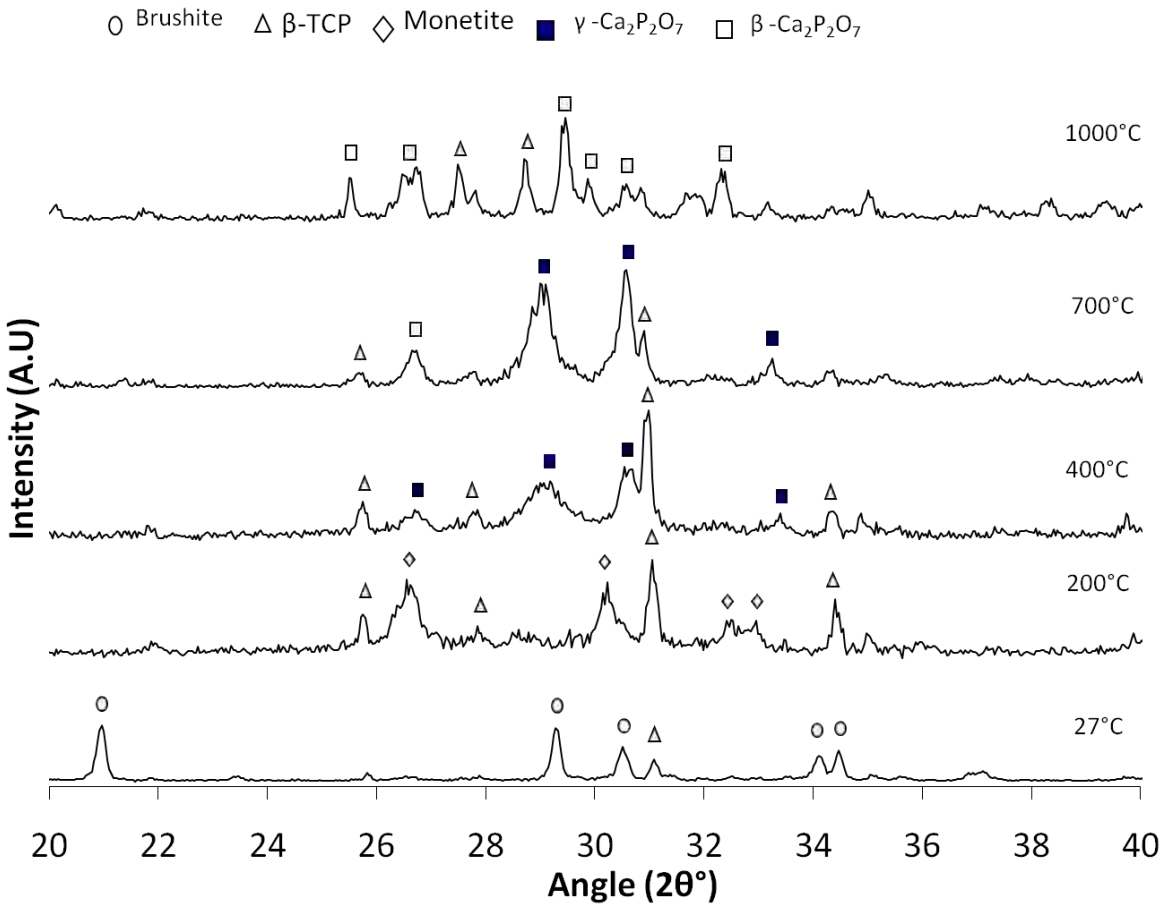

Figure 8.2: XRD patterns showing the phase evolution with temperature during the formation of $Ca_2P_2O_7$.

γ-$Ca_2P_2O_7$ was formed when monetite was heated between 400 – 700°C while there was a phase change to β-$Ca_2P_2O_7$ a more stable phase at 1000°C.

$$CaHPO_4.2H_2O \rightarrow CaHPO_4 + 2H_2O \uparrow \ldots (8.8a)$$

$$2CaHPO_4 \rightarrow Ca_2P_2O_7 + H_2O \uparrow \ldots (8.8b)$$

Further heating of the ceramic to 1200°C resulted in a final phase change to α-$Ca_2P_2O_7$ as shown in figure 8.3. It can be clearly seen that the unreacted β-TCP remained within the ceramic over the sintering regime. Beyond 1200°C, the formation of a glass phase was apparent and the cylindrical samples lost their cylindrical conformation.

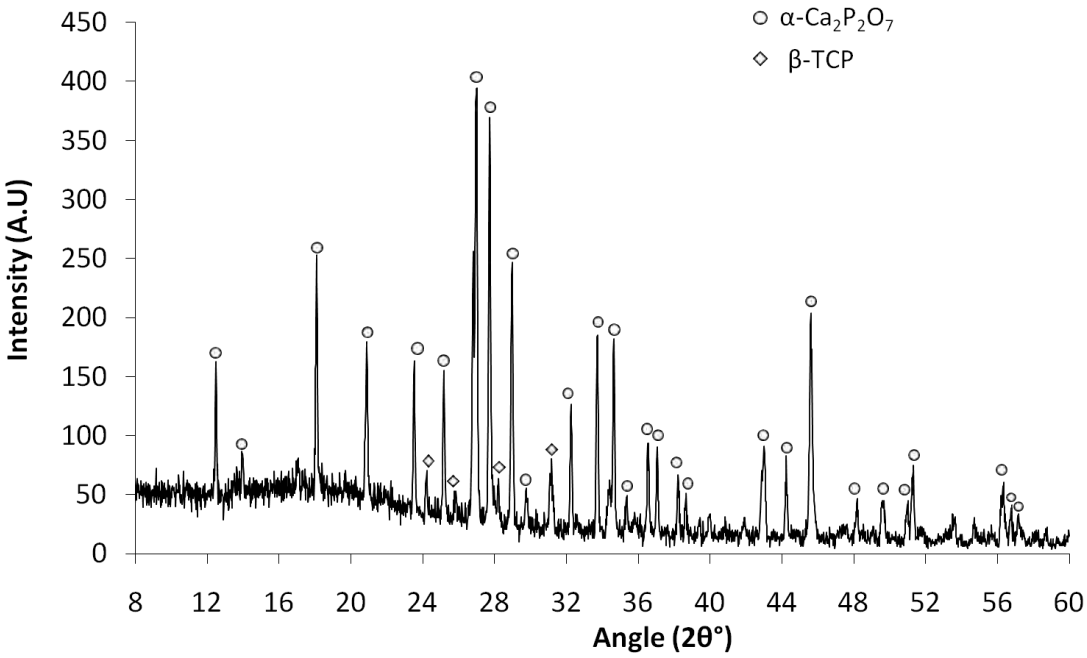

Figure 8.3: XRD pattern of α-$Ca_2P_2O_7$ ceramic (P:L = 1.25 g/mL) when brushite cement was sintered at 1200°C for 5 h.

In addition to the temperature controlled XRD the conversion of brushite to $Ca_2P_2O_7$ was also monitored using TGA and DTA analysis as shown in figure 8.4. The dehydration of the cement up to a temperature of 225°C was associated with a mass loss of 12% and an exothermic reaction that can be associated with the phase change

from brushite to monetite (equation 8.8a). Further heating of the ceramic to 400°C caused a smaller exotherm and the loss of an additional ~6 wt% of the ceramic mass that may be associated with the formation of γ-$Ca_2P_2O_7$ (equation 8.8b) in the matrix of the ceramic (Figure 8.2 and 8.4).

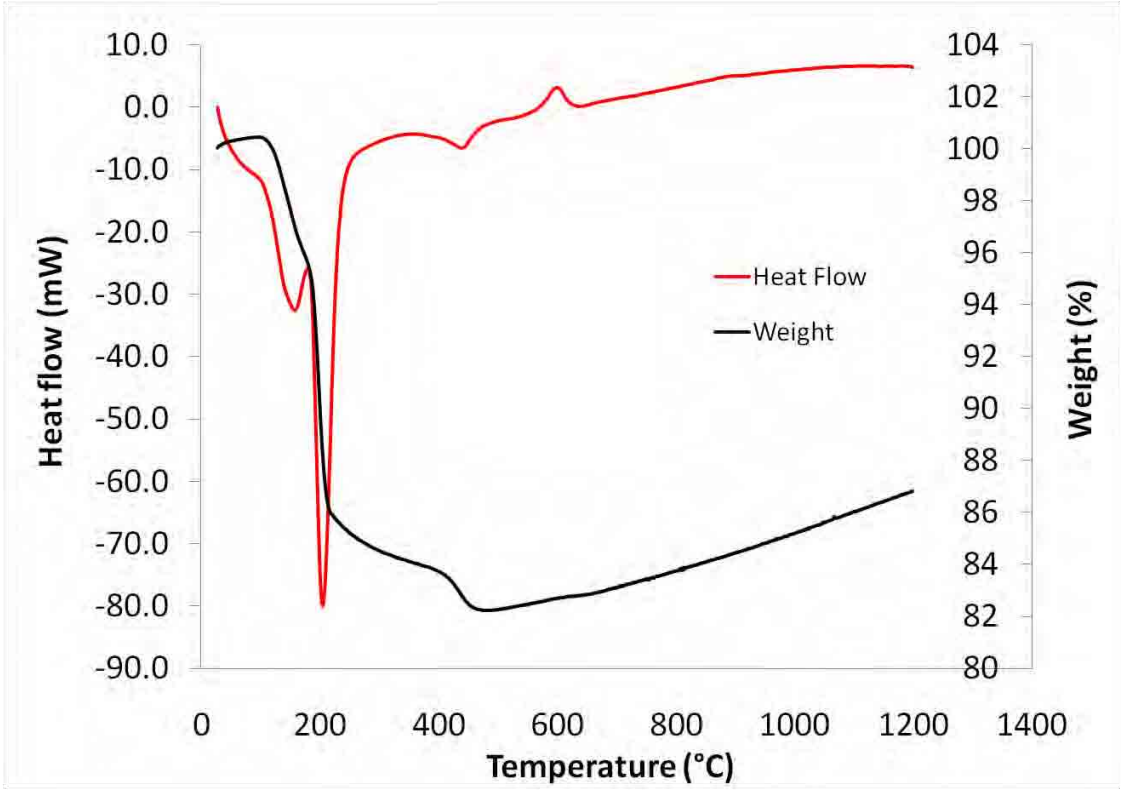

Figure 8.4: Thermal and gravimetric profile for the solid state reaction of the conversion of brushite cement to $Ca_2P_2O_7$.

An endothermic peak at approximately 600°C may indicate an additional phase change that was associated with little or no mass loss (Figure 8.4). Indeed, following heating beyond 700°C, the ceramic was shown to contain β-$Ca_2P_2O_7$ (Figure 8.2). As sintering temperature was increased from 1000 - 1200°C β-$Ca_2P_2O_7$ was converted to α-$Ca_2P_2O_7$ as confirmed on the XRD pattern in figure 8.3.

8.2.2. Effect of varying process condition on $Ca_2P_2O_7$ ceramic

Sintering time and temperature are two of the process variables which determine the conversion of one material to another and the microstructure of the sintered material. This section investigated the effect of varying sintering time and temperature.

8.2.2.1. Sintering time

The pores within the particles of the powder compact are expected to decrease with increase in sintering time i.e. ceramic porosity is expected to decrease as the sintering time increases. β-TCP powder consisted of irregularly shaped particles and agglomerates of 2 – 50 μm in diameter (Figure 8.5a) while the brushite crystals formed were of a rectangular shape of 10 – 30 μm in diameter (Figure 8.5b). The difference in shape and size of component particles of the brushite cement made it difficult to obtain uniform elimination of the pores within the cement (Figure 8.5b). Indeed there was no statistically significant change in ceramic porosity when the sintering time was varied from 3 to 10 h except when sintered at 5 h (Table 8.1). The compressive strength of the ceramic was also not affected by increasing sintering time (Table 8.1). The change in porosity and compressive strength of $Ca_2P_2O_7$ ceramic with increased sintering time was of no statistical significance. The porosity (30%) and compressive strength (11.1 MPa) of $Ca_2P_2O_7$ ceramic was highest when brushite cement was sintered in the muffle furnace for 5 h (Table 8.1).

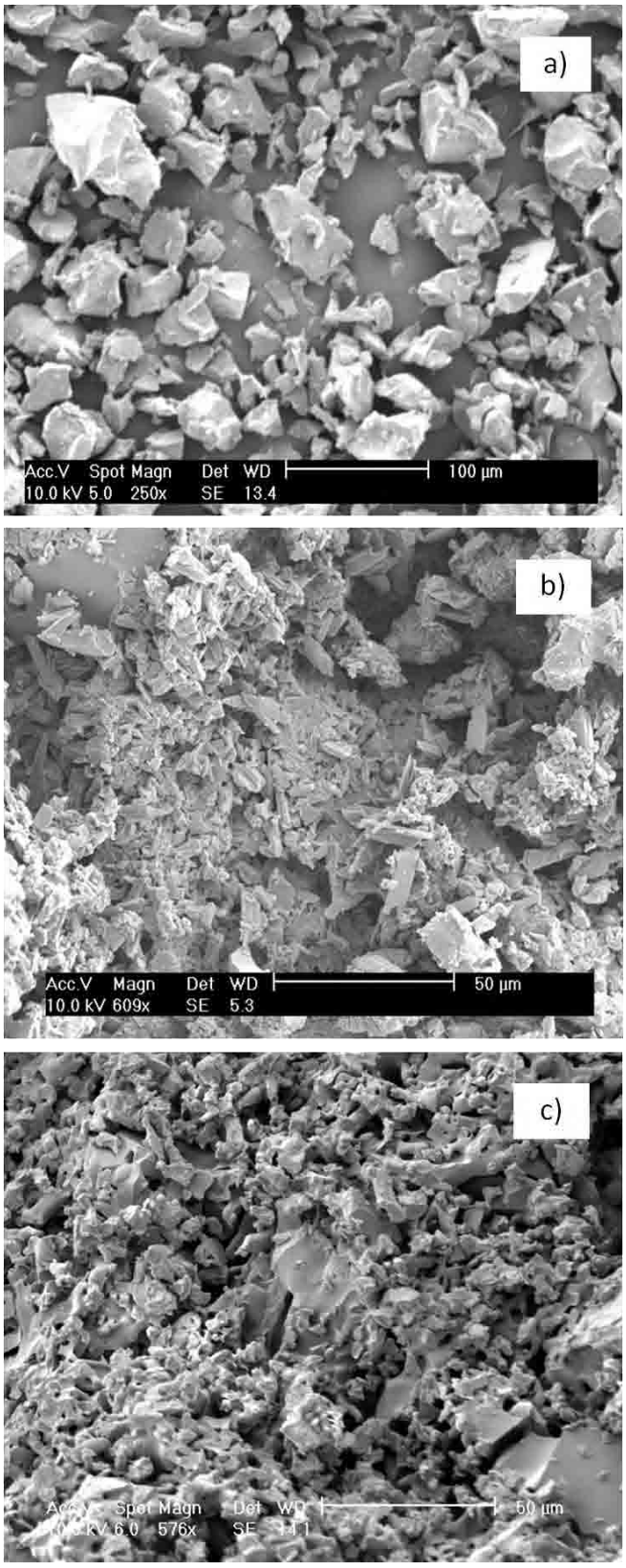

Figure 8.5: Scanning electron micrograph of a) β-TCP particles, b) brushite based cement (P:L = 3.0 g/mL) and c) $Ca_2P_2O_7$ ceramic (P:L = 3.0 g/mL) sintered at 1200°C for 5 h.

Table 8.1: Effect of sintering time on the compressive strength porosity and volumetric change of $Ca_2P_2O_7$ ceramic sintered at 1200°C and P:L 3.0 g/mL.

Time (h)	Compressive Strength (MPa)	Standard Deviation	Porosity (%)	Standard Deviation
3	9.6	1.9	22	3
5	11.1	1.8	30	2
8	9.9	2.8	21	3
10	9.5	1.9	20	2

8.2.2.2. Sintering temperature

Effect of sintering temperature on the specific surface area of $Ca_2P_2O_7$ ceramic

In general, ceramic densification increases as the sintering temperature is increased (German, 2001). The SSA of a ceramic is affected by sintering temperature and it is an important factor in the degradation of the ceramic (Barralet et al., 2002). The particles of the brushite crystals are irregularly shaped and between 10 – 30 μm in diameter (Figure 8.6a). As the brushite cement is sintered, neck formation occurs by mass transfer via solid state diffusion between contacting particles (Figure 8.6b, 8.6c, 8.6d and 8.6e). As the sintering temperature is increased more particles become diffused and the neck formed grows which results in crystallite growth (Figure 8.6b, 8.6c, 8.6d and 8.6e). The pore spaces between the particles also decreased with increasing sintering temperature; ceramics sintered at 400°C (Figure 8.6b) were compared with those at 1200°C (Figure 8.6e). The reduction in pore space might not be obvious from the SEM in figure 8.6 but the porosity was reduced from 44 ± 2% (400°C) to 32 ± 6% (1200°C). The reduction in porosity was of statistical significance ($P < 0.05$).

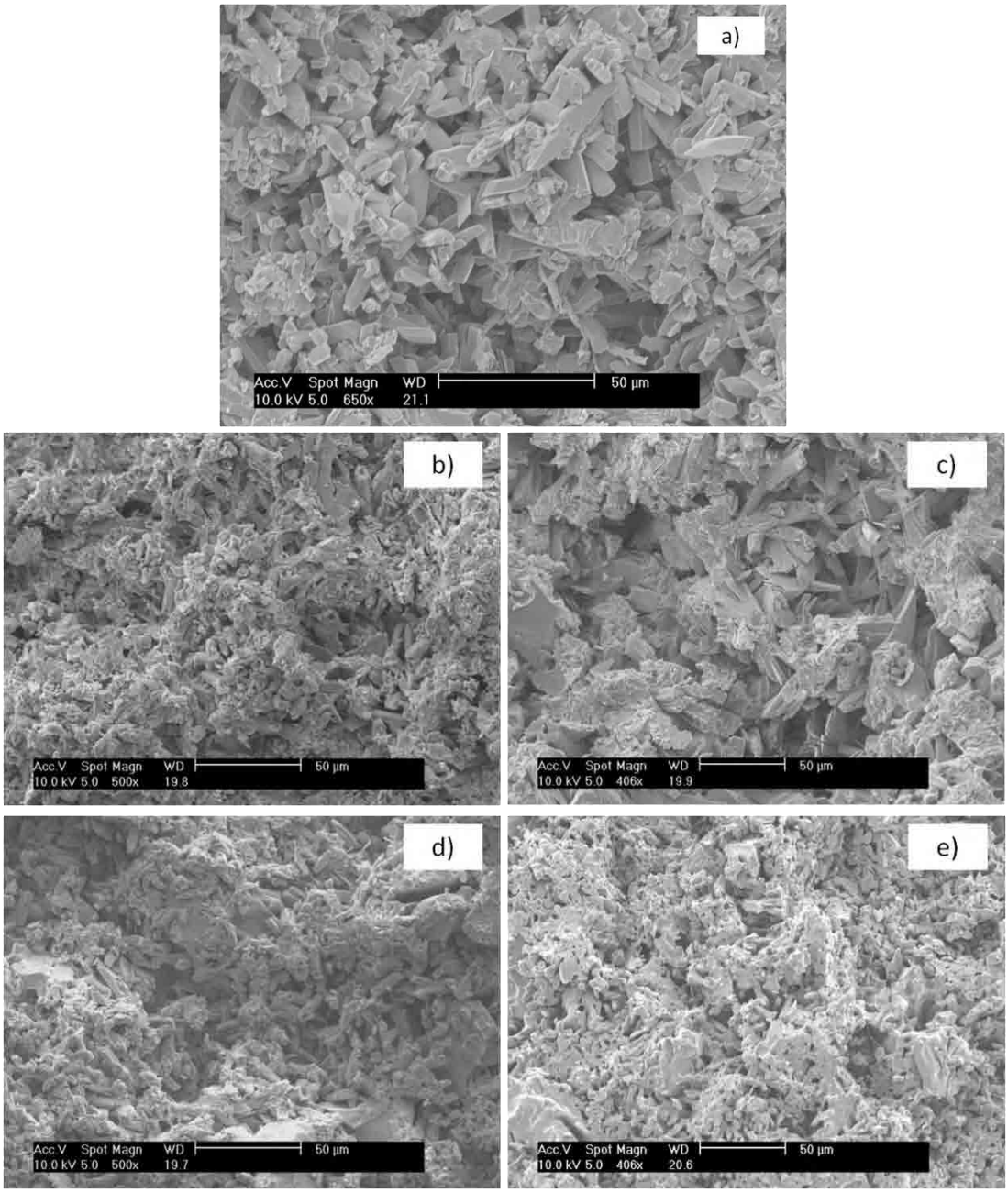

Figure 8.6: Scanning electron micrograph of a) brushite cement (P:L = 1.5 g/mL) and $Ca_2P_2O_7$ ceramic sintered at b) 400°C, c) 700°C, d) 1000°C and e) 1200°C.

The decrease in pore size i.e. ceramic densification leads to increased compressive strength as seen in figure 8.7. Increasing the sintering temperature also led to a decrease in the SSA of the sintered ceramic (Figure 8.7). The SSA could also be affected by the surface roughness of the sintered ceramic although not measured here. The SSA at each sintering temperature is the average SSA data obtained from

three samples collected from nitrogen BET (Tristar Gemini, Micrometrics). Although not measured here the SSA of $Ca_2P_2O_7$ ceramic is expected to decrease with increased sintering temperature irrespective of the P:L ratio.

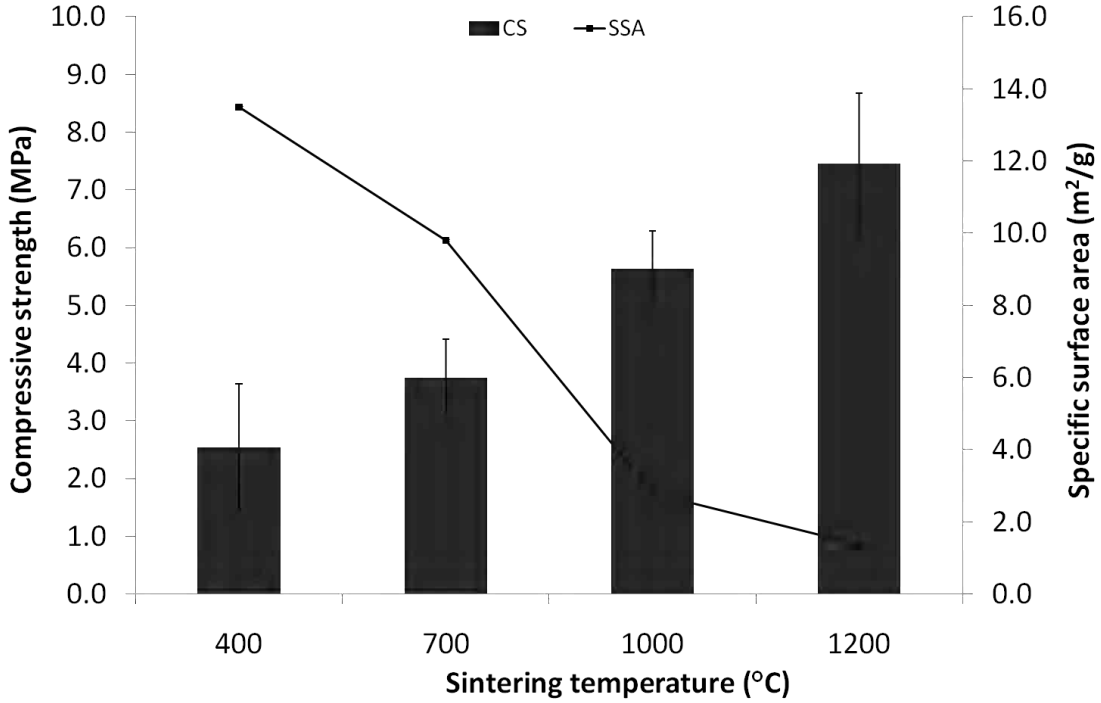

Figure 8.7: Effect of sintering temperature on the specific surface area (SSA) of and compressive strength (CS) of the sintered $Ca_2P_2O_7$ ceramic (P:L = 1.5 g/mL). The error bars on the SSA graph is very small. It is the standard deviation of three data obtained at each sintering temperature.

Although the experiments carried out so far involved ceramics at P:L 1.25 and 1.5 g/mL, further experiments involved increasing the P:L ratio of the sintered ceramic so as to optimise the properties of the ceramic with respect to porosity and compressive strength. This would provide a wider range of clinical applications for the $Ca_2P_2O_7$ ceramic.

Effect of sintering temperature on porosity and compressive strength

$Ca_2P_2O_7$ ceramic is studied for its possible application as a bone replacement material therefore its compressive strength is an important parameter in determining its suitability. The compressive strength of cancellous bone has been reported over a wide range between 0.5 – 50 MPa (Lawson and Czernuszka, 1998). Therefore in other to provide a clinical application for the formulated $Ca_2P_2O_7$ ceramic the compressive strength should also be within the range of the cancellous bone. As the P:L ratio was increased the compressive strengths increased (Figure 8.7, 8.8 and 8.10). The compressive strength of $Ca_2P_2O_7$ ceramic increased from 5.0 ± 0.7 MPa at 400°C to 8.8 ± 2.1 MPa at 1000°C (Figure 8.8).

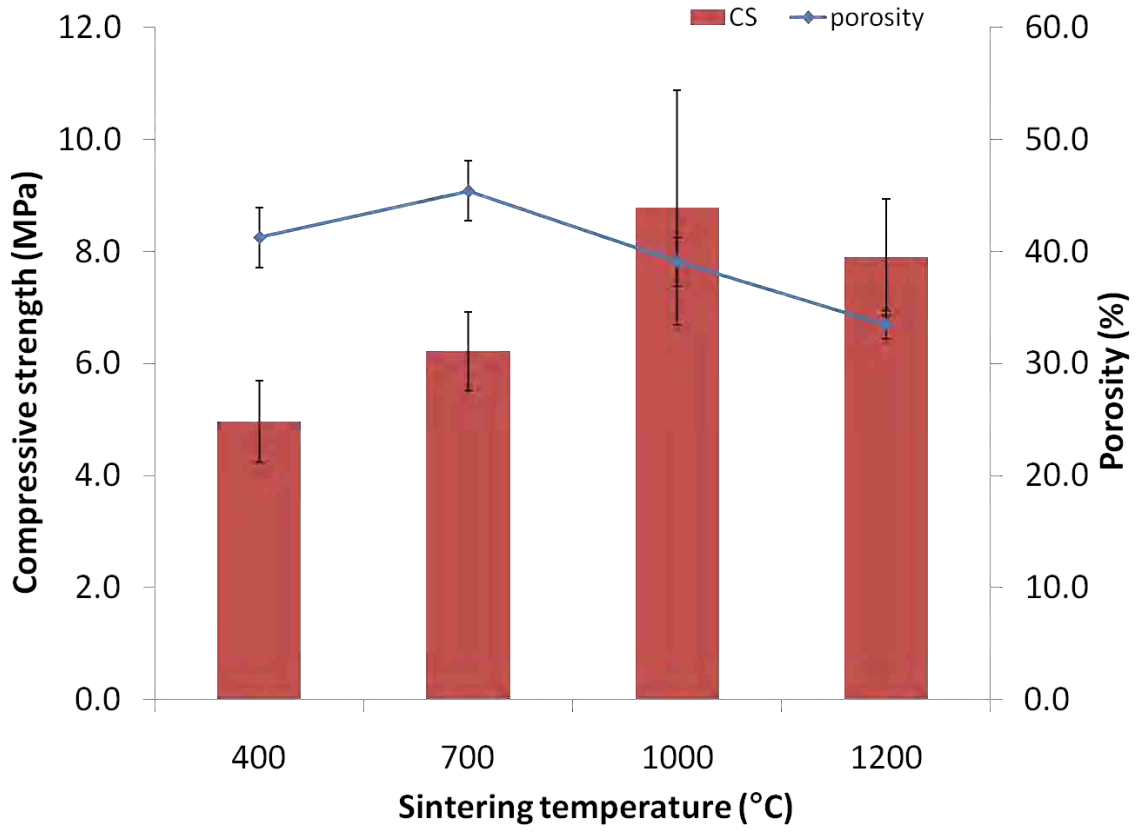

Figure 8.8: Effect of sintering temperature on the porosity and compressive strength of $Ca_2P_2O_7$ ceramic at P:L 2.0 g/mL.

This change was of statistical significance ($P \leq 0.05$). The increase in sintering temperature results in increased particle densification (Figure 8.12). Further increase in sintering temperature to 1200°C resulted in the compressive strength reducing to 7.9 ± 1.0 MPa (Figure 8.8). The decrease in compressive strength when the sintering temperature was increased from 1000°C to 1200°C was statistically insignificant ($P = 0.251$). This decrease in compressive strength from 8.8 ± 2.1 MPa to 7.9 ± 1.0 MPa is associated with the presence of microcracks at 1200°C possibly as a result of tetragonal to monoclinic phase transformation (Figure 8.9).

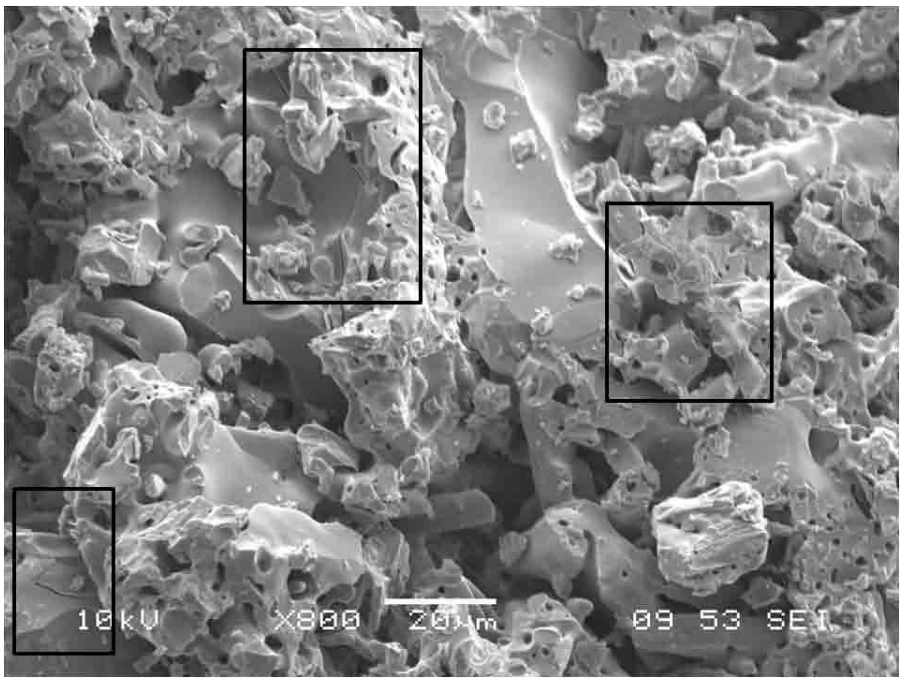

Figure 8.9: Scanning electron micrograph showing the presence of microcracks in $Ca_2P_2O_7$ ceramic when sintered at 1200°C (P:L = 2.0 g/mL).

The porosity of $Ca_2P_2O_7$ ceramic was 45 ± 3% when sintered at 700°C and this reduced to 34 ± 1% when it was sintered at 1200°C (Figure 8.8). The reduction in porosity was of statistical significance ($P \leq 0.05$) and the increase in porosity from 42 ± 3% at 400°C to 45 ± 3% at 700°C was also statistically significant ($P = 0.009$) (Figure 8.8). Irrespective of the increase in P:L ratio the trend observed with compressive strength and porosity over the range of sintering temperature was the same (Figure 8.10). Porosity was found to decrease from 32 ± 2% at 400°C to 23 ± 3% at 1200°C at P:L ratio of 2.5 g/mL (Figure 8.10a). The compressive strength was also increased from 6.9 ± 1.4 MPa to 9.5 ± 1.2 MPa over 400 – 1200°C (Figure 8.10a). The decrease in porosity and increase in compressive strength for the ceramic at P:L of 2.5 g/mL was of statistical significance. Overall the compressive strength of $Ca_2P_2O_7$ ceramic was highest at P:L ratio of 3.0 g/mL (Figure 8.10b). At P:L ratio of 3.0 g/mL the porosity decreased from 33 ± 2% at 400°C to 30 ± 2% at 1200°C (Figure 8.10b). The compressive strength increased significantly from 8.3 ± 1.3 MPa to 11.1 from ± 1.3 MPa over the same temperature range (Figure 8.10b).

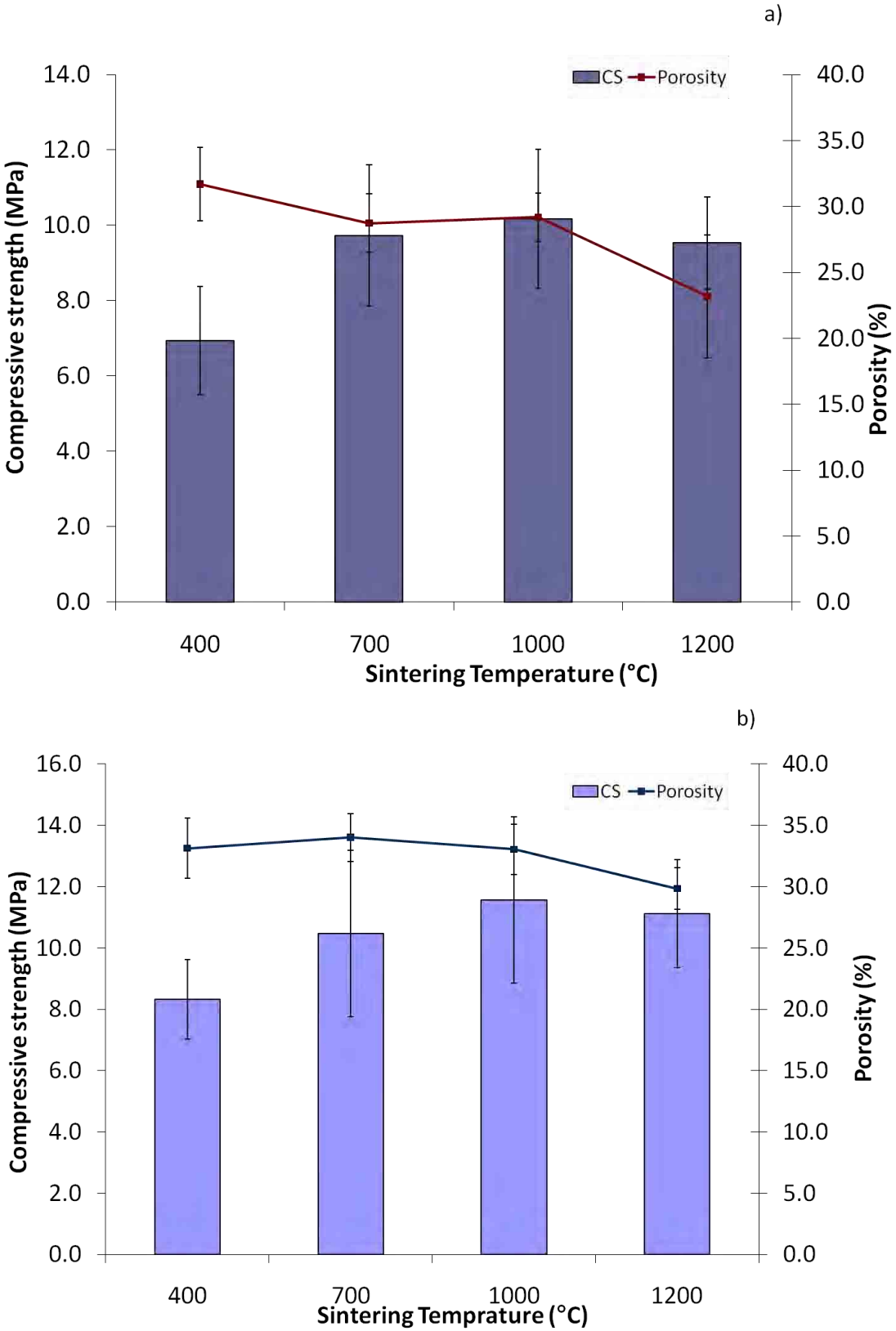

Figure 8.10: Effect of sintering temperature on the porosity and compressive strength of $Ca_2P_2O_7$ ceramic at a) P:L 2.5 g/mL and b) P:L 3.0 g/mL.

Effect of sintering temperature on mass loss and volumetric shrinkage

In the case of materials processed at high temperatures it is important to be able to predict the shrinkage to the $Ca_2P_2O_7$ ceramic to produce graft replacement of a defined size. As sintering temperature is increased the crystals present within the ceramic matrix grow and the pores within the crystals decrease therefore the ceramic shrinks in volume. Figure 8.11a shows that the volumetric shrinkage of the ceramic increased significantly from 3 ± 1% (400°C) to 14 ± 1% (1200°C). At temperatures greater than 400°C brushite was converted to $Ca_2P_2O_7$ and there was no other chemical change within the ceramic over the sintering regime except phase changes. Therefore the mass loss from the ceramic is expected to be unchanged with increasing sintering temperature. There was a little increase in mass loss as shown in figure 8.11b from 16.0 ± 0% at 400°C to 18.0 ± 1% when brushite cement was sintered at 1200°C. The volumetric shrinkage could also be linked to the ceramic densification which also could influence the compressive strength of the sintered ceramic (Figure 8.12).

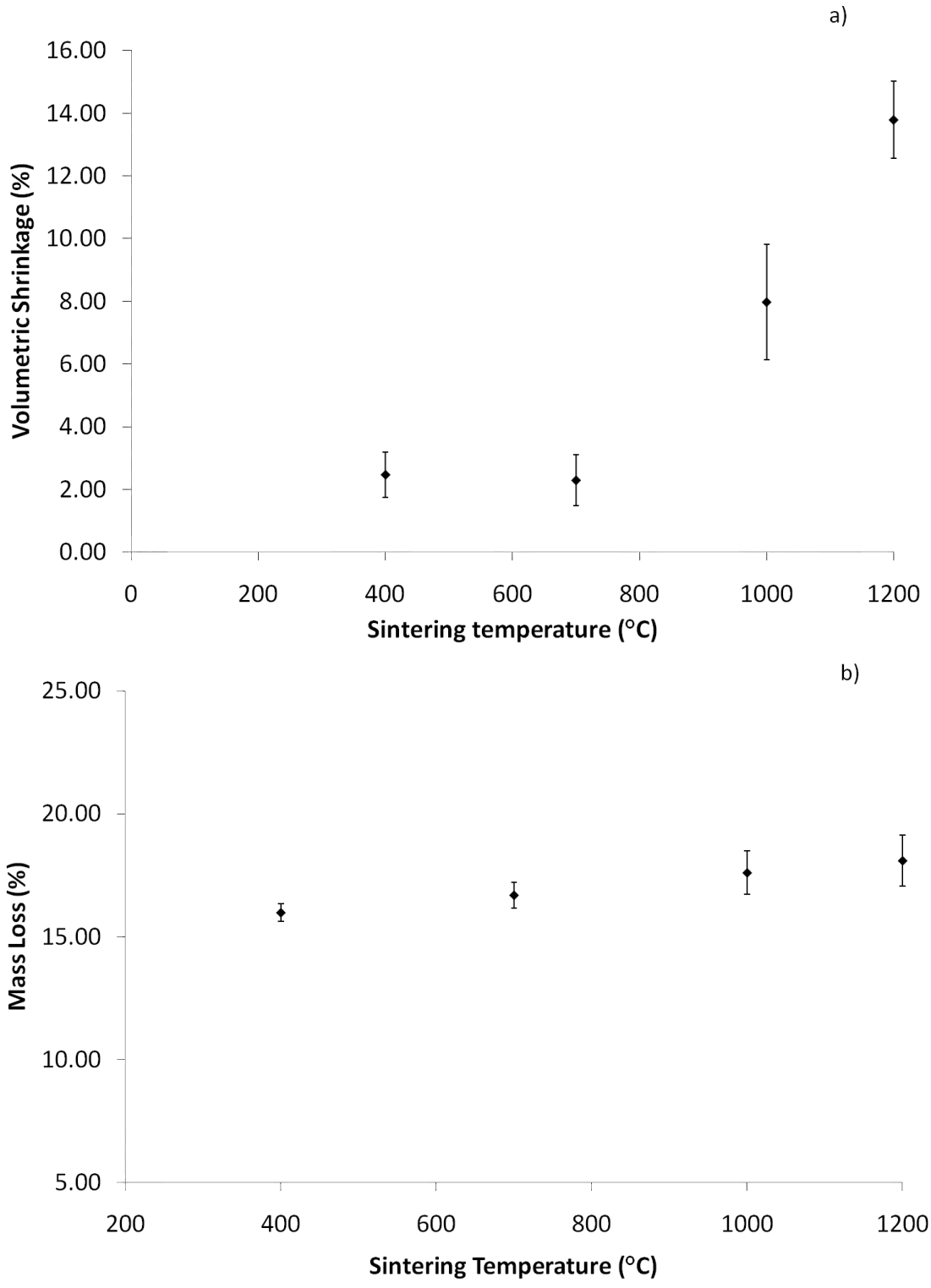

Figure 8.11: The effect of varying sintering temperature on a) volumetric shrinkage and b) mass loss of $Ca_2P_2O_7$ ceramic at P:L 2.0 g/mL.

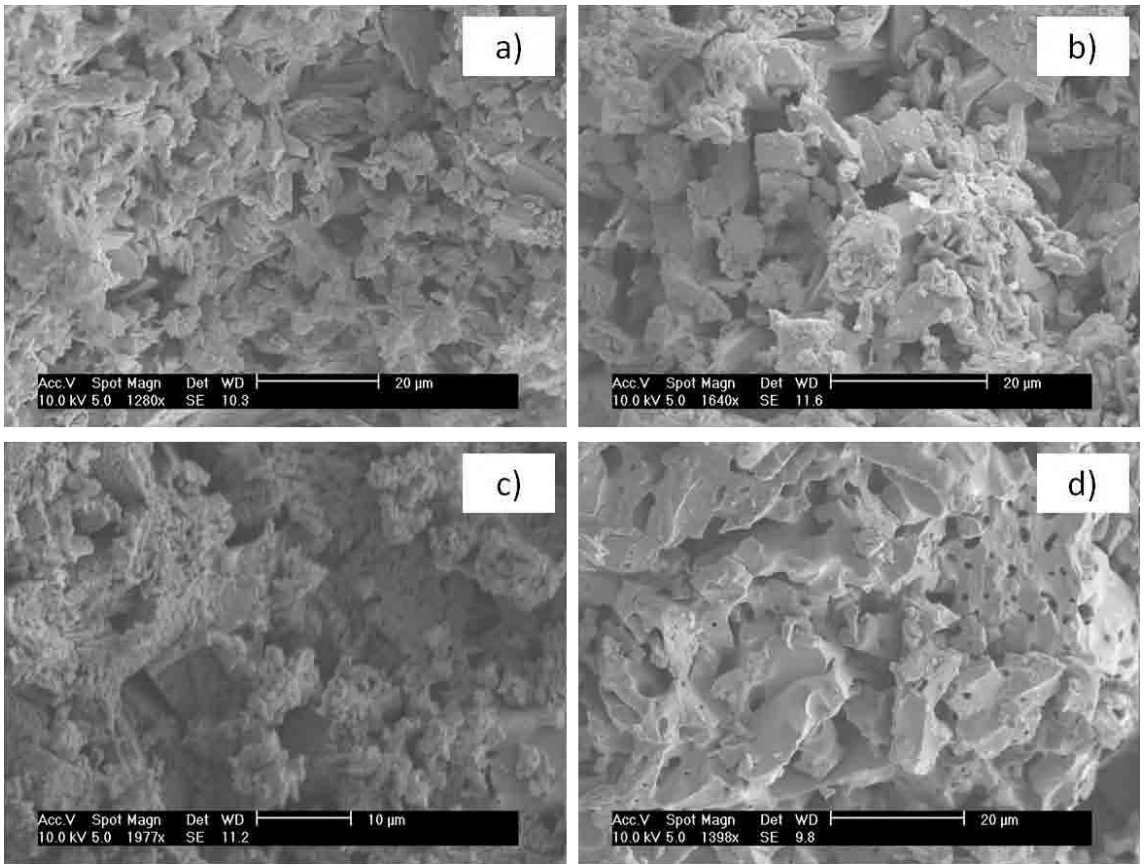

Figure 8.12: SEM micrographs showing the change in ceramic densification with temperature. Ceramic at P:L 2.5 g/mL was sintered at a) 400°C, b) 700°C, c) 1000°C and 1200°C.

8.2.3. Effect of varying cement composition

The relative quantities of brushite and β-TCP crystals varied depending on the H_3PO_4 acid concentration and P:L ratio. This section describes the effect of varying cement composition on mass loss, volumetric shrinkage, compressive strength and porosity of the sintered ceramic.

8.2.3.1. Increasing acid concentration

As H_3PO_4 acid concentration is increased the proportion of brushite present within the cement is increased as shown in table 8.2.

Table 8.2: Relative composition of brushite and β-TCP crystals present within brushite cement with increase in acid concentration.

Acid Concentration (M)	**$CaHPO_4.2H_2O$ (% wt)**	**β- TCP (% wt)**
1.5	43	57
2.5	64	36
3.5	81	19
4.5	96	4

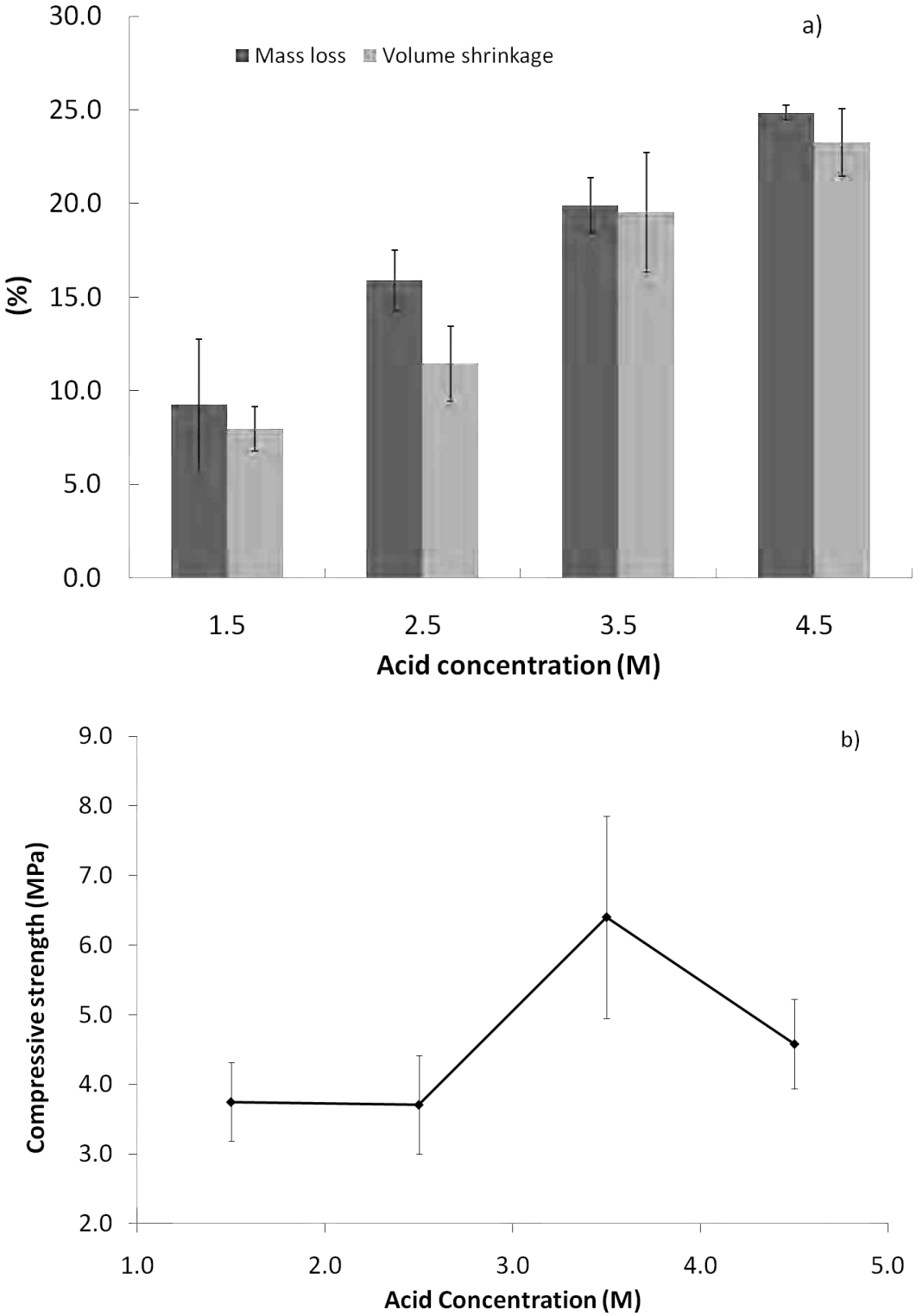

Figure 8.13: Effect of acid concentration on a) volumetric shrinkage and mass loss and b) compressive strength of $Ca_2P_2O_7$ sintered ceramic at 1200°C and P:L 1.5 g/mL.

As the acid concentration was increased from 1.5 M to 4.5 M the amount of brushite also increased from 43% to 96% (Table 8.2). Therefore the amount of water of crystallisation removed from the brushite crystals was increased leading to an increase in mass loss from the cement (Figure 8.13a). The mass loss increased from 9 ± 4% (1.5 M) to 25% (4.5 M). The increase in the proportion of brushite led to an increased proportion of $Ca_2P_2O_7$ so that crystal densification and growth increase with increasing acid concentration. This led to increase in volumetric shrinkage as seen in figure 8.13a. Compressive strength was found to be highest when brushite cement was prepared with 3.5 M H_3PO_4 acid (Figure 8.13b). As acid concentration is increased cement setting times reduce, this makes cement handling difficult. Therefore voids may form within the cement matrix at high acid concentrations leading to the reduction in compressive strength. The compressive strength reduced from 6.4 ± 1.5 MPa at 3.5 M to 4.6 ± 0.6 MPa at 4.5 M (Figure 8.13b). The reduction in compressive strength was of statistical significance ($P \leq 0.05$).

8.2.3.2. Increasing P:L ratio

The ratio of β-TCP to H_3PO_4 acid mixed was varied from 1.25 – 3.0 g/mL. At P:L ratio of 1.25 g/mL the phase composition of $Ca_2P_2O_7$ ceramic sintered at 1200°C was determined by means of Rietveld refinement phase analysis. The Rietveld plot shown in figure 8.14 showed that the ceramic contained 79 wt% α-$Ca_2P_2O_7$ and 21 wt% β-TCP. The bottom line on the Rietveld plot (Figure 8.14) is termed the difference plot which shows the difference between the calculated and observed pattern. The bottom line deviates very little from -1.0×10^2 counts indicating that there was a good agreement between the calculated and observed pattern. The Rietveld plot confirmed

that β-TCP is present in excess and the reaction occurs in accordance with equation 8.9.

$$2Ca_3(PO_4)_2 + H_3PO_4 + 6H_2O \rightarrow 3CaHPO_4.2H_2O + Ca_3(PO_4)_2 \ldots (8.9)$$

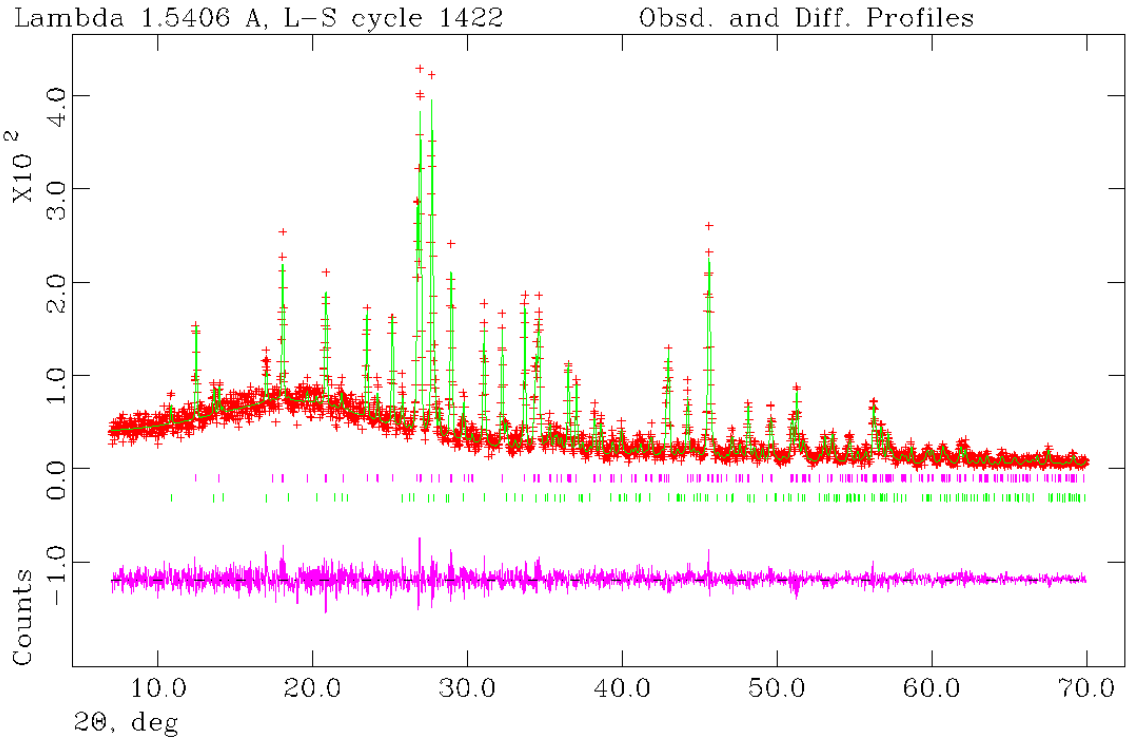

Figure 8.14: Rietveld plot of $Ca_2P_2O_7$ ceramic (P:L = 1.25 g/mL) sintered at 1200°C.

Table 8.3 shows the calculated relative quantities of β-TCP and $Ca_2P_2O_7$ after sintering at 1200°C. The β-TCP content of the ceramic increased from 16 wt% to 45 wt% as the P:L ratio was increased from 1.5 g/mL to 3.0 g/mL (Table 8.3). Compressive strength of the sintered ceramic increased with increase in P:L ratio (Table 8.3). The increase in compressive strength from 6.7 ± 0.8 MPa at a P:L of 1.25 g/mL to 11.4 ± 1.7 MPa at a P:L of 3.00 g/mL was of statistical significance (P = 0.000). The porosity was lowest at P:L ratio of 2.5 g/mL (24%) (Table 8.3). The

difference in porosity at P:L of 1.25, 1.5, 2.0 and 3.0 g/mL was not statistically significance (P = 0.137).

Table 8.3: Effect of P:L ratio on the porosity and compressive strength of $Ca_2P_2O_7$ ceramic sintered at 1200°C.

P:L Ratio	**Phase Composition**		**Porosity**		**Compressive Strength**	
	β-TCP (wt ± 2) %	$Ca_2P_2O_7$ (wt ± 2) %	(%)	Standard Deviation	(MPa)	Standard Deviation
1.25	7	93	33	4	6.7	0.8
1.50	16	84	32	6	7.5	1.4
2.00	25	75	33	1	8.2	0.5
2.50	31	69	25	3	9.7	1.2
3.00	45	55	30	2	11.4	1.7

The volumetric shrinkage and mass loss from the sintered ceramic decreases with increase in P:L ratio (Figure 8.15). According to equation 8.9 water molecule is in excess and the amount present within the cement matrix reduces with increasing P:L ratio. Therefore the mass loss from the ceramic reduces from 24 ± 1% at P:L = 1.25 g/mL to 12 ± 1% at P:L = 3.0 g/mL. As P:L ratio is increased the amount of β-TCP and brushite crystals present within the ceramic matrix is increased therefore the volumetric shrinkage that occurs with crystal growth is reduced. Volume shrinkage reduced from 27 ± 3% at P:L 1.25 g/mL to 10 ± 1% at P:L 3.0 g/mL (Figure 8.15).

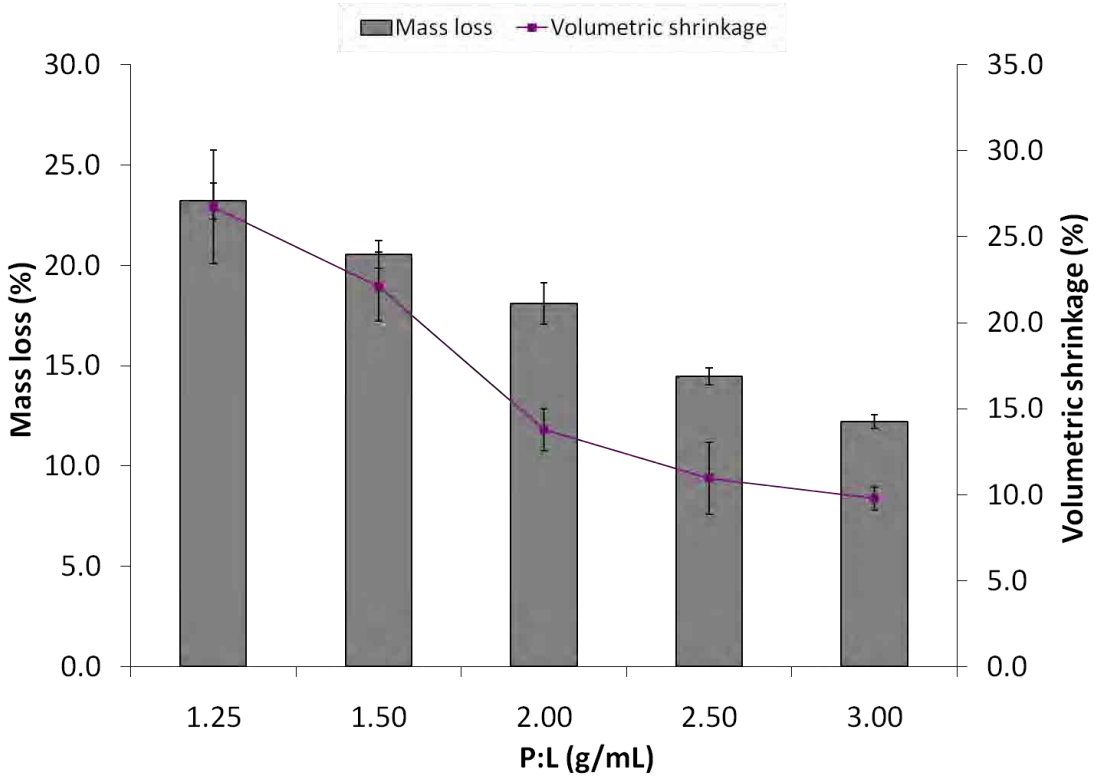

Figure 8.15: Effect of P:L on the mass loss and volumetric shrinkage of $Ca_2P_2O_7$ ceramic at 1200°C.

8.2.4. Degradation profile of $Ca_2P_2O_7$ ceramic

This section investigates the degradation of $Ca_2P_2O_7$ ceramic in the presence of ALP and other proteins present in serum. The ceramics were aged over a period of time and the mass of the ceramic was measured daily from which the mass loss as a percentage of the original was calculated. In other to observe the effect of SSA on the degradation of the sintered ceramics the sintering temperature and P:L ratio were varied. Enzyme concentration was also varied to observe any effect it had on $Ca_2P_2O_7$ ceramic degradation. The degradation of brushite and $Ca_2P_2O_7$ ceramic was also compared in the same ageing solution.

8.2.4.1. Degradation in ALP solution

Standard sized ceramics (height = 12 mm and diameter = 6 mm) were shown to degrade faster in ALP containing solution than in Tris HCl control solution (Figure 8.16). Figure 8.16 shows that 41 wt% of the original ceramic degraded in 75 U of ALP and 48 wt% in 10 U ALP solution while 18 wt% of the original ceramic degraded in 20 mL Tris HCl solution and only 5 wt% in 40 mL Tris HCl solution over the same ageing period. The increase in ALP concentration from 10 U to 75 U did not produce an increase in the mass of $Ca_2P_2O_7$ ceramic which degraded.

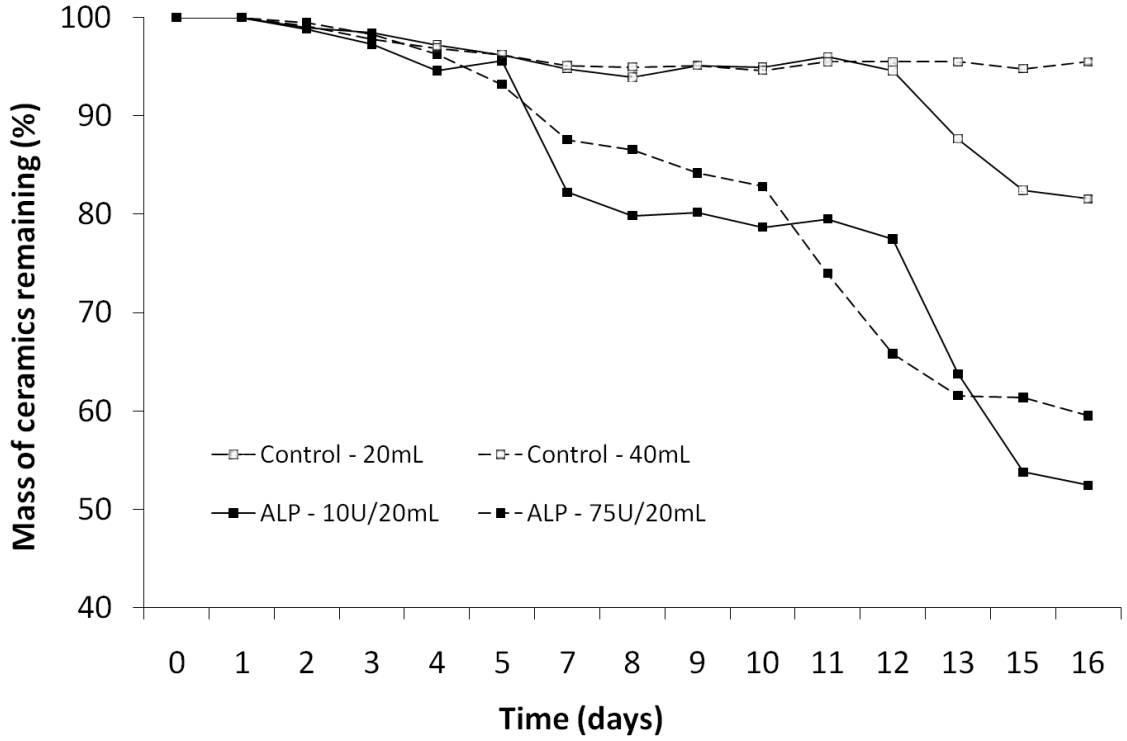

Figure 8.16: Degradation of $Ca_2P_2O_7$ ceramic of P:L of 1.25 g/mL and sintered at 1200°C in 10 U, 75 U and control solution over 16 days.

The degradation of ceramics at P:L ratio of 1.5 g/mL was studied due to the increased compressive strength (Table 8.3). Figure 8.17 shows that 8 wt% of the original $Ca_2P_2O_7$ ceramic degraded in control solution but only 5 wt% of the original ceramic degraded in 15 U and 75 U ALP solutions. Increasing ALP concentration

did not produce an increase in the mass of ceramic which degraded in solution. As it was not possible to increase ALP concentration significantly the ceramics were then degraded in serum which is expected to contain pyrophosphatase that might enhance ceramic degradation. For the control experiment the brushite cement and $Ca_2P_2O_7$ ceramic was degraded in phosphate buffered saline (PBS) solution.

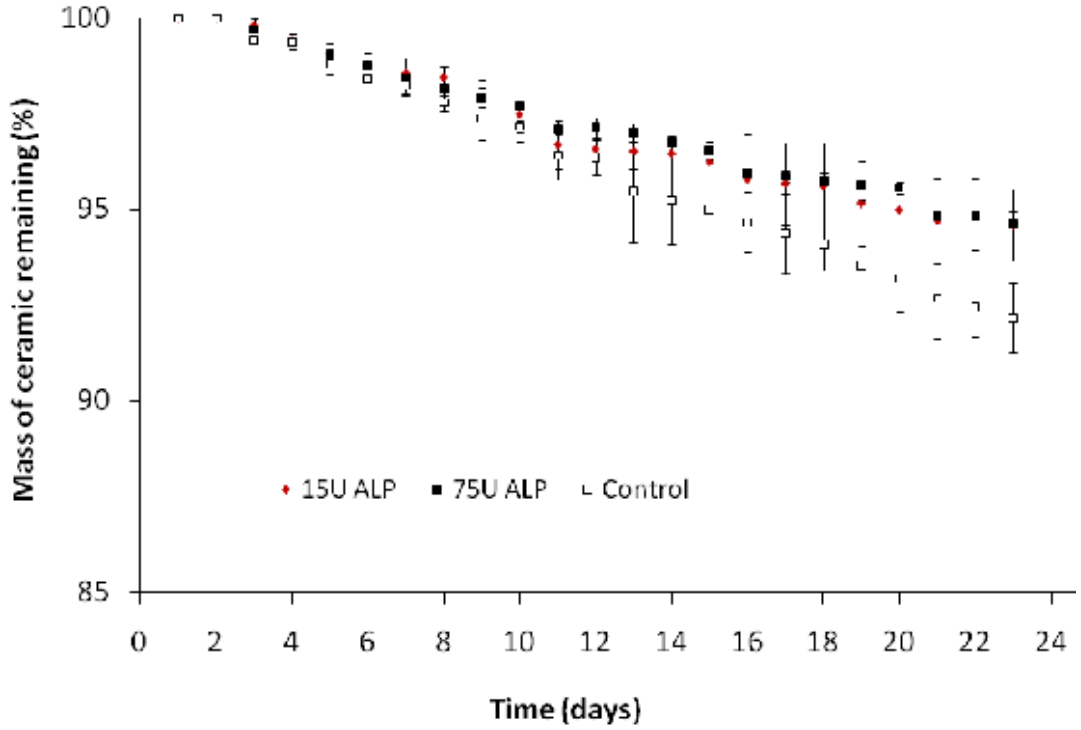

Figure 8.17: Degradation profile of $Ca_2P_2O_7$ ceramic of P:L 1.5 g/mL and sintered at 1200°C in the presence of ALP over 24 days.

8.2.4.2. Degradation in foetal bovine serum solution (serum)

To carry out further degradation experiments, $Ca_2P_2O_7$ ceramics were aged in serum since further increase in the concentration of ALP was found to have no effect (Figure 8.17). Rather than increase the concentration of ALP significantly serum which is cheaper and thought to contain enzymes with pyrophosphatase activity was used. Due to the increased compressive strength ceramics sintered at 1200°C with P:L 3.0 g/mL (Figure 8.10b) were used. The ceramic was degraded over 26 days in

serum and as a negative control brushite cement at the same P:L ratio was degraded in serum and PBS solution. Over a period of 26 days 38 wt% of the original brushite cement was degraded in serum and 14 wt% of the original brushite cement degraded in PBS solution (Figure 8.18). The increased degradation of brushite cement in serum than in PBS solution follows that previously reported by Grover et al. (Grover et al., 2003). Brushite is more soluble than HA in physiological condition, therefore apatite formation within brushite cement decreases the cement degradation (Theiss et al., 2005). Apatite formation within brushite cement is inhibited by serum therefore the brushite cement degrades at a normal rate (Grover et al., 2003). Only 3 wt% of the original sintered $Ca_2P_2O_7$ ceramic degraded in serum (Figure 8.18). The slow degradation of $Ca_2P_2O_7$ ceramic was surprising as the presence of proteins and enzymes such as pyrophosphatases were expected to enhance degradation.

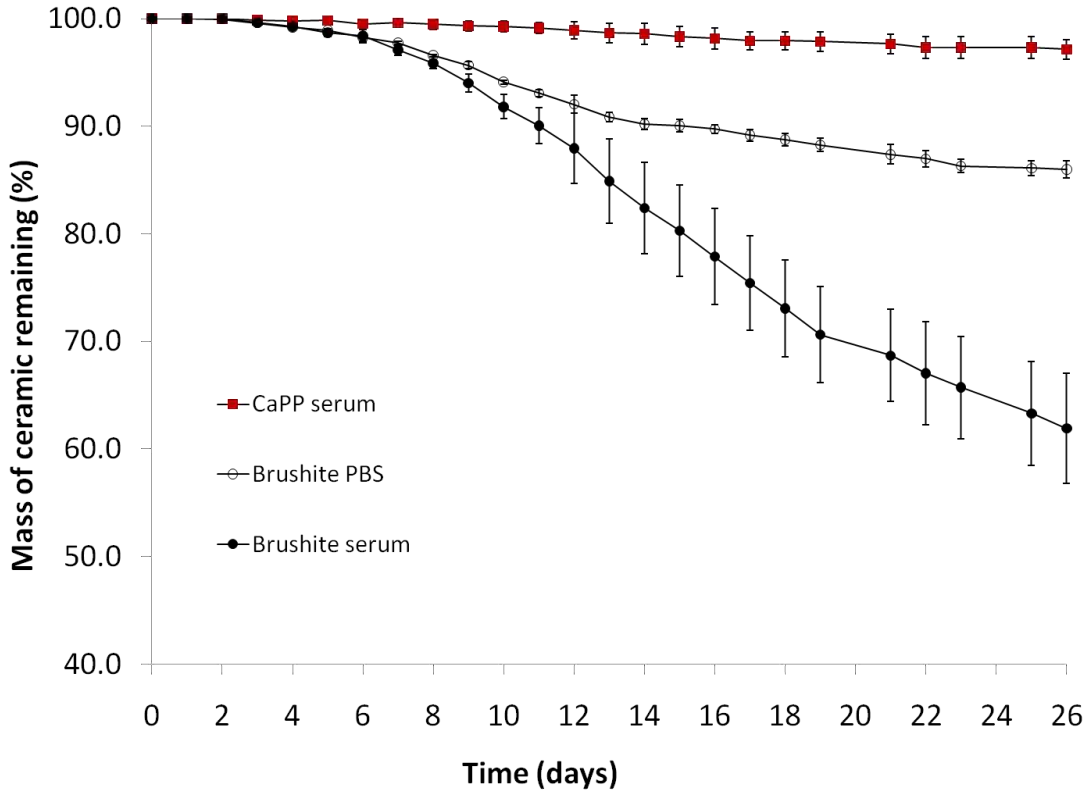

Figure 8.18: Degradation profile of brushite cement and $Ca_2P_2O_7$ ceramic at P:L 3.0 g/mL and 1200°C in foetal bovine serum (serum) for 26 days at 37°C.

The SSA of brushite cement at 3.0 g/mL is 1.013 ± 0.122 m^2/g whereas that of $Ca_2P_2O_7$ ceramic at 1200°C and 3.0 g/mL is 0.318 ± 0.002 m^2/g. The porosity of the brushite cement is 21 ± 1% while that of the $Ca_2P_2O_7$ ceramic is 30 ± 2% illustrating the significant effect SSA has on the rate of materials degradation in comparison to porosity. The sintering temperature and P:L ratio of $Ca_2P_2O_7$ ceramic was reduced to 400°C from 1200°C and to 2.5 g/mL from 3.0 g/mL respectively. These changes produced a significant increase in SSA from 0.318 ± 0.002 m^2/g to 8.658 ± 0.847 m^2/g whereas the porosity increased only slightly from 30 ± 2% to 32 ± 2% a change that was statistically insignificant. 21 wt% of the $Ca_2P_2O_7$ ceramic (P:L = 2.5 g/mL) sintered at 400°C degraded in serum while 50 wt% degraded in PBS solution over 28 days (Figure 8.19).

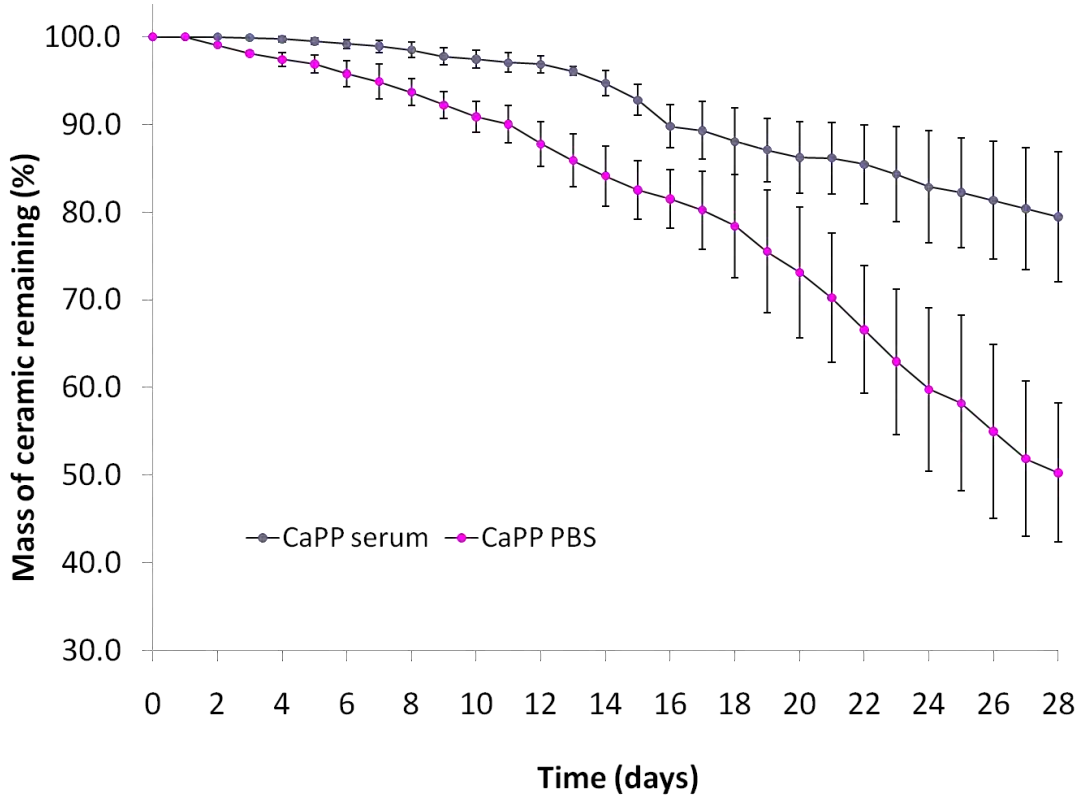

Figure 8.19: Degradation of $Ca_2P_2O_7$ ceramic sintered at 400°C with a P:L of 2.5 g/mL in serum and PBS solution.

At P:L ratio of 2.5 g/mL the microstructure of $Ca_2P_2O_7$ ceramic sintered at 400°C shows that the particles are fused together but the particles are visible and the large pore structure would enable the degradation to proceed easily (Figure 8.20a). The degradation was slowest when the P:L ratio was increased to 3.0 g/mL and the sintering temperature was increased to 1200°C. The microstructure of the ceramic shows that the neck formed during sintering are tightly fused and the pores are reduced making it very difficult for small particles to be released from the ceramic matrix (Figure 8.20b).

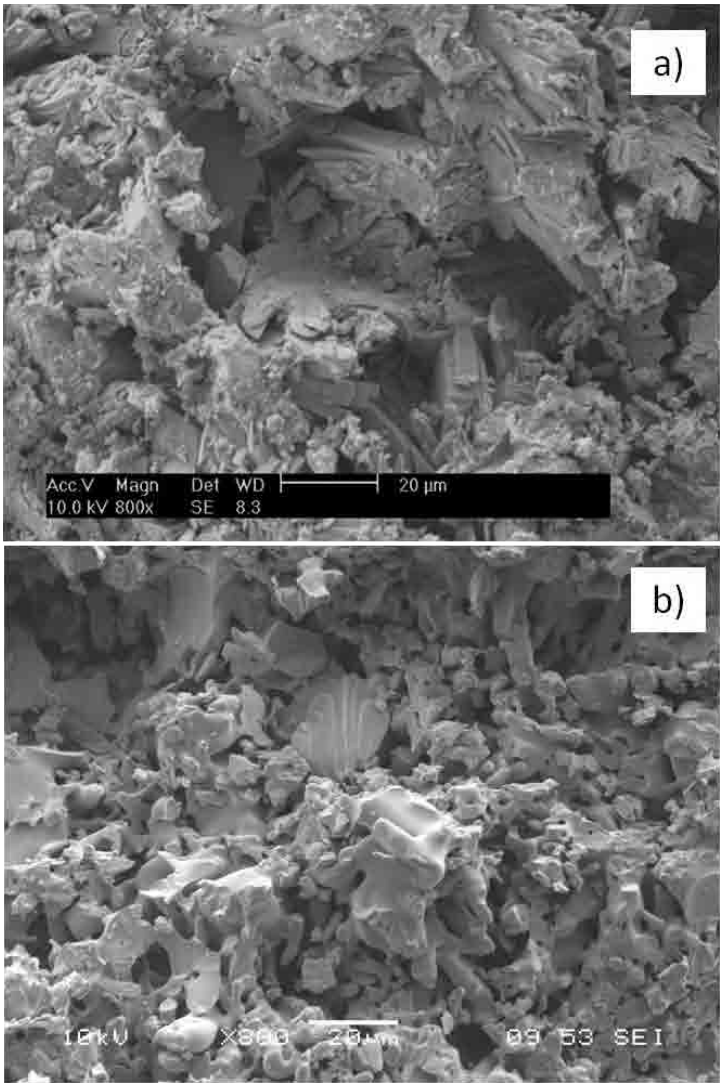

Figure 8.20: Microstructure of a) sintered $Ca_2P_2O_7$ ceramic (P:L = 2.5 g/mL, 400°C) and b) sintered $Ca_2P_2O_7$ ceramic (P:L = 3.0 g/mL, 1200°C).

8.3. DISCUSSION

8.3.1. Ceramic characterisation

Brushite cement was heat treated to temperatures ≥ 400°C to form $Ca_2P_2O_7$ ceramic. The formation of $Ca_2P_2O_7$ occurred in two stages (i) the dehydration of brushite to form monetite and (ii) the condensation of monetite to form $Ca_2P_2O_7$ (equations 8.10b and 8.10c). The dehydration of brushite to form monetite occurs at temperatures ≥ 55°C (Grover et al., 2005; Safronova et al., 2007). The XRD and DTA analysis showed that this reaction takes place at about 100°C and goes to completion at 200°C (Figures 8.2 and 8.4). Assuming the cement setting reaction was in accordance with equation 8.7a using an acid concentration of 3.5M the matrix should consist of 92 wt% brushite and 8 wt% unreacted β-TCP. Based on this the theoretical weight loss following heating to 200°C should be 19 wt%.

$$\beta - Ca_3(PO_4)_2 + H_3PO_4 + 6H_2O \rightarrow 3CaHPO_4.2H_2O \ldots (8.10a)$$

$$CaHPO_4.2H_2O \rightarrow CaHPO_4 + 2H_2O \uparrow \ldots (8.10b)$$

The observed weight loss using the data from the DTA analysis was about 12 wt%, the inconsistency between these two figures could be due to the cement setting reaction not going to completion. At 200 – 500°C all the monetite present was converted to γ-$Ca_2P_2O_7$ by a condensation reaction as illustrated in equation 8.10c. This conversion to γ-$Ca_2P_2O_7$ was confirmed by XRD, DTA and TGA results showing a weight loss of 6.3% between 200 – 400°C, this is in line with theoretical weight loss calculated to be 6%. Further phase changes occur within the ceramic at 550 – 1100°C converting γ-$Ca_2P_2O_7$ to β-$Ca_2P_2O_7$. The phase change from β-$Ca_2P_2O_7$ to α-$Ca_2P_2O_7$ occurs at 1200°C as confirmed by XRD (Figure 8.3) and Rietveld plot (Figure 8.14). These phase changes which occur when brushite is

heated in air is in line with that observed by Safronova et al. (Safronova et al., 2007). At temperatures above 1200°C a glass phase was formed within the ceramic which caused the material to melt and thus lose its shape (Gbureck et al., 2008).

$$2CaHPO_4 \rightarrow Ca_2P_2O_7 + H_2O \uparrow \ldots \text{(8.10c)}$$

There are three stages of sintering: initial, intermediate and final stage. Solid state sintering progresses along these stages as the sintering temperature is increased. The initial phase of sintering is associated with growth and formation of contact points (necks) between the particles of the compact cement/ceramic. The particles of $Ca_2P_2O_7$ ceramic were shown to contact and coalesce between 400 – 700°C (Figure 8.6b and 8.6c). As the sintering temperature is increased further the sintering enters the intermediate stage whereby the necks formed merge and shrink resulting in the formation of interconnected pores along the particle junctions. The microstructure of the ceramic sintered at 1000°C showed the sintering to be at the intermediate stage (Figure 8.6d). The final stage of sintering which occurs at 1200°C involves pore closure and further crystal densification (Figure 8.6e).

As discussed above the increase in sintering temperature results in the densification of the crystals and increased pore closure within the ceramic matrix therefore volumetric shrinkage is increased (Figure 8.11a and 8.12). The conversion of brushite to monetite and then $Ca_2P_2O_7$ were the only chemical reactions that occurred within the ceramic therefore so there was little mass loss as the sintering temperature was increased from 400 – 1200°C (Figure 8.11b). TGA analysis confirmed that there was little change in the weight of the ceramic 400°C (Figure 8.4). The SSA of $Ca_2P_2O_7$ at P:L ratio of 1.5 g/mL reduced with increasing sintering temperature. This

is due to larger particle size which as explained above occurs through crystal growth. The compressive strength increased from 2.5 ± 0.9 MPa to 7.5 ± 2.0 MPa over 400°C to 1200°C due to the reduction in pore sizes i.e. ceramic densification as the sintering temperature is increased (Figure 8.7).

For uniformly shaped and sized crystals the pore spacing is uniform therefore it is uniformly eliminated as the sintering temperature is increased (Figure 8.21a). For irregularly shaped and sized crystals the pore spacing would vary so that it is not uniformly eliminated with increase in sintering temperature (Figure 8.21b).

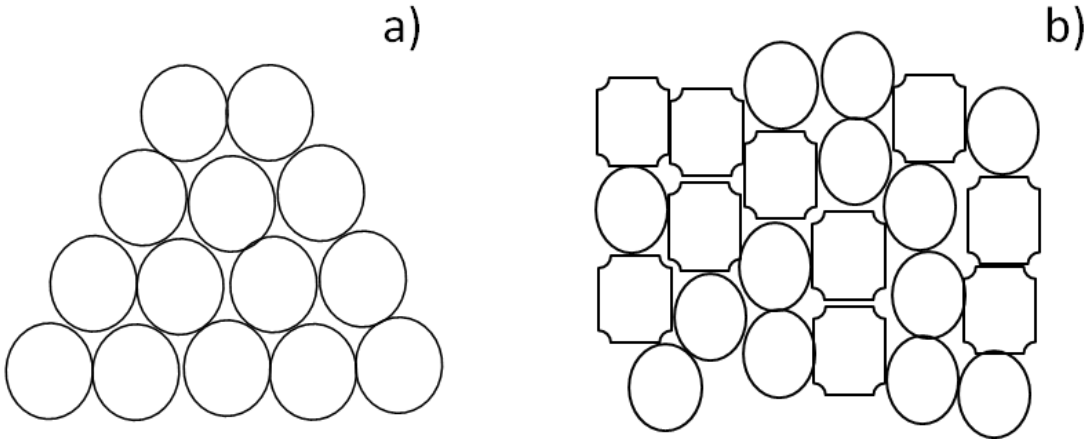

Figure 8.21: Schematic diagram showing the pore spaces between a) uniform crystals of the ceramic and b) crystals of different shape and size within the ceramic.

The uniformity of crystal shape and size also ensures that ceramic densification is increased with increased sintering time i.e. compressive strength should increase with increasing sintering time. Since $Ca_2P_2O_7$ ceramic consists of crystals with irregular shape and size (Figure 8.5) the pore spaces are not uniformly reduced therefore compressive strength did not increase with increase in sintering time (Table 8.1). The porosity of the post sintered $Ca_2P_2O_7$ ceramic did not reduce with increase in sintering time (Table 8.1). This is due to the competing effect of neck formation

and growth (pore formation/closure) which is affected by sintering temperature and crystal densification which is affected by sintering time.

Interestingly, although increasing sintering temperature from 400ºC to 1000ºC caused an increase in the mean compressive strength of the post-sintered ceramic; there was not a corresponding reduction in porosity (Figure 8.8 and 8.10). This is surprising since it is established that compressive strength is inversely proportional to porosity (equation 8.5). For ceramics with P:L ratio of 2.0 g/mL the increase in porosity when the sintering temperature was increased from 400°C to 700°C was statistical significant (Figure 8.8). The increase in porosity is due to the growth of 'neck' formed between the crystals of the ceramic creating larger pores. Further increase in sintering temperature resulted in further densification resulting in the reduction of porosity. For ceramics at P:L ratio of 2.5 and 3.0 g/mL any change in porosity between 400°C and 700°C was of no statistical significant (Figure 8.10). For all the ceramics at P:L 2.0, 2.5 and 3.0 g/mL the compressive strength increased with sintering temperature up to 1000°C (Figure 8.8 and 8.10). The reduction in compressive strength of $Ca_2P_2O_7$ ceramic sintered at 1200°C (Figure 8.8 and 8.10) could be the result of microcracks which were shown to be present within the ceramic matrix (Figures 8.9).

As P:L ratio is increased the amount of crystals present within the cement matrix increases therefore the pore spaces are reduced. This ensures that the pore closure within individual crystals is more uniform as the sintering temperature increases, therefore porosity is gradually reduced as sintering temperature is increased (Figure

8.12). The increase in the number of particles present within the ceramic matrix also ensures that as the crystals grow the volumetric shrinkage of the ceramic is reduced (Figure 8.15). As the P:L ratio of brushite cement is increased the β-TCP content within the cement is increased which means the brushite content reduces (Table 8.3). Therefore the corresponding $Ca_2P_2O_7$ content of the ceramic is reduced and the compressive strength of the ceramic reduced (Table 8.3) (Grover et al., 2003). The corresponding decrease in the amount of brushite present within the cement means that the water which is evaporated through condensation reactions (equation 8.2 and 8.3) is reduced. Therefore mass loss from the $Ca_2P_2O_7$ ceramic is reduced (Figure 8.15). Using equation 8.1, as H_3PO_4 acid concentration is increased the amount of brushite crystals present within the cement is increased (Table 8.3). This means that the amount of water evaporated from the brushite cement post sintering is increased from 9% (1.5 M H_3PO_4 acid) to 21% (4.5 M H_3PO_4 acid), therefore mass loss is increased (Figure 8.13a). The increase in brushite crystals means that the crystals become larger when sintered and the pores present are decreased leading to increase in the volumetric shrinkage of the ceramic.

8.3.2. Ceramic degradation

As noted with CPPD crystals, $Ca_2P_2O_7$ ceramic degradation was enhanced in the presence of ALP (Figure 8.16). The $Ca_2P_2O_7$ ceramic was structurally unstable over 16 days therefore smaller ceramic particles were easily released into solution and degraded into Ca^{2+} and $P_2O_7^{4-}$ ion. The $P_2O_7^{4-}$ ion is then hydrolysed by ALP thereby driving $Ca_2P_2O_7$ ceramic degradation further. Once the P:L ratio was increased from 1.25 – 1.5 g/mL the ceramic matrix became structurally stable in solution and the

effect of ALP was not realised (Figure 8.17). The structural stability of the ceramic at P:L of 1.5 g/mL ensured that smaller particles are not easily released into solution. Increasing the ALP concentration 8 fold did not enhance ceramic degradation confirming the assumption that ceramic degradation just as crystal dissolution did not take place through surface cleaving by ALP enzyme. By increasing the P:L ratio from 1.25 g/mL to 1.5 g/mL (sintering temperature was kept constant at 1200°C) the SSA was reduced from 0.347 m^2/g to 0.319 m^2/g (obtained from a single experiment). This shows that as the SSA in increased the mass of ceramic which degrades in ALP and control Tris HCl solution increases.

Brushite cement was found to degrade faster in serum than in PBS solution (Figure 8.18). This is due to serum inhibiting apatite formation within brushite cement as reported by Grover et al. (Grover et al., 2003). The mass percentage of $Ca_2P_2O_7$ ceramic (3 wt%) which degraded in serum was much lower than that of brushite cement (38 wt%) in the same solution and at the same P:L ratio. The porosity of the brushite cement (21 ± 1%) is lower than that of the calcium pyrophosphate ceramic (30 ± 2%) which was sintered at 1200°C. The SSA of brushite cement was measured as 1.013 ± 0.122 m^2/g but once it was sintered at 1200°C to form $Ca_2P_2O_7$ the SSA was reduced significantly to 0.318 ± 0.002 m^2/g. The increased porosity in the sintered ceramic did not result in an increase in degradation, therefore the degradation rate of the cement and ceramic is affected by the SSA and not porosity (Barralet et al., 2002).

Figure 8.7 shows that at P:L = 1.5 g/mL the increase in sintering temperature results in the reduction of SSA of $Ca_2P_2O_7$ ceramic. Increasing the P:L ratio of the ceramic

from 1.25 g/mL to 1.5 g/mL resulted in the decrease in SSA (stated above). The decrease in sintering temperature from 1200 – 400°C and the reduction in P:L from 3.0 – 2.5 g/mL resulted in an increase in SSA of the $Ca_2P_2O_7$ ceramic from 0.318 ± 0.002 m^2/g to 8.658 ± 0.847 m^3/g. The increase in SSA produced a corresponding increase in the mass of $Ca_2P_2O_7$ ceramic which degraded in serum from 3 wt% to 21 wt% of the original (Figure 8.19). Surprisingly $Ca_2P_2O_7$ ceramic degradation was not enhanced in serum even though it is expected to contain active phosphatase and pyrophosphatase enzyme. Figure 8.19 shows that 50 wt% of the original $Ca_2P_2O_7$ ceramic degraded in PBS solution as compared with 21 wt% in serum. It is suspected that the presence of calcium and orthophosphate ion in serum is responsible for significantly reducing the rate of ceramic degradation as compared with the PBS solution. Besides the SSA, increased ceramic degradation at lower sintering temperature and P:L ratio can be attributed to their microstructure (Figure 8.20). The microstructure of brushite cement shows the presence of crystals which are easily removed from the cement matrix leading to fragmentation (Figure 8.20a). The particles of $Ca_2P_2O_7$ ceramics are tightly held together by strong primary bonds and the crystals are tightly fused (Figure 8.20). As the sintering temperature is increased the crystals grow larger and it is therefore more difficult for ceramic fragmentation to occur.

Finally the degradation of $Ca_2P_2O_7$ ceramic in serum is thought to occur by: (1) the release of smaller particles from the ceramic matrix into solution and (2) the hydrolysis of the small particles into its component ions and (3) enzyme mediated degradation of the component ion.

8.4. CONCLUSIONS

$Ca_2P_2O_7$ ceramic was successfully synthesised by the thermal treatment of brushite cement at temperatures ≥ 400°C. The formation of $Ca_2P_2O_7$ ceramic was confirmed using XRD, TGA and DTA analysis. Generally the compressive strength of the sintered ceramic increased with increased sintering temperature up to 1000°C. The presence of microcracks within the ceramic structure that was sintered at 1200°C was responsible for the decrease in the compressive strength. Although expected, the porosity of $Ca_2P_2O_7$ ceramic did not reduce with increase in compressive strength and sintering temperature. This is due to the competing effect of ceramic densification and density changes associated with phase change. The variations in P:L was found to have an effect on the mass loss, volumetric shrinkage and compressive strength of the ceramic. $Ca_2P_2O_7$ ceramic at P:L of 1.25 g/mL degraded faster in ALP solution than the control. Increasing the P:L ratio resulted in a more structurally stable ceramic, therefore pyrophosphate ion was released into the ageing solution at low concentration and ALP could not enhance the ceramic degradation. The increase in ALP concentration did not produce a corresponding increase in the mass of sintered ceramic which degraded in ageing solution. Therefore $Ca_2P_2O_7$ ceramic was aged in serum solution which is expected to contain phosphatase and pyrophosphatase enzymes. The control experiment involved degrading brushite cement in serum and PBS solution. The brushite cement degraded faster than the sintered $Ca_2P_2O_7$ ceramic and it also degraded faster in serum than in PBS solution. The increased degradation of brushite in serum than PBS solution is the result of serum inhibiting the formation of apatite within the brushite cement. Brushite cement has a larger SSA than $Ca_2P_2O_7$ ceramic and its crystals are easily removed from the

cement matrix result in the fragmentation of the cement. When the sintering temperature was reduced from 1200°C to 400°C and the P:L ratio was reduced from 3.0 g/mL to 2.5 g/mL the SSA of the resulting $Ca_2P_2O_7$ ceramic increased significantly. The increase in SSA was reflected in the reduction in particle size as observed using SEM. The change in cement composition and process variable resulted in an increase in the mass of $Ca_2P_2O_7$ ceramic which degraded in serum solution. The $Ca_2P_2O_7$ ceramic degradation was faster in PBS solution than in serum due to the likelihood that calcium and orthophosphate ion present in serum inhibited the $Ca_2P_2O_7$ ceramic degradation.

9. FABRICATION OF CALCIUM PYROPHOSPHATE CERAMIC USING STEREOLITHOGRAPHY

In this thesis it has been established that CPPD crystal dissolution may be accelerated in the presence of ALP and it has also been demonstrated that this can be scaled up so that sintered $Ca_2P_2O_7$ ceramic exhibit the same degradation profile. Sintered ceramics are difficult to shape as required but this can be made possible by using various rapid prototyping processes. Rapid prototyping also enables the production of reproducible ceramic materials. Some rapid prototyping processes have been discussed below.

Selective laser sintering (SLS)

A thin layer of powder is spread on a flat surface using a cylindrical roller. A high precision carbon dioxide (CO_2) beam scans the powder bed and selectively sinters the powder to fuse certain areas as defined by the geometry of the computer aided design (CAD) model. The areas of the powder which are not sintered by the laser beam are used for support to build subsequent layers. A piston or inkjet printer head is used to spread a new layer of powder which is then fused with the previous one layer by the laser beam. The process is repeated until the desired material is built. SLS can bind powders directly without the aid of binders (Tay et al., 2003).

Three dimensional printing (3D printing)

3D printing uses the technology of an ink jet printer (Gbureck et al., 2007; Safari et al., 2001). A roller or mechanical, acoustic, ultrasonic vibration is used to roll and level dry powder into a thin layer. The inkjet printer then sprays a binder onto the

powder in selected area depending on the material geometry designed using CAD. Once that layer dries a new powder layer is laid down and the process is repeated until the desired shape is realised. 3D printing is a flexible process which employs the use of various powders and binders in a single fabrication process to build a material of various geometries.

Laminated object manufacturing

Laminated object manufacturing was developed in 1985 to build components with layers of paper or plastic (Tay et al., 2003). The sheet feedstock is cut to a defined structure using a laser before it is sprayed with an adhesive solvent. Another layer is placed upon the previous one before pressing with a heated roller and thereby activating the adhesive.

Fusion deposition modelling

The deposition of fused ceramics was developed at Rutgers University (Agarwala et al., 1996) using the fusion deposition modelling technique. A material feedstock (combination of polymer and ceramic) are heated close to the melting point inside a heated liquefier head before being extruded through the nozzle of a small orifice (Leong et al., 2003). The motion of the liquefier is computer controlled (x-and y-direction). Once the material has been extruded it solidifies and welds to the previous layer. Controlling the direction of material deposition ensures that the pore structure and interconnectivity can also be controlled.

Stereolithography

Stereolithography was the first solid freeform fabrication technique to be developed (Hull, 1996) and has since been modified to produce ceramic materials (Griffith and Halloran, 1996). Stereolithography is a process by which 3D biomaterials can be produced in a layer by layer method. The material which is to be produced using stereolithography is designed using CAD. Figure 9.1 is a schematic diagram of the operation of a typical stereolithography apparatus.

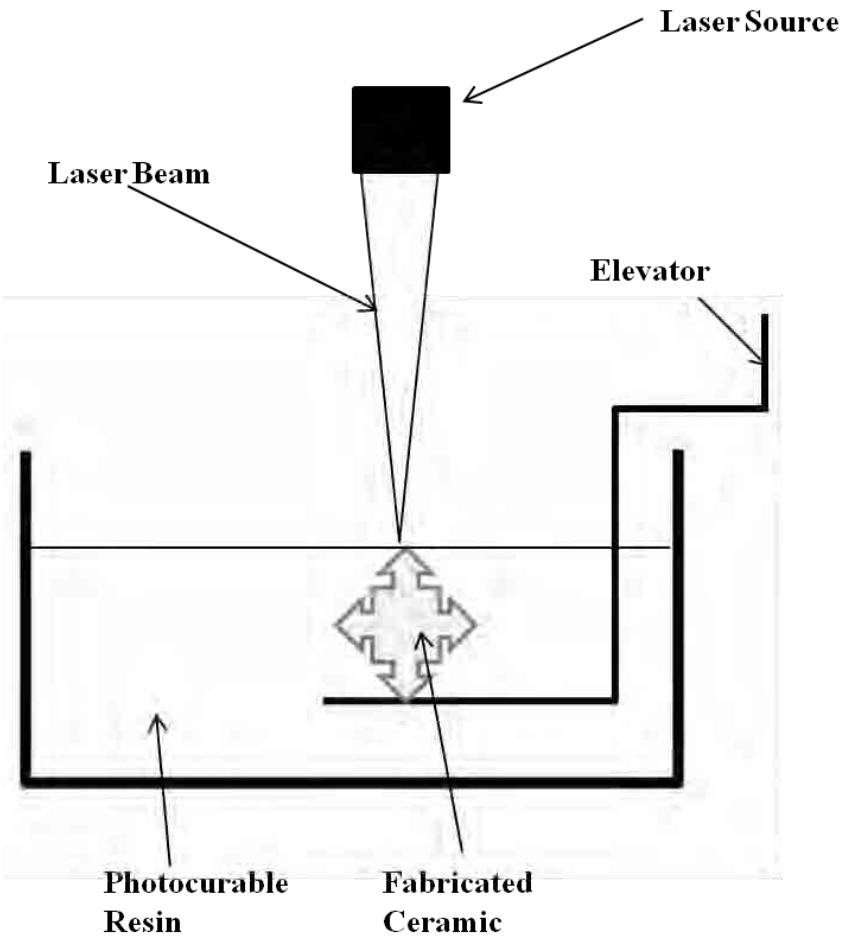

Figure 9.1: Schematic diagram showing the operation of a typical stereolithography apparatus.

The photocurable polymer resin (or polymer/ceramic composite) deposited on a bath plate is exposed to ultraviolet (UV) light (beam) is controlled in x- and y- direction (Tay et al., 2003). The liquid polymer is polymerised (cured) selectively depending on the geometry designed on the CAD program. After the initial layer is cured the elevator raises the sample so that another polymer layer is cured as shown in figure 9.1.

Once the materials fabrication is completed unreacted resin is washed off and the material is post cured. The polymer binder is 'burnt off' through sintering to leave the ceramic material. Although various rapid prototyping processes are used for producing 3D materials, stereolithography was used in this thesis to produce bespoke $Ca_2P_2O_7$ implants. By using stereolithography it is easy to control the microstructural properties of ceramic materials such as porosity and pore connectivity. The operating conditions for the industrial Perfactory$^{3®}$ XGA Desktop (envisionTEC, Germany) stereolithography machine were also investigated. The ceramic loading of the polymer/ceramic suspension was also investigated to ensure that the powder is present in sufficient amount so that the ceramic matrix after sintering is structurally stable materials. Therefore the compressive strength of the sintered ceramic would increase with ceramic loading. The polymer used should be sufficiently viscous in order that is also important that β-$Ca_2P_2O_7$ powder is uniformly distributed within the composite material.

9.1. MATERIALS AND METHODS

9.1.1. Preliminary investigation

Initial experiments involved curing calcium pyrophosphate ceramic and polymer suspension using a light engine which used an LED as its light source before transferring the formulation onto the industrial Perfactory$^{3®}$ XGA Desktop (envisionTEC, Germany) stereolithography machine. The polymer cured using the light engine was a mixture of 70 wt% 1, 6-Hexanediodiacrylate (HDDA; Sigma Aldrich, Dorset) and 30 wt% N-methyl-2-pyrolidone (pyrolidon, Sigma Aldrich, Dorset). β-Calcium pyrophosphate powder (β-$Ca_2P_2O_7$; Sigma Aldrich, Dorset) was added to the polymer mixture at a loading of 40 wt%. To this ceramic suspension Triton XL 100 (Sigma Aldrich, Dorset) a dispersant was added at 4 wt% of the ceramic. The dispersant ensures that the ceramic does not settle or coagulate within the polymer. The suspension was then mixed on a magnetic stirrer for 2-3 days to ensure that large ceramic particles were dispersed within the polymer mixture. α-benzyl-α-(dimethylamino)-4-morpholinobutyrophenon (Sigma Aldrich, Dorset) a photoinitiator was added at 4 wt% of the ceramic content. A thin layer of the ceramic suspension was placed on a glass plate in the light engine with a 0.5 cm^2 aperture exposing it to the LED light source (ENFIS LTD, Swansea). The LED power output is up to 38 W and the wavelength is between 365 – 870 nm. The single layer was cured before being placed in the light box for 10 seconds to cure any unreacted polymer. The cured ceramic material was then cleaned with propan-2-ol (Fisher Scientific, UK) to remove any remaining unreacted polymer.

Although the ceramic suspension of HDDA, pyrolidon and β-$Ca_2P_2O_7$ ceramic was shown to cure on the light engine it was not possible to build a ceramic monolith on the Perfactory$^{3®}$ XGA Desktop. Various polymers were mixed with β-$Ca_2P_2O_7$ powder and precipitated brushite crystals (precipitation method was described in chapter 7) and the viscosity of the resulting suspensions were measured. The viscosities of the suspensions were measured at a shear rate of 0.01 s^{-1} with 40 mm plate geometry on AR-Rheometer (TA Instruments, UK). The polymer mixture investigated are: 1) HDDA and trimethylolpropane triacrylate (TMPTA, Sigma Aldrich, Dorset), 2) HDDA and pyrolidon and 3) dipentaerythritol penta-/hexa-acrylate (DPA; Sigma Aldrich, Dorset) and 1, 6-Hexanediol ethoxylate diacrylate (HDeDA; Sigma Aldrich, Dorset). The particle size of the precipitated brushite crystals and β-$Ca_2P_2O_7$ ceramic powder purchased from Sigma Aldrich were measured using a Mastersizer (Malvern Instruments, UK). The sintered $Ca_2P_2O_7$ ceramic was not used in these experiments as it was not possible to grind it into very fine powder which would be properly suspended within the polymer matrix.

9.1.2. Formation of $Ca_2P_2O_7$ monolith using stereolithography

The new polymer mixture consisted of 70 wt% of DPA and 30 wt% HDeDA. β-$Ca_2P_2O_7$ powder was added gradually to the polymer mix at 40 wt% before mixing for 2 - 3 day depending on the dispersion of the ceramic. The photoinitiator was added at 3 wt% of the polymer and a dye, orange orasul (Sigma Aldrich, Dorset) was also added at 0.05 wt% of the ceramic content. The dye is a photo inhibitor that ensures the ceramic suspension is cured at a controlled rate by preventing spontaneous polymerisation. Prior to successfully fabricating $Ca_2P_2O_7$ monolith on

the Perfactory$^{3®}$ XGA Desktop the viscosity of the ceramic suspension at various ceramic loading was measured. After 2.5 h experimental time nine $Ca_2P_2O_7$ ceramic cylinders with an average height of 8 mm and diameter of 4 mm were produced.

9.1.3. Material characterisation

The ceramic polymer composite was then characterised using simultaneous thermal analysis (STA 1500, Stanton Redcroft). This equipment enables the change in mass and heat flow within the ceramic to be monitored with increasing temperature (25 – 1200°C). The STA was operating at a flow rate of 50 mL/min and at a heating rate of 20°C/min. The crystalline composition of the sintered $Ca_2P_2O_7$ monolith was monitored and confirmed using XRD. The X-ray diffraction was carried out as described in section 8.1.2 using a step size of 0.015° and a step time of 0.25 s.

9.1.3.1. Effect of sintering temperature on ceramic density and microstructure

After burning off the polymer binder the ceramic is left in the furnace for further densification. As the sintering temperature is increased the change in density of the remaining ceramic matrix is measured using a helium pycnometer (Micromeritics, Bedfordshire). The microstructure of the ceramic/polymer composite and the sintered ceramic is observed using SEM. It was not possible to obtain geometrical measurement of the sintered ceramic due to the structural instability of the resulting matrix.

9.2. RESULTS

It is important that the polymer used in binding β-$Ca_2P_2O_7$ powder or brushite crystals cured once exposed to UV light. Therefore initial investigation involved testing various photocurable polymers which would suspend the powder and cure once exposed to the LED light source (Figure 9.2).

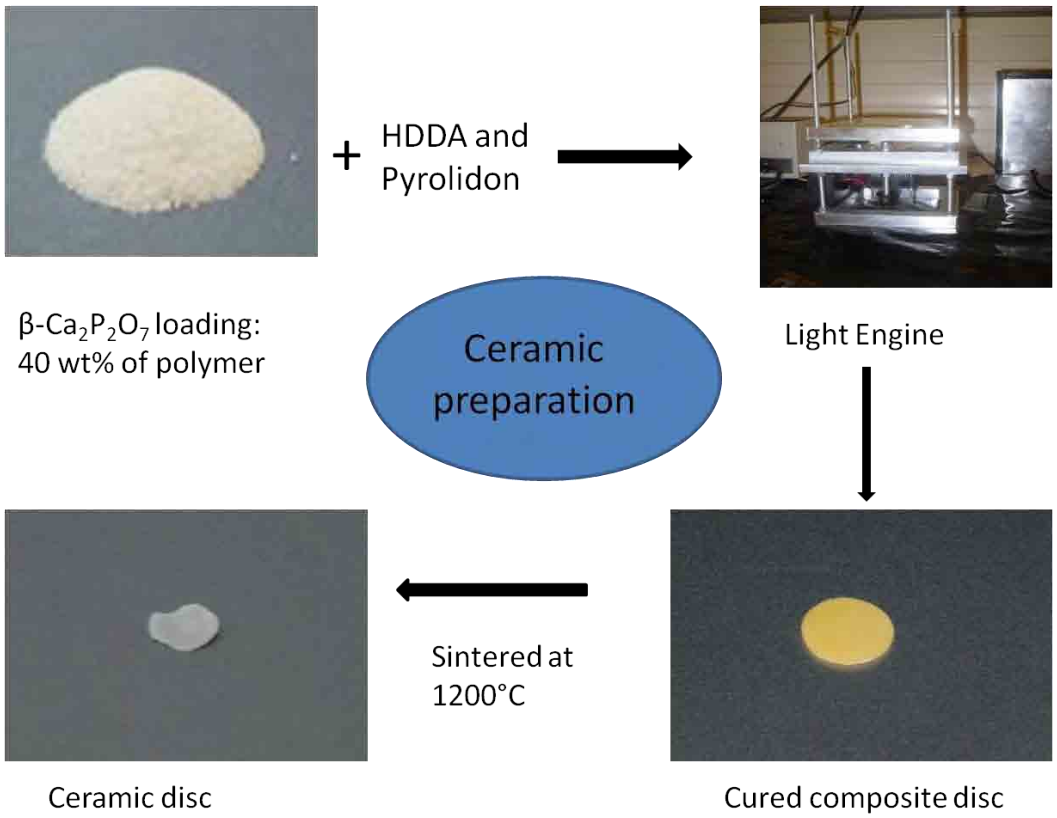

Figure 9.2: Initial investigation into the fabrication of $Ca_2P_2O_7$ ceramic by curing polymer/ceramic suspension on a light engine.

Since it took 2.5 h to produce nine cylindrical ceramic/polymer composites (Figure 9.4a), the viscosity of the polymer is also very important; the polymer should be sufficiently viscous to enable suspension of the ceramic solid component while the material is fabricated on the stereolithography machine. The mixture of HDDA and TMPTA was used as the polymer which when mixed with brushite crystals the viscosity was 207 Pas which fell drastically to 0.4 Pas when β-$Ca_2P_2O_7$ powder was

used. The particle size of β-$Ca_2P_2O_7$ powder is twice as large as that of precipitated brushite crystals (Table 9.1); this is thought to have contributed significantly to the reduction in viscosity.

Table 9.1: Effect of polymer and particle size on the viscosity of ceramic suspension.

Material type	**Particle Size (μm)**	**Viscosity of polymer and cement/ceramic suspension (Pas)**		
		HDDA + TMPTA	HDDA + Pyrolidon	HDeDA + DPA
Brushite	79.90 ± 1.04	207.2	35,640.0	42,800.0
β-$Ca_2P_2O_7$	170.42 ± 41.03	0.418	1.404	9.383

The larger the particle size of the powder component the more difficult it is to be suspended within the polymer. The large particles of the β-$Ca_2P_2O_7$ powder settled to the bottom of the suspension during the fabrication process. By mixing the ceramic/polymer suspension vigorously some of the larger particles are broken down into smaller particles which are easily suspended within the polymer. It was difficult to fabricate brushite materials using the Desktop because of the extremely high viscosity of the brushite/polymer suspension. In comparison, the extremely low viscosity of the HDDA and pyrolidon mixture made it difficult to fabricate the β-$Ca_2P_2O_7$ using the desktop. The polymer mixture was changed but this did not produce a successful fabrication process until a dye was added.

The addition of a dye and photoinitiator to the HDeDA, DPA and β-$Ca_2P_2O_7$ mixture resulted in a decrease in viscosity from 9.38 Pas to 1.47 Pas as shown in figure 9.3. The viscosity of the ceramic suspension at 40 wt% calcium pyrophosphate was measured at shear rates in the range of 0.01 – 100 s^{-1}.

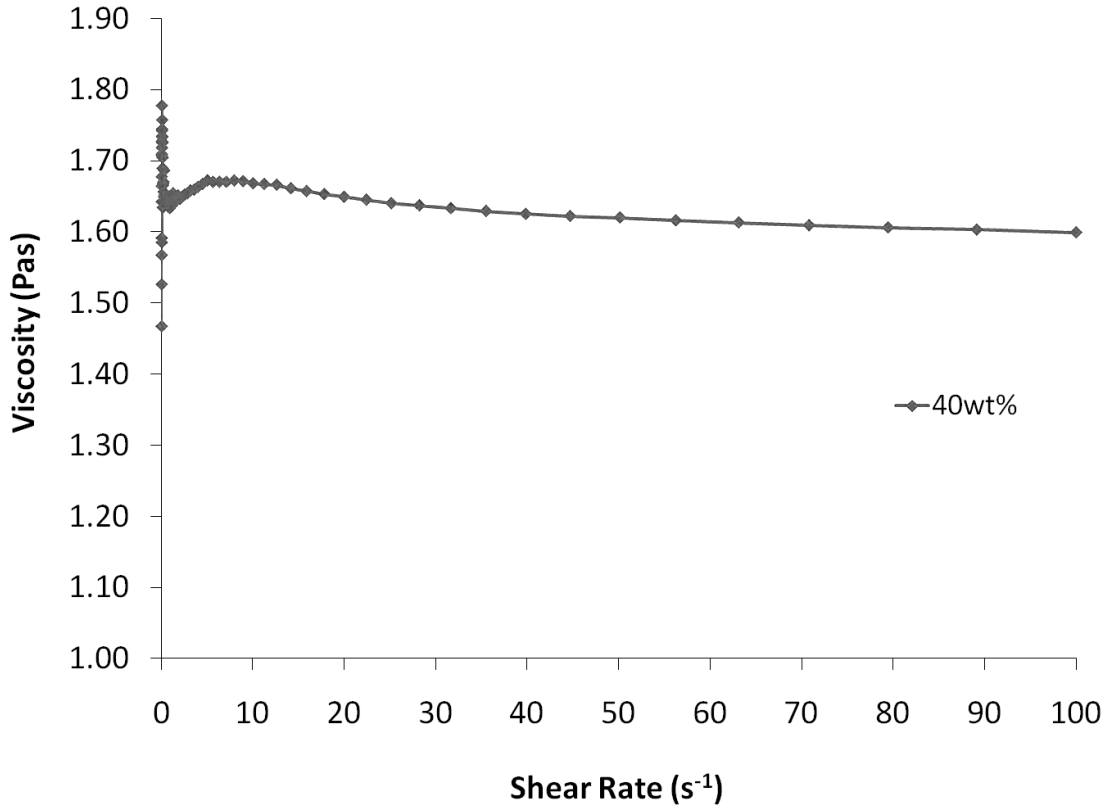

Figure 9.3: Viscosity of β-$Ca_2P_2O_7$ and polymer suspension as a function of shear rate at 40 wt% ceramic loading.

The movement of the elevator over the ceramic suspension (Figure 9.1) can have an effect on the viscosity of the suspension therefore it was of great importance that there was no sudden change in the viscosity of the suspension with changes in shear rate (Figure 9.3). The formulation consisting of β-$Ca_2P_2O_7$ ceramic, HDeDA and DPA polymer was successfully fabricated on the stereolithography machine as is shown in figure 9.4a. Each layer that makes up the ceramic cylinder shown in figure

9.4a is 25 μm thick. Once sintered the orange dye was decomposed at high temperature, along with the polymer binding the ceramic (Figure 9.4b).

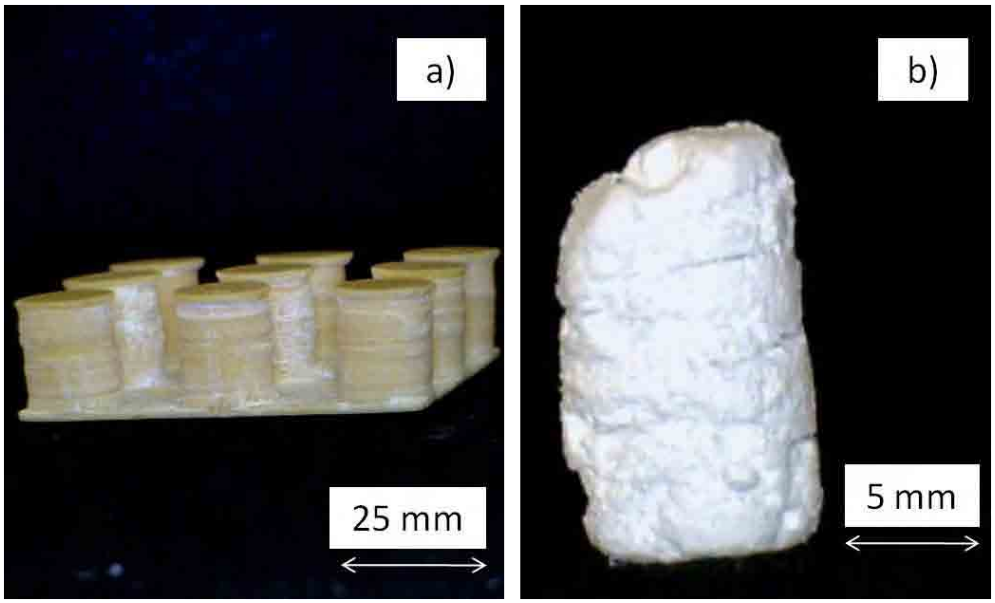

Figure 9.4: Photograph of a) cured 40 wt% calcium pyrophosphate ceramic suspension and b) the ceramic and polymer composite material after sintering at 800°C for 3 h.

Figure 9.4b shows that at 40 wt% β-$Ca_2P_2O_7$ ceramic loading the ceramic matrix did not retain it cylindrical shape. The thermogravimetric analysis shows that the polymer decomposition began at about 315°C and continues to about 600°C (Figure 9.5a). There was no phase change within the $Ca_2P_2O_7$ ceramic as the sintering temperature was increased (Figure 9.5b). The increase in heat flow within the ceramic is associated with the decomposition of HDeDA, DPA, photoinitiator and the dye as shown in figure 9.5a. The β-$Ca_2P_2O_7$ powder added to the polymer mixture was found to contain β-TCP as well as β-$Ca_2P_2O_7$ (Figure 9.5b).

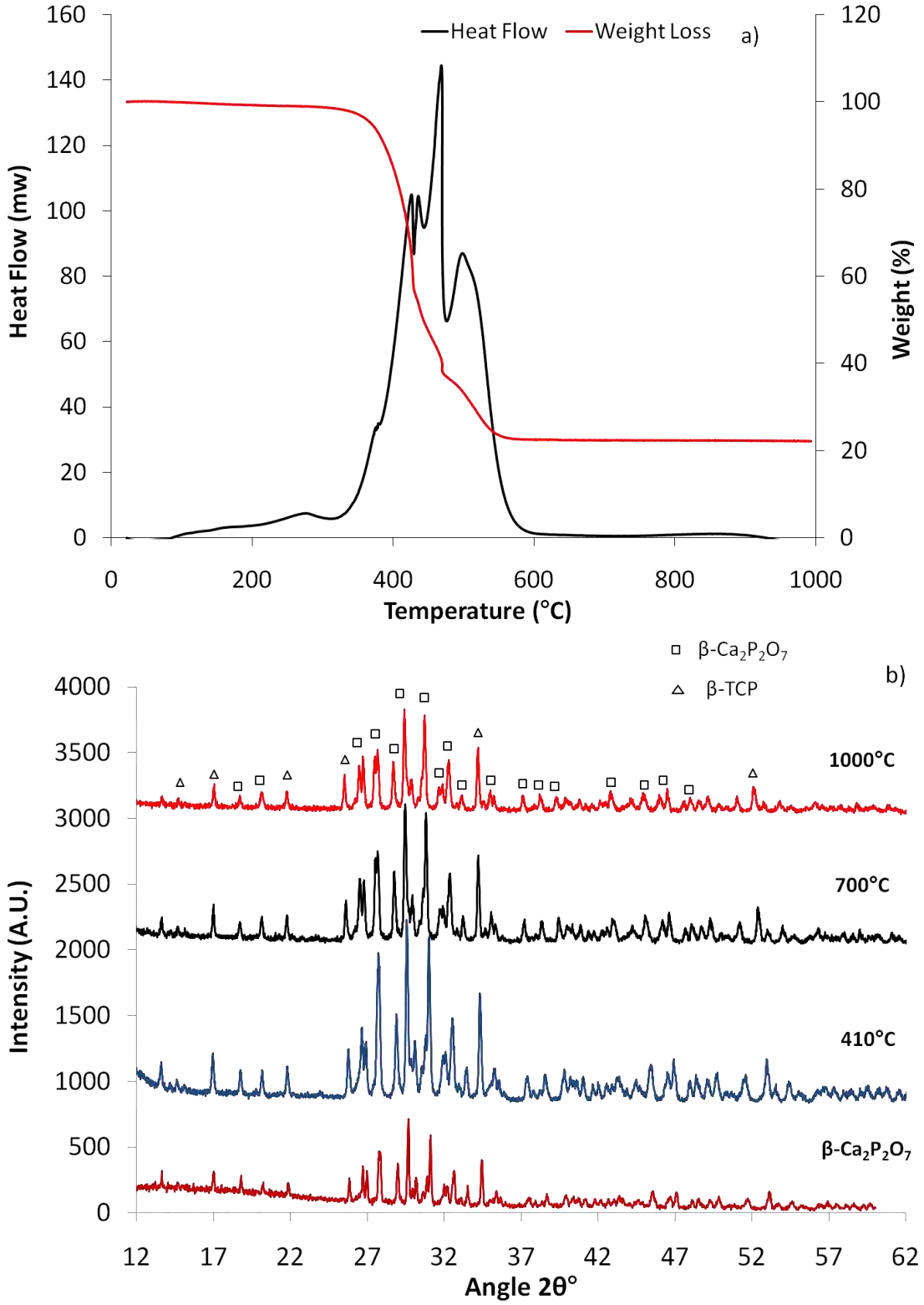

Figure 9.5: a) Effect of temperature on the heat flow and mass changes of the cured 40 wt% $Ca_2P_2O_7$ ceramic and b) effect of sintering temperature on the chemical composition of fabricated $Ca_2P_2O_7$ ceramic.

There was no chemical reaction between the ceramic powder and the polymer as there was no change in the crystalline composition of β-$Ca_2P_2O_7$ after sintering. It was not possible to see the crystals with defined shape and size β-$Ca_2P_2O_7$ within the composite material (Figure 9.6a). As the sintering temperature was increased from 410°C to 1200°C β-$Ca_2P_2O_7$ crystals became densified and the particle size increased (Figure 9.6).

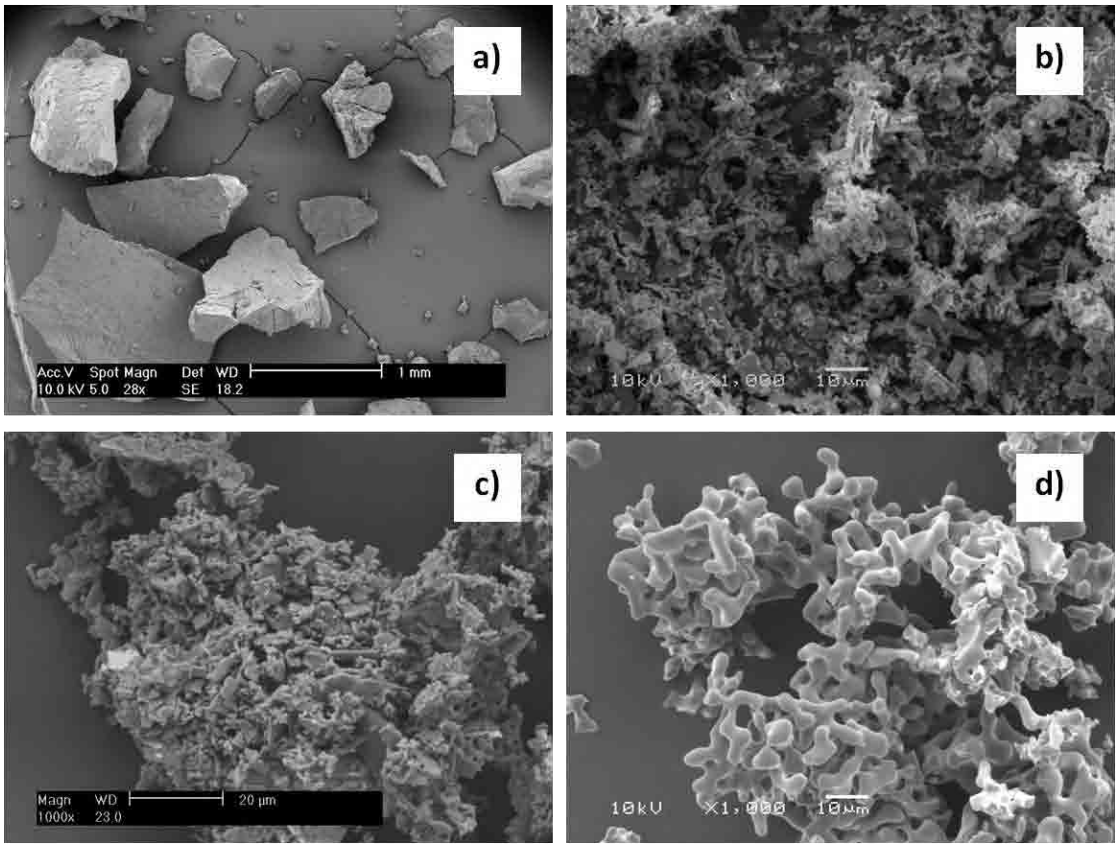

Figure 9.6: SEM micrograph of: a) cured $Ca_2P_2O_7$ ceramic, b) cured ceramic sintered at 410°C to remove the polymer binder, c) sintered at 1000°C for 3 h and d) sintered at 1200°C for 8 h.

The density of the sintered ceramic increased with sintering temperature. In this case, the significant increase in density of the ceramic with temperature can be attributed to the decomposition of the relatively low density (specify) polymeric phase. Figure 9.7 provides further evidence that the polymer was fully decomposed by 600°C as shown in figure 9.5a.

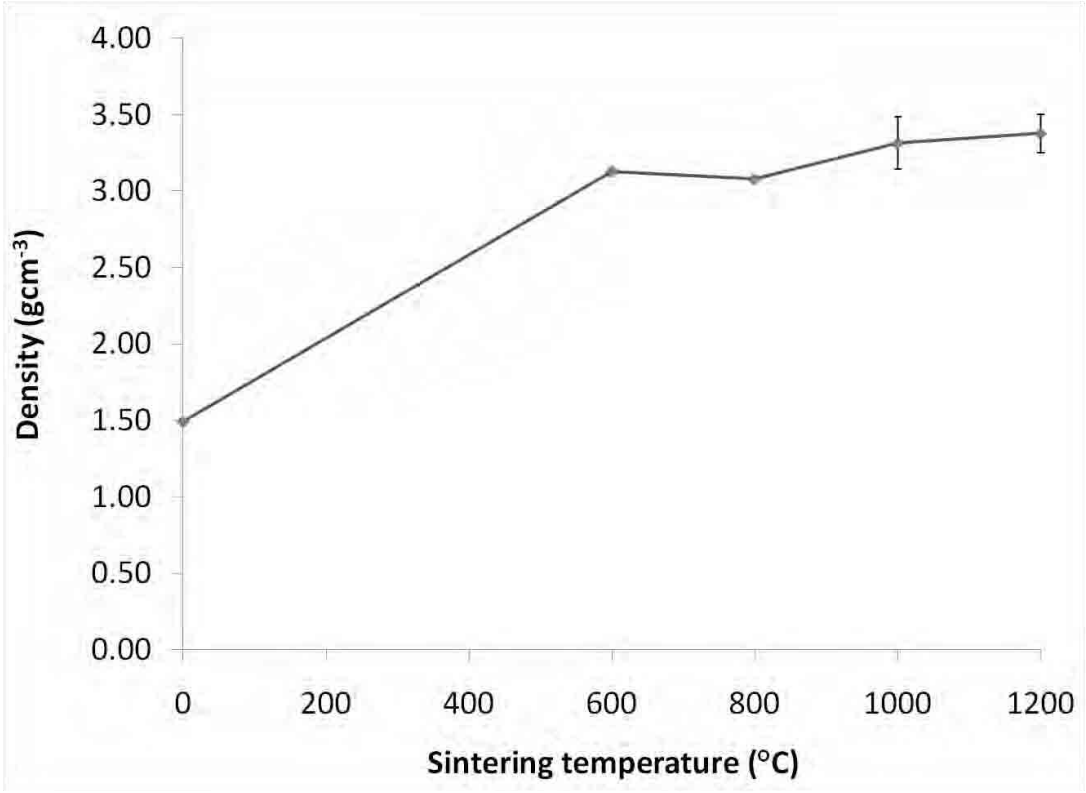

Figure 9.7: Effect of sintering temperature on the density of the fabricated $Ca_2P_2O_7$ ceramic.

9.3. DISCUSSION

Stereolithography is a rapid prototyping process whereby three dimensional materials are produced layer by layer when a photocurable polymer is exposed to UV light. The particle size of ceramic material suspended within the polymer was found to have an effect on the viscosity of the ceramic suspension (Table 9.1). The viscosity of all the brushite suspension studied was found to be greater than that of the $Ca_2P_2O_7$ suspension (Table 9.1). It has been reported that the viscosity of a ceramic suspension be below 5 Pas for its successful fabrication using stereolithography (Porter, Pilliar, & Grynpas 2001). The viscosity of all the brushite suspension was significantly higher than 5 Pas and therefore it was not possible to fabricate monoliths from it. The viscosity of the $Ca_2P_2O_7$ suspension was lower than 5 Pas except were the ceramic was suspended in HDeDA and DPA polymer. It was not possible to fabricate composite materials from the mixture of HDeDA, DPA and $Ca_2P_2O_7$ until a photo inhibitor (dye) was added (Figure 9.4a). Prior to composite fabrication on the Desktop various polymer mixtures were tested one of which was HDDA and pyrolidon. This polymer with the addition of β-$Ca_2P_2O_7$ powder was cured using the light engine (Figure 9.2). As the HDDA and pyrolidon polymer mixture was not sufficiently viscous to suspend a higher ceramic loading it was not used on the Desktop.

Despite preparing sintered $Ca_2P_2O_7$ ceramic (chapter 8) this was not used in this investigation as the particles of the ground ceramic were not small enough to be suspended within the polymer. The ceramic suspension was expected to contain 28 wt% $Ca_2P_2O_7$ ceramic but from the TGA graph 24 wt% of the ceramic was detected

when the polymer was decomposed at 550°C (Figure 9.5a). The $Ca_2P_2O_7$ ceramic was not uniformly distributed throughout the polymer binder which could be the reason why there was a difference in the actual and expected weight of the remaining ceramic. β-TCP was found to be contained within the β-$Ca_2P_2O_7$ powder purchased from Sigma Aldrich (Dorset, UK). The cured monolith has to be sintered at temperatures greater than 410°C for the polymer binder to be removed (Figure 9.5a). Sintering temperature was also shown to have no effect on phase change within the $Ca_2P_2O_7$ ceramic as shown in figure 9.5b. As sintering temperature is increased the crystallites from which the ceramic was composed become larger as is shown in figure 9.6. As discovered using TGA analysis the burning off of the polymer began at about 410°C and finished at about 600°C. Therefore the true density increased from 1.5 gcm^{-3} for the composite material to 3.1 gcm^{-3} when the polymer was burnt off completely at 600°C. Subsequent heating of the remaining ceramic material produced slight increases in the true density of the material (Figure 9.7). The difficulty in using stereolithography is the relatively low ceramic loading which means that the sintered material is structurally unstable and the compressive strength cannot be measured. Further experiment is needed to investigate polymers and various operating conditions which would enable higher ceramic loading and subsequently more structurally stable materials.

9.4. CONCLUSION

$Ca_2P_2O_7$ composite discs were successfully produced on a light engine exposed to an LED light source. The polymer used was then changed and a photo inhibitor added to avoid uncontrolled polymerisation before fabricating composite materials on the Desktop. The viscosity of the polymer/brushite suspension was very high due to its smaller particle size in comparison with that of β-$Ca_2P_2O_7$ powder. The extremely high viscosity prevented the fabrication of brushite composite materials on the stereolithography instrument. The polymer used in the production of $Ca_2P_2O_7$ composite did not affect the crystalline composition of the material. TGA analysis showed that the polymer binder was burnt off at temperature between 410 – 600°C. XRD pattern showed that the powder added to the polymer mixture was a combination of β-$Ca_2P_2O_7$ and β-TCP and remained unchanged with increasing sintering temperature.

The crystallites of the composite were further densified as the polymer was completely burnt off with increased sintering temperature. This followed the trend observed in ceramic materials as shown in chapter 8. The material which remained after sintering was structurally unstable due to low ceramic loading. This also prevents compressive testing and geometrical testing of the ceramic matrix.

10. RESEARCH FINDINGS, CHALLENGES, CLINICAL IMPLICATIONS AND ALTERNATIVE APPROACHES.

Worldwide around 2.2 million bone graft procedures are carried out in the repair of bone defect in orthopaedics and dentistry (Lewandrowski et al., 2000). Bone tissue taken from the patients themselves (autograft) is still the gold standard in the repair of bone defect as it provides the optimum osteoconductive, osteoinductive and osteogenic properties required (Giannoudis et al., 2005). Post operative pain, increased operating time and cost are some of the disadvantages associated with the autograft procedure (Ilan and Ladd, 2002). When a large amount of tissue is required and cannot be obtained from the patient, tissue is taken from another individual (allograft tissue) to be used. Allograft tissue is osteoconductive but it has lost most of its osteoinductive properties (Giannoudis et al., 2005). There is also potential for infection and disease transmission with allograft tissue (Buck et al., 1989). To overcome these problems synthetic materials have been developed as an alternative to the biological bone graft (autograft and allograft). An ideal synthetic bone graft should be osteoconductive, osteoinductive, bioactive and bioresorbable (Giannoudis et al., 2005).

Calcium phosphates cements are synthetic materials with a wide range of applications in the field of orthopaedics and dentistry due to their bioactive and osteoconductive properties, non-toxicity and chemical similarity to the mineral component of mammalian bones and teeth (Dorozhkin, 2010; Ginebra et al., 1997; Bohner, 2000). TCP has a stoichiometry similar to amorphous bone precursors, whereas HA has a stoichiometry similar to bone mineral (Giannoudis et al., 2005).

The low stability of HA in physiological conditions is a limiting factor in its use as an implant. If the implant remains in situ for a long period of time there is likelihood of mechanical failure requiring the patient to return for surgery to replace the failed implant. For materials which degrade too fast it will be impossible for the implant to provide sufficient support to the new tissue formed. It is desirable to have a material that is resorbed over time leaving space for the formation of new tissue. The rate of bone turnover varies with the age, health and sex of the patient (Havill, 2004). Therefore it is difficult to link the rate of bone formation to the resorption of the bone implant. To overcome this problem a bioresponsive material should be used as the bone replacement. A bioresponsive material is one which will degrade in response to the presence of a biological stimulus which in the case of bone formation and mineralisation is ALP. It is therefore possible that each patient will produce ALP which will then regulate the degradation of the implant.

The aim of the thesis was to formulate and produce a calcium pyrophosphate material which would degrade faster in the presence of ALP thereby developing a novel bioresponsive bone replacement. Xu et al. (Xu et al., 1991b) found that CPPD crystals which have the same dimensions as that found in the joints of patients suffering from pseudogout dissolved faster in the presence of ALP. ALP is also thought to perform an important role in bone mineralisation by removing $P_2O_7^{4-}$ ion (a known inhibitor to bone mineralisation) (Anderson et al., 2004). ALP hydrolyses $P_2O_7^{4-}$ ion to form PO_4^{3-} ion which can then be used in the precipitation of apatite crystals which make up the inorganic component of bone (Thouverey et al., 2009). Therefore the research in this thesis began by confirming that CPPD crystals

dissolved faster in the presence of ALP. The results also showed that CPPD crystal dissolution was not achieved by a stereoselective process. The CPPD crystals dissolved in solution to produce Ca^{2+} and $P_2O_7^{4-}$ ion before the $P_2O_7^{4-}$ ion was hydrolysed by ALP to form PO_4^{3-} ion.

Once the interaction between the $P_2O_7^{4-}$ ion and the ALP enzyme has been established, bulk calcium pyrophosphate ceramic was produced by sintering brushite cement at temperatures ≥ 400°C. The composition of the brushite cement was varied between 1.25 – 3.0 g/mL, once sintered for 5 h at temperatures between 400 – 1200°C the compressive strengths of the ceramic was between 2.5 – 11.6 MPa which is within the range of that of cancellous bone (0.5 – 50 MPa, Table 2.1). The porosity of $Ca_2P_2O_7$ ceramic (P:L = 1.25 g/mL) sintered at 1200°C was 32% while its compressive strength was 6.7 ± 0.8 MPa. This ceramic degraded faster in ALP (48 wt%) solution over 16 days but the bulk ceramic was structurally unstable. From this result $Ca_2P_2O_7$ ceramic at P:L 1.25 g/mL and 1200°C would probably not provide sufficient support for the new bone tissue formed. Once the P:L ratio was increased to 3.0 g/mL the compressive strength increased to 11.1 ± 1.8 MPa and the porosity decreased to 30%. Due to the cost of ALP enzyme it was impossible to continue the degradation experiment using ALP therefore the ceramic was degraded in serum solution. Serum is expected to contain proteins and enzymes with pyrophosphatase activity.

$Ca_2P_2O_7$ ceramic at P:L 3.0 g/mL and 1200°C was structurally stable throughout the degradation period but only 3 wt% degraded in serum over 26 days as compared to

38 wt% of brushite cement at the same P:L ratio which degraded in serum (Figure 8.18). The SSA of the ceramic was found to be strongly linked to the degradation of the ceramic (Barralet et al., 2002). The sintering temperature and P:L ratio were reduced to 400°C and 2.5 g/mL respectively. The compressive strength of this ceramic was 9.5 ± 1.2 MPa and the porosity was 23%. The SSA increased from 0.318 ± 0.002 m^2/g (3.0 g/mL and 1200°C) to 8.658 ± 0.847 m^2/g (2.5 g/mL and 400°C). The mass of ceramic which degraded in serum increased to 20 wt% and it was structurally stable throughout the duration of the experiment (Figure 8.19). This confirms the link between SSA and ceramic degradation. Although no i*n vivo* experiments were carried out in this thesis, the $Ca_2P_2O_7$ ceramic is expected to be suitable for use *in vivo* due to suitability of similar materials (Lin et al., 1995b; Sun et al., 2002). The limitation of sintering is that it is difficult to produce an implant which can fit irregular shaped bone defects. Although there has been development in the design of mouldable cements the difficulty in tailoring implant degradation to bone formation still exists (Frayssinet et al., 1998). To overcome this problem the final part of this thesis investigates the use of stereolithography to fabricate $Ca_2P_2O_7$ ceramic which can be designed to fit any size defect.

It is possible to obtain an X-ray of a bone defect requiring bone implant, design the implant using a computer aided design programme before fabricating on the stereolithography machine. Preliminary investigations carried out in this thesis showed that it was possible to fabricate a $Ca_2P_2O_7$ and polymer composite material. Once the material is sintered between 410 – 600°C the polymer is burnt off leaving the $Ca_2P_2O_7$ ceramic. Only 24 wt% of the ceramic remained once the polymer was

burnt off even though the composite mixture was loaded at 40 wt% of the polymer. The low ceramic content led to the production of ceramic materials which were not structurally stable leading to loss of the shape of the implant designed. This problem of loss of ceramic structure does not overcome the limitations associated with material sintering. The main challenge in this part of the research was the difficulty in increasing the ceramic content of the material. It is therefore necessary to further research polymers which would enable the incorporation of larger amounts of ceramic powder and experimental conditions which would also enable higher ceramic content. An alternative approach to using stereolithography would be to investigate a process by which the ceramic powder can be used to make the implant without requiring a polymer binder. Therefore the material would not be sintered, thereby retaining the shape of the bone defect.

To conclude the bulk calcium pyrophosphate ceramics produced in this thesis had compressive strength between 2.5 ± 0.7 MPa to 11.6 ± 2.7 MPa which is within the range of compressive strength recorded for cancellous bone (Table 2.1). Therefore from these compressive data alone it is possible for the ceramics in their present form to be used as replacement for cancellous bone. The ceramics at P:L 1.25 g/mL were shown to degrade faster in ALP solution which is also promising development in the development of a bioresponsive material. Although the ceramic was structurally unstable at 1.25 g/mL, perhaps it could be used in the replacement of bone defects in low load bearing areas.

11. CONCLUSIONS

ALP mediated degradation of calcium pyrophosphate dihydrate crystals

Phase pure CPPD and brushite crystals were successfully precipitated and characterised using XRD, FTIR and SEM analysis. The precipitated CPPD crystals degraded faster in the presence of ALP but the dissolution of brushite crystal was not affected by the presence of ALP. ALP enzyme was found to have high affinity for pyrophosphate ion which results in a large increase in the concentration of orthophosphate ion. The solution becomes saturated with orthophosphate ion which is reprecipitated as apatite onto CPPD crystals inhibiting further CPPD crystal dissolution. Therefore by increasing the volume of aliquot removed from solution the concentration of orthophosphate ion is reduced and CPPD crystal dissolution increased. The use of visking tube to separate CPPD crystals from ALP solution showed that the dissolution occurred in two steps: 1) hydrolysis of the crystals in Tris HCl solution and 2) enzymatic degradation of pyrophosphate ion.

Synthesis and dissolution of calcium pyrophosphate ceramic

$Ca_2P_2O_7$ ceramics were successfully produced by sintering brushite cement at temperatures greater than or equal to 400°C. The mechanical strength of $Ca_2P_2O_7$ ceramic was found to increase with increasing powder liquid ratio i.e. increase in the β-TCP content of the ceramic. Generally as sintering temperature is increased the compressive strength was increased but the porosity did not reduce. This is due to the competition between the densification and phase change within the ceramic which means that the trend expected was not realised. As the sintering temperature was increased the SSA of the ceramic reduced and this was found to have an effect on the

degradation rate of $Ca_2P_2O_7$ ceramic. As the P:L ratio and sintering temperature is reduced the ceramic degradation increased.

Fabrication of calcium pyrophosphate ceramic using stereolithography

Stereolithography was used to successfully produce uniformly formed calcium pyrophosphate ceramic. The layer by layer technology was used to produce a cylindrical matrix with cement loading of up to 50 wt%. It is difficult to achieve uniformly shaped materials at higher ceramic loading (60 – 90 wt %) due to the high viscosity of the ceramic suspension. Using TGA analysis the acrylate binder which is used to hold calcium pyrophosphate powder in place is removed at temperatures between 340 - 540°C. The acrylate binder was found to have no chemical effect on the composition of calcium pyrophosphate as observed on the XRD pattern. This shows that it is possible to fabricate calcium pyrophosphate ceramic of various shapes and size which can be used to fill any size bone defect.

12. FUTURE WORK

This thesis has described the method by which CPPD crystals dissolve in the presence of ALP. The sintering of brushite cement to form $Ca_2P_2O_7$ ceramic and its degradation in ALP containing solution was also investigated. It is difficult to build a mould of varying shapes and sizes from which brushite cement is cast therefore stereolithography a layer by layer technology was investigated. This process uses a computer aided design program therefore $Ca_2P_2O_7$ ceramic of various shapes and size can be built. The mechanism of CPPD crystal dissolution, optimisation of sintered $Ca_2P_2O_7$ ceramic and the mechanism of degradation can be further investigated. Stereolithography process also has to be optimised to increase the ceramic loading of the ceramic/polymer suspension. The following are recommendations for future work on the CPPD dissolution and the optimisation of ceramic manufacturing processes.

ALP mediated degradation of calcium pyrophosphate dihydrate crystals

Using a phosphate assay CPPD crystals were shown to dissolve faster in ALP solution. There are limitations with this procedure as the reprecipitation of orthophosphate ion as apatite crystals might distort the result. Therefore the rate of CPPD dissolution and the mechanism of dissolution might not be accurate. To avoid this discrepancy it is more accurate to measure the calcium ion in solution, a calcium electrode was used in this thesis, however, the results were not sufficiently reproducible or reliable to be used. Future work should use inductively coupled mass spectroscopy to evaluate calcium ion concentration with time.

Effect of process conditions and cement composition on ceramic property and degradation

$Ca_2P_2O_7$ ceramic was successfully produced by sintering brushite cement at temperatures ≥ 400°C. The compressive strength of the human cancellous bone is within 1.9 – 7.1 MPa this corresponds to the ultimate compressive strength measured for the sintered $Ca_2P_2O_7$ ceramic. The effect of sintering temperature on the mass loss and volumetric shrinkage of the sintered ceramic must be explored further in other to determine the shape of the final ceramic. The link between sintering temperature and ceramic porosity and compressive strength of porosity and pore connectivity is important in the degradation of the material, growth of bone tissue and flow of nutrient into the tissue for nourishment. Further systematic experimentation needs to be undertaken to investigate these relationships.

Fabrication of calcium pyrophosphate ceramic using stereolithography

Calcium pyrophosphate ceramics were successfully manufactured using stereolithography. The material produced was sintered to remove the polymer binder leaving the $Ca_2P_2O_7$ ceramic. It is important to investigate different polymer mixture which ensures the suspension of the $Ca_2P_2O_7$ powder over the duration of the manufacturing process. It was not possible to increase the ceramic loading of the ceramic/polymer suspension beyond 50 wt%. At such low ceramic loading the resulting ceramic is not structurally stable. Efforts have been made to increase the ceramic loading but it has been unsuccessful therefore subsequent processes have to be investigated to increase the ceramic loading.

13. REFERENCES

- Addison,W.N., Azari,F., Sorensen,E.S., Kaartinen,M.T., and Mckee,M.D. (2007). Pyrophosphate inhibits mineralization of osteoblast cultures by binding to mineral, up-regulating osteopontin, and inhibiting alkaline phosphatase activity. Journal of Biological Chemistry *282*, 15872-15883.

- Agarwala,M.K., Bandyopadhyay,A., vanWeeren,R., Safari,A., Danforth,S.C., Langrana,N.A., Jamalabad,V.R., and Whalen,P.J. (1996). FDC, rapid fabrication of structural components. American Ceramic Society Bulletin *75*, 60-65.

- Ahmed,I., Lewis,M., Olsen,I., and Knowles,J.C. (2004). Phosphate glasses for tissue engineering: Part 1. Processing and characterisation of a ternary-based P2O5-CaO-Na2O glass system. Biomaterials *25*, 491-499.

- Alkhraisat,M.H., Marino,F.T., Retama,J.R., Jerez,L.B., and Lopez-Cabarcos,E. (2008). Beta-tricalcium phosphate release from brushite cement surface. Journal of Biomedical Materials Research Part A *84A*, 710-717.

- Anderson,H.C., Harmey,D., Camacho,N.P., Garimella,R., Sipe,J.B., Tague,S., Bi,X.H., Johnson,K., Terkeltaub,R., and Millan,J.L. (2005). Sustained osteomalacia of long bones despite major improvement in other hypophosphatasia-related mineral deficits in tissue nonspecific alkaline phosphatase/nucleoticle pyrophosphatase phosphodiesterase 1 double-deficient mice. American Journal of Pathology *166*, 1711-1720.

- Anderson,H.C., Sipe,J.B., Hessle,L., Dhamyamraju,R., Atti,E., Camacho,N.P., and Millan,J.L. (2004). Impaired calcification around matrix vesicles of growth plate and bone in alkaline phosphatase-deficient mice. American Journal of Pathology *164*, 841-847.

- Anee,T.K., Ashok,M., Palanichamy,M., and Kalkura,S.N. (2003). A novel technique to synthesize hydroxyapatite at low temperature. Materials Chemistry and Physics *80*, 725-730.

- Apelt,D., Theiss,F., El-Warrak,A.O., Zlinszky,K., Bettschart-Wolfisberger,R., Bohner,M., Matter,S., Auer,J.A., and von Rechenberg,B. (2004). In vivo behavior of three different injectable hydraulic calcium phosphate cements. Biomaterials *25*, 1439-1451.

- Arellano-Jimenez,M.J., Garcia-Garcia,R., and Reyes-Gasga,J. (2009). Synthesis and hydrolysis of octacalcium phosphate and its characterization by electron microscopy and X-ray diffraction. Journal of Physics and Chemistry of Solids *70*, 390-395.

- Asthana,R., Kumar,A., and Dahotre,N. (2006). Powder Metallurgy and Ceramic Forming. In Materials Processing and Manufacturing Science, Butterworth-Heinemann), pp. 167-245.

- Athanasiou,K.A., Agrawal,C.M., Barber,F.A., and Burkhart,S.S. (1998). Orthopaedic applications for PLA-PGA biodegradable polymers. Arthroscopy-the Journal of Arthroscopic and Related Surgery *14*, 726-737.

- Ayral,A., Phalippou,J., and Woignier,T. (1992). Skeletal Density of Silica Aerogels Determined by Helium Pycnometry. Journal of Materials Science *27*, 1166-1170.

- Balcerzak,M., Hamade,E., Zhang,L., Pikula,S., Azzar,G., Radisson,J., Bandorowicz-Pikula,J., and Buchet,R. (2003). The roles of annexins and alkaline phosphatase in mineralization process. Acta Biochimica Polonica *50*, 1019-1038.

- Barralet,J.E., Gaunt,T., Wright,A.J., Gibson,I.R., and Knowles,J.C. (2002). Effect of porosity reduction by compaction on compressive strength and microstructure of calcium phosphate cement. Journal of Biomedical Materials Research *63*, 1-9.

- Barrere,F., van der Valk,C.M., Dalmeijer,R.A.J., van Blitterswijk,C.A., de Groot,K., and Layrolle,P. (2003). In vitro and in vivo degradation of biomimetic octacalcium phosphate and carbonate apatite coatings on titanium implants. Journal of Biomedical Materials Research Part A *64A*, 378-387.

- Batich,C. and Leamy,P. (2003). Biopolymers. In Standard Handbook of Biomedical Engineering and Design, K.Myer, ed. McGraw-Hill), p. 11.3-11.30.

- Begley,C.T., Doherty,M.J., Mollan,R.A.B., and Wilson,D.J. (1995). Comparative-Study of the Osteoinductive Properties of Bioceramic, Coral and Processed Bone-Graft Substitutes. Biomaterials *16*, 1181-1185.

- Ben-Nissan,B. and Pezzotti,G. (2004). Bioceramics: An Introduction. In Engineering Materials for Biomedical Applications, T.S.Hin, ed. World Scientific), pp. 6-1-6-36.

- Bermudez,O., Boltong,M.G., Driessens,F.C.M., and Planell,J.A. (1994). Development of Some Calcium-Phosphate Cements from Combinations of Alpha-Tcp, Mcpm and Cao. Journal of Materials Science-Materials in Medicine *5*, 160-163.

- Betts,F. and Posner,A.S. (1974). X-Ray Radial-Distribution Study of Amorphous Calcium-Phosphate. Materials Research Bulletin *9*, 353-360.

- Bitar,M., Salih,V., Mudera,V., Knowles,J.C., and Lewis,M.P. (2004). Soluble phosphate glasses: in vitro studies using human cells of hard and soft tissue origin. Biomaterials *25*, 2283-2292.

- Blom,A. (2007). (v) Which scaffold for which application? Current Orthopaedics *21*, 280-287.

- Bohner,M. (2000). Calcium orthophosphates in medicine: from ceramics to calcium phosphate cements. Injury-International Journal of the Care of the Injured *31*, S37-S47.

- Bohner,M., Gbureck,U., and Barralet,J.E. (2005). Technological issues for the development of more efficient calcium phosphate bone cements: A critical assessment. Biomaterials *26*, 6423-6429.

- Bohner,M., Lemaitre,J., and Ring,T.A. (1996). Effects of sulfate, pyrophosphate, and citrate ions on the physicochemical properties of cements made of beta-tricalcium phosphate-phosphoric acid-water mixtures. Journal of the American Ceramic Society *79*, 1427-1434.

- Bohner, M. and Matter, S. Brushite hydraulic cement stabilized with a magnesium salt. 10/149035[6733582B1], 1-10. 11-5-2004. U.S.A.
  Ref Type: Patent

- Bohner,M., vanLanduyt,P., Merkle,H.P., and Lemaitre,J. (1997). Composition effects on the pH of a hydraulic calcium phosphate cement. Journal of Materials Science-Materials in Medicine *8*, 675-681.

- Boskey,A.L., Maresca,M., Ullrich,W., Doty,S.B., Butler,W.T., and Prince,C.W. (1993). Osteopontin-Hydroxyapatite Interactions In-Vitro - Inhibition of Hydroxyapatite Formation and Growth in A Gelatin-Gel. Bone and Mineral *22*, 147-159.

- Boutin,P., Christel,P., Dorlot,J.M., Meunier,A., Deroquancourt,A., Blanquaert,D., Herman,S., Sedel,L., and Witvoet,J. (1988). The Use of Dense Alumina Alumina Ceramic Combination in Total Hip-Replacement. Journal of Biomedical Materials Research *22*, 1203-1232.

- Bow,J.S., Liou,S.C., and Chen,S.Y. (2004). Structural characterization of room-temperature synthesized nano-sized beta-tricalcium phosphate. Biomaterials *25*, 3155-3161.

- Bragg,L. (1975). The Development of X-Ray Analysis. (London: G. Bell and Sons Ltd).

- Brar,H.S., Platt,M.O., Sarntinoranont,M., Martin,P.I., and Manuel,M.V. (2009). Magnesium as a biodegradable and bioabsorbable material for medical implants. Jom *61*, 31-34.

- Brown,E.H., Lehr,J.R., Smith,J.P., and Frazier,A.W. (1963). Preparation and Characterization of Some Calcium Pyrophosphates. Journal of Agricultural and Food Chemistry *11*, 214-&.

- Brown,W.E. (1962). Octacalcium Phosphate and Hydroxyapatite. Nature *196*, 1048-&.

- Brown, W. E. and Chow, L. C. Dental restorative cement pastes. American Dental Association Health Foundation. 539740[4518430], 1-14. 21-5-1985. Washington D.C.
  Ref Type: Patent

- Brown,W.E. and Chow,L.C. (1976). Chemical Properties of Bone-Mineral. Annual Review of Materials Science *6*, 213-236.

- Brown,W.E., Eidelman,N., and Tomazic,B. (1987). Octacalcium phosphate as a precursor in biomineral formation. Adv Dent Res *1*, 306-313.

- Brown,W.E., Smith,J.P., Frazier,A.W., and Lehr,J.R. (1962). Crystallographic and Chemical Relations Between Octacalcium Phosphate and Hydroxyapatite. Nature *196*, 1050-&.

- Brunski JB (1996). Classes of materials used in medicine. In Biomaterials science: an introduction to materials in medicine, B.D.Ratner, A.S.Hoffman, F.J.Schoen, and J.E.Lemons, eds. (London: Academic Press), pp. 37-50.

- Bucholz,R.W. (2002). Nonallograft osteoconductive bone graft substitutes. Clinical Orthopaedics and Related Research 44-52.

- Bucholz,R.W., Carlton,A., and Holmes,R.E. (1987). Hydroxyapatite and Tricalcium Phosphate Bone-Graft Substitutes. Orthopedic Clinics of North America *18*, 323-334.

- Buck,B.E., Malinin,T.I., and Brown,M.D. (1989). Bone Transplantation and Human Immunodeficiency Virus - An Estimate of Risk of Acquired Immunodeficiency Syndrome (Aids). Clinical Orthopaedics and Related Research 129-136.

- Caswell,A.M., Whyte,M.P., and Russell,R.G.G. (1991). Hypophosphatasia and the Extracellular Metabolism of Inorganic Pyrophosphate - Clinical and Laboratory Aspects. Critical Reviews in Clinical Laboratory Sciences *28*, 175-&.

- Chen,P.S., Toribara,T.Y., and Warner,H. (1956). Microdetermination of Phosphorus. Analytical Chemistry *28*, 1756-1758.

- Chevalier,J. (2006). What future for zirconia as a biomaterial? Biomaterials *27*, 535-543.

- Choi,D. and Kumta,P.N. (2007). Mechano-chemical synthesis and characterization of nanostructured beta-TCP powder. Materials Science & Engineering C-Biomimetic and Supramolecular Systems *27*, 377-381.

- Christoffersen,M.R. and Christoffersen,J. (2003). Effects of a bisphosphonate (EHDP) on growth, formation, and dissolution of calcium pyrophosphate crystals. Crystal Growth & Design *3*, 79-82.

- Cini,R., Chindamo,D., Catenaccio,M., Lorenzini,S., Selvi,E., Nerucci,F., Picchi,M.P., Berti,G., and Marcolongo,R. (2001). Dissolution of calcium pyrophosphate crystals by polyphosphates: an in vitro and ex vivo study. Annals of the Rheumatic Diseases *60*, 962-967.

- Constantz,B.R., Ison,I.C., Fulmer,M.T., Poser,R.D., Smith,S.T., Vanwagoner,M., Ross,J., Goldstein,S.A., Jupiter,J.B., and Rosenthal,D.I. (1995). Skeletal Repair by In-Situ Formation of the Mineral Phase of Bone. Science *267*, 1796-1799.

- Cox,R.P., Gilbert,P., and Griffin,M.J. (1967). Alkaline Inorganic Pyrophosphatase Activity of Mammalian-Cell Alkaline Phosphatase. Biochemical Journal *105*, 155-&.

- Currey,J.D. (2001). Bone and natural composites: porperties. In Encyclopedia of Materials: Science and Technology, K.H.J.Buschow, R.W.Cahn, M.C.Flemings, B.Ilschner, E.J.Kramer, and S.Mahajan, eds. Elsevier), pp. 776-782.

- de Groot K. (1984). Calcium Phosphate Ceramics: Their Current Status. In Contemporary biomaterials, Boretos JW and Eden M, eds. (USA: Noyes Publications), pp. 477-492.

- de Groot,K. (1980). Bioceramics Consisting of Calcium-Phosphate Salts. Biomaterials *1*, 47-50.

- de Jong,W.F. (1926). Mineral substance in bones. Recueil des Travaux Chimiques des Pays-Bas *45*, 445-448.

- del Valle,S., Mino,N., Munoz,F., Gonzalez,A., Planell,J.A., and Ginebra,M.P. (2007). In vivo evaluation of an injectable Macroporous Calcium Phosphate Cement. Journal of Materials Science-Materials in Medicine *18*, 353-361.

- Denissen,H.W. and Degroot,K. (1979). Immediate Dental Root Implants from Synthetic Dense Calcium Hydroxylapatite. Journal of Prosthetic Dentistry *42*, 551-556.

- Dias,A.G., Lopes,M.A., Santos,J.D., Afonso,A., Tsuru,K., Osaka,A., Hayakawa,S., Takashima,S., and Kurabayashi,Y. (2006). In vivo performance of biodegradable calcium phosphate glass ceramics using the

rabbit model: Histological and SEM observation. Journal of Biomaterials Applications *20*, 253-266.

- Dion,A., Langman,M., Hall,G., and Filiaggi,M. (2005). Vancomycin release behaviour from amorphous calcium polyphosphate matrices intended for osteomyelitis treatment. Biomaterials *26*, 7276-7285.

- Doherty,M.J., Schlag,G., Schwarz,N., Mollan,R.A.B., Nolan,P.C., and Wilson,D.J. (1994). Biocompatibility of Xenogeneic Bone, Commercially Available Coral, A Bioceramic and Tissue Sealant for Human Osteoblasts. Biomaterials *15*, 601-608.

- Dorozhkin,S.V. (2010). Bioceramics of calcium orthophosphates. Biomaterials *31*, 1465-1485.

- Dorozhkin,S.V. (2007). Calcium orthophosphates. Journal of Materials Science *42*, 1061-1095.

- Dorozhkin,S.V. (2008). Calcium orthophosphate cements for biomedical application. Journal of Materials Science *43*, 3028-3057.

- Dorozhkin,S.V. and Epple,M. (2002). Biological and medical significance of calcium phosphates. Angewandte Chemie-International Edition *41*, 3130-3146.

- Driessens,F.C.M., Boltong,M.G., Bermudez,O., Planell,J.A., Ginebra,M.P., and Fernandez,E. (1994). Effective Formulations for the Preparation of Calcium-Phosphate Bone Cements. Journal of Materials Science-Materials in Medicine *5*, 164-170.

- Dubok,V.A. (2000). Bioceramics - Yesterday, today, tomorrow. Powder Metallurgy and Metal Ceramics *39*, 381-394.

- Ducheyne,P., Hench,L.L., Kagan,A., Martens,M., Bursens,A., and Mulier,J.C. (1980). Effect of Hydroxyapatite Impregnation on Skeletal Bonding of Porous Coated Implants. Journal of Biomedical Materials Research *14*, 225-237.

- Elliot J.C. (1994). Structure and chemicstry of the apatites and other calcium orthophosphates. (Amsterdam: Elsevier).

- Fahrleitner-Pammer,A., Obernosterer,A., Pilger,E., Dobnig,H., Dimai,H.P., Leb,G., Kudlacek,S., and Obermayer-Pietsch,B.M. (2005). Hypovitaminosis D, impaired bone turnover and low bone mass are common in patients with peripheral arterial disease. Osteoporosis International *16*, 319-324.

- Fernandez,E., Gil,F.J., Ginebra,M.P., Driessens,F.C.M., Planell,J.A., and Best,S.M. (1999). Calcium phosphate bone cements for clinical applications -

Part I: Solution chemistry. Journal of Materials Science-Materials in Medicine *10*, 169-176.

- Frame,J.W. (1975). Porous calcium sulphate dihydrate as a biodegradable implant in bone. J Dent *3*, 177-187.

- Fratzl,P., Gupta,H.S., Paschalis,E.P., and Roschger,P. (2004). Structure and mechanical quality of the collagen-mineral nano-composite in bone. Journal of Materials Chemistry *14*, 2115-2123.

- Frayssinet,P., Gineste,L., Conte,P., Fages,J., and Rouquet,N. (1998). Short-term implantation effects of a DCPD-based calcium phosphate cement. Biomaterials *19*, 971-977.

- Friedlander,G.E., Strong,D.M., Tomford,W.W., and Mankin,H.J. (1999). Long-term follow-up of patients with osteochondral allografts - A correlation between immunologic responses and clinical outcome. Orthopedic Clinics of North America *30*, 583-+.

- Friedman,C.D., Costantino,P.D., Takagi,S., and Chow,L.C. (1998). BoneSource (TM) hydroxyapatite cement: A novel biomaterial for craniofacial skeletal tissue engineering and reconstruction. Journal of Biomedical Materials Research *43*, 428-432.

- Gatti,A.M., Zaffe,D., and Poli,G.P. (1990). Behavior of Tricalcium Phosphate and Hydroxyapatite Granules in Sheep Bone Defects. Biomaterials *11*, 513-517.

- Gbureck,U., Hoelzel,T., Biermann,I., Barralet,J.E., and Grover,L.M. (2008). Preparation of tricalcium phosphate/calcium pyrophosphate structures via rapid prototyping. Journal of Materials Science-Materials in Medicine *19*, 1559-1563.

- Gbureck,U., Hozel,T., Klammert,U., Wurzler,K., Muller,F.A., and Barralet,J.E. (2007). Resorbable dicalcium phosphate bone substitutes prepared by 3D powder printing. Advanced Functional Materials *17*, 3940-3945.

- Geesink,R.G.T. (1990). Hydroxyapatite-Coated Total Hip Prostheses - 2-Year Clinical and Roentgenographic Results of 100 Cases. Clinical Orthopaedics and Related Research 39-58.

- Geesink,R.G.T., Degroot,K., and Klein,C.P.A.T. (1988). Bonding of Bone to Apatite-Coated Implants. Journal of Bone and Joint Surgery-British Volume *70*, 17-22.

- German,R.M. (2001). Sintering: Modelling. In Encyclopedia of Materials - Science and Technology, Volumes 1-11, K.H.J.Buschow, R.W.Cahn,

M.C.Flemings, B.Ilschner, E.J.Kramer, and S.Mahajan, eds. Elsevier), pp. 8643-8647.

- Giannoudis,P.V., Dinopoulos,H., and Tsiridis,E. (2005). Bone substitutes: an update. Injury *36 Suppl 3*, S20-S27.

- Gilding,D.K. and Reed,A.M. (1979). Biodegradable Polymers for Use in Surgery - Polyglycolic-Poly(Actic Acid) Homopolymers and Copolymers .1. Polymer *20*, 1459-1464.

- Ginebra,M.P., Fernandez,E., DeMaeyer,E.A.P., Verbeeck,R.M.H., Boltong,M.G., Ginebra,J., Driessens,F.C.M., and Planell,J.A. (1997). Setting reaction and hardening of an apatitic calcium phosphate cement. Journal of Dental Research *76*, 905-912.

- Ginebra,M.P., Traykova,T., and Planell,J.A. (2006). Calcium phosphate cements as bone drug delivery systems: A review. Journal of Controlled Release *113*, 102-110.

- Goldstein,J.I., Romig,Jr.A.D., Newbury,D.E., Lyman,C.E., Echlin,P., Fiori,C., Joy,D.C., and Lifshin,E. (1992). Scannng Electron Microscopy and X-Ray Microanalysis. Plenum Press).

- Gollwitzer,H., Thomas,P., Diehl,P., Steinhauser,E., Summer,B., Barnstorf,S., Gerdesmeyer,L., Mittelmeier,W., and Stemberger,A. (2005). Biomechanical and allergological characteristics of a biodegradable poly(D,L-lactic acid) coating for orthopaedic implants. Journal of Orthopaedic Research *23*, 802-809.

- Gong,J.P., Katsuyama,Y., Kurokawa,T., and Osada,Y. (2003). Double-network hydrogels with extremely high mechanical strength. Advanced Materials *15*, 1155-+.

- Greenfield,S. and Clift,M. (1975). General properties of the condensed phosphates. In Analytical chemistry of the condensed phosphates, (Oxford, New York: Pergamon Press), pp. 1-36.

- Griesser,H.J. and Kambouris,P.A. (2001). Biocompatible Hydrogels. In Encyclopedia of materials science and technology, Vol 1 -11, K.H.J.Buschow, R.W.Cahn, M.C.Flemings, B.Ilschner, E.J.Kramer, and S.Mahajan, eds. Elsevier), pp. 548-551.

- Griffith, E. J. Acicular, crystalline calcium metaphosphate. 153667[4360625]. 23-11-1982. US.
  Ref Type: Patent

- Griffith,M.L. and Halloran,J.W. (1996). Freeform fabrication of ceramics via stereolithography. Journal of the American Ceramic Society *79*, 2601-2608.

- Griffiths,P.R. and de Haseth,J.A. (2007). Fourier Transform Infrared Spectrometry. John Wiley and Sons, INC.,).

- Grimm,M.J. (2003). Orthopedic Biomaterials. In Standard Handbook of Biomedical Engineering and Design, K.Myer, ed. McGraw-Hill), p. 15.1-15.22.

- Grover,L.M., Gbureck,U., Wright,A.J., Tremayne,M., and Barralet,J.E. (2006). Biologically mediated resorption of brushite cement in vitro. Biomaterials *27*, 2178-2185.

- Grover,L.M., Gbureck,U., Young,A.M., Wright,A.J., and Barralet,J.E. (2005). Temperature dependent setting kinetics and mechanical properties of beta-TCP-pyrophosphoric acid bone cement. Journal of Materials Chemistry *15*, 4955-4962.

- Grover,L.M., Knowles,J.C., Fleming,G.J.P., and Barralet,J.E. (2003). In vitro ageing of brushite calcium phosphate cement. Biomaterials *24*, 4133-4141.

- Grynpas,M.D., Bonar,L.C., and Glimcher,M.J. (1984). X-Ray-Diffraction Radial-Distribution Function Studies on Bone-Mineral and Synthetic Calcium Phosphates. Journal of Materials Science *19*, 723-736.

- Grynpas,M.D., Pilliar,R.M., Kandel,R.A., Renlund,R., Filiaggi,M., and Dumitriu,M. (2002). Porous calcium polyphosphate scaffolds for bone substitute applications in vivo studies. Biomaterials *23*, 2063-2070.

- Hamanishi,C., Kitamoto,K., Tanaka,S., Otsuka,M., Doi,Y., and Kitahashi,T. (1996). A self-setting TTCP-DCPD apatite cement for release of vancomycin. Journal of Biomedical Materials Research *33*, 139-143.

- Harold,F.M. (1966). Inorganic Polyphosphates in Biology - Structure Metabolism and Function. Bacteriological Reviews *30*, 772-&.

- Havill,L.M. (2004). Osteon remodeling dynamics in Macaca mulatta: Normal variation with regard to age, sex, and skeletal maturity. Calcified Tissue International *74*, 95-102.

- Hearn,P.R. and Russell,R.G.G. (1980). Formation of Calcium Pyrophosphate Crystals Invitro - Implications for Calcium Pyrophosphate Crystal Deposition Disease (Pseudogout). Annals of the Rheumatic Diseases *39*, 222-227.

- Hedberg,E.L. and Mikos,A.G. (2001). Bone augmentation and repair. In Encyclopedia of Materials: Science and Technology, K.H.J.Buschow, R.W.Cahn, M.C.Flemings, B.Ilschner, E.J.Kramer, and S.Mahajan, eds. Elsevier), pp. 782-787.

- Hench,L.L. (1998). Bioceramics. Journal of the American Ceramic Society *81*, 1705-1728.

- Hench,L.L. (1991). Bioceramics - from Concept to Clinic. Journal of the American Ceramic Society *74*, 1487-1510.

- Hench,L.L. (2001). Bioglass and Similar Materials. In Encyclopedia of Materials: Science and Technology, K.H.J.Buschow, R.W.Cahn, M.C.Flemings, B.Ilschner, E.J.Kramer, and S.Mahajan, eds. Elsevier), pp. 563-568.

- Hench,L.L., Splinter,R.J., Allen,W.C., and Greenlee,T.K. (1972). Bonding Mechanism at the Interface of Ceramic Prosthetic Materials. Journal of Biomedical Materials Research Biomedical Materials Symposium *2*, 117-141.

- Hench,L.L. and Wilson,J. (1984). Surface-Active Biomaterials. Science *226*, 630-636.

- Hesse,A. and Heimbach,D. (1999). Causes of phosphate stone formation and the importance of metaphylaxis by urinary acidification: a review. World Journal of Urology *17*, 308-315.

- Hessle,L., Johnson,K.A., Anderson,H.C., Narisawa,S., Sali,A., Goding,J.W., Terkeltaub,R., and Millan,J.L. (2002). Tissue-nonspecific alkaline phosphatase and plasma cell membrane glycoprotein-1 are central antagonistic regulators of bone mineralization. Proceedings of the National Academy of Sciences of the United States of America *99*, 9445-9449.

- Hing,K.A. (2004). Bone repair in the twenty-first century: biology, chemistry or engineering? Philosophical Transactions of the Royal Society of London Series A-Mathematical Physical and Engineering Sciences *362*, 2821-2850.

- Hsu,H.H.T. and Anderson,H.C. (1978). Calcification of Isolated Matrix Vesicles and Reconstituted Vesicles from Fetal Bovine Cartilage. Proceedings of the National Academy of Sciences of the United States of America *75*, 3805-3808.

- Hulbert,S.F., Hench,L.L., Forbers,D., and Bowman,L.S. (1982). History of bioceramics. Ceramics International *8*, 131-140.

- Hulbert,S.F., Klawitte,J.J., and Bowman,L.S. (1972). History of Ceramic Orthopedic Implants. Materials Research Bulletin *7*, 1239-&.

- Hull, C. W. Method for production of three-dimensional objects by stereolithography. 3D Systems Inc. 462865[5554336]. 10-9-1996. USA. Ref Type: Patent

- Hunter,G.K. and Goldberg,H.A. (1993). Nucleation of Hydroxyapatite by Bone Sialoprotein. Proceedings of the National Academy of Sciences of the United States of America *90*, 8562-8565.

- Hunter,G.K., Hauschka,P.V., Poole,A.R., Rosenberg,L.C., and Goldberg,H.A. (1996). Nucleation and inhibition of hydroxyapatite formation by mineralized tissue proteins. Biochemical Journal *317*, 59-64.

- Hunter,G.K., Kyle,C.L., and Goldberg,H.A. (1994). Modulation of Crystal-Formation by Bone Phosphoproteins - Structural Specificity of the Osteopontin-Mediated Inhibition of Hydroxyapatite Formation. Biochemical Journal *300*, 723-728.

- Ignjatovic,N.L., Liu,C.Z., Czernuszka,J.T., and Uskokovi,D.P. (2007). Micro- and nano-injectable composite biomaterials containing calcium phosphate coated with poly(DL-lactide-co-glycolide). Acta Biomaterialia *3*, 927-935.

- Ilan,D.I. and Ladd,A.L. (2002). Bone graft substitutes. Operative Techniques in Plastic and Reconstructive Surgery *9*, 151-160.

- Ishikawa,K., Matsuya,S., Miyamoto,Y., and Kawate,K. (2003). Bioceramics. In Comprehensive Structural Integrity, Volumes 1-10, I.Milne, R.O.Ritchie, and B.Karihaloo, eds. Elsevier), pp. 170-210.

- Itokazu,M., Yang,W.Y., Aoki,T., Ohara,A., and Kato,N. (1998). Synthesis of antibiotic-loaded interporous hydroxyapatite blocks by vacuum method and in vitro drug release testing. Biomaterials *19*, 817-819.

- Jacobs,J.J., Gilbert,J.L., and Urban,R.M. (1998). Corrosion of metal orthopaedic implants. Journal of Bone and Joint Surgery-American Volume *80A*, 268-282.

- Jarcho,M. (1981). Calcium-Phosphate Ceramics As Hard Tissue Prosthetics. Clinical Orthopaedics and Related Research 259-278.

- Johnson,K.A., Hessle,L., Vaingankar,S., Wennberg,C., Mauro,S., Narisawa,S., Goding,J.W., Sano,K., Millan,J.L., and Terkeltaub,R. (2000). Osteoblast tissue-nonspecific alkaline phosphatase antagonizes and regulates PC-1. American Journal of Physiology-Regulatory Integrative and Comparative Physiology *279*, R1365-R1377.

- Kalita,S.J., Bhardwaj,A., and Bhatt,H.A. (2007). Nanocrystalline calcium phosphate ceramics in biomedical engineering. Materials Science & Engineering C-Biomimetic and Supramolecular Systems *27*, 441-449.

- Kamakura,S., Sasano,Y., Homma,H., Suzuki,O., Kagayama,M., and Motegi,K. (1999). Implantation of octacalcium phosphate (OCP) in rat skull defects enhances bone repair. Journal of Dental Research *78*, 1682-1687.

- Karlkroupa,E., Callis,C.F., and Seifter,E. (1957). Stability of Condensed Phosphates in Very Dilute Solutions. Industrial and Engineering Chemistry *49*, 2061-2062.

- Kasuga,T. (2007). Development of phosphate glass-ceramics for biomedical applications. Journal of the Ceramic Society of Japan *115*, 455-459.

- Kasuga,T. and Abe,Y. (1998). Novel calcium phosphate ceramics prepared by powder sintering and crystallization of glasses in the pyrophosphate region. Journal of Materials Research *13*, 3357-3360.

- Kasuga,T., Sawada,M., Nogami,M., and Abe,Y. (1999). Bioactive ceramics prepared by sintering and crystallization of calcium phosphate invert glasses. Biomaterials *20*, 1415-1420.

- Kitsugi,T., Yamamuro,T., Nakamura,T., Kotani,S., Kokubo,T., and Takeuchi,H. (1993). 4 Calcium-Phosphate Ceramics As Bone Substitutes for Non-Weight-Bearing. Biomaterials *14*, 216-224.

- Kornberg,A., Rao,N.N., and ult-Riche,D. (1999). Inorganic polyphosphate: A molecule of many functions. Annual Review of Biochemistry *68*, 89-125.

- Koster,K., Heide,H., and Konig,R. (1977). Resorbable Calcium-Phosphate Ceramics Under Load. Langenbecks Archiv fur Chirurgie *343*, 173-181.

- Kualev,I.S., Vagabov,V.M., and Kulakovskaya,T.V. (2004). The Biochemistry of Inorganic Polyphosphates. John Wiley & Sons Ltd).

- Kuhn,L.T. (2001). Bone Mineralisation. In Encyclopedia of Materials: Science and Technology, K.H.J.Buschow, R.W.Cahn, M.C.Flemings, B.Ilschner, E.J.Kramer, and S.Mahajan, eds. Elsevier), pp. 787-794.

- Kulkarni,R.K., Moore,E.G., Hegyeli,A.F., and Leonard,F. (1971). Bio Degradable Poly Lactic-Acid Polymers. Journal of Biomedical Materials Research *5*, 169-181.

- Kura,G. (1987b). Hydrolysis Reaction of Inorganic Cyclophosphates at Various Acid Strengths. Polyhedron *6*, 531-533.

- Kura,G. (1991). Hydrolysis of Cyclopentaphosphate, Cycloheptaphosphate, Linear Pentaphosphate and Heptaphosphate in Aqueous-Solution. Polyhedron *10*, 697-702.

- Kura,G. (1987a). Alkaline-Hydrolysis of Inorganic Cyclo-Polyphosphates. Bulletin of the Chemical Society of Japan *60*, 2857-2860.

- Kura,G., Miyazaki,Y., and Sakamoto,J. (1998). Additional reactions of inorganic condensed phosphate oligomers during their degradation reactions in the presence of aluminum(III) ions. Polyhedron *17*, 1907-1912.

- Kura,G. and Tsukuda,T. (1993). Effect of Copper(Ii), Nickel(Ii) and Aluminum(Iii) Ions on the Hydrolysis Rates of Inorganic Condensed Phosphate Oligomers. Polyhedron *12*, 865-870.

- Kurashina,K., Kurita,H., Hirano,M., Kotani,A., Klein,C.P.A.T., and Degroot,K. (1997). In vivo study of calcium phosphate cements: Implantation of an alpha-tricalcium phosphate dicalcium phosphate dibasic tetracalcium phosphate monoxide cement paste. Biomaterials *18*, 539-543.

- Lagow,R.J., Capano,P.C., Hoffman,S.S., Nelson,S.F., Read,L.A., Jacoby,B.H., Ross,A.E., Cooper,O.J., and Davis,W.L. (1991). Calcium Polyphosphate Bioceramic Cpb Implants in Canine Mandibular Block Defects. Journal of Dental Research *70*, 302.

- Lakes,R. (1993). Materials with Structural Hierarchy. Nature *361*, 511-515.

- Lambotte,A. (1932). L'utilisation du magnesium comme materiel perdu dans l'osteosynthese. Bull Mem Soc Nat Chir *28*, 1325-1334.

- Lawson,A.C. and Czernuszka,J.T. (1998). Collagen-calcium phosphate composites. Proceedings of the Institution of Mechanical Engineers Part H-Journal of Engineering in Medicine *212*, 413-425.

- Lee,J.H., Lee,C.K., Chang,B.S., Ryu,H.S., Seo,J.H., Hong,S., and Kim,H. (2006). In vivo study of novel biodegradable and osteoconductive CaO-SiO2-B2O3 glass-ceramics. Journal of Biomedical Materials Research Part A *77A*, 362-369.

- LeGeros,R.Z. (1988). Calcium phosphate materials in restorative dentistry: a review. Adv Dent Res *2*, 164-180.

- LeGeros,R.Z. (2001). Formation and transformation of calcium phosphates: relevance to vascular calcification. Z Kardiol *90 Suppl 3*.

- Lemaitre,J., Mirtchi,A.A., and Mortier,A. (1987). Calcium phosphate cements for medical use: state of the art and perspectives of development. Silicates Industriels *9-10*, 141-146.

- Leong,K.F., Cheah,C.M., and Chua,C.K. (2003). Solid freeform fabrication of three-dimensional scaffolds for engineering replacement tissues and organs. Biomaterials *24*, 2363-2378.

- Levine,B. (2008). A New Era in Porous Metals: Applications in Orthopaedics. Advanced Engineering Materials *10*, 788-792.

- Lewandrowski,K.U., Gresser,J.D., Wise,D.L., and Trantolo,D.J. (2000). Bioresorbable bone graft substitutes of different osteoconductivities: a histologic evaluation of osteointegration of poly(propylene glycol-co-fumaric acid)-based cement implants in rats. Biomaterials *21*, 757-764.

- Li,J. (2004). Polymeric Hydrogels. In Engineering materials for biomedical applications, S.H.Teoh, ed. World Scientific), pp. 7-1-7-18.

- Li,L.C., Gao,J.C., and Wang,Y. (2004). Evaluation of cyto-toxicity and corrosion behavior of alkali-heat-treated magnesium in simulated body fluid. Surface & Coatings Technology *185*, 92-98.

- Lin,C.C., Liao,C.J., Sun,J.S., Liu,H.C., and Lin,F.H. (1996). Prevascularized bone graft cultured in sintered porous beta-Ca2P2O7 with 5 wt% Na4P2O7 center dot 10H(2)O addition ceramic chamber. Biomaterials *17*, 1133-1140.

- Lin,F.H., Liaw,J.R., Hon,M.H., and Wang,C.Y. (1995a). The Effects of Na4P2O7-Center-Dot-10H(2)O Addition on the Mechanical-Properties of Sintered Ca2P2O7 Bioceramic. Materials Chemistry and Physics *41*, 110-116.

- Lin,F.H., Lin,C.C., Lu,C.M., Liu,H.C., Sun,J.S., and Wang,C.Y. (1995b). Mechanical-Properties and Histological-Evaluation of Sintered Beta-Ca2P2O7 with Na4P2O7-Center-Dot-10H2O Addition. Biomaterials *16*, 793-802.

- Liu,D.M., Troczynski,T., and Tseng,W.J. (2001). Water-based sol-gel synthesis of hydroxyapatite: process development. Biomaterials *22*, 1721-1730.

- Liu,T.Y., Chen,S.Y., Liu,D.M., and Liou,S.C. (2005). On the study of BSA-loaded calcium-deficient hydroxyapatite nano-carriers for controlled drug delivery. Journal of Controlled Release *107*, 112-121.

- Llinas,P., Masella,M., Stigbrand,T., Menez,A., Stura,E.A., and Le Du,M.H. (2006). Structural studies of human alkaline phosphatase in complex with strontium: Implication for its secondary effect in bones. Protein Science *15*, 1691-1700.

- Lu,X. and Leng,Y. (2005). Theoretical analysis of calcium phosphate precipitation in simulated body fluid. Biomaterials *26*, 1097-1108.

- Ludwig,S.C., Kowalski,J.M., and Boden,S.D. (2000). Osteoinductive bone graft substitutes. European Spine Journal *9*, S119-S125.

- Malak,S.F.F. and Anderson,I.A. (2008). Orthogonal cutting of cancellous bone with application to the harvesting of bone autograft. Medical Engineering & Physics *30*, 717-724.

- Marks,S.C.Jr. and Odgren,P.R. (2002). Structure and Development of the Skeleton. In Principles of Bone Biology, J.P.Bilezikan, L.G.Raisz, and G.A.Rodan, eds. Academic Press), pp. 3-15.

- Martin,R.B., Burr,D.B., and Sharkey,N.A. (1998). Skeletal Biology. In Skeletal Tissue Mechanics, (New York: Springer), pp. 29-78.

- Mccarty,D.J. (1976). Calcium Pyrophosphate Dihydrate Crystal Deposition Disease - 1975. Arthritis and Rheumatism *19*, 275-285.

- Mccarty,D.J., Kohn,N.N., and Faires,J.S. (1962). Significance of Calcium Phosphate Crystals in Synovial Fluid of Arthritic Patients - Pseusogout Syndrome .1. Clinical Aspects. Annals of Internal Medicine *56*, 711-&.

- Mccarty,D.J., Solomon,S.D., Warnock,M.L., and Paloyan,E. (1971). Inorganic Pyrophosphate Concentrations in Synovial Fluid of Arthritic Patients. Journal of Laboratory and Clinical Medicine *78*, 216-&.

- McComb,R.B., Bowers,G.N., and Posen,S. (1979). Alkaline Phosphatases. (New York: Plenum Press).

- Mckee,M.D. and Nanci,A. (1996). Osteopontin at mineralized tissue interfaces in bone, teeth, and osseointegrated implants: Ultrastructural distribution and implications for mineralized tissue formation, turnover, and repair. Microscopy Research and Technique *33*, 141-164.

- Middleton,J.C. and Tipton,A.J. (2000). Synthetic biodegradable polymers as orthopedic devices. Biomaterials *21*, 2335-2346.

- Millan,J.L. (2006). Alkaline Phosphatases : Structure, substrate specificity and functional relatedness to other members of a large superfamily of enzymes. Purinergic. Signal. *2*, 335-341.

- Miller,R.A., Brady,J.M., and Cutright,D.E. (1977). Degradation Rates of Oral Resorbable Implants (Polylactates and Polyglycolates) - Rate Modification with Changes in Pla-Pga Copolymer Ratios. Journal of Biomedical Materials Research *11*, 711-719.

- Mirtchi,A.A., Lemaitre,J., and Terao,N. (1989). Calcium-Phosphate Cements - Study of the Beta-Tricalcium Phosphate - Monocalcium Phosphate System. Biomaterials *10*, 475-480.

- Monma,H. and Kanazawa,T. (2000). The hydration of alpha-tricalcium phosphate. Journal of the Ceramic Society of Japan *108*, S75-S80.

- Moochhala,S.H., Sayer,J.A., Carr,G., and Simmons,N.L. (2008). Renal calcium stones: insights from the control of bone mineralization. Experimental Physiology *93*, 43-49.

- Mornet,E., Stura,E., Lia-Baldini,A.S., Stigbrand,T., Menez,A., and Le Du,M.H. (2001). Structural evidence for a functional role of human tissue nonspecific alkaline phosphatase in bone mineralization. Journal of Biological Chemistry *276*, 31171-31178.

- Moss,D.W. (1982). Alkaline-Phosphatase Isoenzymes. Clinical Chemistry *28*, 2007-2016.

- Muginova,S.V., Zhavoronkova,A.M., Polyakov,A.E., and Shekhovtsova,T.N. (2007). Application of alkaline phosphatases from different sources in pharmaceutical and clinical analysis for the determination of their cofactors; Zinc and magnesium ions. Analytical Sciences *23*, 357-363.

- Nagano,M., Kitsugi,T., Nakamura,T., Kokubo,T., and Tanahashi,M. (1996). Bone bonding ability of an apatite-coated polymer produced using a biomimetic method: A mechanical and histological study in vivo. Journal of Biomedical Materials Research *31*, 487-494.

- Nair,L.S. and Laurencin,C.T. (2007). Biodegradable polymers as biomaterials. Progress in Polymer Science *32*, 762-798.

- Nancollas,G.H. and Wu,W.J. (2000). Biomineralization mechanisms: a kinetics and interfacial energy approach. Journal of Crystal Growth *211*, 137-142.

- Navarro,M., Michiardi,A., Castano,O., and Planell,J.A. (2008). Biomaterials in orthopaedics. Journal of the Royal Society Interface *5*, 1137-1158.

- Nelson,S.R., Wolford,L.M., Lagow,R.J., Capano,P.J., and Davis,W.L. (1993). Evaluation of New High-Performance Calcium Polyphosphate Bioceramics As Bone-Graft Materials. Journal of Oral and Maxillofacial Surgery *51*, 1363-1371.

- Ng,A.M.H., Tan,K.K., Phang,M.Y., Aziyati,O., Tan,G.H., Isa,M.R., Aminuddin,B.S., Naseem,M., Fauziah,O., and Ruszymah,B.H.I. (2008). Differential osteogenic activity of osteoprogenitor cells on HA and TCP/HA scaffold of tissue engineered bone. Journal of Biomedical Materials Research Part A *85A*, 301-312.

- Ng,K.W., Romas,E., Donnan,L., and Findlay,D.M. (1997). Bone biology. Baillieres Clinical Endocrinology and Metabolism *11*, 1-22.

- Nijiweide,P.J., Burger,E.H., and Klein-Nulend,J. (2002). The osteocyte. In Principles of Bone Biology, J.P.Bilezikan, L.G.Raisz, and G.A.Rodan, eds. Academic Press), pp. 93-107.

- Ohura,K., Bohner,M., Hardouin,P., Lemaitre,J., Pasquier,G., and Flautre,B. (1996). Resorption of, and bone formation from, new beta-tricalcium phosphate-monocalcium phosphate cements: An in vivo study. Journal of Biomedical Materials Research *30*, 193-200.

- Olszta,M.J., Cheng,X.G., Jee,S.S., Kumar,R., Kim,Y.Y., Kaufman,M.J., Douglas,E.P., and Gower,L.B. (2007). Bone structure and formation: A new perspective. Materials Science & Engineering R-Reports *58*, 77-116.

- Omelon,S.J. and Grynpas,M.D. (2008). Relationships between Polyphosphate Chemistry, Biochemistry and Apatite Biomineralization. Chemical Reviews *108*, 4694-4715.

- Omelon,S., Georgiou,J., Henneman,Z.J., Wise,L.M., Sukhu,B., Hunt,T., Wynnyckyj,C., Holmyard,D., Bielecki,R., and Grynpas,M.D. (2009). Control of vertebrate skeletal mineralization by polyphosphates. Plos One *4*, e5634.

- Palazzo,B., Sidoti,M.C., Roveri,N., Tampieri,A., Sandri,M., Bertolazzi,L., Galbusera,F., Dubini,G., Vena,P., and Contro,R. (2005). Controlled drug delivery from porous hydroxyapatite grafts: An experimental and theoretical approach. Materials Science & Engineering C-Biomimetic and Supramolecular Systems *25*, 207-213.

- Pampena,D.A., Robertson,K.A., Litvinova,O., Lajoie,G., Goldberg,H.A., and Hunter,G.K. (2004). Inhibition of hydroxyapatite formation by osteopontin phosphopeptides. Biochemical Journal *378*, 1083-1087.

- Pan,Y.S., Xiong,D.S., and Chen,X.L. (2007). Mechanical properties of nanohydroxyapatite reinforced poly(vinyl alcohol) gel composites as biomaterial. Journal of Materials Science *42*, 5129-5134.

- Parfitt,A. (1994). Osteonal and hemi-osteonal remodeling: The spatial and temporal framework for signal traffic in adult human bone. Journal of Cellular Biochemistry *55*, 273-286.

- Patel,A. and Mequanint,K. (2007). Novel physically crosslinked polyurethane-block-poly(vinyl pyrrolidone) hydrogel biomaterials. Macromolecular Bioscience *7*, 727-737.

- Paul,W. and Sharma,C.P. (1999). Development of porous spherical hydroxyapatite granules: application towards protein delivery. Journal of Materials Science-Materials in Medicine *10*, 383-388.

- Peppas,N.A., Hilt,J.Z., Khademhosseini,A., and Langer,R. (2006). Hydrogels in biology and medicine: From molecular principles to bionanotechnology. Advanced Materials *18*, 1345-1360.

- Peters,F. and Reif,D. (2004). Functional materials for bone regeneration from beta-tricalcium phosphate. Materialwissenschaft und Werkstofftechnik *35*, 203-207.

- Petropoulos,J.H., Tsimillis,K., Savvakis,C., and Havredaki,V. (1983). Simple Sensitive Techniques for Absolute and Differential Helium Pycnometry. Journal of Physics E-Scientific Instruments *16*, 1112-1115.

- Piconi,C. (2001). Oxide Ceramics for Biomedical Applications. In Encyclopedia of Materials: Science and Technology, K.H.J.Buschow,

R.W.Cahn, M.C.Flemings, B.Ilschner, E.J.Kramer, and S.Mahajan, eds. Elsevier), pp. 6595-6601.

- Pietak,A., Mahoney,P., Dias,G.J., and Staiger,M.P. (2008). Bone-like matrix formation on magnesium and magnesium alloys. Journal of Materials Science-Materials in Medicine *19*, 407-415.

- Pilliar,R.M., Filiaggi,M.J., Wells,J.D., Grynpas,M.D., and Kandel,R.A. (2001). Porous calcium polyphosphate scaffolds for bone substitute applications - in vitro characterization. Biomaterials *22*, 963-972.

- Porter,N.L., Pilliar,R.M., and Grynpas,M.D. (2001). Fabrication of porous calcium polyphosphate implants by solid freeform fabrication: A study of processing parameters and in vitro degradation characteristics. Journal of Biomedical Materials Research *56*, 504-515.

- Precheur,H.V. (2007). Bone graft materials. Dent Clin North Am *51*, 729-46, viii.

- Pritzker,K.P.H. (1980). Crystal-Associated Arthropathies - Whats New in Old Joints. Journal of the American Geriatrics Society *28*, 439-445.

- Ramchandani,M. and Robinson,D. (1998). In vitro and in vivo release of ciprofloxacin from PLGA 50 : 50 implants. Journal of Controlled Release *54*, 167-175.

- Rezwan,K., Chen,Q.Z., Blaker,J.J., and Boccaccini,A.R. (2006). Biodegradable and bioactive porous polymer/inorganic composite scaffolds for bone tissue engineering. Biomaterials *27*, 3413-3431.

- Rho,J.Y., Kuhn-Spearing,L., and Zioupos,P. (1998). Mechanical properties and the hierarchical structure of bone. Medical Engineering & Physics *20*, 92-102.

- Rosiak, J., Ruciska-Rybus, A., and Wladyslaw, P. Method of manufacturing hydrogel dressings. Politechnika Lodzka. 140150[4871490]. 3-10-1989. Poland.
  Ref Type: Patent

- Ryu,H.S., Youn,H.J., Hong,K.S., Chang,B.S., Lee,C.K., and Chung,S.S. (2002). An improvement in sintering property of beta-tricalcium phosphate by addition of calcium pyrophosphate. Biomaterials *23*, 909-914.

- Safari,A., Danforth,S.C., Allahverdi,M., and Venkataraman,N. (2001). Rapid Prototyping. In Encyclopedia of Materials - Science and Technology, Volumes 1-11, K.H.J.Buschow, R.W.Cahn, M.C.Flemings, B.Ilschner, E.J.Kramer, and S.Mahajan, eds. Elsevier), pp. 7991-8003.

- Safronova,T.V., Putlyaev,V.I., Shekhirev,M.A., and Kuznetsov,A.V. (2007). Composite ceramic containing a bioresorbable phase. Glass and Ceramics *64*, 102-106.

- Sainz-Diaz,C.I., Villacampa,A., and Otalora,F. (2004). Crystallographic properties of the calcium phosphate mineral, brushite, by means of First Principles calculations. American Mineralogist *89*, 307-313.

- Sandhu,H.S., Grewal,H.S., and Parvataneni,H. (1999). Bone grafting for spinal fusion. Orthopedic Clinics of North America *30*, 685-+.

- Sarkar,S.L., Aimin,X., and Jana,D. (2001). Scanning Electron Microscopy, X-Ray Microanalysis of Concretes. In Handbook of analytical techniques in concrete science and technology, V.S.Ramachandran and J.J.Beaudoin, eds. William Andrew Publishing/Noyes), pp. 231-274.

- Schmaljohann,D., Oswald,J., Jorgensen,B., Nitschke,M., Beyerlein,D., and Werner,C. (2003). Thermo-responsive PNiAAm-g-PEG films for controlled cell detachment. Biomacromolecules *4*, 1733-1739.

- Schoenau,E., Saggese,G., Peter,F., Baroncelli,G.I., Shaw,N.J., Crabtree,N.J., Zadik,Z., Neu,C.M., Noordam,C., Radetti,G., and Hochberg,Z. (2004). From bone biology to bone analysis. Hormone Research *61*, 257-269.

- Schwartz,J.H. and Lipmann,F. (1961). Phosphate Incorporation Into Alkaline Phosphatase of e Coli. Proceedings of the National Academy of Sciences of the United States of America *47*, 1996-&.

- Seal,B.L., Otero,T.C., and Panitch,A. (2001). Polymeric biomaterials for tissue and organ regeneration. Materials Science & Engineering R-Reports *34*, 147-230.

- Seviour,R.J., Mino,T., and Onuki,M. (2003). The microbiology of biological phosphorus removal in activated sludge systems. Fems Microbiology Reviews *27*, 99-127.

- Shelton,R.M., Liu,Y., Cooper,P.R., Gbureck,U., German,M.J., and Barralet,J.E. (2006). Bone marrow cell gene expression and tissue construct assembly using octacalcium phosphate microscaffolds. Biomaterials *27*, 2874-2881.

- Shinozaki,T., Xu,Y., Cruz,T.F., and Pritzker,K.P.H. (1995). Calcium Pyrophosphate Dihydrate (CPPD) Crystal Dissolution by Alkaline-Phosphatase - Interaction of Alkaline-Phosphatase on CPPD Crystals. Journal of Rheumatology *22*, 117-123.

- Skalny,J. and Hearn,N. (2001). Surface Area Measurements. In Handbook of analytical techniques in concrete science and technology, V.S.Ramachandran and J.J.Beaudoin, eds. William Andrew Publishing/Noyes), pp. 505-527.

- Smith,B.C. (1996). Fundamentals of fourier transform infrared spectroscopy. CRC Press Inc.).

- Smith,L. (1963). Ceramic-Plastic Material As A Bone Substitute. Archives of Surgery *87*, 653-661.

- Song,J.S., Lee,Y.H., Kim,S.S., and Park,W. (2002). A case of calcium pyrophosphate dihydrate crystal deposition disease presenting as an acute polyarthritis. Journal of Korean Medical Science *17*, 423-425.

- Staiger,M.P., Pietak,A.M., Huadmai,J., and Dias,G. (2006). Magnesium and its alloys as orthopedic biomaterials: A review. Biomaterials *27*, 1728-1734.

- Stephenson,P.K., Freeman,M.A., Revell,P.A., Germain,J., Tuke,M., and Pirie,C.J. (1991). The effect of hydroxyapatite coating on ingrowth of bone into cavities in an implant. J Arthroplasty *6*, 51-58.

- Suchanek,W. and Yoshimura,M. (1998). Processing and properties of hydroxyapatite-based biomaterials for use as hard tissue replacement implants. Journal of Materials Research *13*, 94-117.

- Sumita,M. and Teoh,S.H. (2004). Durability of Metallic Implant Materials . In Engineering Materials for Biomedical Applications, S.H.Teoh, ed. World Scientific), pp. 2-1-2-31.

- Sun,J.S., Huang,Y.C., Tsuang,Y.H., Chen,L.T., and Lin,F.H. (2002). Sintered dicalcium pyrophosphate increases bone mass in ovariectomized rats. Journal of Biomedical Materials Research *59*, 246-253.

- Sun,J.S., Tsuang,Y.H., Liao,C.J., Liu,H.C., Hang,Y.S., and Lin,F.H. (1997). The effects of calcium phosphate particles on the growth of osteoblasts. Journal of Biomedical Materials Research *37*, 324-334.

- Sun,Z.y. and Zhao,L. (2002). [Feasibility of calcium polyphosphate fiber as scaffold materials for tendon tissue engineering in vitro]. Zhongguo Xiu Fu Chong Jian Wai Ke Za Zhi *16*, 426-428.

- Suzuki,O., Kamakura,S., Katagiri,T., Nakamura,M., Zhao,B.H., Honda,Y., and Kamijo,R. (2006). Bone formation enhanced by implanted octacalcium phosphate involving conversion into Ca-deficient hydroxyapatite. Biomaterials *27*, 2671-2681.

- Suzuki,O., Nakamura,M., Miyasaka,Y., Kagayama,M., and Sakurai,M. (1991). Bone-Formation on Synthetic Precursors of Hydroxyapatite. Tohoku Journal of Experimental Medicine *164*, 37-50.

- Takagi,S., Chow,L.C., and Ishikawa,K. (1998). Formation of hydroxyapatite in new calcium phosphate cements. Biomaterials *19*, 1593-1599.

- Tan,L.L., Gong,M.M., Zheng,F., Zhang,B.C., and Yang,K. (2009). Study on compression behavior of porous magnesium used as bone tissue engineering scaffolds. Biomedical Materials *4*.

- Tay,B.Y., Evans,J.R.G., and Edirisinghe,M.J. (2003). Solid freeform fabrication of ceramics. International Materials Reviews *48*, 341-370.

- Termine,J.D. and Posner,A.S. (1966). Infrared Analysis of Rat Bone - Age Dependency of Amorphous and Crystalline Mineral Fractions. Science *153*, 1523-&.

- Theiss,F., Apelt,D., Brand,B.A., Kutter,A., Zlinszky,K., Bohner,M., Matter,S., Frei,C., Auer,J.A., and von Rechenberg,B. (2005). Biocompatibility and resorption of a brushite calcium phosphate cement. Biomaterials *26*, 4383-4394.

- Thouverey,C., Bechkoff,G., Pikula,S., and Buchet,R. (2009). Inorganic pyrophosphate as a regulator of hydroxyapatite or calcium pyrophosphate dihydrate mineral deposition by matrix vesicles. Osteoarthritis and Cartilage *17*, 64-72.

- Tomatsu,S., Nishioka,T., Gutierrez,M.A., Miyamoto,K., Trandafirescu,G.G., Kanai,R., Kobayashi,H., and Yamaguchi,S. (2006). Enhancement of drug delivery to bone: Characterization of human tissue-nonspecific alkaline phosphatase tagged with an acidic oligopeptide. Journal of Inherited Metabolic Disease *29*, 51.

- Tomazic,B.B., Brown,W.E., and Schoen,F.J. (1994). Physicochemical Properties of Calcific Deposits Isolated from Porcine Bioprosthetic Heart-Valves Removed from Patients Following 2-13 Years Function. Journal of Biomedical Materials Research *28*, 35-47.

- Uemura,T., Dong,J., Wang,Y.C., Kojima,H., Saito,T., Iejima,D., Kikuchi,M., Tanaka,J., and Tateishi,T. (2003). Transplantation of cultured bone cells using combinations of scaffolds and culture techniques. Biomaterials *24*, 2277-2286.

- Ulijn,R.V., Bibi,N., Jayawarna,V., Thornton,P.D., Todd,S.J., Mart,R.J., Smith,A.M., and Gough,J.E. (2007). Bioresponsive hydrogels. Materials Today *10*, 40-48.

- Urech,K., Durr,M., Boller,T., Wiemken,A., and Schwencke,J. (1978). Localization of Polyphosphate in Vacuoles of Saccharomyces-Cerevisiae. Archives of Microbiology *116*, 275-278.

- Vaccaro,A.R. (2002). The role of the osteoconductive scaffold in synthetic bone graft. Orthopedics *25*, S571-S578.

- Vallet-Regi,M. and Gonzalez-Calbet,J.M. (2004). Calcium phosphates as substitution of bone tissues. Progress in Solid State Chemistry *32*, 1-31.

- van Hemert,W.L.W., Willems,K., Anderson,P.G., van Heerwaarden,R.J., and Wymenga,A.B. (2004). Tricalcium phosphate granules or rigid wedge preforms in open wedge high tibial osteotomy: a radiological study with a new evaluation system. Knee *11*, 451-456.

- Van Wazer (1974). Phosphorus and Its Compounds. John Wiley & Sons Limited, New York).

- Vanwazer,J.R. and Callis,C.F. (1958). Metal Complexing by Phosphates. Chemical Reviews *58*, 1011-1046.

- Vanwazer,J.R. and Holst,K.A. (1950). Structure and Properties of the Condensed Phosphates .1. Some General Considerations About Phosphoric Acids. Journal of the American Chemical Society *72*, 639-644.

- Vereecke,G. and Lemaitre,J. (1990). Calculation of the Solubility Diagrams in the System Ca(Oh)2-H3Po4-Koh-Hno3-Co2-H2O. Journal of Crystal Growth *104*, 820-832.

- Waldman,S.D., Grynpas,M.D., Pilliar,R.M., and Kandel,R.A. (2002). Characterization of cartilagenous tissue formed on calcium polyphosphate substrates in vitro. Journal of Biomedical Materials Research *62*, 323-330.

- Wang,X.D. and Puram,S. (2004). The toughness of cortical bone and its relationship with age. Annals of Biomedical Engineering *32*, 123-135.

- Weiner,S. and Wagner,H.D. (1998). The material bone: Structure mechanical function relations. Annual Review of Materials Science *28*, 271-298.

- Whited,B.M., Skrtic,D., Love,B.J., and Goldstein,A.S. (2006). Osteoblast response to zirconia-hybridized pyrophosphate-stabilized amorphous calcium phosphate. Journal of Biomedical Materials Research Part A *76A*, 596-604.

- Wichterle,O. and Lim,D. (1960). Hydrophilic Gels for Biological Use. Nature *185*, 117-118.

- Willmann,G. (1999). Coating of implants with hydroxyapatite material connections between bone and metal. Advanced Engineering Materials *1*, 95-105.

- Woltgens,J. and Ahsmann,W. (1970). Determination of Orthophosphate in Presence of Inorganic Pyrophosphate in Assay of Inorganic Pyrophosphatase Activity. Analytical Biochemistry *35*, 526-&.

- Wuttke,M., Muller,S., Nitsche,D.P., Paulsson,M., Hanisch,F.G., and Maurer,P. (2001). Structural characterization of human recombinant and

bone-derived bone sialoprotein - Functional implications for cell attachment and hydroxyapatite binding. Journal of Biological Chemistry *276*, 36839-36848.

- Xia,Z.D., Grover,L.M., Huang,Y.Z., Adamopoulos,L.E., Gbureck,U., Triffitt,J.T., Shelton,R.M., and Barralet,J.E. (2006). In vitro biodegradation of three brushite calcium phosphate cements by a macrophage cell-line. Biomaterials *27*, 4557-4565.

- Xu,Y., Cruz,T., Cheng,P.T., and Pritzker,K.P.H. (1991a). Effects of Pyrophosphatase on Dissolution of Calcium Pyrophosphate Dihydrate Crystals. Journal of Rheumatology *18*, 66-71.

- Xu,Y., Cruz,T.F., and Pritzker,K.P.H. (1991b). Alkaline-Phosphatase Dissolves Calcium Pyrophosphate Dihydrate Crystals. Journal of Rheumatology *18*, 1606-1610.

- Yamada,M., Shiota,M., Yamashita,Y., and Kasugai,S. (2007). Histological and histomorphometrical comparative study of the degradation and osteoconductive characteristics of alpha- and beta-tricalcium phosphate in block grafts. Journal of Biomedical Materials Research Part B-Applied Biomaterials *82B*, 139-148.

- Zaidi,M. (2007). Skeletal remodeling in health and disease. Nature Medicine *13*, 791-801.

- Zdrahala,R.J. (1996). Hydrogels and vascular grafts - State of the art and beyond. Macromolecular Symposia *109*, 135-143.

- Zreiqat,H., Howlett,C.R., Zannettino,A., Evans,P., Schulze-Tanzil,G., Knabe,C., and Shakibaei,M. (2002). Mechanisms of magnesium-stimulated adhesion of osteoblastic cells to commonly used orthopaedic implants. Journal of Biomedical Materials Research *62*, 175-184.

14. APPENDIX

Part of the research carried out on ceramic fabrication and characterisation (chapter 8) was successfully published in a peer reviewed journal. If you would like to read the article it can be found at http://www.trailab.net/Liam%20-%20Papers/28.pdf.

- Bolarinwa A.O., Wright A.J., Gbureck U., Purnell P., Bold M. and Grover L.M. "Cement casting of calcium pyrophosphate based bioceramics". Advances in Applied ceramics, UK, 2010; 109: 291-295.